Comprehensive Study of Unidirectional Flax/Epoxy Composites; an Evaluation of Material Properties and Fracture Behavior

by

Yousef SAADATI

MANUSCRIPT-BASED THESIS PRESENTED TO ÉCOLE DE TECHNOLOGIE SUPÉRIEURE IN PARTIAL FULFILLMENT OF THE REQUIREMENTS FOR THE DEGREE OF DOCTOR OF PHILOSOPHY Ph.D.

MONTREAL, DECEMBER 7, 2020

ÉCOLE DE TECHNOLOGIE SUPÉRIEURE
UNIVERSITÉ DU QUÉBEC

BOARD OF EXAMINERS

THIS THESIS HAS BEEN EVALUATED

BY THE FOLLOWING BOARD OF EXAMINERS

Prof. Jean-François Chatelain, Thesis Supervisor
Department of Mechanical Engineering at École de technologie supérieure

Prof. Gilbert Lebrun, Thesis Co-supervisor
Department of Mechanical Engineering at Université du Québec à Trois-Rivières (UQTR)

Prof. Yves Beauchamp, Thesis Co-supervisor
Office of the Vice-Principal at McGill University

Prof. Simon Joncas, President of the Board of Examiners
Department of Systems Engineering at École de technologie supérieure

Prof. Ilyass Tabiai, Member of the jury
Department of Mechanical Engineering at École de technologie supérieure

Prof. Rachid Boukhili, External Evaluator
Department of Mechanical Engineering at Polytechnique Montreal

THIS THESIS WAS PRESENTED AND DEFENDED

IN THE PRESENCE OF A BOARD OF EXAMINERS AND PUBLIC

ON DECEMBER 1, 2020

AT ÉCOLE DE TECHNOLOGIE SUPÉRIEURE

DEDICATION

Dedicated to my beloved parents, my wife and my children, Amirheerad, Helma and Hosna for their endless love and supports…

ACKNOWLEDGMENT

Étude approfondie des composites lin / époxy unidirectionnels; évaluation des propriétés et du comportement en rupture en vue de la simulation numérique des processus d'usinage

Yousef SAADATI

RÉSUMÉ

Les matériaux composites sont couramment utilisés dans divers domaines comme l'industrie aérospatiale, l'automobile, le transport, l'énergie éolienne, les articles récréatifs et de sport, et beaucoup d'autres en raison de leurs propriétés spécifiques supérieures qui leur permettent de remplacer les matériaux conventionnels comme les métaux. Le matériau composite renforcé par des fibres de verre (GFRP) est largement utilisé pour ses propriétés comparables voire supérieures aux matériaux métalliques. Cependant, il n'est pas recyclable, est cher et cause des problèmes de santé pendant le processus d'usinage. Pour surmonter les difficultés de recyclage et les dangers pour la santé de ce type de matériau, le composite à base de fibres de lin (FFRC), qui s'est révélé avoir des propriétés intrinsèques comparables au GFRP, peut être une solution de remplacement intéressante pour de nombreuses applications.

Les pièces à base de fibres de lin et d'époxy (FFREC), bien qu'elles soient habituellement fabriquées sous forme de pièces quasi-finies, doivent être usinées pour l'assemblage, le dimensionnement et l'amélioration de la qualité. L'usinage des FFREC est un processus difficile en raison de leur hétérogénéité et de leur comportement anisotrope et peut endommager la pièce à usiner et générer un mauvais état de surface usinée par épluchage des fibres, arrachement des fibres, dégâts matriciels, délamination, etc. Une connaissance approfondie de leurs processus d'usinage est essentielle pour réduire ces dommages et améliorer leur qualité d'usinage. Le processus de détourage est fréquemment utilisé pour les corrections géométriques; cependant, seules quelques études expérimentales ont abordé son application aux FFREC. La complexité de leur processus de découpe nécessite de faire appel à la méthode des éléments finis (FEM) pour l'étudier, mais cela est impossible en raison de l'absence des propriétés mécaniques adéquates. Par conséquent, l'objectif principal de cette étude sera l'évaluation complète du FFREC unidirectionnel (UD) afin de déterminer ses propriétés mécaniques requises dans le code de calcul des éléments finis pour modéliser le détourage.

Tout d'abord, des UD-FFREC avec une teneur en fibres unique ont été moulés et durcis dans des conditions similaires. Ensuite, des éprouvettes ont été préparées et testées selon les procédures de tests standards adaptés, initialement développées pour les (composite renforcé par fibres) FRC synthétiques.

Les propriétés physiques, y compris la densité, la capacité thermique spécifique et la diffusivité thermique et conductivité thermique, ont été déterminées selon des méthodes d'essai standard.

X

Les propriétés de résistance et rigidité sous charges de tension, compression, cisaillement et flexion dans les directions longitudinales at transversale ont été évaluées selon les normes ASTM. En outre, une analyse fractographique a été menée pour comprendre les mécanismes de défaillance à l'échelle macro et microscopique. Les résultats sont en bon accord avec ceux de la littérature, lorsqu'ils sont disponibles, mais ils montrent principalement le comportement spécifique des composites UD-lin/époxy soumis à différents modes de sollicitation.

Des éprouvettes appropriées ont été conçues et testées pour évaluer les taux de restitution d'énergie en rupture interlaminaire en mode I, mode II et mode mixte I / II. Les tests ont été réalisés selon les normes ASTM. Les résultats sont en bon accord avec les données de la littérature, lorsqu'elles sont disponibles.

Pour les stratifiés UD, l'application des méthodes de test conventionnelles pour le mode de défaillance translaminaire est difficile; il n'existe pas non plus de méthode standard pour les tester en compression. Cette étude a utilisé deux méthodologies, ainsi qu'une enquête sur le comportement à la rupture et la viabilité des procédures d'essai standards pour les FFREC. Tout d'abord, le composite a été testé pour la résistance à la rupture translaminaire en traction selon la norme ASTM E1922 existante. Ensuite, en utilisant une méthodologie basée sur la thermographie infrarouge (IRT), ainsi que la norme ASTM D5045, l'énergie de fracture translaminaire des UD-FFREC en traction et en compression a été déterminée. Pour les tests de traction, les résultats de l'IRT sont en accord avec ceux de l'ASTM, alors que les tests de compression montrent un écart significatif, indiquant l'inadéquation de l'IRT pour ces tests.

Dans l'ensemble, pour un UD-FFREC de qualité unique, une connaissance approfondie a été développée et un ensemble complet de propriétés de matériaux et d'énergies de fracture précises et fiables, répondant aux exigences FEM, a été généré.

Mots-clés: Composites renforcés de fibres de lin; propriétés matérielles; énergie de fracture interlaminaire; résistance à la fracture translaminaire (taux de restitution d'énergie en rupture de fibres en mode I); Thermographie Infrarouge; détourage; méthode des éléments finis

Comprehensive study of unidirectional flax/epoxy composites; an evaluation of material properties and fracture behavior in view of numerical simulation of machining processes

Yousef SAADATI

ABSTRACT

Fiber-reinforced polymer composites (FRCs) are extensively used in various commercial applications such as aerospace, transportation industry, recreational and sporting goods due to their enhanced properties. However, they are costly and are not eco-friendly. Offering competitive properties at a lower cost and improved sustainability, flax fiber-reinforced epoxy composites (FFRECs) are recognized as an attractive alternative to glass fiber polymer composites for various applications.

FFREC parts are produced to their final geometry; still, some machining processes are often unavoidable for technical and quality purposes. However, machining of FFRCs remains challenging due to their heterogeneity and anisotropic nature that induce workpiece damages such as delamination and generate inferior surface finish. In-depth knowledge of their machining processes is vital for reducing these damages and improving their machining quality. Edge trimming is frequently used for geometrical corrections of FRCs; however, only few experimental studies have addressed its application to FFRECs. The complexity of their cutting process requires involving the finite element method (FEM) to study it, but it is impossible due to a lack of adequate material properties. Therefore, this study aims at a comprehensive evaluation of unidirectional (UD) FFRECs to provide their essential material characteristics for finite element modeling of their edge trimming process.

Accordingly, first, UD-FFRECs with unique specifications were molded via resin transfer molding (RTM). Then, test specimens were prepared and tested according to the adapted standard test procedures, initially developed for synthetic FRCs.

Physical properties, including density, specific heat capacity, and thermal diffusivity/thermal conductivity, were determined according to standard test methods.

Strength/stiffness properties under tension, compression, shear, and flexural loading, in longitudinal/transverse directions were evaluated following standard test methods. Also, the failure mechanisms were investigated via fractography. The results are in good agreement with those of the literature, when available, while they mainly show the specific behavior of UD-flax composites subject to different solicitation modes.

Proper test specimens were designed and tested for the interlaminar fracture energies in Mode I, Mode II, and Mixed-Mode I/II. The tests were carried out following ASTM standards. The results are in good agreement with literature data for similar cases, where available.

For UD laminates, the application of the conventional test methods for translaminar failure mode is challenging; also, there is no standard method for testing them in compression. Two methodologies were employed, along with an investigation of the fracture behavior and viability of the standard test procedures for FFRECs. First, the composite was tested for translaminar fracture toughness in tension according to the existing ASTM E1922. Then, employing an Infrared Thermography (IRT)-based methodology, as well as ASTM D5045, the translaminar fracture energy of UD-FFRECs in tension and compression was determined. For tension tests, the results of IRT agree with those of ASTM, whereas compression tests showed a significant discrepancy, indicating the inappropriateness of IRT for these tests.

Overall, for a UD-FFREC with unique quality, an in-depth knowledge was developed, and a full set of precise and reliable material properties and fracture energies, fulfilling FEM requirements were generated.

Keywords: Flax fiber-reinforced composites; material properties; interlaminar fracture energy; translaminar fracture toughness; Infrared Thermography; edge trimming; Finite element method

TABLE OF CONTENTS

XV

LIST OF TABLES

LIST OF FIGURES

Page

XXII

LIST OF ABBREVIATIONS

2D/3D	2-Dimensional/3-Dimensional
ABS	Acrylonitrile Butadiene Styrene
AE	Acoustic Emission
ANN	Artificial Neural Network
ANOVA	Analysis of Variance
ASTM	American Society for Testing Material
CC	Compact Compression; Compliance Calibration
CFRP	Carbon Fiber-Reinforced Polymer
COD	Crack Opening Displacement
COV	Coefficient of Variation
CT	Compact Tension
DCB	Double Cantilever Beam
DIC	Digital Image Correlation
DoE	Design of Experiment
DSC	Differential Scanning Calorimetry
ECT	Extended Compact Tension
EHM	Equivalent Homogenous Material
ENF	End-Notched Flexure
FE/FEM	Finite Element/Finite Element Method
FFREC	Flax Fiber-Reinforced Epoxy Composite
FFRC	Flax Fiber-Reinforced Polymer Composite
FRC	Fiber-Reinforced Polymer Composite

GFRP	Glass Fiber-Reinforced Polymer
HBP	Hyperbranched Polymer
HDPE	High-Density Polyethylene
IFE	Interlaminar Fracture Energy
IFT	Interlaminar Fracture Toughness
IRT	Infrared Thermography
LEFM	Linear Elastic Fracture Mechanics
LLSRA	Least-Squares Regression Analysis
MBT	Modified Beam Theory
MMB	Mixed-Mode Bending
NF	Natural Fiber
NFRC	Natural Fiber-Reinforced Polymer Composite
NL	Non-linear
NMOD	Notch Mouth Opening Displacement
NPC/PC	Non-Precracked/Precracked
PEEK	Polyether Ether Ketone
PHB	Polyhydroxybutyrate
PLA	Polylactic Acid
PP	Polypropylene
PPS	Polyphenylene Sulfide
PTFE	Polytetrafluoroethylene
PU	Polyurethane

PVC	Polyvinyl Chloride
RTM	Resin Transfer Molding
SBT	Simple Beam Theory
SF	Synthetic Fiber
SFRC	Synthetic Fiber-reinforced Composite
SG	Strain Gauge
SLB	Single-Leg-Bending
STD	Standard Deviation
TFT	Translaminar Fracture Toughness
TPB	Three-Point-Bending
UD	Unidirectional
VE	Vinyl-ester
VIS	Visualized

LIST OF SYMBOLS

Symbol	Unit	Description
a	mm	Delamination crack length
a_0	mm	Initial delamination crack length
a_{calc}	mm	Calculated crack length
a_f	(mm/tooth)	Feed per tooth
A	mm/N	Compliance calibration coefficient
A_f	g/m^2	Fiber surface density
b	mm	Width of DCB and MMB specimens
B	mm	Width of ENF specimen
c	mm	Length of the lever in MMB fixture
C	mm/N	Compliance of the specimen
C_p	J/(g.K)	Specific heat capacity
dW_{diss}	J	Energy dissipated as heat
dW_{irrev}	J	Total irreversible energy
D	(m)	Diameter of cutting tool
E_{11}, E_{22}	GPa	Stiffness of laminate in the fiber and transverse directions respectively
E_f	GPa	Flexural modulus
f	(mm/rev)	Feed per revolution
F	–	Large-displacement correction factor of DCB specimen
G	J/m^2	Strain energy release rate
G_{12}, $G_{21,}$ and G_{13}	GPa	Shear moduli

G_C	J/m^2	Critical strain energy release rate or fracture energy
G_C^{Comp}, G_C^{Ten}	J/m^2	Translaminar fracture energy in compression and tension respectively
$G_C^{Comp}\|_{fiber\ kinking}$	J/m^2	Fracture energy in fiber-kinking failure mode
$G_C^{Comp}\|_{lam\ comp}$	J/m^2	Fracture energy of laminate in compression
$G_C^{Ten}\|_{fiber\ tensile}$	J/m^2	Fracture energy in fiber tensile failure mode
$G_C^{Ten}\|_{lam\ tensile}$	J/m^2	Fracture energy of laminate in tension
G_I	J/m^2	Strain energy release rate in Mode I delamination
G_{IC}, G_{IIC}, $G_{(I/II)C}$	J/m^2	Mode I, Mode II, and Mixed-mode I/II interlaminar fracture energy respectively
G_{IC}^0	J/m^2	Fracture energy in fiber tensile failure mode
G_{IC}^{90}	J/m^2	Mode-I intralaminar matrix failure fracture energy
G_{IC}^{ini}	J/m^2	Crack initiation value of G_{IC}
$G_{IIC}\|_{matrix\ intra}$	J/m^2	Mode-II matrix failure intralaminar fracture energy
$G_{IC}\|_{matrix\ intra}$	J/m^2	Mode-I intralaminar matrix failure fracture energy
$G_{(I/II)C}^{est}$	J/m^2	Estimated value of Mixed-mode I/II fracture toughness
h	mm	Thickness of laminate; Half thickness of MMB specimen
K_C	MPa m$^{1/2}$	Stress intensity factor
K_{IC}	MPa m$^{1/2}$	Translaminar fracture toughness
K_{xx}, K_{yy}, and K_{zz}	W/(m.K)	Thermal conductivity in x, y, and z directions
L	mm	Half-span length of MMB fixture
m	1/(N.m^2)	Compliance calibration coefficient
m	N/mm	Slope of the load-displacement curve in MMB test

n	–	Number of plies in the composite plate
N	rpm	Spindle speed
P	N	Applied load
P_1, P_2	MPa	Pressure after fill and after expansion respectively
P_C, P_{Max}	N	Critical load and Maximum load respectively
P_i	N	Initial compliance calibration forces
R_a	μm	Arithmetic mean value
R_p, R_t	μm	Maximum peak to mean and maximum peak to valley height respectively
R_v, R_z	μm	Mean to valley and ten-point average height respectively
S_{the}	J	Thermo-mechanical coupling term
t_{lam}, t_0, t_{90}	mm	Thicknesses of the cross-ply laminate, 0° layers, and 90° layers within the laminate
T, T_0	(°C)	Temperature in the current and initial situation
v	(m/min)	Cutting speed
v_f	(mm/min)	Feed speed
V_f	(%)	Fiber volume fraction
V_s, V_c, V_x	mm^3	Volumes of the sample, sample chamber, and expansion chamber respectively
W_a, W_{fl}	g	Weight in air and in the immersion fluid respectively
α	m^2/S	Thermal diffusivity
β	–	Taylor–Quinney coefficient
δ	mm	Crack opening displacement on the load line
$\varDelta$	mm	Crack length correction factor

$\varepsilon_{11}{}^{max}$, $\varepsilon_{22}{}^{max}$	%	Failure strain in the fiber and transverse directions respectively
$\varepsilon_{12}{}^{max}$, $\varepsilon_{21}{}^{max}$	%	Shear failure strain in the fiber and transverse directions respectively
η	–	B-K (Benzeggagh & Kenane) fitting parameter
θ	(°)	Fiber orientation relative to the cutting edge speed
$\theta = T - T_0$	(°C)	Temperature change
λ	W/(m.K)	Thermal conductivity
ρ	g/cm^3	Density
ρ_a, ρ_{fl}	g/cm^3	Density of air and the immersion fluid respectively
ρ_f, ρ_c	g/cm^3	Density of fiber and composite respectively
$\sigma_{11}{}^{max}$, $\sigma_{22}{}^{max}$	MPa	Strength of laminate in the fiber and transverse directions respectively
$\tau_{12}{}^{max}$, $\tau_{21}{}^{max}$	MPa	Shear strength in fiber and transverse directions respectively
υ	–	Poisson's ration
ϕ	(°)	Tool rotation angle
$\emptyset_{int}$, $\emptyset_{irrev}$	J	Intrinsic and irreversible dissipation respectively
$\emptyset_{stored}$	J	Stored energy
χ	–	Crack correction parameter in MMB test
ψ	(°)	Fiber angles in the laminate

INTRODUCTION

Fiber-reinforced polymer composites (FRCs) have been widely used in various industrial applications for several decades owing to the progress in composites technology with enabling the production of outstanding composite components with combined desired properties such as high strength, low density, high fatigue, and corrosion resistance (Ismail, Dhakal, Popov, & Beaugrand, 2016; La Mantia & Morreale, 2011; Mohanty, Misra, & Hinrichsen, 2000; Netravali & Chabba, 2003; Wambua, Ivens, & Verpoest, 2003). However, having two dissimilar and non-biodegradable constituents, synthetic fiber-reinforced composites (SFRCs) cannot be easily reused or recycled, so that most of them have to be disposed of in the landfills, and some are incinerated after reaching their end-of-service-life (La Mantia & Morreale, 2011; Netravali & Chabba, 2003). Furthermore, most of the polymers and fibers used to produce engineered FRCs are derived from the ever-depleting petroleum-based resources and are produced via high energy-consuming processes (Chandrasekar *et al.*, 2019; Fuqua, Huo, & Ulven, 2012; Netravali & Chabba, 2003; Shekar & Ramachandra, 2018). Thus, using these composites leads to costly products, which is not favorable.

Over the recent past decades, the growing global environmental consciousness, depletion of petroleum resources, and commencement of new legislation have triggered demanding more sustainable and ecologically efficient products (La Mantia & Morreale, 2011; Netravali & Chabba, 2003). Numerous research efforts have been dedicated to finding sustainable replacements for the human-made FRCs. They have confirmed that plant-based natural fiber-reinforced polymer composites (NFRCs) are the most promising alternatives to petroleum-based FRCs for many applications (Bodros, Pillin, Montrelay, & Baley, 2007; Chandrasekar *et al.*, 2019; Dicker *et al.*, 2014; Gurunathan, Mohanty, & Nayak, 2015; Lotfi, Li, Dao, & Prusty, 2019; Pickering, Efendy, & Le, 2016; Ramesh, Palanikumar, & Reddy, 2017). NFRCs have many advantages over their SFRC counterparts, particularly glass fiber-reinforced polymer (GFRP), such as enhanced sustainability and competitive properties at a lower cost. Substituting the SFRCs with fully biodegradable composites (composed of biodegradable matrix and fibers) is not yet an economically and technically desirable solution in many

applications; nevertheless, the petroleum-based polymers reinforced with natural fibers to produce economic and partially biodegradable composites are suitable for a wide variety of uses (John & Thomas, 2008; Netravali & Chabba, 2003; Ramesh *et al.*, 2017). Flax, hemp, and ramie fibers are the most widely used reinforcement in NFRCs, offering comparable mechanical properties to GFRP (Ahmad, Choi, & Park, 2015; Fuqua *et al.*, 2012; Pickering *et al.*, 2016; Ramamoorthy, Skrifvars, & Persson, 2015; Ramesh, 2019). Among them, flax fibers have superior performances, and many manufacturers use them in NFRCs for various applications (Chandrasekar *et al.*, 2019; Goudenhooft, Bourmaud, & Baley, 2019; Moudood, Rahman, Öchsner, Islam, & Francucci, 2018; Pil, Bensadoun, Pariset, & Verpoest, 2016; Darshil U. Shah, Schubel, & Clifford, 2013; Yan, Chouw, & Jayaraman, 2014; Yan, Wang, & Kasal, 2017). NFRCs have attracted much attention worldwide and have entered the composites industry with a rapidly growing commercial application extending from packaging to structural parts (Cristaldi, Latteri, Recca, & Cicala, 2010; Dicker *et al.*, 2014; Fuqua *et al.*, 2012; Lotfi *et al.*, 2019; Sanjay *et al.*, 2019; Darshil U Shah, 2013). Figure 0.1 and Figure 0.2 show different components made of NFRCs.

Figure 0.1 Various applications of NFRCs
Taken from Cristaldi et al. (2010, p318)
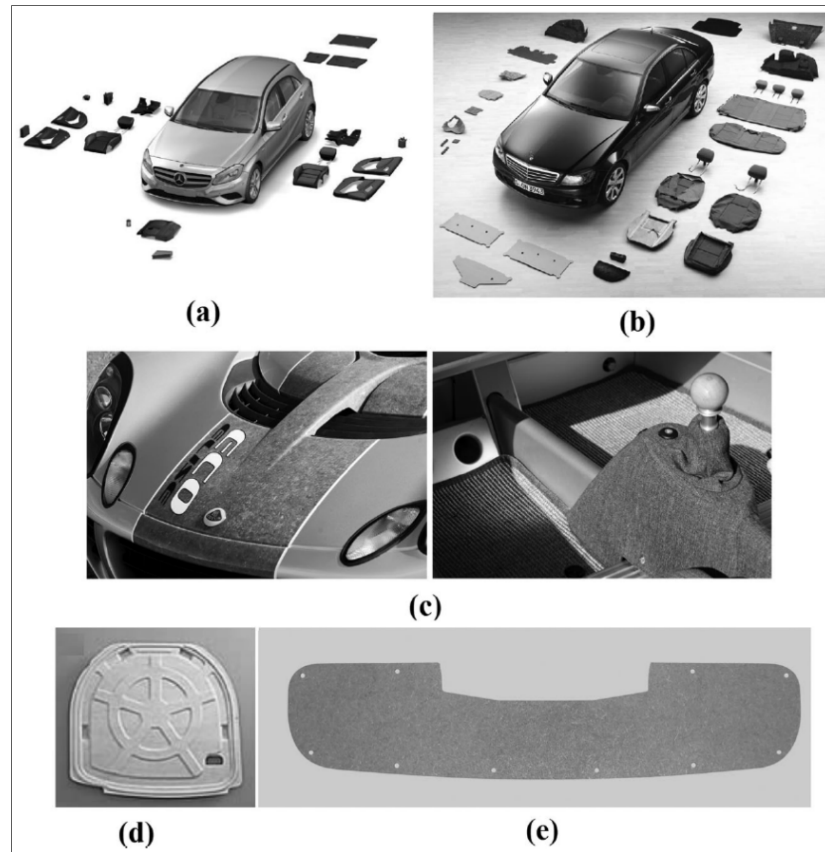
Figure 0.2 NFRCs in automotive applications: (a) Mercedes-Benz A-Class, (b) Mercedes-Benz C-Class, (c) Eco Elise, (d) Toyota RAUM, and (e) Mitsubishi i-MiEV

Taken from Ahmad et al. (2015, p. 21)

Components made of FRCs, including NFRCS, are usually produced near to their final net-shape, still, due to some technical and quality reasons, some secondary production processes such as drilling, and edge trimming are often required. The machining of fiber-reinforced composite materials has always been a challenge because of inducing critical flaws, such as delamination, matrix burning, fiber pullout, burring, uncut fibers, fiber fuzzing, fiber-matrix debonding, and matrix microcracking, due to their heterogeneous and anisotropic nature (Ghafarizadeh, 2015; Lotfi *et al.*, 2019; Mohamed, Rashid, Muhamad, & Ismail, 2019; Nasir, Azmi, & Khalil, 2015; Nassar, Nassar, Arunachalam, & Alzebdeh, 2017). Apart from requiring further finishing operations for machined parts, these defects reduce the static and dynamic strength of the final components, which ultimately affect the short-term and long-term

performances. Moreover, these defects are extremely detrimental, particularly to the service life degradation of NFRCs, due to inducing cavities and cracks, increasing exposure surface, and thus increasing the humidity absorption. All these issues will downgrade the mechanical behavior of these composites and hinder extending their application. Therefore, in order to promote the use of NFRCs, study, evaluation, understanding, and prediction of these machining-induced damages are essential for improving their performance to overcome such downsides. Undoubtedly, for these machinability studies, a deep understanding of their complex structure, their mechanical, physical, and fracture behavior/characteristics is vital.

A large number of research studies have addressed evaluating and improving the machinability of SFRCs via experimental (A. Azmi, Lin, & Bhattacharyya, 2013; Ghafarizadeh, 2015; Ghafarizadeh, Chatelain, & Lebrun, 2014; S. O. Ismail *et al.*, 2016) and numerical methods (Chakrapani & Sekar, 2018; Ghafarizadeh, 2015; Ghafarizadeh, Chatelain, & Lebrun, 2016; S. O. Ismail *et al.*, 2016). However, due to the complex and varying microstructure of the natural fibers (NFs) and the differences in the mechanical, thermal, and hydrolytic behaviors between NFs and conventional fibers, the results obtained for SFRCs do not apply to NFRCs. On the other hand, only limited experimental investigations have been carried out in studying the milling of NFRCs, particularly flax fiber-reinforced polymer composites (FFRCs) (Chegdani, Mezghani, & El Mansori, 2015a; Chegdani, Mezghani, & El Mansori, 2016; Chegdani, Takabi, Tai, Mansori, & Bukkapatnam, 2018; Mustafa, Azmi, Zakaria, & Lih, 2019). To date, no work in the literature has been reported for the numerical study of machining processes of NFRCs, particularly flax/epoxy composites. Because of the complex structure of NFs, their hydrophilicity, and resilient behavior, machining defects in NFRCs are more severe and complex; thus, resolving them is also more complicated.

Some researchers have focused on using the Design of Experiment (DoE) in combination with different statistical techniques to study the machining processes of NFRPs. They mainly investigated the influence of machining parameters on the quality of cut aiming at empirical modeling and optimizing the quality of the machined parts. Analysis of Variance (ANOVA) (Singh & Samanta, 2016), Grey Relational Analysis (Sridharan & Muthukrishnan, 2013),

fuzzy logic (R. Vinayagamoorthy, Rajeswari, Sivanarasimha, & Balasubramanian, 2015), artificial neural network (ANN) (Chandramohan & Rajesh, 2014) are some methods used by previous researchers for NFRCs, with a minimal work reported for FFRCs. However, all these methods are based on some experiments and confined to the selected ranges of the variable parameters. Besides, they do not take into account the cutting process and the chip formation mechanisms. Consequently, these methods are unable to predict the underlying workpiece damages and the extent of damages for different conditions.

Numerical modeling of FRC milling processes, in contrast to experimental methods, considers the material failures occurring during the cutting process, enabling to predict chip formation and workpiece damages (Ghafarizadeh, 2015; Ghafarizadeh *et al.*, 2016). The finite element method (FEM) is a powerful numerical approach that models composite failure by applying specific failure criteria and using material characteristics and fracture properties of the composite. Hence, it is necessary to study and better understand the cutting mechanisms aiming at improving the machining quality. Exploring the behavior and characteristic of the composite is, a fortiori, requisite for numerical modeling. However, a reliable and consistent set of the necessary material and fracture properties of the flax/epoxy composites is missing in the literature.

Therefore, a full evaluation of the physical/mechanical characteristics and fracture behavior of flax/epoxy composite, fulfilling the requirements of the numerical simulation of the machining (cutting) process, is required. In this research, a comprehensive experimental study and evaluation of the physical, mechanical, and fracture characteristics of unidirectional (UD) flax fiber-reinforced epoxy composite (FFREC) have been accomplished. The main purpose is to achieve adequate knowledge of the composite behavior and obtain a full, accurate set of its desired material properties. This is the primary step demanded in FEM to model the material failure for simulating the cutting process and predicting workpiece damages.

This research thesis is organized in five chapters, as follows. A description of the challenges regarding the machining of NFRCs, the research objectives, and the original contributions of

the present study are provided in the first chapter. Chapter 2 is the literature review that includes a brief knowledge of NFRCs, in particular FFRECs, an overview of the FRCs edge trimming process, and a critical review of the previously published research works addressing the milling of FFRCS. Also, the application of FEM in analyzing the cutting process of FRCs, including theory and literature reviews, as well as a comprehensive review of the characterization of FFRECs are presented in this chapter.

Chapter 3 presents the first published journal article (Saadati, Lebrun, Chatelain, & Beauchamp, 2020c). This article reports the results of the literature review and the experimental research conducted to study the failure mechanisms and to evaluate the physical/mechanical properties of the UD flax/epoxy composites. It investigates the material behavior and the involved failure mechanisms under different modes of solicitation and evaluates different mechanical properties of the composite in its principal (longitudinal/transverse) directions. Some physical properties of the composite are also measured in this work. The results are a consistent set of properties and knowledge about the composite that are required at the first step of the numerical modeling of its machining process. The findings of this study are used in the continuation of the research to design the test specimens and determine test parameters for the subsequent experiments reported in the next chapters.

Chapter 4 is the second published article (Saadati *et al.*, 2020a). In this chapter, the interlaminar fracture behavior of the UD flax/epoxy composite under mode I, mode II, and mixed-mode I/II delamination failure is investigated. Also, the interlaminar fracture toughness is evaluated to obtain the fracture energies for corresponding modes of failure. A Digital Image Correlation (DIC) system was used to precisely detect the crack initiation and follow its propagation. These quantities need to be fed into failure criteria employed to predict the material failure in numerical modeling of the cutting process. The knowledge of material behavior in delamination failure will help understand the cutting mechanism and predict the delamination damages that are one of the most prevalent failure modes in these materials. The outcome of

this study is a prerequisite for determining translaminar fracture toughness in the next part of the research.

Chapter 5 presents the third article published in Composites Part C: Open Access (Saadati, Lebrun, Bouvet, Chatelain, & Beauchamp, 2020b). This research work uses the results of the previous chapter and focuses on the translaminar fracture of the understudy UD-FFREC. Translaminar fracture of UD-FRCs, as a primary failure mode of these materials, is one of the most challenging experimental studies of these materials. There are two problems in terms of translaminar fracture testing of NFRCs: no standard test method has been developed for testing in compression loading of FRCs, in general, and those existing for tension loading of SFRCs are inapplicable to UD-FFREC laminates. The former is managed by employing a novel methodology developed based on Infrared Thermography (IRT) and the latter by an intelligent design of the laminate lay-up. The outcome of the study offers a full understanding of the composite behavior under translaminar failure and provides the translaminar fracture energy of UD-FFRECS in tension and compression. Also, valuable results regarding the efficiency of testing methods using two different standards, as well as IRT methods, are achieved. It was concluded that the IRT method could not be efficient in compression and that ASTM D5045 overestimates the translaminar fracture energy for FFRECs, however, compact compression tests using the maximum load of the first linear loading cure is recommended. The translaminar fracture property of the composite is the last essential input into the material failure criteria used by numerical methods implemented to model the cutting processes. The knowledge of the composite behavior in this mode helps to manage the cutting process to optimize the quality of machining and minimize or eliminate the workpiece damages.

The thesis ends with the research conclusion drawn from the present study and the recommendations for future work.

CHAPTER 1

STATE OF THE PROBLEM, RESEARCH OBJECTIVES, AND ORIGINAL CONTRIBUTIONS

1.1   State of problem

The application of FFRCs is rapidly growing in various commercial sections due to their numerous advantageous properties compared to the conventional FRCs, such as comparable specific properties, cost-effectiveness, eco-friendliness, lower tool wear, and lower health impact. Despite these superiorities, machining of FFRCs remains a challenge due to the host of some machining defects such as delamination, matrix burning, fiber pullout, burring, uncut fibers, fiber fuzzing, fiber-matrix debonding, and matrix microcracking. These flaws result from their anisotropic and heterogeneous nature, as well as the composite microstructure and resilient behavior of the flax fiber. These microscale flaws attenuate the static and dynamic strength of the material and may cause catastrophic failure of the components undergoing dynamic loadings. Some of the machined parts require further post-machining operations, such as deburring, that increase production cost and time. Moreover, due to the formation of cavities and voids in the matrix and high hydrophilicity of FFRCs, these defects increase water absorption of the material, which deteriorates the service life of the component (Lotfi *et al.*, 2019; Rajmohan, Vinayagamoorthy, & Mohan, 2018; R. Vinayagamoorthy & Thiagarajan, 2018). To overcome these shortcomings and reach high quality machined surfaces, it is crucial to have an in-depth knowledge of FFRCs behavior in different failure modes, their cutting mechanism, and the influence of machining parameters on their quality of cut.

Experimental studies of the milling process of NFRCs can help to some extent; however, due to the complexity of their milling process, a large number of experiments are required that make them time-consuming and costly. Furthermore, not only the analysis and interpretation of the results are intricate; their validity is confined to the selected range of the machining parameters and the configuration of the composite structure. In contrast, FEM can be efficiently used (at a lower cost and time and without limitations) to simulate the milling

process of FFRCs and study many phenomena, including chip formation, workpiece damages, the evolution of cutting forces as well as the effects of machining parameters and workpiece specifications (reinforcement configuration) on machining quality. Recently, some researchers benefited from advanced computer technology and FEM to study the machining process of SFRCs (Ghafarizadeh *et al.*, 2016; Lasri, Nouari, & El Mansori, 2009; Wan, Li, Yuan, & Zhang, 2019; W. Xu & Zhang, 2017). However, the results of the numerical models obtained for SFRCs are not applicable to NFRCs. This is due to the different fiber/matrix interface, complex microstructure, and contrasting distribution patterns of NFs (they are gathered in bundles rather than distributed as elementary fibers) inside the composite (compared to engineered fibers), resulting in a different cutting behavior of NFRCs. On the other hand, no numerical study in the literature has addressed the milling process of FFRECs. Furthermore, the lack of appropriate knowledge and sufficient reliable set of material and fracture properties of the UD flax/epoxy in the literature, a requirement for numerical modeling, is hampering finite element (FE) modeling of machining processes of these composites.

1.2   Research objectives

Involving FEM to study the milling process of FFRECs and improve their machining quality is vital to facilitate their applications for more complex parts and assemblies. However, adequate knowledge of this composite material, including complete and exact mechanical characteristics, precise fracture energies, and failure behavior, which is the first step to conduct a FE modeling, is missing in the literature.

Therefore, first, this study aims at investigating the material behavior and properties of the FFRECs under different loading modes present in the cutting process, including tension, compression, shear, and flexion. Then, their fracture behavior in various failure modes also occurring during the cutting process, such as Mode I, Mode II, and Mixed-mode I/II interlaminar failure, as well as tensile/compressive translaminar failure, are evaluated. Also, their quantitative physical/mechanical characteristics and fracture energies are determined in

view of FE modeling of the cutting process. Finally, a consistent and complete set of the quantities required in FRCs failure criteria that are used by FEM solutions are extracted.

1.3   Original contributions of the study

A comprehensive investigation and evaluation of UD-FFRECs is elaborated in this research project as a part of the FE modeling process. The obtained results will be used in the future developments of finite element models to analyze their milling process to study and improve their machining quality. Flax/epoxy composite laminates were designed with precise thickness and fiber content and were molded in consistent fabrication conditions to meet the requirements of the targeted standard test procedures. Then, the composites were tested and evaluated for the characteristics required for FEM. The original achievements of this research can be outlined as follows:

- The physical properties of UD-FFRCs (including density, specific heat capacity, thermal diffusivity/conductivity) were determined following standardized methods. Applying different density measurement methods and comparing their results, the proper method for accurately measuring the density of this composite was achieved.

- The behavior of UD-FFRECs in the longitudinal and transverse directions and under various loading modes, namely, tension, compression, shear, and flexion, were evaluated. The corresponding mechanical properties were determined and validated. Also, the fracture surfaces were examined for the failure mechanisms. The complex microstructure and low resin compatibility of NFs led to some particular material properties for this composite. Thus, using reliable procedures and unique composition of composite, the basic requirements of the FEM analysis for this material were generated.

- Specific pre-cracked UD composite specimens were designed and tested following existing standard test methods for human-made FRCs to investigate Mode I, Mode II,

and Mixed-mode I/II interlaminar (delamination) failure. The material behavior under these predominant failure modes of laminated composites was studied, and the corresponding fracture energies were determined and validated. DIC technique was employed to precisely detect and follow the initiation and propagation of delamination failure in the specimens. The outcomes will fulfill the essentials to develop material failure criteria in FEM to model the failure of the composite during the cutting process. This is a basis to simulate chip formation and predict the machining damages to the workpiece.

- Using classic mechanical techniques, following ASTM standards, and an IRT-assisted methodology, the translaminar failure mode (failure in fiber cutting direction) of the UD-FFREC under tensile and compressive loading was studied. Due to the lack of standardized test methods for NF composites, innovative laminate stacking was developed for tensile loading. Also, a novel technology that was already developed based on IRT for the engineered FRCs was applied in combination with existing standard test methods to determine the translaminar fracture energies in tension and compression. Despite its validity for SFRCs, it was concluded that the IRT-based method could not be efficiently applied for NFRECs in compression loading, though, it is proper for tensile translaminar fracture tests. The failure paths were examined for the dominant failure modes. The obtained results provide the last failure mode characteristics and complete the material knowledge to run composite material failure criteria in FEM analysis. This will be utilized for modeling chip formation and predicting workpiece machining damages.

CHAPTER 2

LITERATURE REVIEW

2.1 Flax fiber-reinforced polymer composites

Laminated fiber-reinforced polymer composites are composed of a polymeric matrix and a synthetic or natural fiber structure reinforcement that are combined at the macroscopic level, as shown in Figure 2.1. Offering enhanced properties, and improved sustainability at a lower cost have rendered NFRCs attractive alternatives to SFRCs in many applications. Various NFs and matrices can be used to produce NFRCs, as classified and presented in Figure 2.2. However, this study focuses on plant-based flax natural fiber used to reinforce epoxy resin. Plant-based NFRCs offer many advantages when compared to SFRCs but exhibit some drawbacks (Baley, Gomina, Breard, Bourmaud, & Davies, 2019; Pickering *et al.*, 2016; Ramesh *et al.*, 2017). Some of the pros and cons of NFRCs are summarized in Table 2.1.
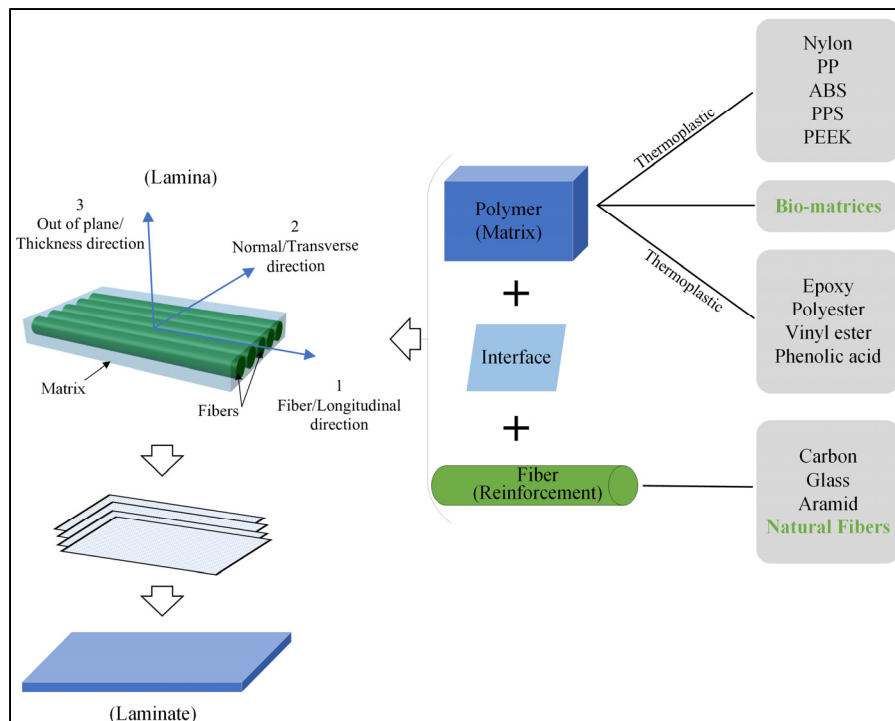
Figure 2.1 FRC laminate composed of unidirectional plies
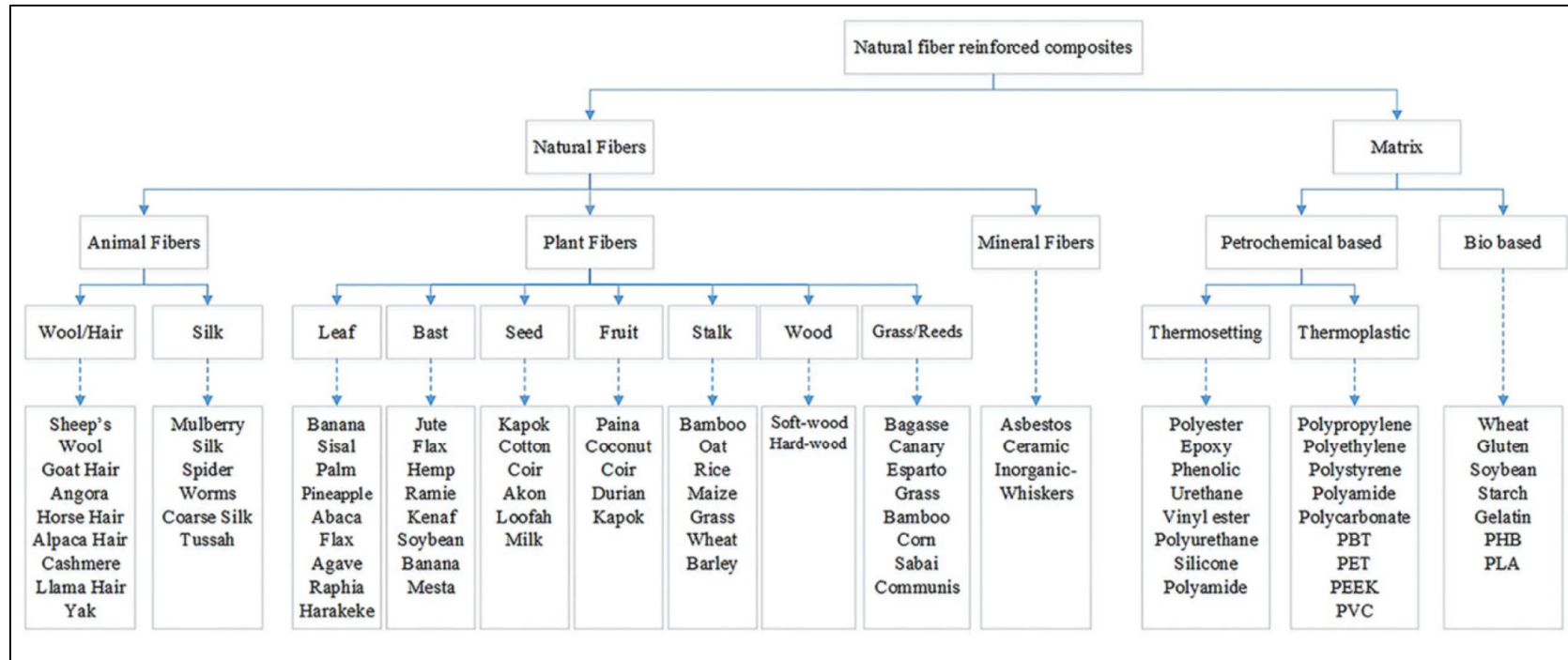
Figure 2.2 Classification of natural fiber reinforcements and different matrices used in NFRCs

Taken from Lotfi et al., 2019

Table 2.1 Advantages and disadvantages of NFRCs

(Baley *et al.*, 2019; Lotfi *et al.*, 2019; Pickering *et al.*, 2016; Ramesh *et al.*, 2017)

Advantages	Disadvantages
➢ NFs are abundantly available	➢ High variability in properties
➢ NFs are less costly than SFs	➢ Lower durability compared to SFRCs (can be enhanced significantly with fiber treatment)
➢ NFs are from renewable resources (biodegradable); require little production energy, are CO_2-neutral	➢ Poor moisture absorption resistance and low dimensional stability (shrinkage, swelling)
➢ Low density and thus high specific strength and stiffness	➢ Limited maximum processing temperature
➢ Low health hazard during manufacturing processes	➢ Weak fiber-matrix adhesion
➢ Low toxic emission when subjected to heat and during incineration at the end of the lifecycle	➢ Poor machinability
➢ Less abrasive compared to SFRCs (reduced tool wear)	
➢ Excellent heat, sound, and electrical insulation properties	

Flax fibers are extracted from the stem (bast) of the flax plant and are composed of about 64% of cellulose. They usually come in bundles, at the mesoscopic level, a bundle contains 10 to 40 elementary fibers linked together by pectin. The elementary fibers, which have a 5-7-side polyhedron shape, have an extremely complex microstructure. It is composed of concentric primary and secondary walls forming an open channel in the middle that is named lumen that contributes to water absorption (K. Charlet *et al.*, 2007; Yan *et al.*, 2014; Jinchun Zhu, Zhu, Njuguna, & Abhyankar, 2013). Flax is one of the most promising NFs that is broadly used as reinforcement in NFRCs for various applications due to its enhanced mechanical, thermal, and damping properties (Chandrasekar *et al.*, 2019; Moudood *et al.*, 2019a; Moudood *et al.*, 2018;

Darshil U. Shah *et al.*, 2013; Yan *et al.*, 2014; Yan *et al.*, 2017). Flax fiber has a complex microstructure in different scales. A general view of the composition and multi-scale composite structure of flax is illustrated in Figure 2.3.
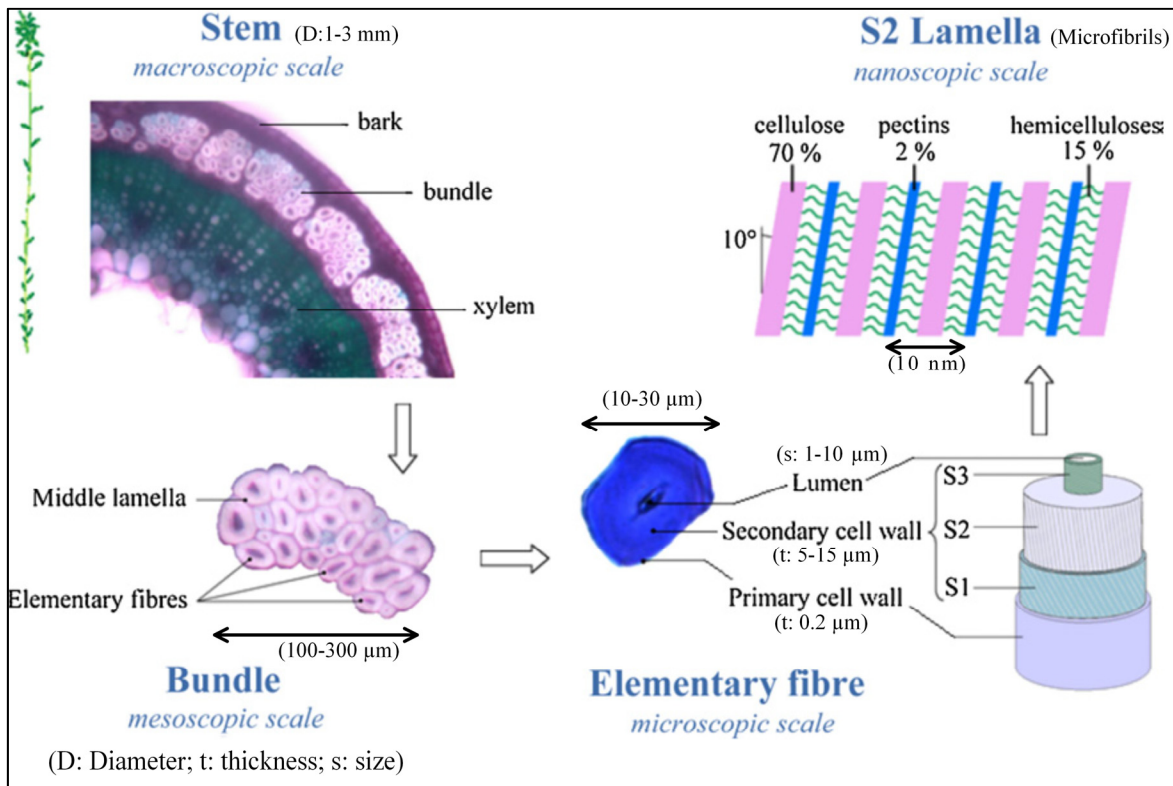
Figure 2.3 Composition and multi-scale composite structure of flax fiber

Taken from K. Charlet et al., 2010 and dimensions adapted from K. Charlet et al., 2007

Flax has a composite structure from Macroscale to the Nanoscale (K. Charlet, Jernot, Eve, Gomina, & Bréard, 2010). They are found in bundles and concentrically arranged in the stem of the plant. They are placed between the xylem, which is responsible for supplying nutrition to the fibers, and the bark which is a protective layer for the stem. During retting and scutching processes, these layers are eliminated and the flax bundles are extracted. The retting process is very important and influences the properties of the fibers (Chabbert *et al.*, 2020; Martin, Mouret, Davies, & Baley, 2013). In mesoscale, the elementary fibers are connected to each other by pectin and form bundles. In practice, these bundles may be broken into smaller bundles, called technical fibers. Elementary fibers have a more complex microstructure,

consist of two concentric walls and a central hole, called Lumen. At the Nanoscale, the cell walls are composed of cellulosic fibrils embedded inside a matrix of mainly pectins and hemicelluloses. These microfibrils are the most important load-carrying part of the fibers (K. Charlet *et al.*, 2010).

Flax/epoxy composites are one of the most frequently used flax fiber-reinforced composites due to their superior performance (Liang, Gning, & Guillaumat, 2015; Pil *et al.*, 2016; Yan & Chouw, 2013). However, similar to other NFRCs, machining of these composites is challenging.

2.2 Milling of flax fiber-reinforced polymers

Usually, milling (edge trimming) is unavoidable for the assembly of complex parts and finishing purposes. These operations are usually being performed by conventional cutting operations due to their simplicity, cost-effectiveness, and restrictions of using unconventional methods to machine these materials. However, due to the heterogeneous and anisotropic nature of FFRCs, milling these materials is more difficult compared to homogenous materials. This is because traditional cutting processes produce high surface roughness and emerge workpiece damages at the cutting zone. These defects deteriorate their mechanical properties and service-life and thus limit their application area. In a milling operation, cutting is carried out by the edges of a multi-teeth rotating tool, often having multiple teeth engaged with the workpiece. In this condition, the cutting direction with respect to the fiber orientation, composite failure modes, chip size, and the cutting forces vary with the rotation angle of the tool. These varying chip formation mechanisms (tool/workpiece interaction condition) make the milling process of FFRCs highly complicated. So, the theory and machining models associated with metals do not apply to these composites, and their machinability needs to be studied in more detail to better understand the machining induced defects to improve their machinability.

Although some researchers have investigated their machinability in drilling via experimental studies (Aiman Akmal, Azmi, & Khalil, 2014; Nasir *et al.*, 2015), only a few others reported

experimental studies of the milling process of flax/PP (Chegdani & Mansori, 2018; Chegdani *et al.*, 2015a; Chegdani *et al.*, 2016; Chegdani *et al.*, 2018), flax/Acrodur bio-resin (Chegdani & El Mansori, 2018), and flax/epoxy composites (J. Delahaigue, Chatelain, & Lebrun, 2017; Karabibene, Chatelain, Beauchamp, & Lebrun, 2018). Nevertheless, these methods are not able to predict machining induced defects, and advanced numerical solutions such as FEM are required. Still, to the author's knowledge, there is no research work addressing modeling of the milling process of UD-FFRECs via numerical techniques, for instance, FEM.

Comprehensive knowledge of material behavior and characteristics is required for FE modeling of FFRECs. There are some works in the literature addressing the behavior and properties of flax composites; however, they have used various compositions (reinforcement structure, fiber content, matrix type), processing techniques, and testing methods (Almansour, Dhakal, & Zhang, 2018; Ravandi, Teo, Tran, YONG, & TAY, 2016b; Yan *et al.*, 2014). Hence, not only a full set of the required properties have not been determined; the reported values are very scattered and cannot be confidently used in FEM analysis.

Therefore, in this study, the edge trimming process, as well as FE modeling of this process will be overviewed to explore the material properties needed for FEM. Then, a literature review will be carried out to find the missing properties. Finally, comprehensive characterizations will be performed to provide the required material properties of UD-FFRECs in view of FE modeling of the cutting process. This will help to understand and minimize the machining induced defects and improve their machinability. This section gives an overview of the profile milling (edge trimming) process of FFRCs.

2.2.1 Profile milling (Edge trimming) configuration

The configuration of the profile milling (edge trimming) process is shown in Figure 2.4a. Depending on how the cutting edges engage and disengage the workpiece, milling operations are categorized into up-milling, Figure 2.4b, and down-milling, Figure 2.4c.
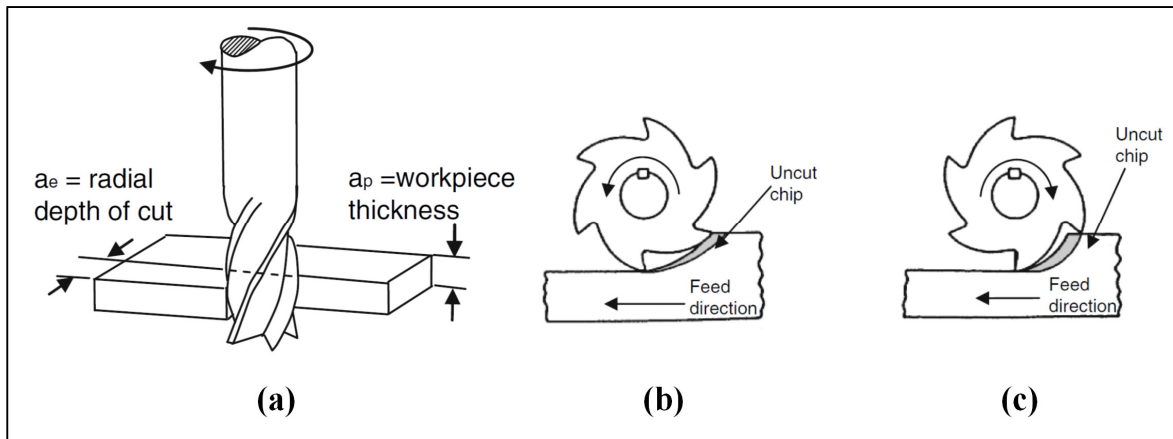
Figure 2.4 (a) Configuration of profile milling (edge trimming), (b) up-milling and down-milling operations

Adapted from Sheikh-Ahmad, (2009, pp.43-44)

Figure 2.5 illustrates the cutting geometry of a cutting edge at a specific cross-section (for the helical tool) in up milling operation.
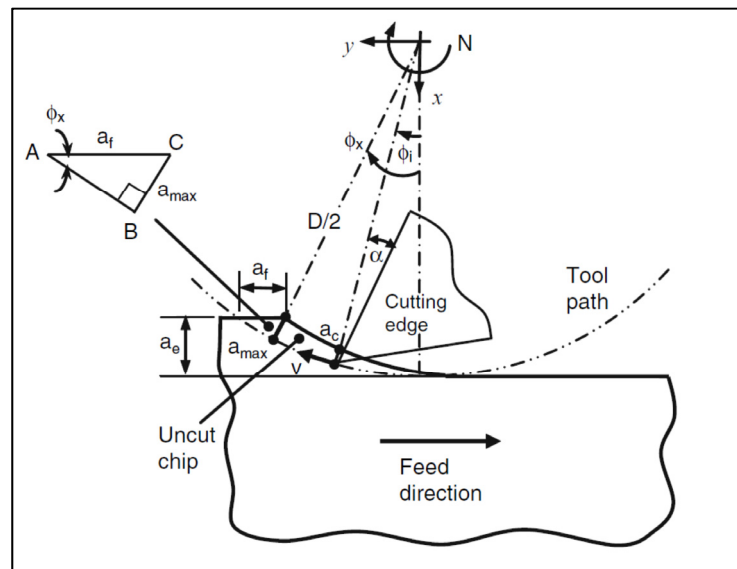
Figure 2.5 Cutting geometry in up milling operation

Taken from Sheikh-Ahmad, (2009, p.45)

The tool has a trochoidal path, generated by rotational and translational motions. The rotation of the spindle generates the cutting speed, v, which is a function of spindle speed, N (rpm), and cutter diameter, D. It is calculated using the following equation:

$$v = \pi DN$$
(2.1)

The feed speed, v_f, and feed per revolution f, influential to material removal rate and machined surface quality, are related by equation 2.2.

$$f = \frac{v_f}{N}$$
(2.2)

The feed per tooth, a_f, determines the movement of the workpiece between the engagement of two successive cutting edges in multi-tooth cutters. It is a function of v_f, N, and the number of teeth of the cutter, T, given by:

$$a_f = \frac{v_f}{TN}$$
(2.3)

2.2.2   Mechanisms of chip formation

The chip formation in machining the metals is predominantly caused by plastic deformation, and then the shearing of material that forms a continuous chip. Accordingly, under fixed conditions, machining approaches a steady-state with relatively constant and predictable cutting forces and machining quality. On the other hand, the cutting mechanism in thermosetting SFRCs usually takes place by uncontrolled intermittent compression shearing (plastic deformation) of the ductile matrix and brittle fracture of the fibers. The discontinuous fracture of the fibers results in the oscillation of the cutting forces. The machinability of FRCs is primarily determined by the physical and mechanical properties of the fiber and matrix, fiber content, and fiber orientation (Sheikh-Ahmad, 2009). Accordingly, flax fibers that are much more resilient than synthetic fibers (SFs) are expected to resist shear cutting and tend to bend at the edge of the cutting tool. Thus, FFRECs are expected to exhibit different machinability compared to SFRCs. Similar behavior was observed for comparatively tougher aramid fiber

composites (Sheikh-Ahmad, 2009). The results of several studies addressing the machining of UD-FRCs revealed that the fiber orientation and the cutting edge rake angle control the chip formation mechanism in milling unidirectional FRCs (Ramulu, 1997; Sheikh-Ahmad, 2009). As shown in Figure 2.6, in a milling operation, the fiber orientation with respect to the cutting direction depends on the cutter rotation angle and varies continuously with tool rotation. In Figure 2.6, the position of the cutting edge is shown by ϕ, θ indicates the fiber orientation relative to the instantaneous cutting-edge speed, and ψ is the fiber angles in the UD laminate measured from the feed opposite direction.

Therefore, during the milling process, the composite will be subjected to and fail under various modes of loading; thus, depending on the cutting situation, different cutting mechanisms are responsible for chip formation. As illustrated in Figure 2.7, chip formation mechanisms in cutting UD-FRCs are classified into five types, depending on the relative fiber orientation/cutting direction angles and tool rake angle (Sheikh-Ahmad, 2009):

- *Type I, delamination type*: When cutting the 0° fibers with positive rake angles, the sharp edge of the tool penetrates the FRC laminate in the fiber direction, Figure 2.7a. At the tool-workpiece contact point, inducing Mode I interlaminar loading and fracture, a crack initiates and propagates along with the fiber-matrix interface. As the tool advances into the composite, the delaminated plies, sliding up the tool surface, bend, and eventually fracture in the perpendicular direction ahead of the tool edge, and a small discontinuous chip is formed. Accordingly, a knowledge of the Mode I interlaminar behavior and fracture properties of FFRECs is crucial for modeling and analysis of this type of cutting mechanism.
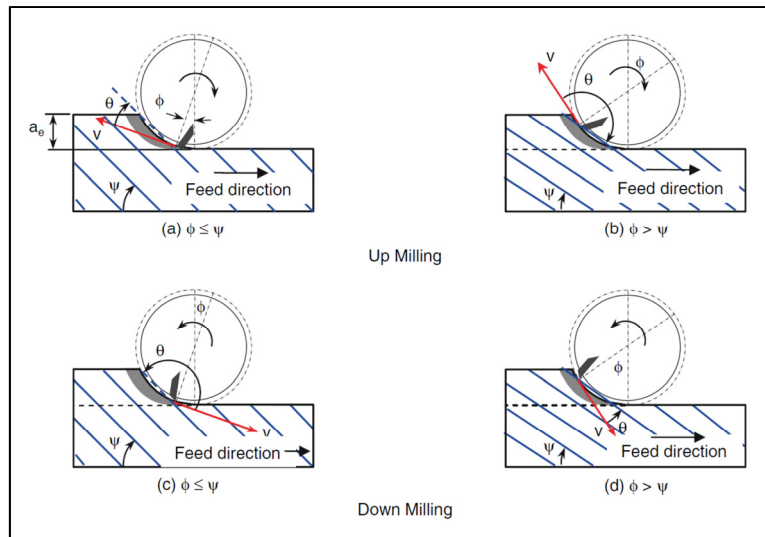
Figure 2.6 Kinematics of milling process of UD laminates:
(a, b) up milling and (c, d) down milling

Taken from Sheikh-Ahmad, (2009, p.161)
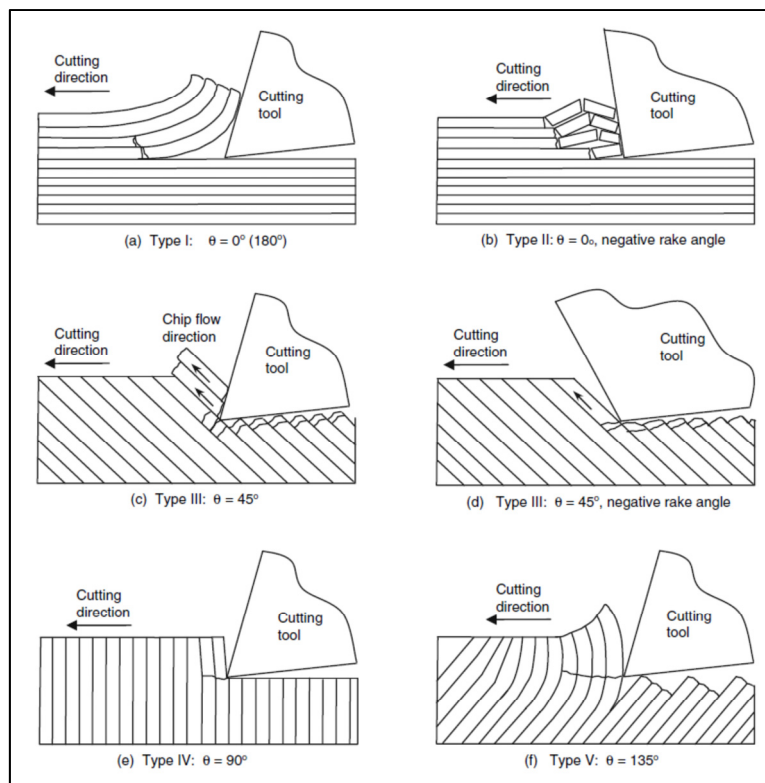
Figure 2.7 Cutting mechanisms of UD-FRCs

Taken from Sheikh-Ahmad, (2009, p.75)

- *Type II, fiber buckling type*: When machining 0° fibers with 0° or negative rake angles, Figure 2.7b, the plies are exposed to compression loading in their longitudinal direction that causes fiber buckling. Further advancement of the cutting tool induces Mode II interlaminar fracture at the fiber/matrix interface. Consecutive buckling of the fibers leads to the fiber fractures in perpendicular direction. The fractures take place in close proximity of the cutting edge, resulting in small distinct chips. Hence, understanding of the Mode II interlaminar and compressive fracture behavior/properties of FFRECs is essential for understanding and modeling of this chip formation mode in milling operation.

- *Type III, fiber cutting type (with continuous chip)*: This type of cutting mechanism occurs during the machining with fiber orientations greater than 0° and less than 90°, and for all rake angles, Figure 2.7 c-d. The chip formation process starts with the fracture of the fibers caused by transverse compression-induced shear stress. By further advancement of the cutting tool, interlaminar shear fracture at the fiber-matrix interfaces completes the chip formation. Some cracks are generated in the fibers above and below the cutting plane during the first stage of the chip formation process. The cracks created below the cutting plane are a source of surface integrity problems. In these cases, the chip is continuous and flows parallel to the fibers. The predominant material failure mode in these cases is in-plane shear. So, in-depth knowledge of the in-plane shear, tensile, interlaminar, and translaminar failure is required for modeling and analysis of the responsible cutting mechanism.

- *Type IV, fiber cutting type (with discontinuous chip)*: In this case, the cutting mechanism is similar to type III, Figure 2.7e. However, the interlaminar shear at the fiber-matrix interface increases, leading to a fracture of chip segments and the formation of small chips. Likewise, the material characteristics in tensile, shear, interlaminar, and translaminar failure modes for numerical modeling of the trimming process of this composite are necessary.

- *Type V, macrofracture type*: The cutting mechanism in edge trimming with large fiber orientation angles (105°-150°) is rather a macrofracture, Figure 2.7f. Entering the workpiece, cutting tool induces large fiber deformations leading to delamination, intralaminar shear, and large out-of-plane displacement. In this case, material failure may occur below the cutting plane. This results in the formation of discontinuous chips, which are at times greater than the depth of cut, and a poor surface finishing (Sheikh-Ahmad, 2009; Teti, 2002). Therefore, due to the presence of different modes of material failure in this chip formation type, comprehensive knowledge of composite behavior and its characteristics are indispensable for modeling and analysis.

Nonetheless, flax fibers have a much more complex microstructure, contrasting high resilience and different distribution patterns (they are gathered in bundles rather than distributed as elementary fibers inside the composite) compared to SFs. Consequently, the cutting behavior of FFRCs significantly differs from those of engineered FRCs and is more challenging to analyze. For example, their machining behavior is largely affected by the selected analysis scale, as shown in Figure 2.8 (Chegdani *et al.*, 2015a), whereas, SFs are spread more evenly in the composites that prevents this effect. In another study, Chegdani et al. concluded that the cutting mechanisms in NFRCs are affected by fiber stiffness, and the real cutting condition is far from the ideal one, as shown in Figure 2.9 (Chegdani, Mezghani, El Mansori, & Mkaddem, 2015b). In fact, the particular characteristics and composition of the NFs are the source of machining difficulties. Their viscoelastic behavior provokes large fiber deformation during the cutting process so that, instead of fracturing under shear, the fibers slide between the tool and the machined surface. This behavior of the NFs induces fiber/fiber and fiber/matrix interface fracture, leading to the generation of uncut fibers that cause inferior surface finish (Chegdani *et al.*, 2015b). Likewise, this is a consequence that does not occur in SFRCs and renders the machining of NFRCs different and more intricate.

Also, Chegdani et al. realized that for NFRCs, the trimming specific energy in up-milling is higher that down-milling (Chegdani *et al.*, 2015a). This was explained by different levels of

fiber support during the cutting process, leading to more efficient shearing of the fiber in the up-milling than in down-milling, as illustrated in Figure 2.10.
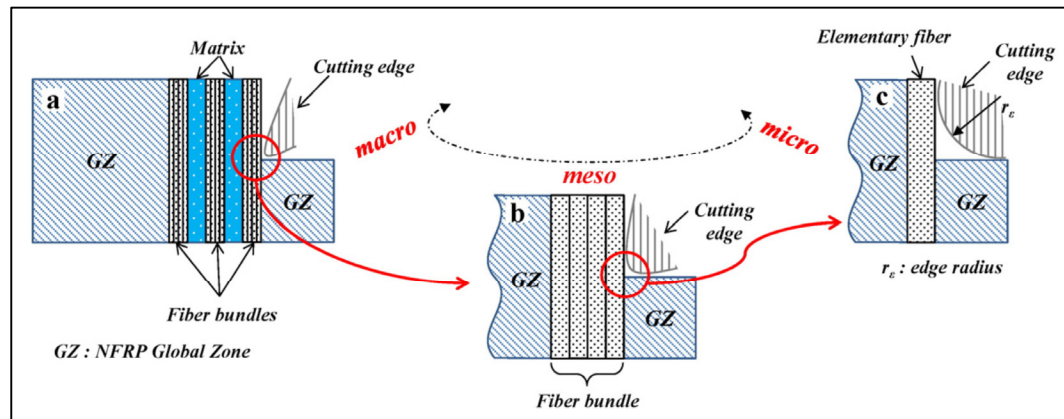
Figure 2.8 Principal cutting scales for NFRP. a) Macroscopic scale. b) Mesoscopic scale. c) Microscopic scale

Taken from Chegdani, Mezghani, & El Mansori, (2015)
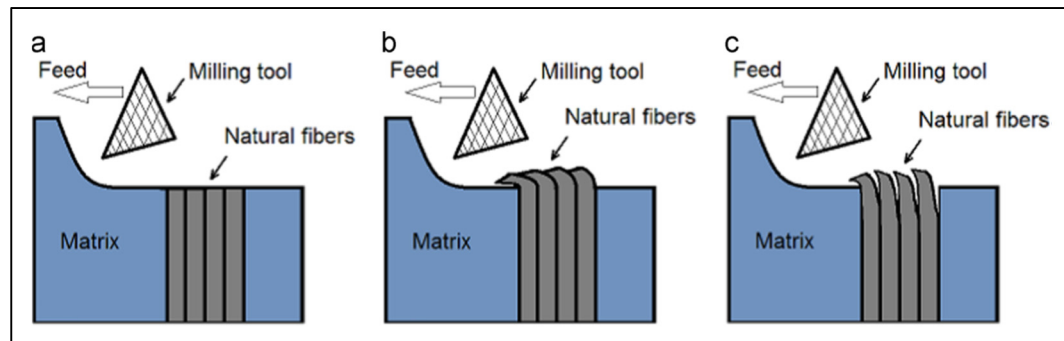
Figure 2.9 NFRP cutting mechanisms: (a) ideal shearing of fibers, (b) real shearing of fibers, and (c) real shearing of fibers showing interfaces

Taken from Chegdani, Mezghani, & El Mansori, et al., (2015)

In a recent study, Chegdani et al. investigated the effects of cutting inserts, cutting speed, and depth-of-cut on the mechanisms of chip formation during orthogonal cutting of UD-flax/PP composite (Chegdani & Mansori, 2018). They observed continuous chips for all cutting conditions that are entirely in contrast with SFRCs. The authors related this to the specific behavior of flax fibers inside the thermoplastic polymer.
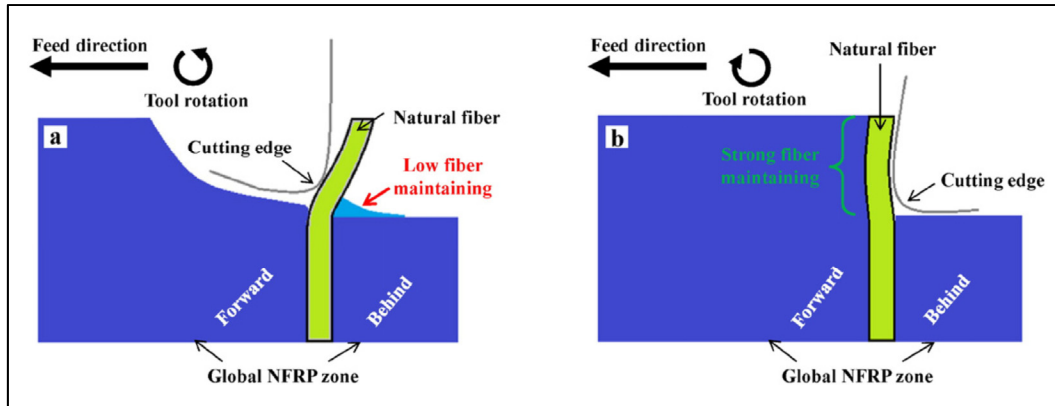
Figure 2.10 Natural fiber behavior during milling operation: a) Down-milling,
and b) Up-milling configurations

Taken from Chegdani, Mezghani, & El Mansori, (2015)

As explained above, the findings of researchers show that not only the cutting mechanisms in NFRCs, and thus their cutting behavior is significantly different from those of SFRCs; they also depend on the NF type. Moreover, understanding the chip formation mechanisms in the trimming of flax/epoxy composites is a basis for studying their machinability and needs to be explored in more detail than existing knowledge about engineered FRCs. Numerical analysis can be efficiently used for this purpose; however, it requires appropriate knowledge of FFRECs, including precise and reliable mechanical characteristics that are missing in the literature.

2.2.3 Cutting force patterns in milling of FRCs

Cutting forces in machining FRCs have been the subject of many studies due to their effect on many machining aspects such as cutting temperature, process stability, machined part quality, cutting tool, and energy consumption. Several researchers investigated the influence of machining parameters (cutting speed and feed rate), fiber orientation, and tool geometry on cutting forces in milling UD-SFRCs through experimental and numerical studies (Arola & Ramulu, 1997; Ghafarizadeh *et al.*, 2016; Sheikh-Ahmad, 2009; Wan *et al.*, 2019; Zaghbani, Chatelain, Berube, Songmene, & Lance, 2012a; Zaghbani, Chatelain, Songmene, Bérubé, & Atarsia, 2012b; Zenia, Ayed, Nouari, & Delamézière, 2015). Likewise, some others studied

the milling process of UD-NFRCs through experimental studies (J. Delahaigue *et al.*, 2017; Karabibene, 2017). In general, these studies showed huge fluctuations in the cutting forces during milling FRCs. The principal cutting force exhibited a higher degree of fluctuations than the trust force. The majority of these studies agree that these forces are mainly influenced by fiber orientation that determines the modes of chip formation. However, Zaghbani et al. obtained different results (Zaghbani *et al.*, 2012a). The machining parameters, such as feed rate, cutting speed, and depth of cut, as well as tool geometry, also affect the cutting forces, albeit to a lower extent (Ghafarizadeh, 2015). Figure 2.11 presents some general profiles of the cutting forces obtained during the milling of carbon fiber-reinforced polymer (CFRP) composites (Sheikh-Ahmad, 2009).

Experiment	(m/min)	a_c (mm)	a_w (mm)	Cutting tool	α_o (deg)	γ_o (deg)	r_n (μm)
a	1.00	0.05	4.00	–	20	7	50
b	0.02	0.10	2.28	K10	10	10	2
c	4.00	0.25	4.00	PCD	10	17	–
d	1.18	0.25	2.20	K20	12	–	–
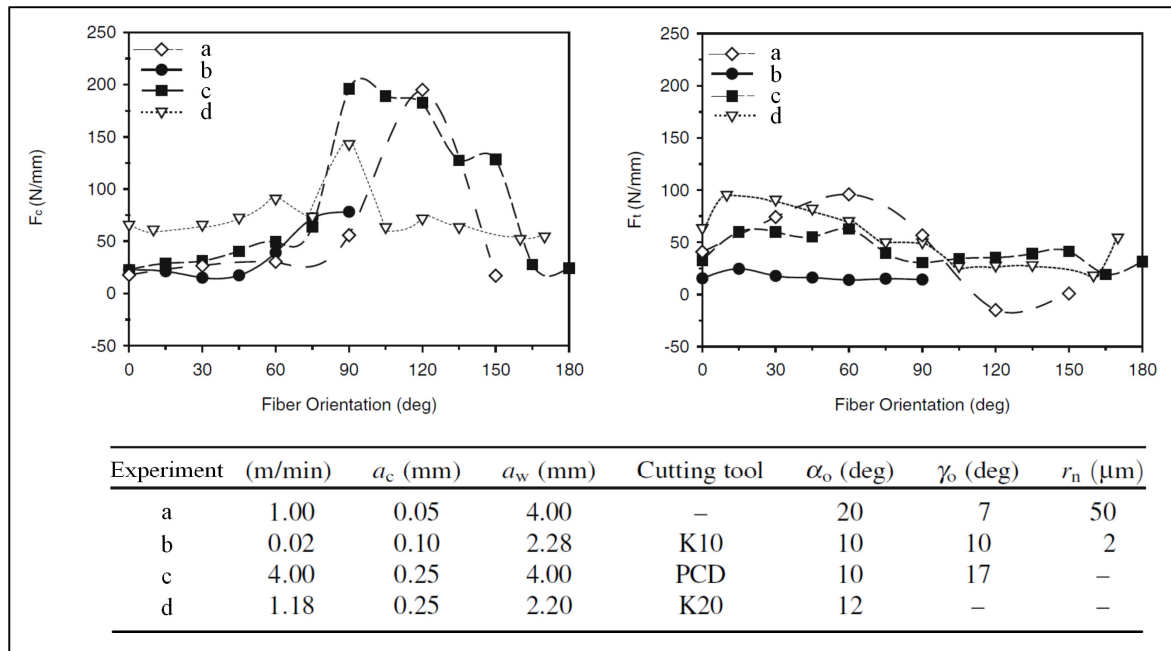
Figure 2.11 Variation of cutting and thrust forces per unit width with fiber orientation for: a- F593/epoxy, b- Torayca T300, c- IM6/epoxy, and d- T300/epoxy

Taken from Sheikh-Ahmad, (2009, p.83)

Delahaigue et al. (2017) conducted an experimental analysis on the milling process of UD and cross-ply flax/epoxy composites and investigated the effect of tool geometry, feed rate, and fiber orientation on the cutting forces. Figure 2.12 shows the results obtained for UD composite in 0° fiber orientation, where Vc1 = 200, Vc2 = 350, Vc3 = 500, Vc4 = 650, Vc5 = 800 m/min;

tool A is a diamond-coated cemented carbide with Ø9.5 mm, 6 flutes, 15 μm edge radius and 10°-helix angle; tool B is a PCD insert with Ø9.5 mm, 2 flutes, 5 μm edge radius and 0°-helix angle. The authors observed that the cutting forces were in general very low, and almost no tool wear occurred, explaining the ease of machining of these composites. Also, the cutting forces were 3–5 times lower for tool B than for tool A, taking the most significant effect from fiber orientation, followed by feed rate and then cutting speed for both tool case. These are interesting and useful information about the milling of UD-FFRECs; nevertheless, the study is confined to the observation of the effects of machining parameter and fiber orientation on the
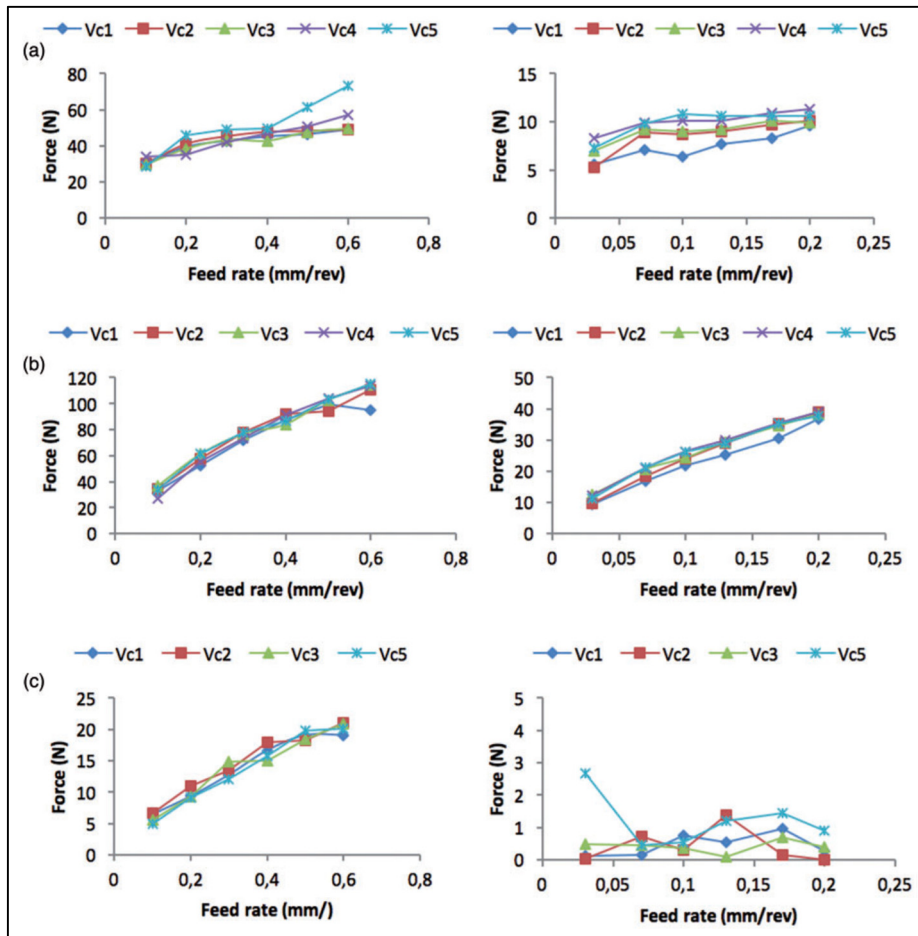
Figure 2.12 Cutting forces for fibers at 0° machined with tool A (left) and tool B (right): (a) feed force, (b) normal force and (c) axial force

Taken from Delahaigue et al. (2017)

cutting forces and surface quality. Hence, it rather covers a basic step of the machinability study, i.e., identifying some issues and their severity when machining UD-flax/epoxy composites.

Karabibene (2017) also performed a similar experimental investigation aiming at optimizing machining parameters for improved machining quality; some typical results are shown in Figure 2.13. In this Figure, Tool #1 is a diamond-coated PCD with Ø9.525 mm, 2 flutes, 0° helix angle, and 5 µm cutting edge radius. Tool #2 has the same diameter, helix angle, and flute numbers but is uncoated, and its cutting-edge radius is 4 µm. The findings of this study are in agreement with those of (J. Delahaigue *et al.*, 2017); fiber orientation is the most, and the cutting speed is the least influential factor in cutting forces. Tool geometry and feed rate have some effects on them. However, the author concluded that the evolution of cutting forces with fiber orientation contradicts those of CFRP found in the literature. Through empirical methods, cutting parameters were optimized to improve the surface roughness and the cutting forces.
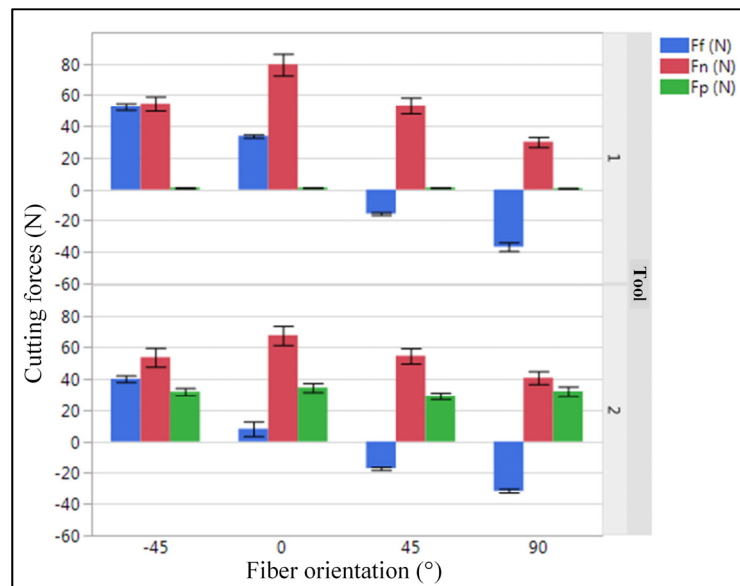
Figure 2.13 Cutting forces vs. fiber orientation and tool
geometry

Taken from Karabibene, (2017, p.145)

Nevertheless, due to the variety of parameters, the optimizations are performed for individual purposes such as minimizing surface roughness, minimizing cutting forces, minimizing delamination, etc. Thus, it has not covered a general multipurpose optimization targeting a superior machining quality. Furthermore, despite the high number of experiments, the validity of the results is limited to the range of selected parameters, i.e., the chosen tool geometries and fiber orientations, cutting speed, and feed rate range. This limitation is a common shortcoming of experimental studies, anyhow, they are always required as a basis for the validation of numerical studies.

Instead, having the mechanical characteristics of the composites, a FEM of the milling process can be developed and validated with minimal experiments covering a wider range of parameters. FE modeling can significantly reduce the number of experiments, and enable more efficient optimization of cutting parameters for improved machining quality. However, due to the high complexity of FRCs, FEM cannot consider all of the macroscopic and microscopic fractures occurring in the composite, including those inside the fibers. Therefore, the results of FEM need to be evaluated by comparing them to experimental results. It means that the experimental and numerical methods as a supplement of each other can help understand and further improve the machinability of FRCs.

2.2.4   Machining-induced defects in milling FRCs

Subsurface damages and machined surface finish are the main features determining the quality of the trimmed edge. Subsurface damages are referred to defects induced by a cutting process, including delamination, microscopic cracks, and fiber/matrix debonding. The irregularities on the surface characterize the surface finish. Figure 2.14 illustrates the different definitions used to describe machined surface geometry (Sheikh-Ahmad, 2009).
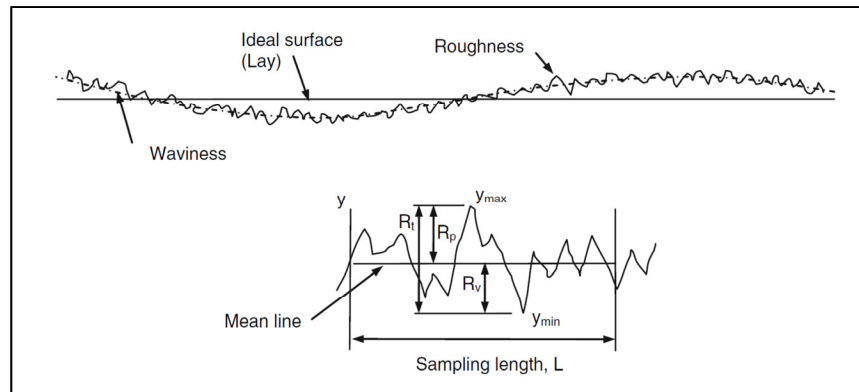
Figure 2.14 Characteristics of machined surface geometry

Taken from Sheikh-Ahmad, (2009, p.55)

Lay defines the macroscopic contour of the surface. Waviness is, in general, the course deviations from an ideal surface, and roughness is the fine surface irregularities, as shown in Figure 2.14. Machined surfaces are usually characterized using surface roughness, which is globally quantified by statistical parameters such as the arithmetic mean value R_a, maximum peak to valley height R_t, maximum peak to mean height R_p, mean to valley height R_v, and ten-point average height R_z, shown in Figure 2.14 (Sheikh-Ahmad, 2009). Machining parameters (feed rate, cutting speed, and depth-of-cut), tool shape, tool wear, and fiber orientation in the composite are the most influencing factors on surface roughness (Sheikh-Ahmad, 2009).

Several previous researchers studied the surface roughness of SFRCs and showed that generally, R_a and R_z increase with feed rate and decreases with cutting speed. Though, the effect of cutting speed is not as significant as feed rate (Chatelain, Zaghbani, & Monier, 2012; Davim & Reis, 2005; Ghafarizadeh, 2015). Also, a smaller depth of cut leads to a decreased extent of subsurface damages (X. Wang & Zhang, 2003).

Nevertheless, as explained earlier, the results obtained for SFRCs may not be applicable to NFRCs, due to their different machining behavior and mechanical properties. On the other hand, limited experimental works have addressed the surface quality in the milling process of flax composites. Some works investigated the effect of cutting parameters, tool shape, and machining direction (fiber orientation in the composite) on the resulting surface roughness of flax/PP composites (Chegdani & Mansori, 2018; Chegdani *et al.*, 2015a; Chegdani *et al.*,

2016). A few others conducted similar studies on UD-FFRECs (Jérémy Delahaigue, 2015; J. Delahaigue *et al.*, 2017; Karabibene, 2017; Karabibene *et al.*, 2018). Chegdani et al. (Chegdani *et al.*, 2015a) studied the influence of coated tools and up-milling/down-milling configuration on the machinability of UD flax/PP composites. They achieved a better surface finish with up-milling. They explained that by efficient fiber cut, as shown in Figure 2.15, which was later confirmed by Delahaigue et al. (J. Delahaigue *et al.*, 2017) for FFRECs. They also concluded that the cutting edge radius has a significant effect on surface finish, and NF shearing is more efficient when the chip thickness is greater than the cutting edge radius.
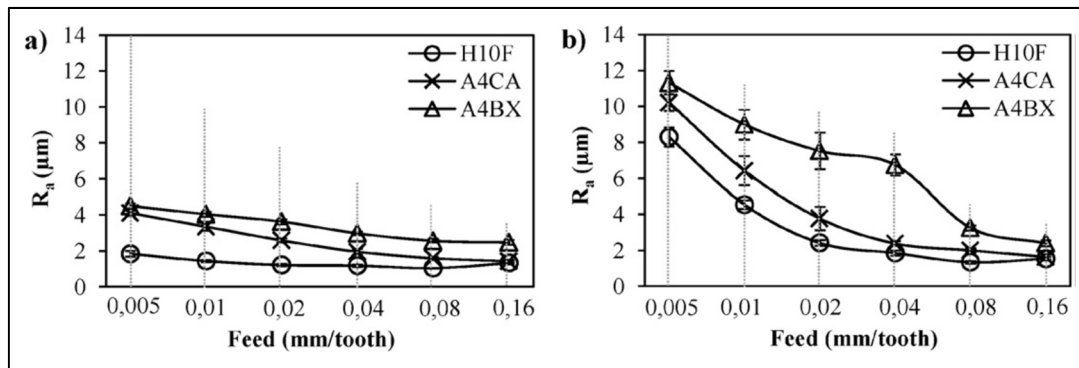
Figure 2.15 Surface roughness after the profile milling of UDF/PP. a) Up-milling
and b) Down-milling configurations
Taken from Chegdani et al. (2015)

Delahaigue et al. (2017) investigated the effects of milling configuration, cutting parameters (cutting speed and feed rate), tool geometry, and fiber orientation on the profile milling of UD and cross-ply FFRECs. Some typical results are shown in Figure 2.16. Tool A and B are the same tools in Figure 2.12. The authors concluded that the feed rate had a greater effect and cutting speed smaller effect on the surface roughness. Also, it was observed that tool A with a 0°-helix angle, provided a cleaner cut with a better surface finish and a lower delamination factor. They recommended down milling to be avoided due to poor surface finish and severe workpiece damage, also found that optimal machining could be achieved with a moderate feed rate and a high cutting speed.
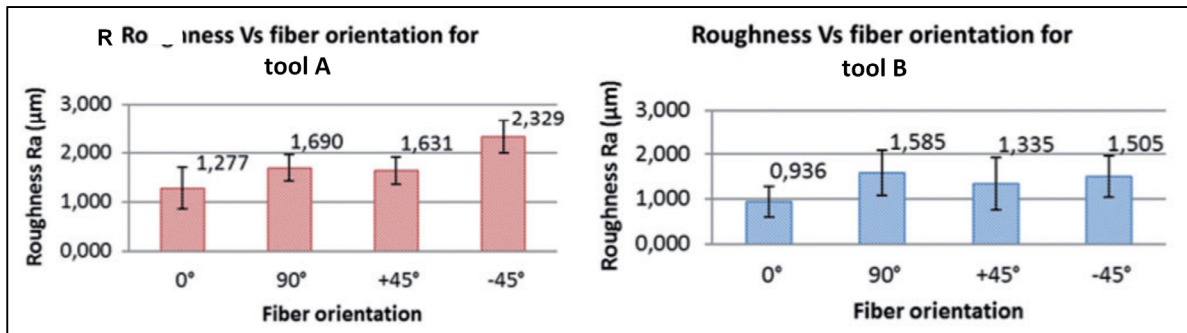
Figure 2.16 Effect of fiber orientation and tool geometry on surface roughness of FFREC

Taken from Delahaigue et al. (2017)

Karabibene (2017) conducted a large number of experiments and performed a similar study. Their finding regarding tool type and fiber orientation on delamination damage is shown in Figure 2.17 (Tools specifications are given above). The comparison between the machining behavior of flax/epoxy and glass/epoxy reveals that the former exhibited better machinability with lower cutting forces and lower delamination damages. In this study, through statistical analysis and empirical modeling, the author tried to optimize the cutting parameters leading to the best machining results. However, similar to cutting forces, this is performed for individual targets and is limited to the range of experiments parameters; thus, comprehensive optimization of cutting conditions leading to overall desired machining quality is missing.

To avoid such time-consuming and costly experiments and benefit the advantages of the numerical simulations, involving FEM in studying the milling process of flax/epoxy composites is inevitable. Nevertheless, the required material knowledge of UD-FFRECs for FE modeling is not available; consequently, FEM has not yet been implemented for investigating the trimming process of these composites.
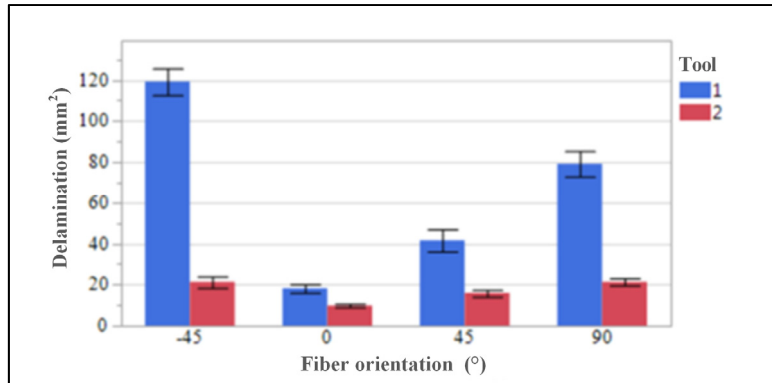
Figure 2.17 Tool and fiber orientation effect on delamination

Taken from Karabibene, (2017, p.105 and p.125)

2.3 Finite element modeling of cutting process of FFREC

During recent decades, special attention is given to DoE and modeling techniques to minimize machining experiments of FRCs. Some researchers used DoE and statistical analysis to study the milling of NFRCs (Harun Azmi *et al.*, 2016; H. Azmi, Haron, Ghani, Suhaily, & Yuzairi, 2018; Babu, Babu, & Gowd, 2013; J. Delahaigue *et al.*, 2017; Mustafa *et al.*, 2019; R Vinayagamoorthy & Rajeswari, 2012). Among these works, very few addressed statistical modeling of the edge trimming process of UD-FFRECs (Karabibene, 2017). In general, two approaches have been used in modeling FRCs machining: (I) analytical and empirical modeling and (II) numerical techniques (Ghafarizadeh, 2015; Wan *et al.*, 2019). Theoretical and empirical models were used to investigate the milling process of FRCs (Zaghbani *et al.*, 2012a; Zaghbani *et al.*, 2012b), nevertheless, employing these models is very complicated due to the high nonlinearity and inhomogeneous nature of these materials. Lack of cutting force coefficients required for tool/workpiece combinations is another obstacle for these techniques (Kevin A Calzada, 2010). Moreover, these approaches do not involve the cutting mechanisms and are not capable of a complete understanding of the machining complexities.

Many researchers have employed numerical techniques such as FEM to study the machining of FRCs (Che, Saxena, Han, Guo, & Ehmann, 2014; Chinmaya R Dandekar & Shin, 2012; Ghafarizadeh *et al.*, 2016). Applying FEM to study machining processes enables predicting

chip formation mechanisms, the cutting forces, and workpiece damages of complex two-phase and anisotopic FRCs (Kevin A Calzada, 2010). Many researchers have successfully implemented FEM to model the cutting processes of SFRCs, including CFRPs (Kevin A. Calzada, Kapoor, DeVor, Samuel, & Srivastava, 2012; Chinmaya R Dandekar & Shin, 2012; Ghafarizadeh *et al.*, 2016; Wan *et al.*, 2019), but there is no finite FE model developed for simulating the trimming process of FFRECs with highly complex microstructure. This is without a doubt crucially required for studying machining complications of FFRECs; nevertheless, a lack of adequate knowledge of these composites prevents any progress in this regard.

2.3.1   Definition of FFREC material in FEM

Three approaches have been implemented to FE modeling of the machining processes of FRCs: a micro-mechanical-based approach, a macro-mechanical approach, and a macro-micro combined approach (Kevin A. Calzada *et al.*, 2012; Shetty, Shahabaz, Sharma, & Divakara Shetty, 2017). The micromechanical-based method models the composite as two individual phases, with their specific material properties. In this approach, the fiber-matrix interface modeling is needed to model failure in the form of phase separation. The macro-mechanical approach models the two-phase composite with an equivalent homogenous material (EHM) with equivalent anisotropic properties; this is done to simplify the machining simulation, but the FE model will be less accurate because do not consider the fiber-matrix interfacial bonding. The macro-micro approach is the combination of the macro-mechanical and micro-mechanical approach.

The micromechanical-based approach has been successfully applied to simulate the orthogonal cutting of FRCs and accurately predict the cutting forces and workpiece damages (Kevin A. Calzada *et al.*, 2012; Chinmaya R. Dandekar & Shin, 2008; Chinmaya R Dandekar & Shin, 2012; Nayak, Bhatnagar, & Mahajan, 2005). However, it is more complicated than the EHM approach. It needs much higher modeling and computation time and more precise details of composite microstructure, including details of reinforcement structure, fiber-matrix interface,

and material properties of fibers and matrix (Chinmaya R Dandekar & Shin, 2012). Because of the complexities of the microstructure-based FE modeling approach, the macro mechanical approach with EHM is preferred for modeling the intricate milling process. Since 1995, the EHM method has been broadly implemented to study the machining process of SFRCs (Chinmaya R Dandekar & Shin, 2012). Some authors reported shortcomings regarding its accuracy in the prediction of the cutting forces (Arola & Ramulu, 1997; Arola, Sultan, & Ramulu, 2002; Santiuste, Soldani, & Miguélez, 2010), though, this deficiency was overcome by combining micro and macro mechanical approaches (Mkaddem, Demirci, & El Mansori, 2008).

NFRCs are more intricate in terms of microstructure compared to SFRCs; thus, the macro mechanical approach is evidently preferable for modeling the trimming process of FFRECs. Therefore, investigation of the composite properties as a whole is required for the FE modeling of the trimming process.

2.3.2   Composite material failure modes and chip formation criteria

Applying an appropriate chip separation criterion is of great importance in the FE formulations of the machining processes where the material undergoes extreme deformation and fails under a complex combination of several fracture mechanisms (Chinmaya R Dandekar & Shin, 2012; Sheikh-Ahmad, 2009). As explained in section 2.2.2, different fracture mechanisms may be responsible for the failure of UD-FRCs in the cutting processes, for instance, fiber micro-buckling, fiber breakage, matrix cracking, delamination (in-plane damage and buckling delamination), or a combination of these factors. An effective failure and damage criterion should be capable of modeling and predicting all these failure modes.

Various fracture mechanisms are illustrated in Figure 2.18 (Anderson & Anderson, 2005). Tensile stresses (Figure 2.18a) can induce matrix cracking, fiber fracture, fiber pullout, and fiber-matrix debonding. For fibers having a lower ultimate strain, the fibers fail before matrix under longitudinal tensile loading. This is true for flax/epoxy composites where flax fiber and

epoxy matrix have respectively 1–4% (Yan *et al.*, 2014) and 1–8.5% (Bensadoun, 2016) failure strains. After a fiber rupture, the matrix transfers the tensile load along the created microcrack from the broken to the neighboring fibers. With increasing tensile load, the number of broken fibers on the crack surface rises gradually. Consequently, the stress concentration developed by the failed fibers causes the failure of adjacent fibers up to the ultimate failure of the composite (Daniel, Ishai, Daniel, & Daniel, 2006). A final tensile failure of FRCs often contains several of these mechanisms.
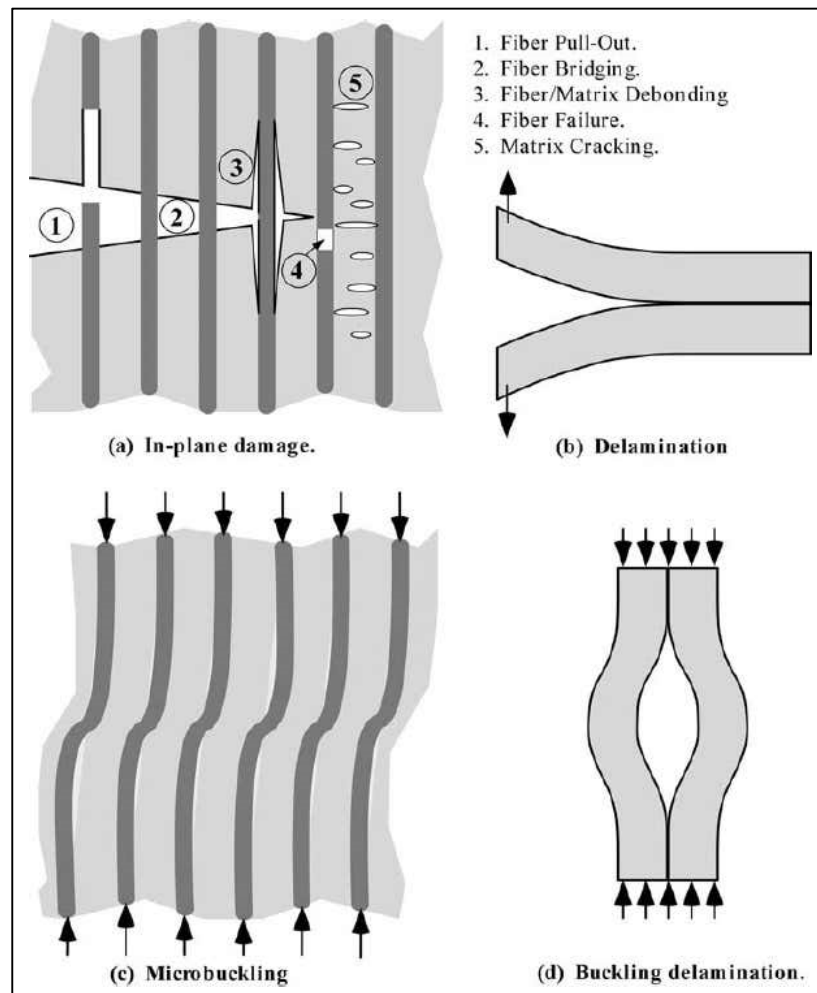
Figure 2.18 Typical damages and fracture mechanics in FRCs

Taken from Anderson, (2005, p273)

Out-of-plane loading can produce Mode I delamination or interlaminar fracture (Figure 2.18b). Delamination can occur in Mode II, under shear stress between the plies. Under dynamic loads, interlaminar damages may grow to a critical extent and cause laminate failure. Longitudinal compression loading can lead to microbuckling of the fibers and the creation of kink bands in the composite (Figure 2.18c). The relatively soft polymer matrix partially supports the fibers; thus, they are unstable in compression, yet, buckling does not necessarily cause immediate failure. Compressive loading can also create macro-scale delamination buckling in the composite (Figure 2.18d), particularly in the presence of a preexisting delaminated region (Anderson & Anderson, 2005).

It should be noted that these general failure modes are recognized for SFRCs. The complex microstructure and different distribution patterns of NFs, as well as the poor fiber/matrix interface in NFRCs, may cause other failure modes such as NF bundle failure. However, Habibi et al. have mentioned similar failure modes for FFRCs in tensile loading (Habibi, Laperrière, Lebrun, & Toubal, 2017a).

Several theoretical criteria have been developed to determine the failure of composite materials for instance, (I) maximum stress theory, (II) maximum strain theory, (III) Energy-based interaction theory (Tsai-Hill), (IV) Tsai-Wu failure theory, (V) Hoffman failure theory, and (VI) Hashin failure theory (Daniel *et al.*, 2006). According to maximum stress theory, the composite laminate failure occurs when one of the stress components along one of the principal material axes reaches the corresponding strength in that direction. Lasri et al. (Lasri *et al.*, 2009) applied it to model the chip separation in UD-GFRPs. They concluded that using this failure criterion, fiber-matrix debonding was the first damage initiated ahead of the cutting tool edge and progressed during the chip formation process. Then, matrix failure began and gradually developed in the close proximity of the tooltip. Fiber fracture was the last failure mechanism activated during chip separation.

Hill modified the von Mises criterion (applied to predict isotropic materials failure by the Von Mises yield criterion) for ductile and anisotropic materials (Daniel *et al.*, 2006). Tsai-Hill or maximum work failure criterion, which has been developed based on Hill criterion, has been

used in several studies for simulation of CFRP machining (Arola & Ramulu, 1997; Mahdi & Zhang, 2001; Mkaddem *et al.*, 2008; Mkaddem & El Mansori, 2009; Nayak *et al.*, 2005; Rao, Mahajan, & Bhatnagar, 2008). Rao et al. (Rao, Mahajan et Bhatnagar, 2008) used this criterion in modeling the orthogonal cutting of CFRP. Their model accurately predicted the cutting forces and chip formation. The main shortage of the Tsai-Hill failure criterion is that it is not able to differentiate tensile and compressive strengths. Tsai-Wu and Hoffman criteria are improved versions of the Tsai-Hill criterion to resolve this drawback (Daniel *et al.*, 2006; Schellekens & de Borst, 1990). Mkaddem et al. (Mkaddem *et al.*, 2008) investigated the orthogonal cutting of composites by following a micro-macro mechanical approach and using the Tsai-Hill criterion. They found that the chip size, chip shape, and the cutting forces were mainly dependent on the fiber orientation.

Hashin established a three-dimensional (3D) failure criterion for UD-FRCs that separately models four distinct failure modes, namely, fiber tensile failure, fiber compressive failure, matrix tensile failure (matrix cracking), and matrix compressive failure (matrix crushing) (Hashin, 1980). Hashin's failure criterion has been widely used to investigate FRP cutting processes (Chakrapani & Sekar, 2018; Ghafarizadeh *et al.*, 2016; Y.-L. He, Davim, & Xue, 2018; Lasri *et al.*, 2009; Siddharth, Anand, Vijay Sekar, & Suresh Kumar, 2015). For example, Lasri et al. (Lasri *et al.*, 2009) investigated the orthogonal cutting GFRP composites implementing Hashin, Maximum stress, and Hoffman failure criteria. Their results showed that the principal cutting forces predicted using the Hashin criterion were closer to the experimental results than the other two criteria. However, similar to other macro-mechanical models, the simulated thrust forces for all failure criteria were much lower than the experimental ones. They also found that chip formation was significantly dependent on fiber orientation. All failure criteria predicted the first damage initiation in the vicinity of the cutting tool edge that propagated parallel and perpendicular to the direction of the fibers within the composite workpiece.

Despite the extensive application of FEM to model the behavior of SFRCs, including their cutting process, it has been used to model NFRCs in relatively limited applications, and there

is no work modeling the trimming process of UD-FRECs (Bavan & Kumar, 2013; V. Prasad, Venkatachalam, Rathi, & Rajakumar, 2014; Ravandi, Teo, Yong, & Tay, 2018; Xiong *et al.*, 2018). According to a recent review (Xiong *et al.*, 2018), FEM is mainly used for modeling thermal properties, mechanical properties, and fiber-matrix interface damage of NFRCs. Further extension of the application of FEM to simulate the cutting process of FFRECs is even not feasible and practical without providing the missing appropriate material properties of these composites.

2.4 Material properties of FFRECs

Rapidly increasing commercial and engineering applications of FFRCs necessitates the implementation of advanced computational engineering design and analysis techniques such as finite element modeling. These techniques are mandatory to efficiently investigate their behavior when undergoing complex conditions such as cutting processes and to optimally design and develop components made of these composites. These methods are developed based on some theoretical formulations and numerical methods that use material characteristics to simulate the behavior of the material under different loading conditions. Several researchers have studied FFRCs for different purposes and have published some of their material properties, for instance, their stiffness and strength in tensile, compressive, and flexural loading (Harriëtte L Bos, 2004; H. L. Bos, Molenveld, Teunissen, van Wingerde, & van Delft, 2004; El Sawi, Bougherara, Zitoune, & Fawaz, 2014; Liang *et al.*, 2015; Muralidhar, 2013b; Ramesh, 2019; Sanjay *et al.*, 2018).

However, due to the large variety of the reinforcement contents and architectures, processing methods, and test procedures used in these studies, the results are not consistent and cannot be considered belonging to a unique composite. Thus, they are not accurate enough for numerical analysis applications of a specific composite. Besides, many other material properties and knowledge of UD-FFRCs for FE analysis have never been evaluated and are absent. These issues prevent FE modeling of complex phenomena such as the cutting processes, for which failure criteria requiring a set of accurate material properties are required.

Therefore, a comprehensive characterization of UD-FFRECs with unique specifications is an actual need for research. However, for most of the properties, no specialized, standardized test method, taking into account the complexity of natural fibers, is available. Moreover, due to their complex microstructure, anisotropy, and heterogeneity, more specific properties need to be evaluated in comparison to isotropic materials.

In general, material properties of composites can be classified into (a) physical properties such as density and thermal diffusivity/conductivity, (b) mechanical properties, including all properties determining their stiffness and strength under various modes of loading such as tension, compression, shear and flexion, and (c) fracture properties characterizing their resistance to crack growth under different loading modes and in different directions inside the laminate, denoted as fracture energy or fracture toughness, for instance, interlaminar and translaminar fracture energies.

A review of the reported literature works, particularly for UD-FFRCs, is given in the following sections for each category of these properties. More specific literature reviews are presented in CHAPTER 3 to CHAPTER 5 to raise the important aspects described in each chapter.

2.4.1 Physical properties

This study includes measurement of density, specific heat capacity, and thermal diffusivity/thermal conductivity as physical properties. As a fundamental physical property of composites, density enters many engineering designs and numerical analysis calculations, and its value is an influential factor in the results. Specific heat capacity and thermal diffusivity are required for processing IRT experiments in the continuation of this study.

Although the density measurement of flax fibers has been studied in few works (Amiri *et al.*, 2017; Le Gall, Davies, Martin, & Baley, 2018), the sensitivity of FFRECs to different density measurement methods has not been investigated yet. The literature data are scattered, ranging

from 1.117 to 1.32 g/cm^3 (Liang, Gning, & Guillaumat, 2014; Mahmoudi *et al.*, 2019; Yan *et al.*, 2014). Besides, because the density value depends on factors like fiber volume fraction, fabrication process, measurement method, and the condition of fibers in the composite, it is often not possible to use values published in other works. There are no reported values for specific heat capacity and thermal diffusivity/thermal conductivity of these composites in the literature. Accordingly, it is imperative to precisely measure the density value to develop efficient numerical models for the machining process of the FFREC. This part of the study was presented in a conference paper (Saadati, Chatelain, Lebrun, & Beauchamp, 2019). Also, specific heat capacity and thermal conductivity are required for IRT experiments. Density measurement with different methods, along with a discussion of their precision, is the subject of CHAPTER 3 of this thesis.

2.4.2   Mechanical properties

The elastic properties and strength of FRCs under tension, compression, shear, and flexural loadings are required in FE modeling for engineering design and research purposes. CHAPTER 3 presents the evaluation of these properties and the failure behavior of UD-FFRECs. The laminate was examined under corresponding loading modes in its longitudinal and transverse directions. This is done in view of the simulation of their cutting mechanisms in the edge trimming processes. A concise literature review is given below, and a comprehensive report is presented in CHAPTER 3.

Several authors have studied the mechanical properties of FFRCs and published some values for the investigated properties, but the works using UD reinforcements are reviewed here. Oksman measured the absolute and specific tensile strength and stiffness properties of UD high-quality ArcticFlax FFREC manufactured by the Resin Transfer Molding (RTM) process (Oksman, 2001). Then, they compared them to those of GFRP, traditionally retted UD-FFREC and of pure epoxy. The authors found out that the ArcticFlax FRECs at $V_f = 0.47$ had stiffness and tensile strength of 39 GPa and 280 MPa, respectively, which are higher than those of traditional UD-FFREC and were even stiffer than GFRP with $V_f = 0.48$. They found RTM a

suitable process for manufacturing high-quality NFRCs. Romhany et al. studied the tensile behavior of UD and cross-ply flax fiber-reinforced starch composites (Romhány, Karger-Kocsis, & Czigány, 2003). They observed that for 40 wt.% UD reinforcement content, the tensile strength of the composite increased by three times and the tensile modulus by several orders of magnitude relative to that of the pure starch matrix.

Investigating the effects of processing method and chemical treatment of the fibers on the flexural properties of UD-FFRECs, Van de Weyenberg et al. tested an untreated UD flax/epoxy composite with V_f = 0.40 (Van de Weyenberg *et al.*, 2003). They reported values of 133 and 4.5 MPa for the tensile strength, as well as 28 and 2.7 GPa for the elastic modulus of the composite, respectively, in longitudinal and transverse directions. Also, flexural strengths of 218 and 8 MPa along with flexural moduli of 17.7 and 0.36 GPa was measured respectively, in longitudinal and transverse directions. Charlet et al. compared hand lay-up impregnation and compression molding processing methods for processing UD flax/unsaturated polyester composite (Karine Charlet, Jernot, Gomina, Bizet, & Bréard, 2010). The authors concluded that the latter allows producing composites with higher V_f, but fibers may be damaged. Comparing the properties of fibers and matrix to the properties of composites, they interpreted the similarity of the tensile curves of the composites and elementary fibers as results suggesting a proper fiber-matrix adhesion in the composites. Also, the authors used the mechanical properties of the composite to estimate the properties of reinforcement elements, i.e., flax bundles and the reinforcement efficiency. Their study shows that a maximum of 30% of the fibers contained in the composite would be efficiently reinforcing it when processing with hand lay-up impregnation method and a maximum of 25% when processing with the compression molding method. They found the maximum V_f to be theoretically limited to 41% for the applied compression level. El Sawi et al. studied the influence of manufacturing processes (compression molding and autoclave) and water absorption on the mechanical properties of UD-FFRECs (El Sawi *et al.*, 2014). Their composites, composed of 50 wt% flax fibers, had a 25 GPa longitudinal modulus independent of the production process, and tensile strength of 275 and 307 MPa for 110°C and 150°C curing temperature respectively. They proposed the

compression molding as a competitive process to Autoclave molding, leading to less than 1% small void content.

Using a hot compression molding process, Avril et al. fabricated and evaluated UD fabric/epoxy composites with a 50 wt% fiber content and tested them for tensile properties. (Avril, Bailly, Njuguna, Nassiopoulos, & De Larminat, 2012). They published values of 223 MPa, 22.3 GPa, and 1.24% respectively for tensile strength, Young's modulus, and ultimate strain of the composite. Also, the authors concluded that it meets vehicle design mechanical requirements and is suitable for structural applications. Zhu et al. studied different layups of flax/tannin-based bio-degradable composites to be used in superlight electric car bodies (Jinchun Zhu, Abhyankar, Nassiopoulos, & Njuguna, 2012). They found that the UD laminate offered the highest tensile properties of 150 MPa and 9.6 GPa, respectively, for tensile strength and modulus.

Some researchers have investigated the effect of adding some other types of reinforcing agents on the mechanical properties of UD-FFRECS. Some of the mechanical properties of the original composites are also published in these works. Couture et al. measured the tensile, flexural, and impact properties of UD-flax (roving)/polylactic acid (PLA) laminates and compared them to those determined for flax-paper/PLA composites (Couture, Lebrun, & Laperrière, 2016). For UD-flax/PLA composite with V_f= 0.44, they measured tensile strength, tensile modulus, flexural strength, and flexural modulus of 339 MPa, 20 GPa, 363 MPa, and 26 GPa, respectively. Due to the limited dimensions of their molded composite laminates, they had to follow ASTM D638 to determine tensile properties for comparison purposes. However, this standard recommends using ASTM D3039 for plastics reinforced with oriented continuous high-modulus (>20 GPa) fibers. Therefore, D3039 could be better for evaluating the material properties of flax fibers that have elastic modulus between 47 to 64.4 GPa (Lefeuvre, Bourmaud, Lebrun, Morvan, & Baley, 2013). They also concluded that the specific tensile properties of both PLA composites were similar to those of GFRP. Habibi et al. studied the effects of combining flax-mat with UD-flax yarns on the biaxial mechanical properties and failure behavior of the UD-flax/epoxy composites (Habibi *et al.*, 2017a). In this work, they

used acoustic emission (AE) to study the material damage behavior and tested the composites in the longitudinal and transverse directions for their tensile and flexural properties. For the UD-flax yarns/epoxy composites with V_f = 0.40, the authors published the values of 30.2 GPa, 329 MPa, 22.1 GPa, and 287.5 MPa respectively for tensile modulus, tensile strength, flexural modulus, the flexural strength of the laminate in the longitudinal direction. Also, values of 3.1 GPA, 36.5 MPa, 1.3 GPa, and 44.6 MPa are reported for the corresponding values in the transverse direction. Considering that flax yarns have been used in this work, the results may be different from those of UD non-twisted fibers. Mbakop et al. studied the effect of compaction parameters on tensile and flexural properties of UD-flax yarns combined with short flax fibers mat; however, they didn't test any UD-flax laminate (Mbakop, Lebrun, & Brouillette, 2019). The authors concluded that the hot and wet compaction did not change the permeability of the fibers. They observed that using compacted reinforcements in the composite increased the tensile strength but did not affect the tensile stiffness. Also, flexural strength and modulus were substantially improved.

Overall, in these studies, the mechanical properties were determined mostly for comparison purposes, aiming at investigating the effect of different factors on them or comparing them to those of other composites. Thus, none of the above-mentioned literature works was clearly dedicated to evaluating the mechanical properties of FFREC in view of reusing the data as material properties for numerical modeling purposes, etc. Based on our survey, there is no literature work reporting a complete set of material properties for a well-defined FFRC. In response to the increasing demand for an extended set of properties for this material and considering the large quantity of mechanical and physical properties required for modeling, it was considered necessary to develop a set of precise properties complete enough to fulfill the modeling requirements for a unique type of composite in terms of fiber type, fiber content, molding process, etc.

2.4.3   Fracture properties

In addition to strength and stiffness, fracture toughness is an essential property of FRCs for most engineering applications (Haldar, Herráez, Naya, González, & Lopes, 2019; Hughes, Hill, & Hague, 2002; Q. Liu & Hughes, 2008). Fracture toughness is a fundamental material property and can be determined based on either the Stress Intensity Factor (K_C) or the Critical Strain Energy Release Rate (G_C) of the material. The former is known as fracture toughness, and the latter is commonly named Fracture Energy. They are, respectively, a measure of the stress intensity level and energy required for an increment of the crack growth (Anderson, 2017). For the isotropic, homogeneous, and relatively brittle metallic materials, fracture toughness depends on the energy dissipation at the crack tip and can be characterized by K_C. However, for FRCs, the stress field in the vicinity of the crack tip is more complicated, and fracture toughness is affected by the result of energy losses of different failure mechanisms such as matrix cracking, fiber fracture, fiber pullout, and fiber-matrix debonding (M. S. Prasad, Venkatesha, & Jayaraju, 2011; Y. Zhu, 2009). Therefore, G_C is commonly used for the study of fracture toughness in FRC laminates for different failure modes (ASTM, 2013a, 2019a, 2019b; Nasuha, Azmi, & Lih, 2017; M. S. Prasad *et al.*, 2011). By comparing the energy release rate (G) for a loading case to the G_C of the material, the capability of the material to resist crack extension can be assessed.

Nowadays, the engineering desire for an optimized, efficient, sustainable, cost-effective, and damage tolerant product design in conjunction with the ever-growing research works on FFRECs necessitate characterizing the fracture toughness of these composites. FE modeling of cutting processes, where the material failure criteria are applied to model several failure modes, is one of the research areas that critically need fracture properties of the FFRECs. Therefore, to better exploit the potential of FFRCs, their fracture behavior in different fracture modes needs to be investigated. At least four fracture energies are required to evaluate composite failure using commonly used criteria, such as Hashin's failure criteria. Two of them characterize composite fracture in interlaminar (delamination) fracture, i.e., Mode I (G_{IC}) and Mode II (G_{IIC}) fracture energies. They respectively represent the equivalent laminate failure in

transverse tension and compression loading which is dominantly a matrix mode failure. Two others are the fracture toughness in translaminar mode, perpendicular to fibers, in tension (G_C^{Ten}) and compression (G_C^{Comp}).

2.4.3.1 Interlaminar fracture (delamination) toughness

One of the commonly observed and major damage phenomena in laminated composites is the separation of two adjacent laminae (plies), which is known as the interlaminar failure or delamination damage. It is one of the chip formation mechanisms and the most crucial workpiece damage occurring during machining operations of laminated composites (Almansour, Dhakal, & Zhang, 2017a; Almansour *et al.*, 2018; Nassar *et al.*, 2017). This failure mode is the primary challenge for the laminated FRCs that generally affects the in-service functionality of the component by reducing its overall stiffness and load-bearing capacity and subsequently leading to the failure of the entire component (Chen, Li, & Yu, 2014; Nasuha *et al.*, 2017; Tay, 2003).

In fracture mechanics, the interlaminar failure, according to the relative displacement of crack surfaces, has been classified into three fracture modes: opening or tensile mode (Mode I), in-plane shear or sliding mode (Mode II), and out-of-plane shear or tearing mode (Mode III) (Anderson, 2017; Tay, 2003). Figure 2.19 illustrates the crack propagation caused by different modes of failure and the corresponding loadings acting on the cracks. Delamination can initiate and propagate due to any of these fracture modes or any combinations of them (mixed modes) (Anderson, 2017).
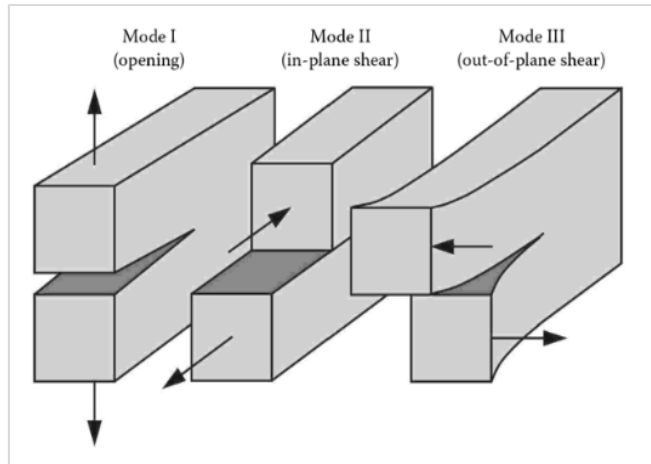
Figure 2.19 Fracture modes and applied loadings
Taken from Anderson (2017, p.45)

Interlaminar fracture toughness (IFT), as a primary property of a material, is required for engineering design purposes as well as numerical analysis methods such as the FEM. The interlaminar fracture of the SFRCs under different modes of failure has been extensively investigated, and its state of the art has been comprehensively reviewed by many authors (Nasuha *et al.*, 2017; Ooi, Tan, & Azmi, 2019; M. S. Prasad *et al.*, 2011; Tay, 2003; Y. Zhu, 2009). However, in the literature, limited works have been documented addressing the interlaminar fracture behavior of the laminated NFRCs, particularly FFRECs that show better toughness (Bensadoun, Verpoest, & Van Vuure, 2017). Some of the works addressing FFRCs with UD and fabric reinforcement structures are reviewed here; a more general and comprehensive review for NFRCs is presented in CHAPTER 4.

Zhang et al. (Zhang, Li, Ma, & Yu, 2013) investigated the properties of a hybrid phenolic resin composite reinforced with UD-fabric (twisted flax yarns) of flax/glass fibers and measured G_{IC} = 550 J/m^2 for flax composite that increased by hybridization to 560 J/m^2 for [(flax/ glass)$_n$]$_s$ composite. Their study shows that adding off-center plies of different fibers to the laminate will change the IFT, although the delamination is happening between the same type of composite plies. Chen et al. (Chen *et al.*, 2014) investigated the potential of carbon nanotube buckypaper interleaf for improving the IFT of flax-fabric/phenolic resin composites with $V_f \approx$

0.73. They followed ASTM D5528 and tested some partially and fully interleaved laminates at the mid-plane as well as laminates without interleaf for IFT. Compared to the initiation G_{IC} and propagation G_{IC} of respectively ≈4.4 and ≈5.6 kJ/m² for the original composite, these values increase by 26% and 29% for the partially interleaved composite, and 22% and 51% for the fully interleaved composite. They believed that these increases are associated with the fibrillations in the interleaved laminates.

Trying to enhance the IFT of flax-fabric/epoxy composite of V_f = 0.60, Li et al. (Y. Li, Wang, & Ma, 2015) interleaved them at the mid-plane with chopped flax yarns of different lengths and content and followed ASTM D5528 to evaluate their G_{IC}. The authors observed a 4% to 31% improvement in the propagation G_{IC}, with the maximum increase for the moderate length and content of the chopped yarns, compared to that of the original composite, G_{IC} =1.40 kJ/m². It should be noted that they have used the Modified Compliance Calibration method but have stated that they used the Modified Beam Theory (MBT). It will be shown in CHAPTER 4 that using different data reduction methods may lead to different results.

Ravandi et al. conducted some experimental investigations, and FE analysis to study and predict the effects of through-the-thickness stitching and reinforcement architecture on the G_{IC} of UD (V_f ≈ 0.31) and woven fabric (V_f ≈ 0.40) FFRECs (Ravandi, Teo, Tran, Yong, & Tay, 2016a; Ravandi *et al.*, 2016b; Ravandi *et al.*, 2018). The authors tested double cantilever beams (DCBs), according to ASTM D5528, to determine the G_{IC} of the FFRECs as well as UD-glass/epoxy (V_f = 0.60) composites. They observed that the average G_{IC} of the UD-glass/epoxy was less than half of that of unstitched UD-FFRECs (G_{IC} ≈ 1.3 kJ/m²). Also, their findings showed that the average G_{IC} value of the UD-FFREC was three times lower than that of woven-FFRECs (G_{IC} ≈ 3.2 kJ/m²). In general, stitching with flax yarns induced continuous improvement in IFT of the laminates, increasing with the stitch density to a maximum of 21% for the highest investigated level of the stitch density. Besides, they reported that their FEM results agreed with the experimental ones giving the G_{IC} values of 0.771 and 1.25 kJ/m², respectively, for the crack initiation and propagation of UD-FFRECs as well as 0.671 kJ/m² for the G_{IC} value of glass/epoxy composite.

Bensadoun et al. investigated the effect of the reinforcement architectures on the G_{IC} and G_{IIC} of flax/epoxy composites with $V_f = 0.40$ (Bensadoun *et al.*, 2017). They tested FFRECs reinforced with seven different fiber configurations; i.e., a plain weave, a twisted-yarn-fabric cross-ply and an untwisted-fiber cross-ply architecture. The two twill weave laminates had low and high twist, and the cross-ply laminates were tested in both 0°/90° directions. In terms of delamination fracture, their composites with untwisted-fiber cross-ply reinforcement denoted as UD [90,0], has a 0°/0° ply interface at the mid-plane of the laminate and is the closest one to the UD-FFRECs assessed in the current study. They reported initiation G_{IC} values between 457 J/m^2 for plain woven and 777 J/m^2 for twisted-yarn-fabric cross-ply composite when tested in [90,0] direction, as well as $G_{IC} = 496$ J/m^2 for UD [90,0] tests. In comparison, the propagation values of G_{IC} vary from 663 J/m^2 for UD [90,0] to 1597 J/m^2 for the low-twist twill-woven composites. Besides, they obtained G_{IIC} values between 728 J/m^2 for UD [90,0] and 1872 J/m^2 for plain weave laminates. The authors named the cross-ply twisted-yarn-fabric and the UD-untwisted-fiber architecture respectively "quasi-UD" and "UD" architecture, whereas, their interlaminar fracture behavior could be different with those of UD laminates, where all plies lay in one direction. Therefore, the results may not coincide exactly with the results of UD laminates.

Almansour et al. investigated the effect of hybridization and water absorption on G_{IC} (Almansour *et al.*, 2017a) and G_{IIC} (Almansour *et al.*, 2018; Almansour, Dhakal, Zhang, & Ghasemnejad, 2017b) of flax/vinyl-ester (VE) composites. They tested woven flax reinforced VE composites, as well as woven flax/basalt reinforced VE hybrid composites in [±45°] arrangement. In their hybrid composites, the basalt plies replaced the top and bottom (surface) plies of the flax laminates. The former had a $V_f = 0.31$, and the later had an overall $V_f = 0.33$. In the hybrid composites, basalt plies were the surface plies of the laminates. Their DCB test results showed that upon immersion in water, the initiation and propagation G_{IC} of the flax/vinyl-ester, as well as the initiation G_{IC} of flax/basalt hybrid composites, decreased by 27%, 10%, and 23%, respectively. In contrast, the propagation G_{IC} of flax/basalt hybrid composites increased by 15%. They obtained average initiation and propagation G_{IC} values of

3870 and 12093 J/m^2 respectively for the flax composites in dry conditions. Likewise, for flax-basalt hybrid composites tested in similar conditions, the authors published values of 4431 and 9738 J/m^2, respectively, for average initiation and propagation G_{IC} values. The concerning issue in this study is that the crack did not propagate in the mid-plane of the laminate and deviated from that by crossing the layers; it thus cannot be considered a pure interlaminar failure. Along with the high G_{IC} value of VE (410 J/m^2 compared to 69–150 J/m^2 of epoxy (Bensadoun et al., 2017)), this might be another reason for the higher measured values of IFT. An increase in initiation G_{IC} was observed for the hybrid composites; however, their propagation G_{IC} values were lower. The latter can be associated with the ever-increasing R-curves of hybrid composites, where the final crack was shorter compared to those of flax composites. In hybrid composites, the crack deviated from the midplane and ended in a shorter length, thus resulted in lower development of R-curves and smaller growth in the propagation G_{IC}. Though, the propagation G_{IC} of hybrid composites at their final crack length was higher than that of flax composite at the crack length equal to the final crack length of hybrid composites. In terms of G_{IIC} values, the authors observed that hybridization by basalt fibers improved the initiation G_{IIC} value of flax composite by 58%. Also, moisture absorption improved the initiation G_{IIC} of flax composite by 29% and that of hybrid composite by 20%. The authors attributed it to improved matrix ductility. Their published average initiation G_{IIC} values for the dry flax and flax/basalt hybrid composites are 253 J/m^2, and 400 J/m^2, respectively.

Nevertheless, it should be noticed that the basalt plies are located at the surface of the laminate, while the IFT is being evaluated between flax plies at the mid-plane. Also, some researchers measuring the IFT of flax composites bonded tabs to the surface of DCB and ENF test specimens to avoid large deformations and specimens arm failure (Bensadoun et al., 2017; Ravandi et al., 2016a, 2016b; Ravandi et al., 2018; Vo Hong et al., 2018). Here, the basalt layers have the same function that those stiffeners have. Accordingly, the findings of these studies show that the stiffeners affect the values of both Mode I and Mode II IFT. This result contradicts the assumption of the researchers using stiffeners. As a result, stiffening the arms of the DCB and ENF specimens will affect the IFT values and is not a proper solution. Instead,

increasing the thickness or changing the initial crack length to improve the specimen stiffness seems desirable, as recommended by the corresponding ASTM standards (ASTM, 2013a, 2019a).

Vo Hong et al. investigated the influences of some processing conditions, fiber surface treatment, and matrix plasticization on IFT of UD-flax fiber-reinforced gliadin composites with V_f = 0.40 (Vo Hong *et al.*, 2018). Testing the original composite DCB specimens according to ISO 15024 standard, the authors reported G_{IC} = 50 to 100 J/m^2 and G_{IC} = 450 to 550 J/m^2, respectively, for crack initiation and propagation measurements. Their findings show that the optimum value of IFT, $G_{IC} \approx 1000$ J/m^2, was obtained with a combination of fiber treatment, adding glycerol to the matrix, and a medium cooling rate. Rajendran et al. investigated the behavior of twill-weave flax/epoxy composites in Mode I and Mode II delamination (Rajendran, Johar, Hassan, & Wong, 2018). The V_f of the composites is not mentioned in this work. The authors tested DCB and ENF specimens and, following the experimental calibration method, calculated a G_{IC} = 485 J/m^2 and G_{IIC} = 962 J/m^2 for the composite. In another work, they published their findings of the Mode I, Mode II, and Mixed-mode I/II interlaminar fracture toughness of the same composite with $V_f \approx 0.44$ (Rajendran, Johar, Low, Abu Hassan, & Wong, 2019). In this work, they followed ASTM D5528 and D7905 standards and tested standardized DCB and ENF specimens to determine the IFT in Mode I and Mode II, respectively. However, they tested not standardized single-leg-bending (SLB) specimens to measure the Mixed-mode I/II fracture toughness ($G_{(I/II)C}$). In this report, they published values of G_{IC} = 363 J/m^2, G_{IIC} = 962 J/m^2 and $G_{(I/II)C}$ = 649 J/m^2 for a $G_{II}/(G_I + G_{II})$ = 0.43. Although the V_f of the composites is not mentioned in the previous work, by comparing the presented graphs the composites seem the same in both works. Nevertheless, comparing the G_{IC} value in their two different reports, a discrepancy can be seen in G_{IC} value for the same material. This can be associated with the two different data reduction methods used in these works.

In a recent study, Saidane et al. used the AE method to investigate the Mode I fracture toughness of flax, glass, and hybrid flax/glass woven-fiber/epoxy composites (Saidane, Scida,

Pac, & Ayad, 2019). Their flax and hybrid laminates had a $V_f = 40\%$, and GFRP had a $V_f = 50\%$, though, for comparison purposes, all laminates should have the same V_f. They conducted DCB tests according to ASTM D5528 standard but used AE to detect the onset of delamination and the corresponding critical load to calculate G_{IC}. The initiation G_{IC} values of 1079 J/m^2, 945 J/m^{2,} and 923 J/m^2 were determined respectively for flax, hybrid flax/glass, and glass composites. Nevertheless, the method used in this work to detect the delamination initiation and the corresponding critical load used in the calculation of G_{IC} influences the obtained values; thus, this fact should be considered when using the results for comparison purposes. The interesting point in this study is that the propagation G_{IC} value of flax composites (R-curve) continuously increased with delamination length. This contradicts the findings of previously cited studies, including those of Zhang et al. (2013) for the similar materials that show a stabilized plateau value after a certain crack length. The prevalent fiber bridging, which causes the initial increase in R-curve, usually stabilizes after certain delamination length. Hence, this could be due to the deviation of crack from the laminate midline towards other plies during propagation. Also, their findings for hybrid flax/glass composites regarding the behavior of R-curves and the decrease in G_{IC} are not consistent with those of Zhang et al. (2013) for similar materials.

As summarized above, the literature review shows that the previous works addressing the IFT of FFRCs have mostly studied flax-fabric reinforced composites. Also, few researchers investigated the IFT of UD-FFRECs in Mode I, however, to the knowledge of the author, no study has investigated their delamination behavior in Mode II and Mixed-mode I/II. Therefore, the damage tolerance and behavior knowledge of UD-FFRECs, as the basic building block of the FFRECs, particularly in Mode II and Mixed-mode I/II are missing. Consequently, an in-depth understanding of their delamination behavior in different modes is essential both for improving their material properties and for generating knowledge for future studies. This is of paramount importance in the engineering design field and in employing FEM numerical analysis techniques to study FFRECs.

2.4.3.2 Translaminar fracture toughness

Mode I intralaminar fracture propagating perpendicular to fiber direction is known as translaminar fracture mode (M. J. Laffan, Pinho, Robinson, & McMillan, 2012). The fracture toughness associated with translaminar failure mode is denoted by G_C when expressed in terms of energy and by K_C when expressed in terms of stress intensity factor. It determines the resistance of a material against crack growth perpendicular to the fibers where the dominating fiber failure mechanism in composites occurs. The translaminar fracture toughness (TFT) is one of the primary mechanical properties of FRCs. This is particularly true when using FEM to simulate specific material damages occurring in composite laminates, like fiber failure, matrix breaking, and delamination (El-Hajjar & Haj-Ali, 2005; Faggiani & Falzon, 2010; Falzon & Apruzzese, 2011; Israr, Rivallant, Bouvet, & Barrau, 2014; Jose, Kumar, Jana, & Rao, 2001). While the significance of TFT measurement was recognized since the late '70s, it has attracted little interest (M. J. Laffan *et al.*, 2012). This is because FRCs were not used in primary structures, where this property is mostly required. At the same time, the advanced numerical simulation methods referring to this property were not yet developed (M. J. Laffan *et al.*, 2012). The situation is now different as FRCs are used in structures, and FEM is a commonly used numerical method. With the growing applications of FFRECs, their TFT in tension and compression loadings are expected to play an essential role in the future. Currently, it is required in many research fields, such as the machining of composite materials, where numerical models based on FEM are implemented.

In the literature, the translaminar fracture toughness measurement of NFRCs is limited to a few studies that are all conducted only in tension. Besides, to the author's knowledge, there is no work in the literature investigating the TFT of UD-FFRECs, neither in tensile nor in compressive loading. Hughes et al. (2002) studied the tensile TFT of polyester composites reinforced with chopped jute and hemp fibers and compared them to that of a glass fiber mat composite. Assuming that the composite is isotropic, they followed the BS-7448 standard but highlighted the inappropriateness of the evaluation method for these materials. Generally, the G_C^{Ten} value of GFRP was three-fold higher than those of NF composites. By formulating the

relationship between the extent of the damaged zone and the fracture toughness (K_{IC}), they concluded that different micro-structural toughening mechanisms were activated in the NFRCs compared to GFRP. Following ASTM D5045, Li et al. studied the fiber surface treatment effect on fracture properties of textile-sisal/vinyl-ester composite (Y. Li, Mai, & Ye, 2005). They obtained K_{IC} = 4.2 MPa-m½ for the untreated fiber composite, which increased to 5.5 and 6.0 MPa-m½ respectively, with Silane and KMnO$_4$ fiber treatments. Silva et al. (2006) tested polyurethane (PU) reinforced with sisal and coconut short fibers as well as a woven sisal fabric for the tensile TFT. The sisal fabric composite exhibited the best performance (G_C^{Ten} = 11.8 kJ/m^2), whereas coconut composites displayed the lowest toughness, even lower than the neat matrix (G_C^{Ten} = 6.3 kJ/m^2). G_C^{Ten} of the composites increased with V_f, but they were not affected by the strain-rate. Also, the alkaline treatment impaired G_C^{Ten} of sisal composites but improved that of the coconut composites.

Q. Liu and Hughes (2008) investigated the effects of textile yarn linear density (Tex), weave configuration, and stacking sequence on G_C^{Ten} of woven FFRECs (Q. Liu & Hughes, 2008). They tested compact tension specimens to measure K_{IC} of the anisotropic woven-flax/epoxy composites. They followed BS 7448 standard, which is developed for metallic materials. According to their findings, reinforcing epoxy resin with woven textiles resulted in a 2-4 fold increase in K_{IC}. Also, they observed that the fracture behavior and K_{IC} of the composites were strongly dependent on the linear density of yarns and the direction of the test but were independent of the weave type. The authors reported K_{IC} values in the range of 3-8.5 MPa m½ for the composites and concluded that the fracture toughness is more dominated by the fiber properties and V_f rather than the reinforcement configuration.

Shakir Radif and Ali investigated the effect of the kenaf mat-fiber content on K_{IC} of polyester composites (Shakir Radif & Ali, 2011). They tested compact tension specimens and followed ASTM E1820. The authors observed an improvement with fiber content increase and published K_{IC} = 0.76 and 2.0 MPa m½ respectively for 20% and 40% kenaf fiber content (not mentioned if they are the weight or volume fractions). Ismail et al. reported values of $K_{IC} \approx$ 8.5 and $K_{IC} \approx$

4.5 MPa m½ respectively for UD-twisted yarn and cross-ply woven kenaf/polyester composites tested based on ASTM D5045 (A. E. Ismail *et al.*, 2016).

Chizyuka and Kanyanga investigated the effects of hydrothermal aging and moisture absorption on the K_{IC} of sisal/polyester composites (Chizyuka & Kanyanga, 2013). They followed the ASTM E1922 procedure to evaluate K_{IC} of the composites and obtained $K_{IC} \approx$ 6.25 MPa m$^{1/2}$. They observed that during the first 60 days, K_{IC} dropped rapidly. The fractographic study revealed that the reduction of K_{IC} was mainly due to fiber/matrix debonding, which was the dominant fracture mechanism in the composite. Manjunath et al. followed ASTM E1922 and investigated the influences of the dimensions of the Extended Compact Tension (ECT) specimens on the K_{IC} of jute fabric reinforced epoxy composites (G B, Vijaykumar, K N, & Jmsse, 2015). However, the criteria of the standard were not carefully respected. Moreover, there is a mismatch between their reported test data and the reported K_{IC} values. Substituting their reported test data in the equations given in the E1922 standard results in a 50-fold lower K_{IC} value compared to their reported K_{IC} values. Their published result is also one order of magnitude higher than that of Ashik et al., $K_{IC} = 7.71$ MPa m$^{1/2}$, for an analogous material (Ashik, Sharma, & Raghavendra, 2017). Khan et al. reported values between 1.61 and 2.67 MPa m½ for K_{IC} of NaOH-treated bamboo fiber/epoxy composites with different fiber lengths (Khan, Yousif, & Islam, 2017), while Naik et al. published K_{IC} values between 1.69 and 2.91 MPa m½ respectively for 30 wt% and 40 wt% fiber contents of banana/epoxy composites (Naik, Londe, Yogesha, Laxmana Naik, & Pradeep, 2018).

Translaminar fracture toughness in tension

The ASTM E1922 standard (ASTM, 2015b) suggests the extended compact tension (ECT) specimen for measuring the tensile translaminar fracture toughness of FRCs. ECT (Figure 5.1) is an extended configuration of the compact tension (CT) specimen that is used for metals in ASTM E399, shown in Figure 5.2a. ECT was developed to avoid undesirable failure modes such as crack growth perpendicular to the pre-notch (Piascik, Newman, & Underwood, 1997; Underwood *et al.*, 1995). It was formulated by the numerical boundary-force method and based on isotropic elasticity. Considering the orthotropy of composites, it defines some criteria to

validate the tests for FRCs. ASTM E1922 was developed and adapted to measure the fracture toughness of FRCs in tension. Nevertheless, a number of studies have used CT specimens, along with ASTM E399, D5045, or other methods, to study the fracture toughness of carbon and glass FRCs (Catalanotti, Camanho, Xavier, Dávila, & Marques, 2010; M. J. Laffan, Pinho, Robinson, & Iannucci, 2010a, 2010b; Leonard, Wong, Low, & Yousif, 2009; H. Liu, Falzon, Catalanotti, & Tan, 2018; S. T. Pinho, Robinson, & Iannucci, 2006). Though, they have highlighted that some errors may originate from the use of the finite width correction factor derived for isotropic materials.

Without mentioning any particular reason, all of these studies have tested cross-ply laminates to determine the fracture toughness of UD-FRCs. Generally, two approaches have been used to determine the tensile fracture toughness of the 0° plies by testing multidirectional and cross-ply laminates (M. J. Laffan *et al.*, 2012). In the first approach, Vaidya and Sun used a method to determine the fracture toughness of the 0° plies in a multidirectional laminate (Vaidya & Sun, 1997). However, it was rather complex and required classical lamination theory for the determination of a coefficient for the material, thus was not used by other researchers. In the second approach, several other researchers tested cross-ply laminates and utilized a rule-of-mixtures type approach to directly measure the fracture toughness of UD-FRCs. This method is more practical and has been frequently used in the literature.

Jose et al. evaluated TFT associated with tensile failure of a carbon/epoxy cross-ply laminate $[0/90]_{15}$, as well as its constituent UD laminates, $[0]_{30}$ and $[90]_{30}$, according to ASTM E399 standard (Jose *et al.*, 2001). In their $[0]_{30}$ and $[90]_{30}$ specimens the fibers were directed respectively perpendicular and parallel to the load direction. They obtained a $K_{IC} \approx 809$ MPa $m^{1/2}$ for their cross-ply laminate, $[0/90]_{15}$, and a much lower $K_{IC} \approx 138$ MPa $m^{1/2}$ for their $[90]_{30}$ laminate whereas, the latter evidently should be higher. They presented an analytical relationship between the K_{IC} of the cross-ply laminate and those of its constituent UD laminates. However, the failure pass of their $[90]_{30}$ specimen was perpendicular to the notch, so it was not representative of a translaminar fracture. Besides, their derived analytical relationship seems to have inconsistent dimensions. Therefore, their results are not discussed.

Pinho et al. used a similar approach to determine the critical energy release rate associated with the tensile and compressive failure of UD carbon/epoxy laminates using a cross-ply [0/90]₈ₛ laminate (S. T. Pinho *et al.*, 2006). They used CT and CC specimens with the dimensions and fiber direction shown respectively in Figure 5.2a and 5.2b and followed the ASTM E399 procedure. However, they regenerated a finite-width correction factor based on FEM to replace the one defined in ASTM derived for isotropic materials. The authors assumed: (i) that the mode-I critical energy release rate of the cross-ply laminate is the sum of energies associated with the fiber fracture in the 0° layers and matrix cracking in the 90° layers, and (ii) that the matrix cracking in the 90° layers occurred as a single crack parallel to the notch, similar to delamination mode-I. By making the first assumption, they neglected other damage modes and interactions between neighboring layers. With the last assumption, the critical energy release rate in tension is quantitatively equivalent to that of mode-I delamination. This assumption seems reasonable, as the 0° layers are much tougher than the 90° layers, and is found to be a good approximation based on their findings in a previous work (S. Pinho, Robinson, & Iannucci, 2009). For the particular cross-ply layup studied, they used the following equation to calculate the G_C^{Ten} for the 0° layer or UD laminate in fiber direction;

$$G_C^{Ten}\big|_{fiber\ tensile} = 2G_C^{Ten}\big|_{lam\ tensile} - G_{IC}\big|_{matrix\ intra} \qquad (2.1)$$

where $G_C^{Ten}\big|_{lam\ tensile}$ is the critical energy release rate of the laminate, as measured by CT test, $G_{IC}\big|_{matrix\ intra}$ is the mode-I matrix failure intralaminar fracture energy, and $G_C^{Ten}\big|_{fiber\ tensile}$ is the fracture energy associated with fiber tensile failure mode. Furthermore, they omitted the last terms in Equations (2.1), as, in carbon/epoxy composites, the fracture energies in matrix failure modes are much lower than in fiber failure modes. The factor "2" indicates that in this laminate with half of its plies oriented in the 0° direction, the TFT of UD laminate is nearly twice as high as that of the cross-ply laminate. With the same assumptions, Laffan et al. used the generalized form of Equation (2.1) to study the layup effects on the fracture toughness of carbon/epoxy composites in tensile fiber failure mode (M. J. Laffan *et al.*, 2010b);

$$G_{IC}^0 = \frac{t_{lam}}{t_0} G_{IC}^{lam} - \frac{t_{90}}{t_0} G_{IC}^{90} \qquad (2.2)$$

where t_{lam}, t_0 and t_{90} are the thicknesses of the cross-ply laminate, 0° and 90° layers within the laminate, respectively. G_{IC}^0 is the fracture energy associated with the fiber tensile failure mode, and G_{IC}^{90} represents the intralaminar mode-I matrix cracking fracture energy. In another study, Laffan et al. observed that there was no interaction between the failure modes occurring in the 0° and 90° plies (M. J. Laffan, Pinho, Robinson, & McMillan, 2011). This result confirms this approach. Nevertheless, it has been shown that the lay-up in the cross-ply laminates can affect the *G*_{IC} measured for the 0° plies (M. Laffan, Pinho, Robinson, & Iannucci, 2009; M. J. Laffan *et al.*, 2012; M. J. Laffan *et al.*, 2010b; Teixeira, Pinho, & Robinson, 2016). Donadon et al. followed the same approach to calculate the fracture energy in woven cross-ply laminates along with a numerical method (Donadon, Falzon, Iannucci, & Hodgkinson, 2007). The agreement of the experimental and numerical results confirmed the validity of this approach.

Translaminar fracture toughness in compression

By contrast to TFT in tension, there is no standard test method available to evaluate the fracture toughness of FRCs in compression. In a few works, modified CT specimens are used in compression with the test coupon renamed compact compression (CC) (Catalanotti *et al.*, 2010; S. T. Pinho *et al.*, 2006). Pinho et al. used the same approach explained in the previous section for determining TFT in compression of UD laminates (S. T. Pinho *et al.*, 2006). They tested CC specimens illustrated and shown in Figure 5.2c and Figure 5.2d and followed the ASTM E399 procedure. They made the same assumptions considering that in compression loading, the matrix cracking in the 90° layers is close to what happens in delamination mode-II. Thus, the critical energy release rate in compression is quantitatively equivalent to that of mode-II delamination. They used Equation (2.3) to calculate the G_C^{Comp} for the UD laminate in the fiber direction;

$$G_C^{Comp}|_{fiber\ kinking} = 2G_C^{Comp}|_{lam\ comp} - G_{IIC}|_{matrix\ intra} \qquad (2.3)$$

where $G_C^{Comp}|_{lam\ comp}$ is the critical energy release rate of the laminate, as measured by a CC test, $G_{IIC}|_{matrix\ intra}$ is the mode-II matrix failure intralaminar fracture energy, and $G_C^{Comp}|_{fiber\ kinking}$ is the fracture energy associated with fiber-kinking failure mode (in the 0° direction). Similar to tension, they ignored the last term in Equation (2.3). In a different approach, Laffan et al. used a four-point-bend specimen to measure the fracture toughness of a UD-CFRP with the help of AE and micromechanical FEM (M. Laffan, Pinho, Robinson, Iannucci, & McMillan, 2012). Their study revealed that compressive failure starts before any signs appear on the load-displacement graph.

Overall, there is a significant difference between the fracture toughness values reported by the authors using different approaches to measure compressive TFT (M. J. Laffan *et al.*, 2012; H. Liu *et al.*, 2018). Perhaps this indicates that conventional mechanical tests are not suitable for this purpose. The compressive fiber failure mode in laminated composites is known as a very complex phenomenon, which is the result of fibers micro-buckling and formation of kink-bands or crushing (Gutkin, Pinho, Robinson, & Curtis, 2010; S. T. Pinho *et al.*, 2006; Soutis & Curtis, 2000). So, and unlike tension, the authors observed large damage zones. Therefore, to measure the pure TFT in compression, the damage mechanisms should be separated.

Infrared thermography/Translaminar fracture toughness measurement

In order to overcome the problems experienced with experimental methods, it was proposed to develop an approach allowing estimating the energy release rate via temperature measurement by IRT (Teddy Lisle *et al.*, 2015; T. Lisle, Bouvet, Pastor, Margueres, & Prieto Corral, 2013; Teddy Lisle *et al.*, 2014; Naderi, Kahirdeh, & Khonsari, 2012). The relation between fracture toughness and dissipative work has already been proved (Freund & Hutchinson, 1985). Characterizing the fracture energy utilizing IRT is an idea conceptualized based on the principles of irreversible thermodynamics and thermo-mechanical laws (Thermodynamics of Continuous Media). The complete details of the methodology are described and employed for evaluating the tensile and compressive fracture energy of FRCs in (T. Lisle *et al.*, 2013) and in (Teddy Lisle *et al.*, 2015; Teddy Lisle *et al.*, 2014), respectively.

The original idea of the IRT method is solving the heat diffusion equation, Equation (2.4), to determine the energy dissipated as heat or the intrinsic dissipation in the damaged material (Teddy Lisle *et al.*, 2015). In this approach, the right term of the equation, including the dissipated energy, is estimated by evaluating the left term using the recorded spatial and temporal data (Teddy Lisle *et al.*, 2015; T. Lisle *et al.*, 2013; Naderi *et al.*, 2012):

$$\rho C_p \frac{d\theta}{dt} - \left\{ K_{xx} \frac{\partial^2 \theta}{\partial x^2} + K_{yy} \frac{\partial^2 \theta}{\partial y^2} + K_{zz} \frac{\partial^2 \theta}{\partial z^2} \right\} = \emptyset_{int} + S_{the} \qquad (2.4)$$

where $\theta = T - T_0$ denotes the temperature difference between the current and the initial situation T_0, ρ is the density, C_p the specific heat capacity, K_{xx}, K_{yy} and K_{zz} are the thermal conductivity coefficients in x, y, and z directions respectively, $\emptyset_{int}$ represents the intrinsic dissipation, and S_{the} the thermo-mechanical coupling term. In the literature, it has been accepted that the thermo-mechanical coupling term in the heat diffusion equation is negligible compared to dissipated energy, ($S_{the} \ll \emptyset_{int}$) (Teddy Lisle *et al.*, 2015; T. Lisle *et al.*, 2013; Naderi *et al.*, 2012). Therefore, this term is neglected and eliminated from the equation. According to the second law of thermodynamics, fracture damage is an irreversible process related to the irreversible dissipation, $\emptyset_{irrev}$. This is required to evaluate the fracture toughness and is composed of two parts: the intrinsic dissipation $\emptyset_{int}$ evaluated using IRT and the stored energy $\emptyset_{stored}$, Equation (2.5) (T. Lisle *et al.*, 2013).

$$\emptyset_{irrev} = \emptyset_{int} + \emptyset_{stored} \qquad (2.5)$$

Determining the stored energy is not trivial and requires the Taylor–Quinney coefficient (β) that indicates the ratio of energy dissipated as heat (dW_{diss}) to the total irreversible energy (dW_{irrev}), as defined in Equation (2.6) (Teddy Lisle *et al.*, 2015; Taylor & Quinney, 1934).

$$\beta = \frac{dW_{diss}}{dW_{irrev}} = \frac{\int_V \emptyset_{int}.dV}{\int_V \emptyset_{irrev}.dV} \qquad (2.6)$$

β varies in the range of 0 and 1 for different failure modes and materials; $\beta = 1$ means that all the dissipated energy is converted into heat (Kapoor & Nemat-Nasser, 1998; Z. Li & Lambros, 2001). Having β and the dissipated energy evaluated with IRT, the fracture energy, G_{IC}, can be determined using Equation (2.7) (Teddy Lisle *et al.*, 2015; T. Lisle *et al.*, 2013);

$$G_{IC} = \frac{dW_{irrev}}{dA} = \frac{dW_{diss}}{\beta.dA} \qquad (2.7)$$

where dA denotes the crack surface growth.

Following this approach, IRT opened the way for the measurement of local fracture energy. However, it requires precise estimation of β, which depends on damage mechanisms (Teddy Lisle *et al.*, 2015; T. Lisle *et al.*, 2013). Some authors studied β parameter for metallic materials and reported β close to 1 for Tantalum (Kapoor & Nemat-Nasser, 1998; Teddy Lisle *et al.*, 2015) and depending on the applied strain rate, β between 0.5 and 1 for stainless steel (Teddy Lisle *et al.*, 2015). β values between 90% and 100% have been published for CFRP with epoxy resin (Teddy Lisle *et al.*, 2015; T. Lisle *et al.*, 2013; Naderi *et al.*, 2012; Taylor & Quinney, 1934). Nevertheless, this value can vary significantly; thus, a precise assessment of the energy release rate or the fracture energy associated with the crack growth seems uncertain (Teddy Lisle *et al.*, 2015; T. Lisle *et al.*, 2013). This is a debatable issue for employing IRT technique to evaluate the magnitude of G_{IC} (Teddy Lisle *et al.*, 2015; T. Lisle *et al.*, 2013).

Allocating values for β remains a delicate issue in this study because no values are available for the under-investigation flax/epoxy composite. Furthermore, the magnitude of the coefficient is strain and strain-rate dependent (Z. Li & Lambros, 2001; Teddy Lisle *et al.*, 2015; T. Lisle *et al.*, 2013). Li and Lambros (Z. Li & Lambros, 2001) investigated PMMA and PC polymers in terms of the value of β and its sensitivity to strain and strain-rate. The authors found it impossible to measure β for PMMA; however, they reported values between 50% for high strain and 100% for low strain, independent of the strain-rate in the ranges of the investigation. Considering the available values for β of polymers in the literature, the values

of $\beta = 0.5$ and $\beta = 0.9$ were chosen for this study. The results are then compared to the result obtained from the ASTM E1922 standard test method to evaluate the validity of the assumptions.

Recently, IRT has been broadly used to investigate the energy-dissipative processes in materials, for example, plastic deformation in metals (Dumoulin, Louche, Hopperstad, & Børvik, 2010) or damage in polymeric materials (Wattrisse, Muracciole, & Chrysochoos, 2002). For FRCs, Naderi et al. used IRT to characterize the damage evolution in fatigue loading of woven-glass/epoxy composites (Naderi *et al.*, 2012). They found that the results were consistent with those obtained by acoustic emission. Lisle et al. used IRT to study damage development in fabric-glass/epoxy composites under tensile loading (T. Lisle *et al.*, 2013; T. Lisle, Bouvet, Pastor, Rouault, & Marguerès, 2015). The authors also measured the fracture toughness of the GFRP in tension (T. Lisle *et al.*, 2013). In another study, Lisle et al. used IRT to measure the fracture toughness of UD-CFRP composite in compression. They showed that for a carbon/epoxy composite, the ratio of dissipative work converted to heat should be close to 100% (Teddy Lisle *et al.*, 2015; Teddy Lisle *et al.*, 2014). IRT helped them to assess the dissipated energy due to fiber failure in compression separately and eliminate those associated with material crushing at loading points or secondary cracks. They obtained a value of G_C^{Comp} = 42.5 N/mm and found their results consistent with those of Hongkarnjanakul et al. (Hongkarnjanakul, Bouvet, & Rivallant, 2013) (40 N/mm) and other researchers (S. T. Pinho *et al.*, 2006; Soutis & Curtis, 2000). There is no previous research using this approach to address NFRCs.

In summary, no standard test methods have been developed for measuring TFT of NFRCs in any loading modes, and that of any FRC in compression. Besides, a very limited number of studies have addressed these topics, and in all of these studies, NFRCs have been tested in tension. These are essential properties for engineering design purposes and for the modeling of these materials with numerical methods, such as FEM. Moreover, and to our knowledge, no fractographic and micrographic analysis of this subject have been performed for UD-FFRECs.

2.5 Summary

An overview of natural fibers, natural fiber-reinforced composites, particularly flax fiber and flax/epoxy composites, edge milling process of these composites, as well as implementation of FEM to simulate the cutting process, was presented in this chapter. The existing experimental works on milling unidirectional flax/epoxy composites, and the studies applying FE modeling to investigate the trimming process of FRCs are briefly reviewed. It was shown that using FEM to study machining operations was indispensable; accordingly, numerous studies have implemented FEM to simulate the cutting processes of SFRCs. Also, it was concluded that it is impractical to use FE models developed for engineered FRCs to study those of FFRECs. This is mainly due to the complex microstructure of flax fibers and different behavior of FFRECs. Therefore, involving FEM in modeling the cutting process of NFRCs is imperative. Fundamentally, FEM relies on a full set of precise and reliable physical, mechanical, and fracture properties of FFRECs, in the current case, to model several failure modes occurring during the cutting process.

Seeking for the material properties required for FE modeling of the composite, they are classified into physical, mechanical, and fracture properties; then, comprehensive literature reviews for these properties is conducted. However, in general, the reviews revealed that only some material properties are available for FFRECs with different specifications. Thus, they are scattered and unreliable; moreover, many other required material properties are absent in the literature. Consequently, the full characterization of FFRECs is essential, as the first step, to enable implementing FEM to investigate their cutting process.

The current study is carried out to fulfill this deficiency. First, unidirectional flax/epoxy laminates with unique fiber volume fraction were molded and cured under similar conditions to satisfy the requirements of the related standard test methods. Then, they were tested according to the adapted standard test procedures. These test methods were initially developed and recommended for the evaluation of corresponding properties for their synthetic

counterparts, where available. The properties were categorized into three categories, and each one was investigated and published in a separate work as follows.

The first category covers the physical and mechanical properties. The physical properties consist of density, specific heat capacity, and thermal diffusivity. The mechanical properties include tension, compression, shear, and flexural properties in longitudinal and transverse directions. Here, it was observed that none of the literature studies particularly addressed determining the physical and mechanical properties of FFRC in view of providing the data for numerical resolutions and design process. Moreover, a complete set of material properties for a well-defined FFRC is absent in the literature. These are the primary material properties that are also needed for determining the fracture properties. Therefore, at first, an experimental investigation of failure mechanisms and evaluation of the physical and mechanical properties of UD-FFRECs, covering this category, was conducted and is presented in CHAPTER 3.

CHAPTER 4 presents a study of the interlaminar fracture toughness of UD-FFRECs and covers the second category, i.e., the interlaminar fracture properties. According to the literature review, the required interlaminar fracture energies for FE modeling of this composite are not available. Hence, using the previously determined properties, the test specimens were designed and tested for the interlaminar fracture energies in Mode I, Mode II, and Mixed-Mode I/II. These quantities will also be used for the evaluation of the properties classified in the third category.

The translaminar fracture toughness in tension and compression are classified in the third category. The conducted literature review showed that no study targeted investigation of the translaminar fracture toughness of UD-FFRECs, and it is totally absent in the literature. Therefore, the previously measured properties were used to conduct an experimental study aiming at determining these properties. The study is presented in CHAPTER 5. This study used two methodologies, along with an investigation of the fracture behavior and viability of the standard test procedures for FFRECs, considering that they were developed for FRCs. In the first method, the composite was tested for translaminar fracture toughness in tension according

to the existing ASTM E1922 standard. A fractography was also conducted to investigate the failure mechanisms. In the second method, an IRT-based methodology and ASTM D5045 standard were employed. The translaminar fracture energy of UD-FFRECs in tension and compression was determined, and the material behavior was assessed.

CHAPTER 3

EXPERIMENTAL INVESTIGATION OF FAILURE MECHANISMS AND EVALUATION OF PHYSICAL/MECHANICAL PROPERTIES OF UNIDIRECTIONAL FLAX-EPOXY COMPOSITE

Yousef Saadati [1], Gilbert Lebrun [2], Jean-François Chatelain [3] and Yves Beauchamp [4]

[1,3] Mechanical Engineering Department, École de technologie supérieure (ÉTS), 1100 Notre-Dame Street West, Montreal, Québec H3C 1K3, Canada
[2] Mechanical Engineering Department, Université du Québec à Trois-Rivières (UQTR), 3351 boul. des Forges, Trois-Rivières, Québec G9A 5H7, Canada
[4] McGill University, 845 Sherbrooke Street West, Montreal, Québec H3A 0G4, Canada

3.1   Abstract

Using natural fibers as reinforcement in polymer matrix composites necessitates evaluating the latter under different modes of solicitation. This allows extracting its material properties for engineering design and research purposes. The main objective of the study is to prepare a consistent set of material properties for unidirectional (UD) flax fiber-reinforced epoxy composite (FFREC) with defined composition and basic configuration. These data are prerequisites for growing researches on FFRECs, especially for numerical analysis purposes using the Finite Element Method (FEM). In this work, partially green UD-FFRECs are tested for physical and mechanical properties and studied for their failure modes. Tension, compression, flexion, and shear properties, as well as physical properties like density, specific heat capacity and thermal diffusivity, are evaluated according to ASTM standard test methods. Flax fibers, which are composites by themselves, come in bundles in the composites and demonstrate a complex behavior. So, a fractographic analysis has been conducted to understand the macro and microscale failure mechanisms to correlate them with the material properties. The results are in good agreement with those of the literature, when available, but they mainly show the specific behavior of UD-flax composites subject to different solicitation

modes, especially compression and direct shear modes evaluated this way for the first time for UD-FFREC. They cover most of the data required for engineering design and numerical analysis by methods like FEM, particularly for simulating the machining process of FFREC in the ongoing works.

Keywords: Natural fiber composites; UD Flax-epoxy composites; Mechanical properties; Physical properties; Composite testing; Fracture analysis; Failure mechanisms

3.2　　Introduction

Having improved sustainability, competitive properties, and lower cost, in the recent few decades, natural fiber-reinforced polymer composites (NFRCs) have attracted the attention of researchers as a potential substitute for man-made fiber-reinforced polymer composites (FRCs) (Fuqua *et al.*, 2012; Gurunathan *et al.*, 2015; La Mantia & Morreale, 2011; Netravali & Chabba, 2003; Sanjay *et al.*, 2018; Väisänen, Das, & Tomppo, 2017). For now, producing completely bio-based composites is neither an economical nor a mechanical solution in many applications; however, combining synthetic polymers with plant-based natural fibers to develop economic and partially green composites has been a viable alternative for petroleum-based FRCs (John & Thomas, 2008; Netravali & Chabba, 2003; Wambua *et al.*, 2003).

Several bast fiber composites have specific elastic modulus and strength (property/density ratio) comparable to and sometimes better than glass fiber-reinforced polymer composites (GFRP) (Ahmad *et al.*, 2015; Yan *et al.*, 2014; Jinchun Zhu *et al.*, 2013). Flax fiber-reinforced polymer composites (FFRCs) mechanical failure mechanism, properties degradation, and in performance failure have been the subject of several researches (Khanlou *et al.*, 2018; Khanlou, Woodfield, Summerscales, & Hall, 2017; Mohammad Khanlou, Hall, Woodfield, Summerscales, & Francucci, 2018; Jinchun Zhu *et al.*, 2013). To design and develop FFRC parts, knowing their physical and mechanical properties is an essential prerequisite. Particularly, numerical analysis methods like FEM, which is widely used in many engineering fields, need these properties. Relatively limited data regarding the mechanical properties of

FFRC are currently available, and due to their complex microstructure, their anisotropy, and heterogeneity, more specific properties need to be evaluated in comparison to isotropic materials. Moreover, for most NFRCs, there are no specific standard test methods available that consider the complexity of natural fibers in the mechanical behavior of these composites.

Garkhail et al. studied the stiffness, strength, and impact strength of flax mat fiber-reinforced polypropylene composites (Garkhail, Heijenrath, & Peijs, 2000). They reported the influence of fiber diameter and length on these properties and compared the experimental results to micro-mechanical models. Their results show that strength depends on fiber strength rather than interfacial bond strength; however, they used a test method adapted for plastics, rather than for FRCs. Oksman measured the absolute and specific tensile strength and elastic properties of a unidirectional (UD) high-quality flax fiber-reinforced epoxy composite (FFREC) and compared the results to those of GFRP, traditionally retted UD-FFREC and of pure epoxy (Oksman, 2001). They found out that the high-quality FFREC at V_f of 50% had stiffness and tensile strength of 40 GPa and 280 MPa, respectively, which are higher than those of traditional FFREC and were even stiffer than GFRP. Romhany et al. studied the tensile behavior of UD and cross-ply flax fiber-reinforced starch composites and observed that for the fiber content of 40 wt.% of UD reinforcement, the tensile strength increased by a factor of three and the tensile modulus by several orders of magnitude relative to that of the matrix (Romhány $et\ al.$, 2003). Singleton et al. studied the effect of V_f on the tensile and impact properties of a recycled HDPE composite reinforced by randomly oriented flax mat and compared it to a polyethylene composite (Singleton, Baillie, Beaumont, & Peijs, 2003). The tensile stiffness and strength increased with V_f, while the strain at failure decreased (maximum V_f of 30% studied). They suggest a V_f of 15–20% as an optimum value to maximize the mechanical properties under study. Baiardo et al. fabricated composites based on polyester (Bionolle) and short randomly distributed flax fibers (Baiardo, Zini, & Scandola, 2004). Stiffness changed with fiber content according to the modified rule-of-mixture, while strength tended to decrease with V_f, showing a weak matrix-fiber adhesion. Arbelaiz et al. used some surface MAPP modifiers for short flax fiber bundles to reinforce polypropylene (PP) and compared their effects on the tensile, flexural, and impact behavior of the composites (Arbelaiz

et al., 2005a; Arbelaiz *et al.*, 2005b). Using MAPP, the water uptake rate decreased, and the mechanical properties were improved, but after water immersion, they drastically decreased. Charlet et al. compared the properties of fibers and matrix to the properties of the flax-polyester composite and interpreted the similarity of the tensile curves of the composite and elementary fibers as the result of a good fiber-matrix adhesion in the composite(Karine Charlet *et al.*, 2010). Using hand lay-up and compression molding approaches, they found the maximum V_f to be theoretically limited to 41%. Zhu et al. studied different lay-ups of flax reinforced tannin-based bio-degradable composites and found that the UD laminate offers the highest tensile strength and modulus of 150 MPa and 9.6 GPa, respectively (Jinchun Zhu *et al.*, 2012). In another work, Zhu et al. reviewed the FFRCs and found that many researchers have proposed flax fibers as a good replacement for glass fibers in some applications and that resin transfer molding (RTM) and compression molding are recognized as preferred processes for the production of high-performance flax/epoxy composites (Jinchun Zhu *et al.*, 2013). El Sawi et al. studied the influence of compression and autoclave molding on the mechanical properties of flax/epoxy composites (El Sawi *et al.*, 2014). They used a 50/50 weight content flax/epoxy prepreg to produce plates and measured a 25 GPa longitudinal elastic modulus independent of the production process, and ultimate tensile strength of 275 and 307 MPa for 110°C and 150°C curing temperature, respectively. Seeking for a fully biodegradable composite, Zhu et al. fabricated some 50/50 weight content of flax nonwoven mat and UD fabric composites based on bio-epoxy and tannin resin (J Zhu *et al.*, 2014). The UD fabric gave the best tensile properties for both epoxy and tannin composites, but only a few properties were compared and reported.

None of those, as mentioned earlier, literature studies particularly addressed determining the mechanical properties of FFRC in view of providing the data as input for numerical resolutions and design process, and there is no published work reporting a complete set of material properties for a well-defined FFRC. Therefore, a deep understanding of their behavior under different modes of solicitation is necessary, not only for ameliorating their mechanical performance but also to develop the required knowledge and properties for future design purposes and future studies aiming at analytic and numerical resolutions. Some drawbacks that

arise during secondary production processes like the machining process limit widening the application of NFRC. Due to their complex and varying microstructure, resolving these drawbacks is also involved. Considering the large quantity of mechanical and physical properties required for their modeling, with knowledge associated with their specific fracture behavior, it was considered necessary to develop such a set, complete enough to fulfill the modeling requirements for a unique composite in terms of matrix, fiber type, and fiber content. Therefore, some of the required physical and mechanical properties of the composite are determined and analyzed in this present work. Our study includes measurement of density, specific heat capacity, and thermal diffusivity (thermal conductivity) as physical properties, as well as the tension (longitudinal and transverse), compression (longitudinal and transverse), shear, and flexural properties as mechanical properties. In the absence of standards specific to NFRCs, all tests were conducted according to ASTM standards developed for synthetic fibers and recommended for the evaluation of these properties. Therefore, precisely defined UD-FFRECs were fabricated and tested based on these standards and already published test methods.

3.3   Fabrication of test specimens

3.3.1   Materials

For the flax/epoxy composites, FLAXTAPE™ 200 (from LINEO, France), consisting of a UD tape of flax fibers with a surface density of 200 g/m^2 and width of 40 cm, was used as reinforcement. Marine 820 Epoxy Laminating System composed of Marine 820 epoxy resin mixed with 18 Wt.% Marine 824 hardener (from ADTECH® Plastic Systems) was used as a polymer matrix.

3.3.2   Fabrication of laminates

All flax/epoxy laminates were molded using the RTM process, which was proved to be a suitable process for manufacturing high-quality NFRCs (Oksman, 2001). The layers of flax

fibers were cut to the proper size and stacked up according to the required number of layers and orientation of fibers, see Figure 3.1a. The fibers were dried for 40 minutes in an oven at 70°C. All plates were produced in 300 mm × 300 mm dimensions, with $[0]_n$ stacking sequences. The number of layers (n) was determined based on the thickness required for the preparation of each test sample, as detailed in Table 3.1. The thicknesses of laminates were precisely calculated according to the ASTM D3171 (ASTM, 2015c) procedure using the fiber specifications given in Table 3.1, to result in a constant fiber volume fraction of 41% for all composite plates following Equation (3.1);

$$V_f = \frac{nA_f}{\rho_f h} \tag{3.1}$$

where A_f is the surface density of flax tape, ρ_f the fiber density, h the laminate thickness, and n the number of plies in the laminate. After fiber impregnation by the resin, the laminate was post-cured and prepared for cutting the specimens. Steel spacers were placed between the mold halves to control the thickness, and after closing, the two parts of the mold were fixed with clamps. The resin was injected at a pressure of 60 psi using a pressure pot, and a vacuum of 1 atm applied to the mold vent to evacuate the air inside of the mold and prevent the void formation and help the resin flow. Plates were demolded ~24 h after completion of the injection to allow curing at room temperature. Next, the laminates were cleaned and post-cured in an oven at 65°C for 4 h; Figure 3.1b shows a typical molded plate.

Figure 3.1 Mold and typical reinforcement stack used for RTM injection of composite laminates (a) and final UD flax-epoxy composite (b)

3.3.3   Tabbing

According to the ASTM standards, end tabs were bonded to the tension, compression, and shear specimens to ensure a proper failure mode and to reduce the risk of breakage in the gripping jaws. Following recommendations of the standard, glass-fiber-reinforced epoxy composite (GFREC) laminates with appropriate configurations were fabricated (Table 3.1). For this purpose, the same epoxy matrix used for the FFRECs was reinforced with Texonic TG-10-T glass fabric (twill 2/2, 320 gsm) to produce an eight-ply/1.91 mm-thick laminate, with approximately 70% weight of fiber content. They were produced using the resin infusion process (full vacuum with the medium flow at the surface) and post-cured for 4 hours at 65 °C. Subsequently, GFRECs were cut to recommended dimensions and bonded on pre-trimmed FFRECs coupons after proper surface preparation for composites. Araldite® 2015 adhesive was used for bonding.

3.3.4   Preparation of samples

Each type of test samples is described and illustrated in the corresponding section below. A 10 inches/90-tooth, DIABLO's cutting saw blade, with high-density carbide tooltips was selected to perform all the specimens cutting. To reach the required geometrical accuracy, the

specimens were cut from the plates (comprising the bonded tabs, when applicable) to the sizes recommended by the standards. Any further remaining operations such as notching and installing strain gauges (SGs) on the specimens were performed separately for each coupon after cutting their overall shapes.

Table 3.1 Composite plates specifications and applications

Plate	Test	ASTM	Fiber	n	Lay-up	A_f (g/m^2)	ρ_f (g/cm^3)	V_f (%)	h (mm)
1	Tension	D3039	Flax	7	$[0]_7$	200	1.45	*41*	2.35
2	Tabs		Glass	8	$[\pm45]_4$	305.15	2.56	*>50*	1.91
3	Compression	D6641	Flax	12	$[0]_{12}$	200	1.45	*41*	4.04
4	Tabs		Glass	8	$[fabric]_8$	305.15	2.56	*>50*	1.91
5	Shear	D5379	Flax	12	$[0]_{12}$	200	1.45	*41*	4.04
6	Tabs		Glass	8	$[0/90]_4$	305.15	2.56	*>50*	1.91
7	Flexion	D7264	Flax	12	$[0]_{12}$	200	1.45	*41*	4.04

3.4　　　Physical properties measurement

3.4.1　　Density

Density is a decisive factor in determining one of the most critical advantages of flax fiber-reinforced polymer (FFRP) composites, i.e., their relatively low weight leading to high specific properties. Considering that the density value depends on factors like the fiber volume fraction, fabrication process, measurement method, and the condition of fibers used, it is often not possible to use values published in other studies. In this work, three conventional methods, which are frequently used by researchers to determine the density of composites, were used to measure the density of the FFRCs, evaluated and compared to obtain a reliable density value: Helium-gas pycnometry, Archimedes with water used as immersing liquid and Archimedes with ethanol used as immersing liquid. For each method, at least five tests were conducted.

Helium-gas pycnometry: Helium-gas pycnometry is a very quick, clean, and convenient density measurement method, based on which some commercially available equipment and the ASTM-D4892 (ASTM, 2014) standard test method were developed. In this method, based on the volume of displaced gas and Boyle's law, the volume of a material sample of known mass is measured, and accordingly, the density is calculated. For this purpose, two chambers are used, and the solid volume of specimen is calculated based on Equation (3.2);

$$V_s = V_c - \frac{V_x}{\dfrac{P_1}{P_2} - 1}$$

(3.2)

where V_s refers to the sample volume, V_c to the sample chamber volume, V_x to the expansion chamber volume, P_1, and P_2 to the pressures after fill and after expansion, respectively. The disadvantage of this method is that when a certain level of pressure is reached, Helium can enter into the open cavities so as to measure the density of the constituent materials of the composite rather than the composite density in its specific form and configuration. This issue will be evaluated by comparing the results with those of the other two methods. An ACCUPYC$^®$ II gas displacement pycnometer (from Micromeritics Instrument Corporation) was used in this work. The test was automatically repeated ten times by the equipment for each sample. The average value and standard deviation (STD) were then calculated.

Archimedes method: This is a buoyancy method based on the Archimedes' principle. It is simple to implement and has been traditionally used for measuring the density of materials. ASTM-D792 Standard test method (ASTM, 2013c) has been developed based on this principle for measuring the density of plastic materials, but It has been used for composites (Madsen, 2004; Madsen & Lilholt, 2003). We used a Sartorius YDK03 (from Sartorius Weighing Technology GmbH) density measurement kit in this study. The density is calculated according to Equation (3.3);

$$\rho = \frac{W_a(\rho_{fl} - \rho_a)}{W_a - W_{fl}} + \rho_a \qquad (3.3)$$

where ρ refers to the density, W to Weight, fl to the immersion fluid, and a to air. In order to monitor the absorption of liquid by the composite samples, the surface of the coupon was dried immediately after testing, and the coupon reweighted. Water is the most common liquid with this method. Due to the hydrophilic nature of natural fibers, immersing their composites in water may cause the absorption of water by the fibers, thus affecting the value of measured density. However, in some studies, water has been used to measure the density of natural fiber composites (Madsen, 2004; Madsen & Lilholt, 2003). In this method, the weight of the samples in the water started to increase without stabilizing. This is evidence of absorbing water rather than the removal of bubbles around the sample that usually stops in a short period of time. This was validated by reweighting the samples after testing. To avoid this problem, before immersing the samples, they were rapidly wetted to remove air bubbles surrounding the sample and then weighted in water in a short time after immersion to avoid absorption.

As an alternative to water, ethanol was used. It can be easily cleaned off, does not affect the samples, and can be safely used at room conditions. It has been used by some researchers to measure the density of natural fibers (Le Gall *et al.*, 2018; Truong, Zhong, Boyko, & Alcock, 2009). The weight of samples in ethanol was very well stabilized after a reasonable immersion time.

3.4.2   Specific Heat Capacity / Thermal Diffusivity

ASTM-E1269 method (ASTM, 2018) was followed to measure the specific heat capacity (C_p) of composite samples by differential scanning calorimetry (DSC). For this purpose, a Perkin Elmer Pyris-1 DSC device was used. A NETZSCH LFA 447 Nano Flash^{TM} apparatus was used to measure the thermal diffusivity of FFREC laminate in normal (thickness) direction at 25°C, 80°C and 135°C. The results of this test were used to calculate the thermal conductivity using the fundamental relationship between thermal diffusivity (α), thermal conductivity (λ), specific

heat capacity (C_p), and density (ρ) via the fundamental equation $\alpha = \lambda/(\rho C_p)$. The experiments were performed according to ASTM E1461 method (ASTM, 2013b). Six samples were prepared to fit in the specimen holders of the instrument. The samples were tested in two sets, with three repetitions for each set.

3.5   Mechanical properties measurement

The samples were exposed to room conditions at least 24 hours before testing. Following ASTM procedures, their dimensions were measured and recorded before testing. According to ASTM standards, for tension, compression, and shear testing, appropriate SGs were selected and bonded on the specimens for strain measurement, when required

3.5.1   Tensile tests

Uniaxial tensile tests on UD-FFRECs were carried out according to the ASTM-D3039 test method (ASTM, 2017). Using an MTS Landmark 370 hydraulic machine with mounted 100 kN load cell capacity and MTS 647/10 hydraulic grips, the coupons were tested at 2 mm/min crosshead speed; the configuration is shown in Figure 3.2a. The specimens were cut from a [0]$_7$ composite laminate and were tested in the longitudinal and transverse directions. Nominal dimensions of 250 mm × 15 mm × 2.35 mm were used for the longitudinal test with end-tabs of 56 mm × 15 mm × 1.91 mm made of cross-ply GFREC laminate pieces bonded in ±45°ply orientation, Figure 3.2b. The specimens with the nominal dimensions of 175 mm × 25 mm × 2.35 mm were used for the transverse direction test, similarly end-tabbed with the dimensions of 25 mm ×25 mm × 1.91 mm, as shown in Figure 3.2c. Biaxial SGs were bonded on one side while uniaxial-longitudinal ones were bonded on the opposite side of the specimens. These were used to indicate the strain in longitudinal and transverse directions and to monitor a possible bending of the specimen, as shown in Figure 3.2. At least five valid tests were conducted under ambient conditions.
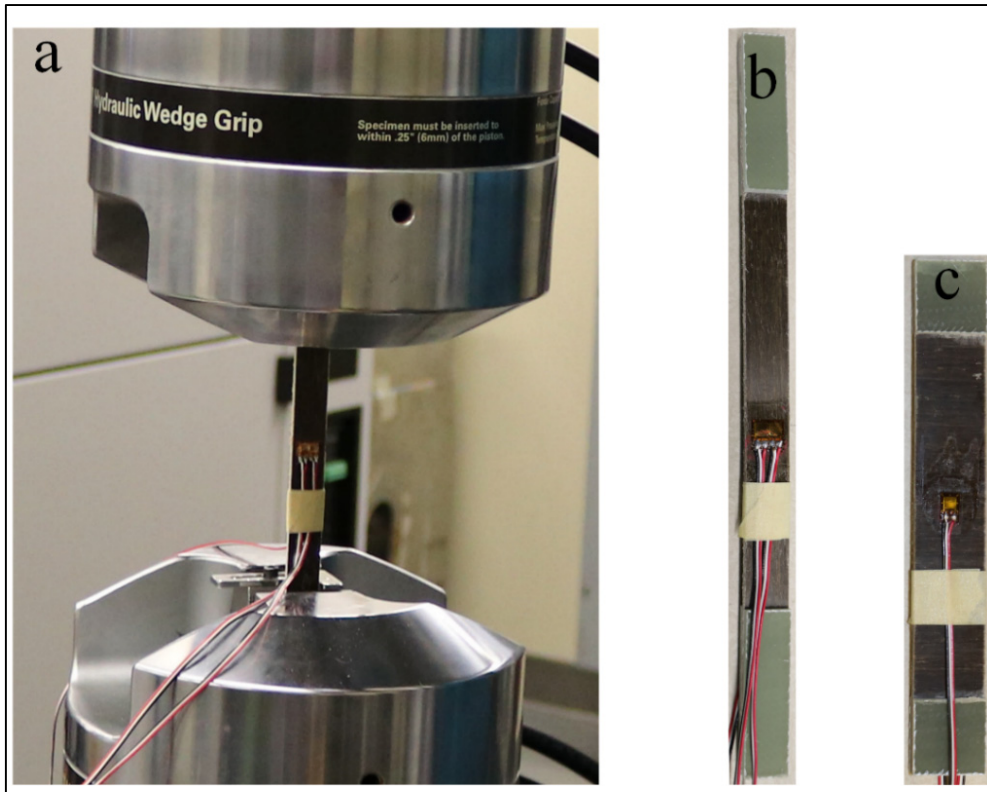
Figure 3.2 Tensile test setup (a), longitudinal (b) and transverse (c) specimens

3.5.2   Compressive tests

Compression tests were conducted following ASTM-D6641 (ASTM, 2016). An electromechanical machine, MTS RF/200 Alliance, with a load cell capacity of 200 kN was used to perform the compression tests at a constant displacement rate of 1 mm/min. A holding fixture described in the test standard was used to introduce the compressive force to the specimens, as shown in Figure 3.3a. End-tabbed specimens with 13 mm gauge-length and dimensions of 140 mm × 13 mm × 4.05 mm were cut from the $[0]_{12}$ pre-tabbed FFREC plates in longitudinal and transverse directions, see Figure 3.3b. According to guidelines of the corresponding ASTM test method, 1.91 mm-thick square-ended tabs were cut from the fabricated glass fabric/epoxy plate (Table 3.1) and orthogonally bonded to FFEC with Araldite adhesive. SGs were used as a strain measurement device, a biaxial gauge on one side, and a longitudinally installed uniaxial gauge on the other side of the specimen, as shown in Figure

3.3b. The longitudinal compressive strain was measured on both sides of the specimens to monitor the degree of bending of the specimen based on the criteria of ASTM standard, and for calculating the average axial strain, which was used next to determine the compressive elastic modulus of the UD composite. Avoiding bending for the whole test range was critical; however, adequate valid tests, meeting ASTM criteria, were conducted.
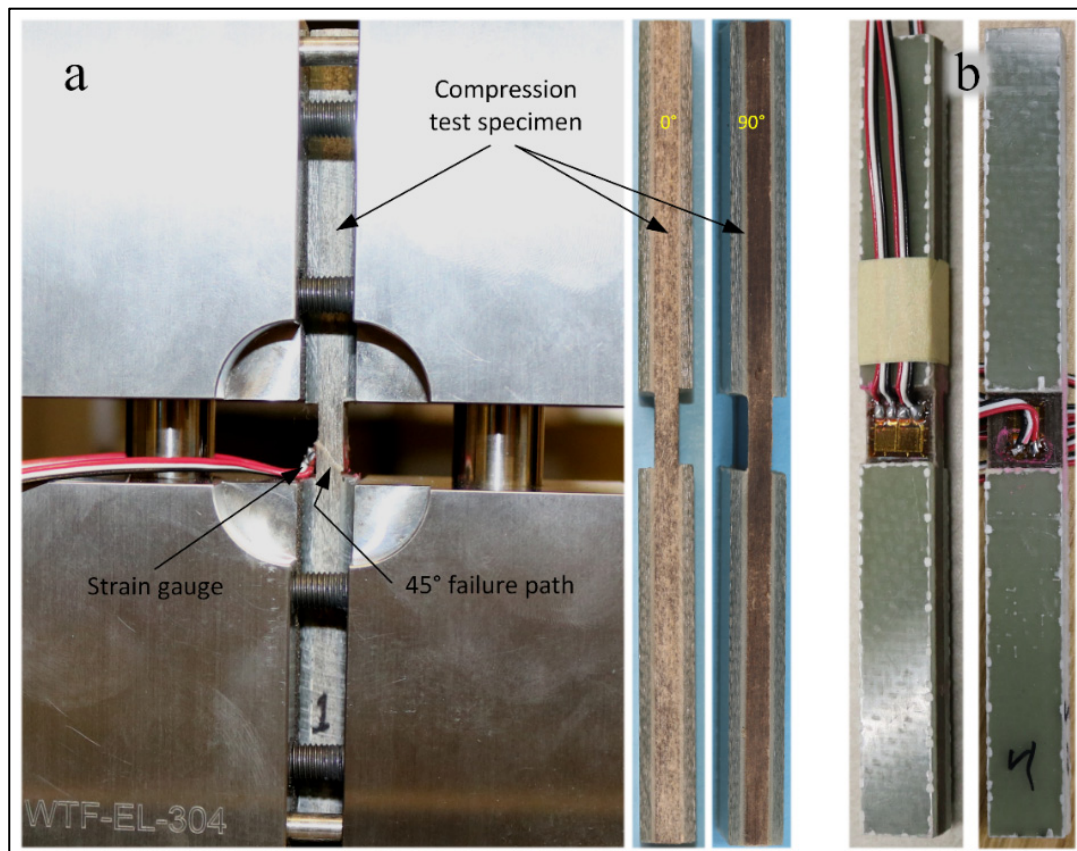
Figure 3.3 Compression test setup/sample (a) and specimens with mounted strain gauges (b)

3.5.3   Shear tests

Characterization of composite for in-plane shear properties was conducted with an Iosipescu shear test fixture according to the ASTM-D5379 method (ASTM, 2012). The V-notched beam specimens of dimensions 76 mm × 19 mm × 4.05 mm were prepared from $[0]_{12}$ FFREC laminates according to ASTM recommendations in the longitudinal and transverse directions.

Because of the inferior surface quality of the machined FFPECs, reaching the defined dimensional tolerances for this test coupon was critical; but by applying post-machining manual modifications, the accuracy of the specimens was maximized. The specimens were end-tabbed with [0/90] GFREC pieces of dimensions 32 mm × 19 mm × 1.91 mm, as shown in Figure 3.4a. The tests were performed on an MTS RF/200 Alliance, electromechanical machine, with a load cell capacity of 10 kN at a constant displacement rate of 2 mm/min. An ideal pure shear force was designed to be applied to the shear specimen at V-notch, shown in Figure 3.4b. Two orthogonal SGs in a stacked rosette were mounted at ±45° to the loading axis. Two specimens were tested, for each of the longitudinal and transverse testing directions, with rosettes on both faces of the coupon to evaluate the amount of twist according to ASTM force efficiency criteria. Consequently, specimens with a longitudinal fiber direction could be tested with two SGs on one side, whereas the specimens with fibers in transverse direction had to be tested with SGs on both sides. Due to having some specimens failing in a non-valid way, more tests than required had to be conducted to obtain five good ones.

3.5.4   Flexural tests

The flexural properties of the composite in the fiber direction were evaluated based on the ASTM-D7264 (ASTM, 2015a). For this purpose, rectangular samples of dimension 180 mm × 13 mm × 4.18 mm were tested on a 3-point bending fixture with a 134 mm span (the standard span-to-thickness ration, [32:1] was used) at a constant 1 mm/min loading rate. An MTS RF/200 Alliance with a load cell capacity of 1 kN was used to apply the displacement and measure the load.
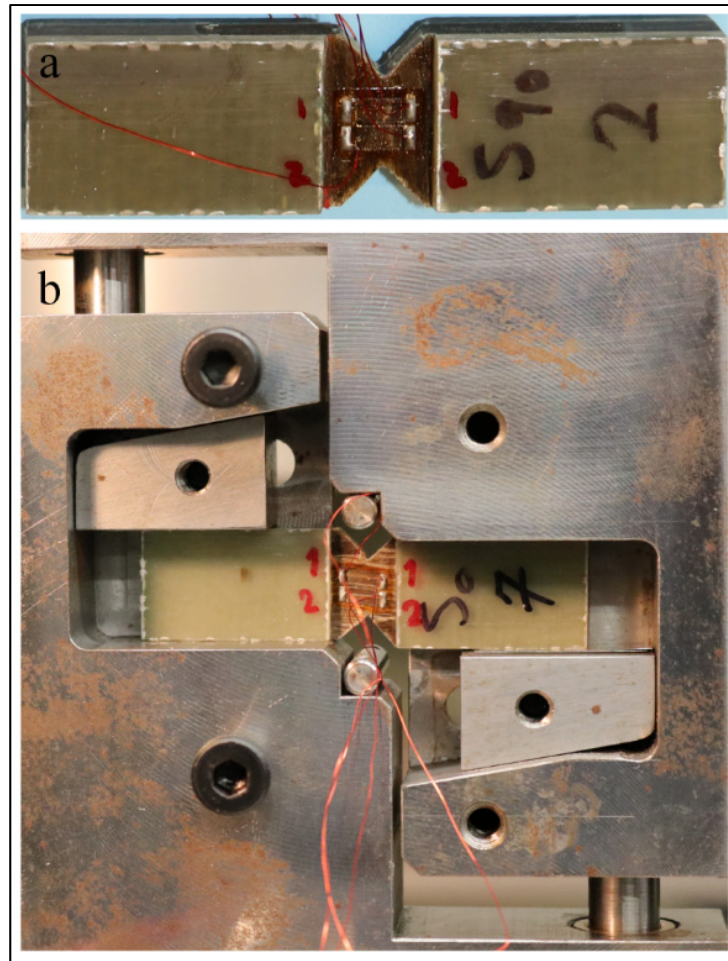
Figure 3.4 Typical shear test coupon (a) and Iosipescu
shear test fixture (b)

3.6   Results and discussion

3.6.1   Physical properties

3.6.1.1 Density

The results of the density measurement tests are shown in Table 3.2. The small coefficients of variations calculated from the measured values show that the tests were quite repeatable. Considering the influences of the variations in the constituent materials and fiber content on the density of composite, the results are in the range of the previous works (Oksman, 2001).

However, according to the findings of this study, Archimedes' method using water is not recommended for measuring the density of FFRP composites. Because the samples have to be weighted in a short immersion time to avoid absorption, this leaves air bubbles trapped at the surface of the coupon, thus leading to measure a lower immersing weight (W_{fl}) and, consequently, lower density values following Equation (3.3). Using ethanol as immersion fluid or the gas pycnometry method gives much more repeatable results. So, these methods are recommended.

Back calculation of the fiber density (ρ_f) using the rule of mixtures and based on $V_f = 0.41$, ρ_m = 1.09 g/cm^3 (following the supplier datasheet) and ρ_c = 1.281 g/cm^3 for the composite (from Table 3.2) gives ρ_f = 1.556 g/cm^3. This value is higher than ρ_f = 1.45 g/cm^3 that we considered at the beginning of the study (Table 3.1) based on the literature. Both of the values are in the range of recently reported density values for flax fiber (1.41 to 1.59 g/cm^3), measured using different methods (Amiri *et al.*, 2017; Goudenhooft *et al.*, 2019; Le Gall *et al.*, 2018; Lefeuvre, Bourmaud, & Baley, 2015).

Table 3.2 Measured density values and its variations

Method	Gas Pycnometry (with Helium)	Archimedes (with water)	Archimedes (with ethanol)
Density (g/cm^3)	1.2813[a]	1.2594[a]	1.2804[a]
STD[b]	0.0005	0.0065	0.0009
COV[c] (%)	0.04	0.52	0.07

[a] Mean value, [b] Standard deviation, [c] Coefficient of variation = STD/Mean value ×100

3.6.1.2 Specific Heat Capacity and Thermal diffusivity

The results of the C_p measurements are summarized in Table 3.3. The samples being small, composite homogeneity could vary from sample to sample, and an 8.6% coefficient of variation (COV) was observed for different test samples. However, the results are reasonably

repeatable, and the ASTM standard criterion was respected. There is no such data at room temperature for flax fiber composites in the literature for comparing the obtained results; nevertheless, Behzad et al. (Behzad & Sain, 2007) reported a $C_p = 2.07$ J/g/K for an acrylic thermoset/hemp composite (compared to 0.66 J/g/K in Table 3.3). Considering that acrylic has a C_p twice as high as epoxy, the results of Table 3.3 are in good agreement. Li et al. (X. Li, Tabil, Oguocha, & Panigrahi, 2008) studied the thermal properties of HDPE/treated-flax composites with 30% fiber content between 170°C and 200°C and found a $C_p = 2.25$ J/g/K at 170°C. Compared to $C_p = 0.6649$ J/g/K measured at $V_f = 41\%$ and room temperature in the present study, considering that HDPE has a doubled C_p (2.48 J/g/K compared to 1.11 J/g/K for epoxy) at 170°C and that C_p of the composite increases with temperature and decreases with V_f (according to Li's study), it is concluded that our result is in agreement with the literature findings.

The measured thermal diffusivity (α) is summarized in Table 3.3. The measurements gave good repeatability of the results. The results are comparable to $\alpha = 1.40 \times 10^{-7}$ m^2/S reported by Li et al. (X. Li *et al.*, 2008) for HDPE/flax, obtained at $V_f = 0.30$ and 170°C. Considering their observation regarding the drastic decrease of α with V_f, the influence of temperature on α (also shown in Table 3.3), and the higher thermal diffusivity of HDPE compared to epoxy, our results are in line with their finding and representative of the actual flax/epoxy composite.

Table 3.3 Thermal properties of FFREC

	Specific heat capacity (J/g/K)	Thermal Diffusivity (m^2/S)		
		25°C	80°C	135°C
Mean value	0.6649	1.35E-07	1.05E-07	9.40E-08
STD	0.057	1.50E-09	5.00E-10	5.00E-10
COV (%)	8.6	1.1	0.5	0.5

STD: Standard deviation; COV: Coefficient of variation

3.6.2 Mechanical properties

3.6.2.1 Tensile properties

Typical tensile loading curves for the longitudinal and transverse directions are shown in Figure 3.5. The curves of two specimens only are shown for clarity. As shown, they are very close to each other. A knee point appears at around 0.1% tensile strain, which corresponds to the nonlinear behavior of the flax fibers originating from the reorientation of micro-fibrils in the flax fibers and straightening of fibers during loading (Baley, 2002; Karine Charlet *et al.*, 2010; Liang *et al.*, 2015). After this point, a fairly linear response is obtained up to fracture.

In the transverse direction, the composite presents a bilinear loading curve with a mild slope change of around 0.25-0.3% strain. Baley et al. (Baley, Perrot, Busnel, Guezenoc, & Davies, 2006) observed an analogous behavior for flax/polyester composite. The elastic properties of the composite were determined according to the ASTM standard, in longitudinal direction using the second part of the curve (after the knee point), and in the transverse direction using the initial portion of the curve (before the slope change). The results are summarized in Table 3.4. Despite the inherent variable properties of flax fibers, and consequently of the flax/epoxy composites, a good repeatability of the results was obtained. As expected, the stiffness and strength are much higher in the fiber direction than counterparts in the transverse direction.

Table 3.4 Mechanical properties of FFREC in tension (1: fiber and 2: transverse direction)

	E_{11} (GPa)		v_{12}	σ_{11}^{max}	ε_{11}^{max}	E_{22}	v_{21}	σ_{22}^{max}	ε_{22}^{max}
	Initial [a]	Secondary [b]		(MPa)	(%)	(GPa)		(MPa)	(%)
Mean	30.04	21.26	0.373	298.39	1.35	4.24	0.054	14.73	0.38
STD	1.21	1.10	0.027	17.53	0.03	0.05	0.004	0.48	0.01
COV (%)	4.0	5.2	7.2	5.9	2.4	1.1	7.3	3.3	3.8

[a] Before the knee point; [b] After the knee point
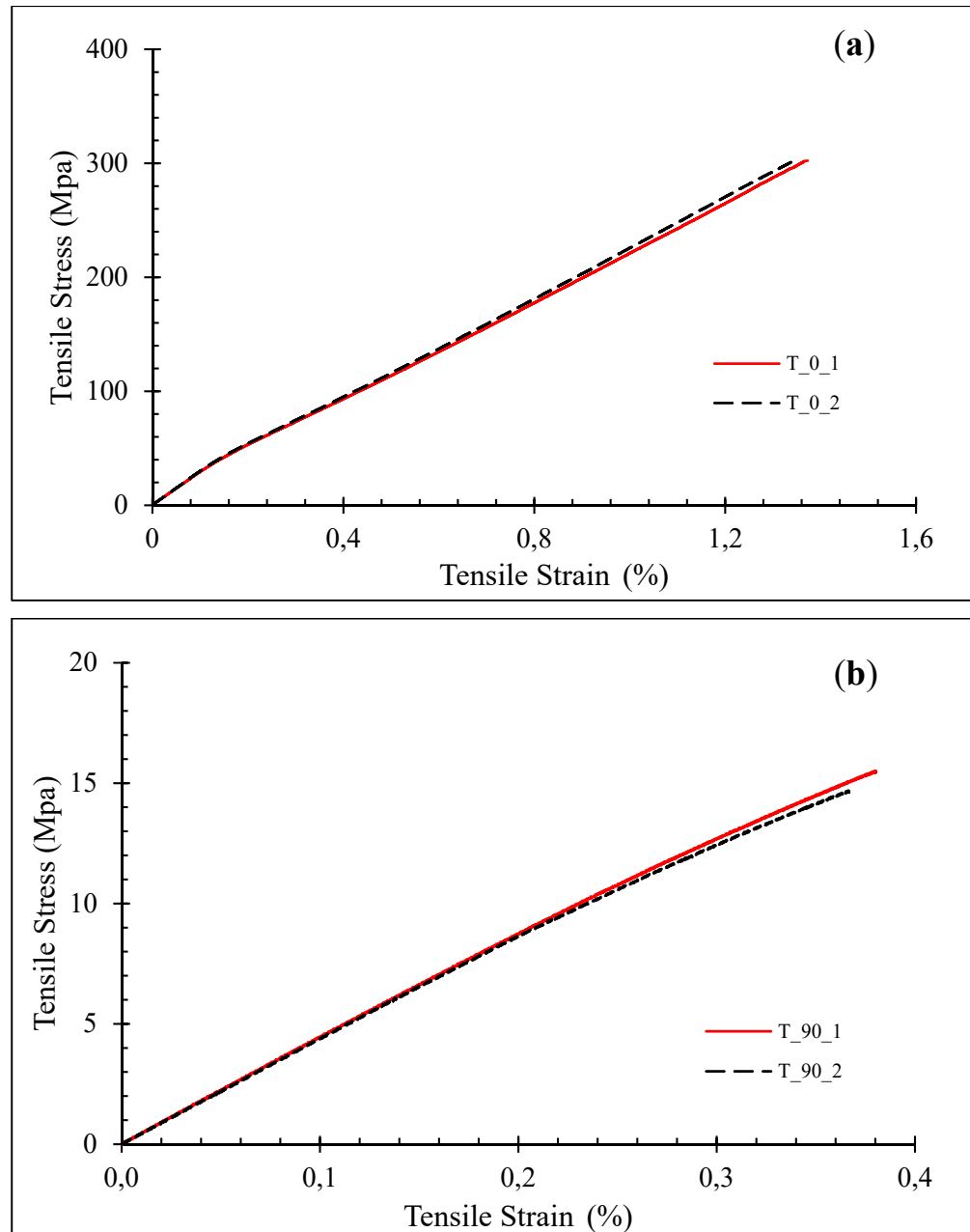
Figure 3.5 FFRC behavior in tension; longitudinal (a) and transverse directions (b)

The failure strains in both loading cases are lower than the values reported by Liang et al. for a flax/epoxy composite with $V_f = 43\%$ ($\varepsilon_{11}^{max} = 1.65$ and $\varepsilon_{22}^{max} = 0.62\%$) (Liang *et al.*, 2015). However, the values of the other properties are in a good agreement. This difference may be due to the higher fiber content and the variations in the fiber and matrix type, and the production methods used to fabricate the composite. Flax fiber properties vary significantly

depending on their origin; consequently, variation in fiber type can remarkably affect the composite properties (Coroller *et al.*, 2013). However, the results are in the range of values reported for similar flax/polymer composites (Baley *et al.*, 2006; Coroller *et al.*, 2013; El Sawi *et al.*, 2014; Oksman, 2001; Yan *et al.*, 2014).

Figure 3.6a shows a photograph of a fractured sample under tensile loading and the failure mechanisms in the fiber direction. It can be noticed that a serrated fracture surface, mainly generated by transverse fracture of fiber and matrix, is accompanied by longitudinal splittings subsequent to longitudinal matrix shear. The observed rupture is recognized as an acceptable failure mode by ASTM criteria, coded LGM(2) (ASTM, 2017). The longitudinal cracking results from the shear stress generated during failure between adjacent fiber yarns and adjacent layers.

In order to conduct a microstructural study and explore the fracture mechanisms, the fracture surfaces and fracture paths of the tested specimens were examined using a digital microscope (KEYENCE VHX-500F). Post-failure examinations of the split surface, shown in Figure 3.6b and Figure 3.6c, reveal an important amount of fiber pullout demonstrating a weak fiber-matrix interfacial bonding. The matrix is broken, and the flax fiber bundles are ruptured and splintered to smaller bundles and single fibers. The micrograph of longitudinal shear, Figure 3.6d, shows broken fiber bundles, matrix fracture, and flax fiber bundle pullout and fracture. Mohammad Khanlou et al. observed similar fracture mechanisms for flax/poly(lactic acid) bio-composites (Mohammad Khanlou *et al.*, 2018).

The failure path in the transverse direction under tensile loading is a straight line (Figure 3.7a) and is recognized as an acceptable failure mode by ASTM, code LGM (ASTM, 2017). Matrix fracture, fiber-matrix debonding, and flax bundle fuzzing are observed in this loading case (Figure 3.7b). Fiber bridging is happening due to crack crossing the flax bundles because of the slight misalignment of fibers with the normal direction to the loading axis and their different positions in different layers.
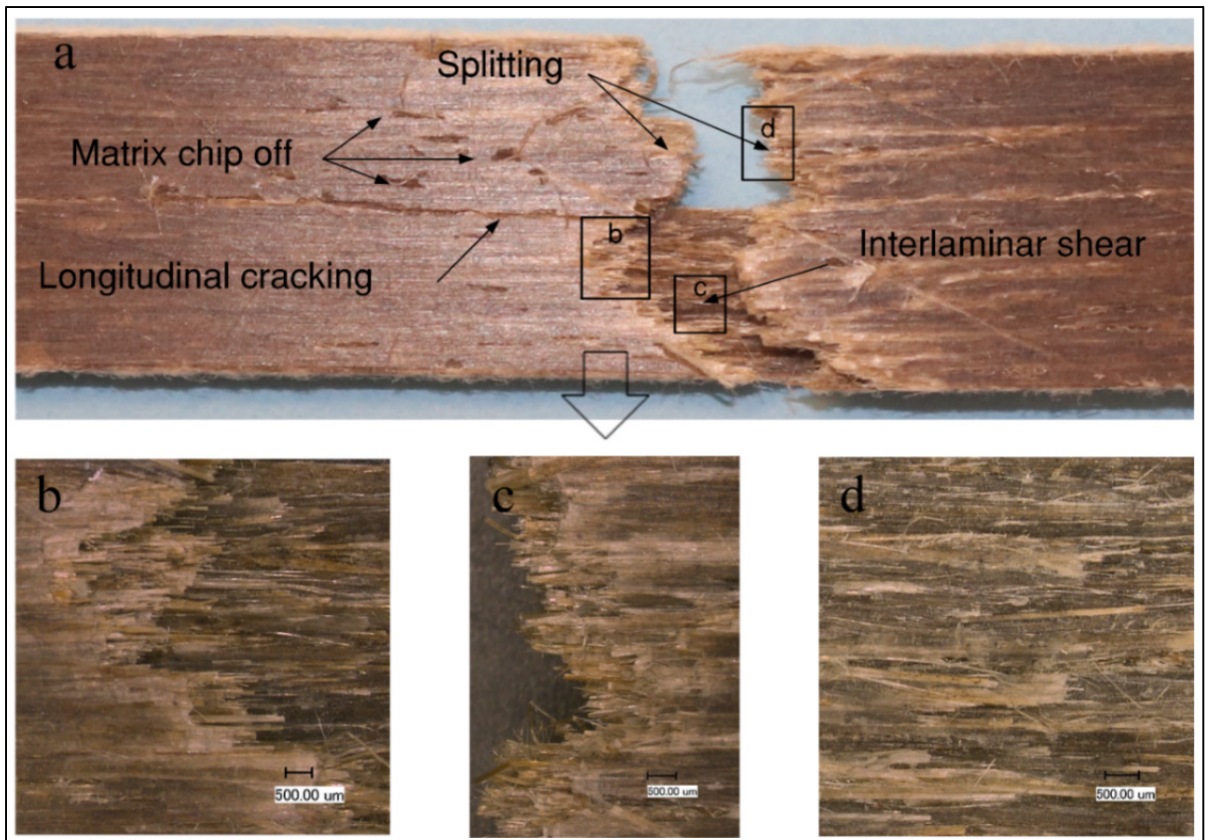
Figure 3.6 Fracture path in longitudinal tensile loading (a), fiber fracture and longitudinal shear (b), fiber pullout, fracture and fuzzing (c) and longitudinal shear (d)

Figure 3.7 Failure modes in transverse tensile loading; fracture path (a) and failure mechanisms (b)

3.6.2.2 Compressive properties

The responses of the UD flax/epoxy laminate to a compression force in the fiber and transverse directions are plotted in Figure 3.8. In the fiber direction, a linear behavior turning to nonlinear at around 0.3%–0.4% strain is observed. The bending of the specimen during compression was monitored using longitudinal SGs installed on both faces of the specimen. In the fiber direction, it is critical to remove the bending and buckling failure modes of the test specimen and measure the net strength in compression. In addition, the local compressive failure mechanism of a long fiber-reinforced composite, as accepted by the researchers, comprises a sequence of phenomena: a small fiber misalignment initiates fiber buckling; then the matrix supporting the fibers deforms plastically, deformation amplifying the instability of fibers; which fail successively by developing a kink band (Grandidier, Casari, & Jochum, 2012). This sequence of phenomena could also be promoted by kink bands already present in the fibers as fiber defects. These defects create weak spots and a slight deviation from the straight line (Muralidhar, 2013a). Therefore, initial small fiber deviations combined to kink bands may trigger premature micro-buckling of the fibers and failure of the composite. As a result, the actual value can be considered as a lower limit for this property that was here influenced by micro-buckling.

The failure modes and areas correspond to the accepted ones by ASTM and coded as KGM and BGM (ASTM, 2016) (Figure 3.9a, c, and e). Post-failure examinations of the specimen (Figure 3.9) show that the compressive failure modes in the fiber direction are one or two 45°-kink band, fiber failure, fiber-matrix debonding, and propagated delamination from the kink band. This combination of failure modes can explain the stress-strain curve of the composite. Before micro-buckling of the reinforcement, the composite behavior is linear. Then, when the micro-buckling occurs, along with the internal failure modes, its behavior turns to be nonlinear, with a rigidity dropping continuously with the occurrence of these modes. By the end of the test, the slope of the curve approaches zero, and the sample cannot support any further load and is considered failed. In the transverse direction, the composite presents an obvious bilinear response. In this case, where the matrix property is dominant, the composite presents a linear

behavior up to a strain of 1.3% (almost 80% of the deformation), after initiation of failure, the rigidity decreases, and the second part starts with a slightly lower slope ending to a somewhat brittle shear-failure. The compressive properties shown in Table 3.5 are determined using the data of the first parts of the graphs.
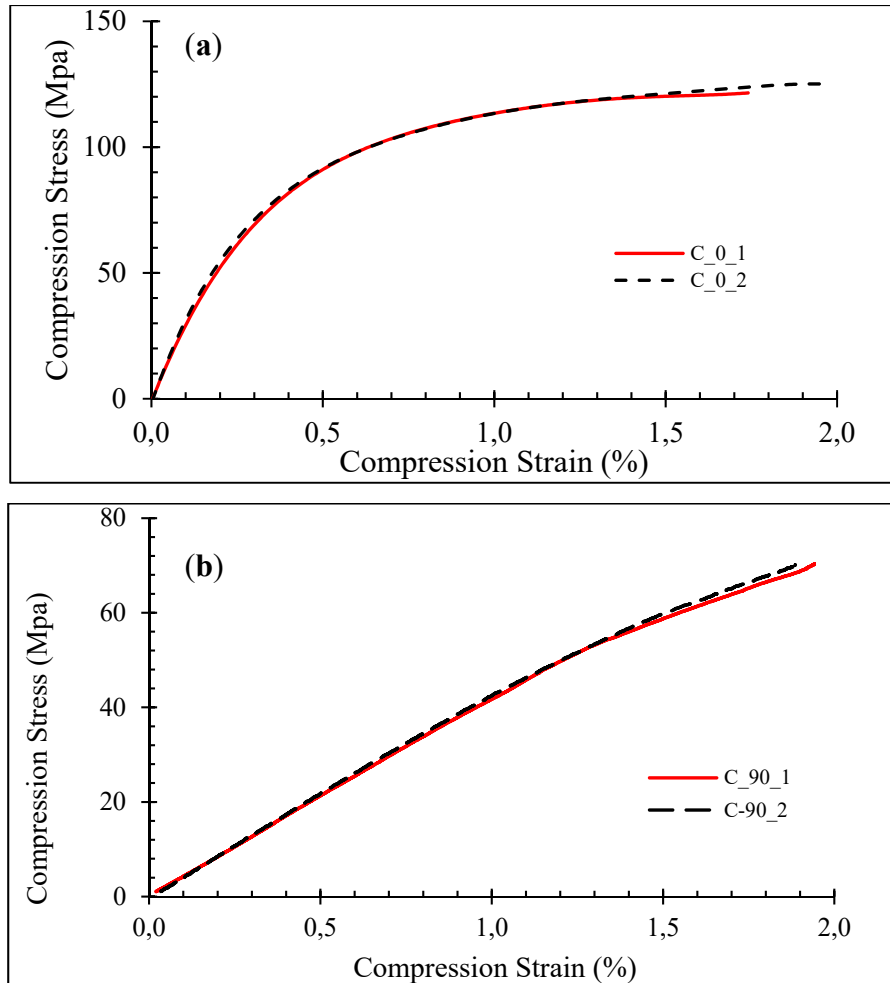
Figure 3.8 Behavior of composite under compressive load in fiber (a)
and Transverse directions (b)

The fractographic analysis shows that the transverse shear fracture in the transverse compressive loading occurs on a $30° \pm 5°$ fracture plane (Figure 3.10a), which is recognized as an acceptable failure mode by ASTM (ASTM, 2016) (Figure 3.9e). This angle is a material property for a UD laminate, and its typical value for synthetic UD laminates is reported as 37° (Davila, Camanho, & Rose, 2005). The corresponding angle for graphite-epoxy and glass-

epoxy composites are determined respectively, as $37° \pm 2°$ and $38°$ (Davila *et al.*, 2005). This fracture angle might be different for NFRCs; however, E. Petersen et al. (Petersen, Cuntze, & Hühne, 2016) reported fracture angles between $29°$-$37°$ for a T700GC carbon-epoxy UD laminate, which are very close to the observed angles in Figure 3.10a.
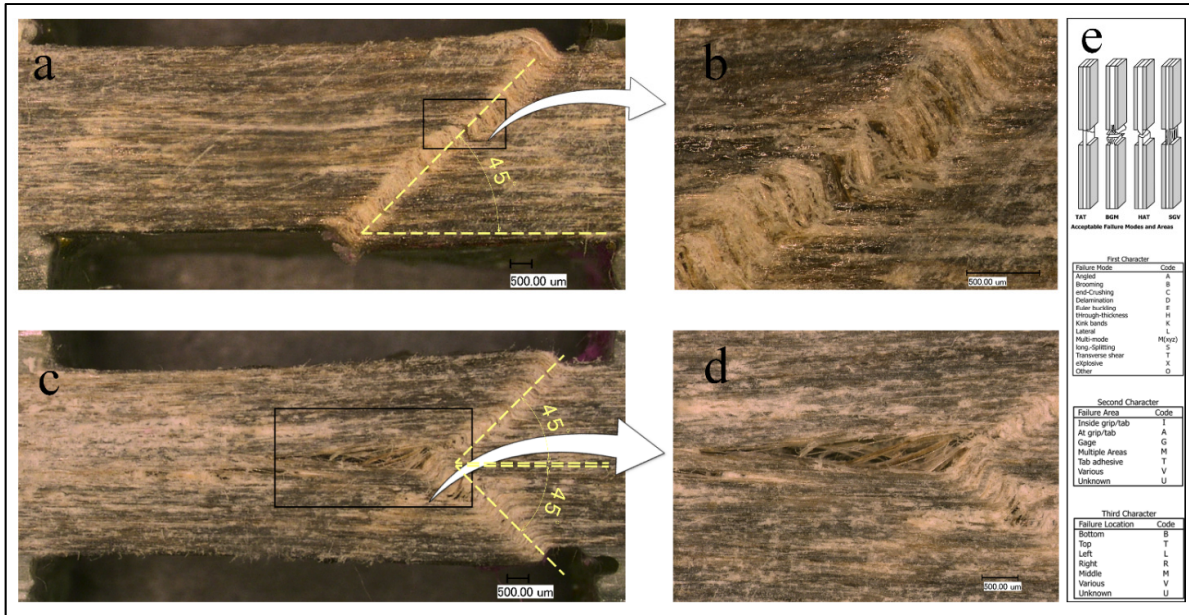
Figure 3.9 Failure modes in fiber direction under compression loading; Sample A (a, b), Sample B (c, d) and ASTM criteria (ASTM-International, 2016) (e)

Table 3.5 Mechanical properties of FFREC in compression (1: fiber and 2: transverse direction)

	E_{11} (GPa)	v_{12}	$\sigma_{11}{}^{max}$ (MPa)	$\varepsilon_{11}{}^{max}$ (%)	E_{22} (GPa)	v_{21}	$\sigma_{22}{}^{max}$ (MPa)	$\varepsilon_{22}{}^{max}$ (%)
Mean	24.12	0.431	126.05	2.02	4.44	0.054	72.02	2.10
STD	1.53	0.043	3.33	0.25	0.12	0.004	0.85	0.11
COV (%)	6.3	9.9	2.6	12.3	2.6	3.6	1.2	5.4
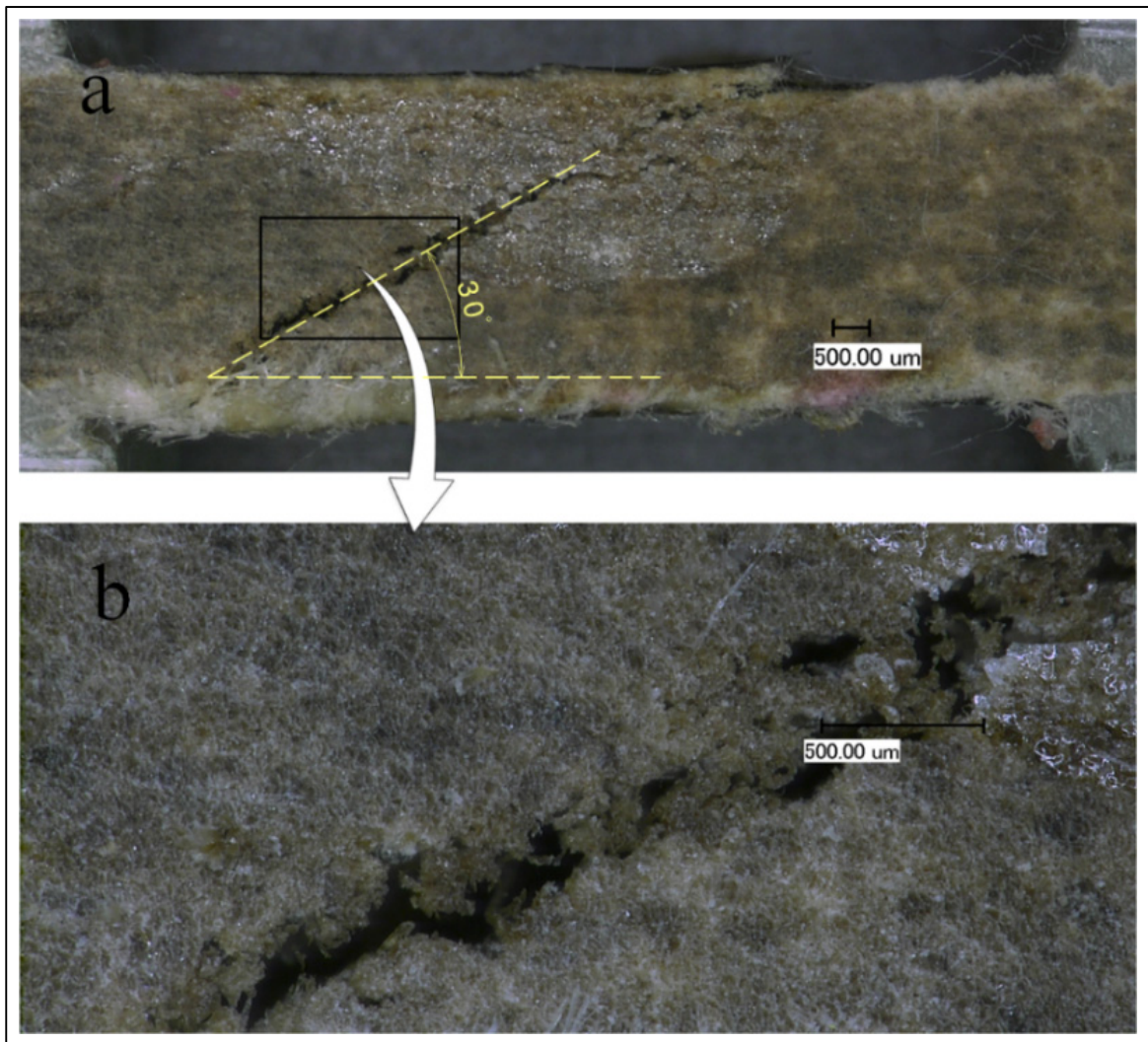
Figure 3.10 Failure modes in transverse direction under compression loading; failure
path in the gauge area (a) and failure modes (b)

There are limited data for equivalent composite to compare with the results presented in Table
3.5. However, the results shown are in the range of reported results for twisted flax fiber and
flax fabric/epoxy composite (Liang *et al.*, 2015; Mahboob, Chemisky, Meraghni, &
Bougherara, 2017). The STDs of the results are in a reasonable range; however, a 12.3% COV
is calculated for the ultimate strain in the fiber direction. This could be due to the unclear failure
location of the test specimen. Considering it was not possible to clearly establish the occurrence
of failure, it was determined using the stress-strain curves by considering failure as the stress
level approaching the flat (nearly horizontal) zone of the curve, where the load reaches its

maximum. This choice is based on the fact that the specimen cannot tolerate higher loads, so the constant load is due to crushing the failed material. According to the ASTM standard, the ultimate compression strength is also calculated based on the maximum load. Globally, the results are satisfactorily repeatable.

A 15% difference is observed between the Poisson's ratios measured in tension and compression loading for tests in the fiber direction. Theoretically, this material property should be identical in tension and compression loadings. Despite the difference in mean values of the property, the ranges of the measured values in this study are overlapping, i.e., 0.373 ± 0.027 and 0.431 ± 0.043 for tension and compression, respectively. Poisson's ratio is generally measured in tension only; therefore, this dissimilarity was not observed and discussed in previous studies in the literature. The difference could also be related to the complex structure of flax fibers containing microfibrils, which may induce different behavior in tension and compression. This issue has not been studied in the literature and needs to be investigated in more detail.

3.6.2.3 Shear properties

The in-plane shear properties of the FFREC were evaluated in the principal material directions. Figure 3.11a shows a typical load-displacement plot of a shear V-notched beam in the fiber direction. As can be noticed, it follows the pattern presented in the ASTM standard for the corresponding specimen (Figure 3.11c).

Figure 3.12a shows the photograph of a failed specimen tested in the fiber direction. According to ASTM, the observed failure mode is an accepted one and coded as HGN (Horizontal cracking at Gage section-between Notches, Figure 3.12c). The micrograph of the gage section shows that the root notch crack, described in the ASTM and observed by previous researchers (J. He, Chiang, Hunston, & Han, 2002), happened, and the horizontal cracks inducing the HGN failure mode can be recognized (Figure 3.13a). The corresponding slight load drop due to the root notch crack can be seen on the load-displacement graph (Figure 3.11a). Therefore, the

tests are meeting the requirements of the standard, and the results will be representing the composite shear properties.
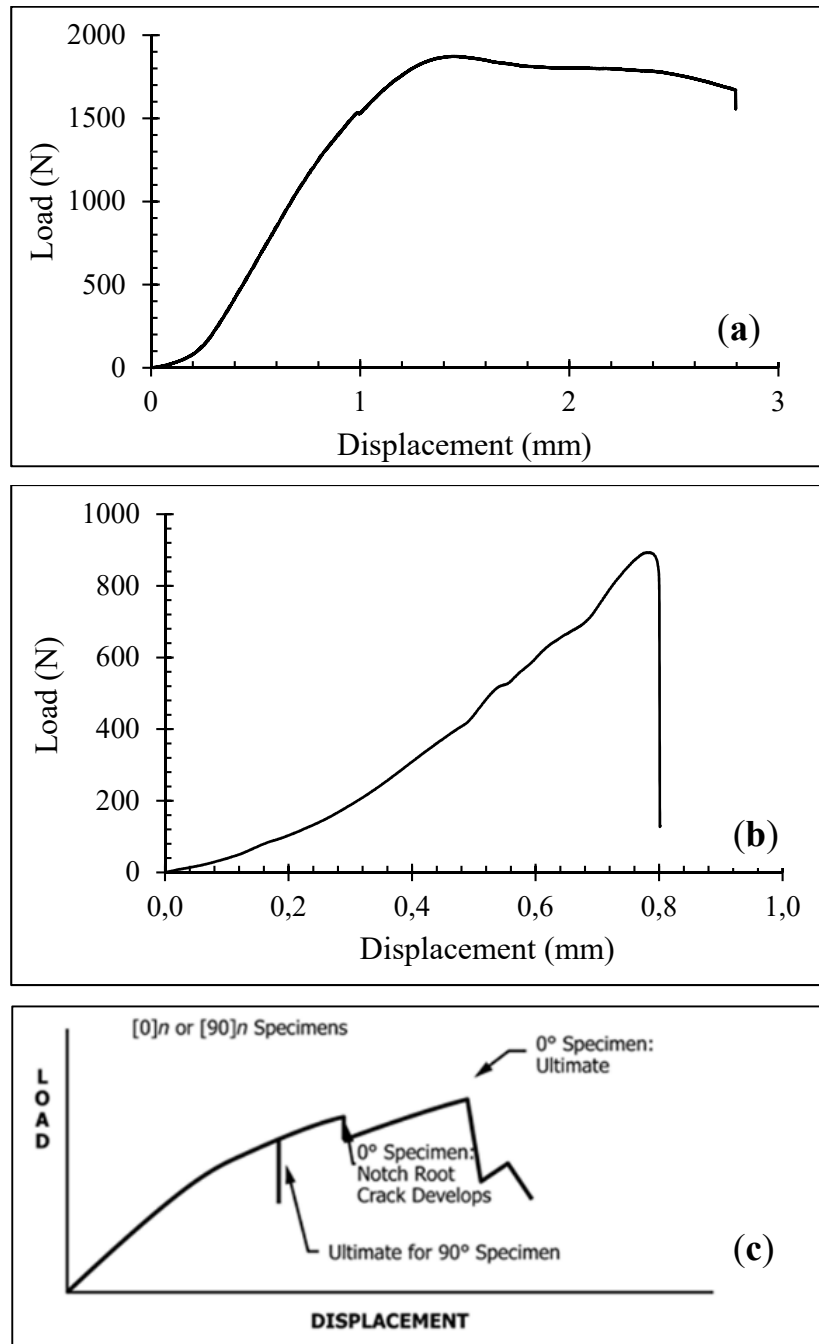
Figure 3.11 V-notched Beam load-displacement plots in;
longitudinal (a) and transverse (b) loadings; typical plots
from ASTM (ASTM, 2012) (c)
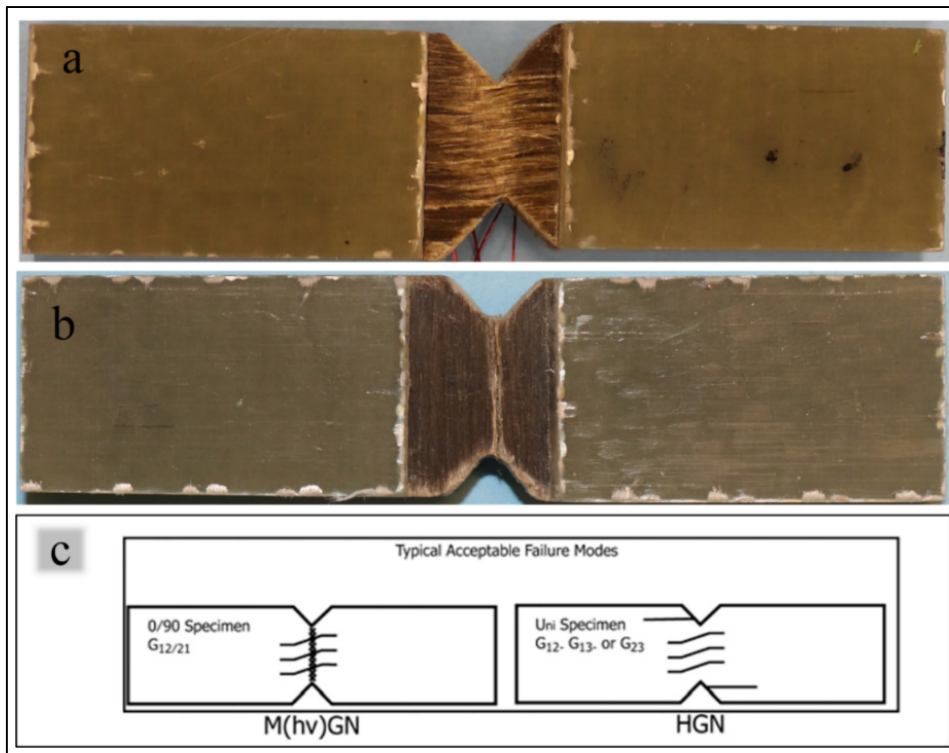
Figure 3.12 Shear failure mode in; longitudinal (a) and transverse (b) loadings, ASTM coding for acceptable failure modes (ASTM, 2012) (c)
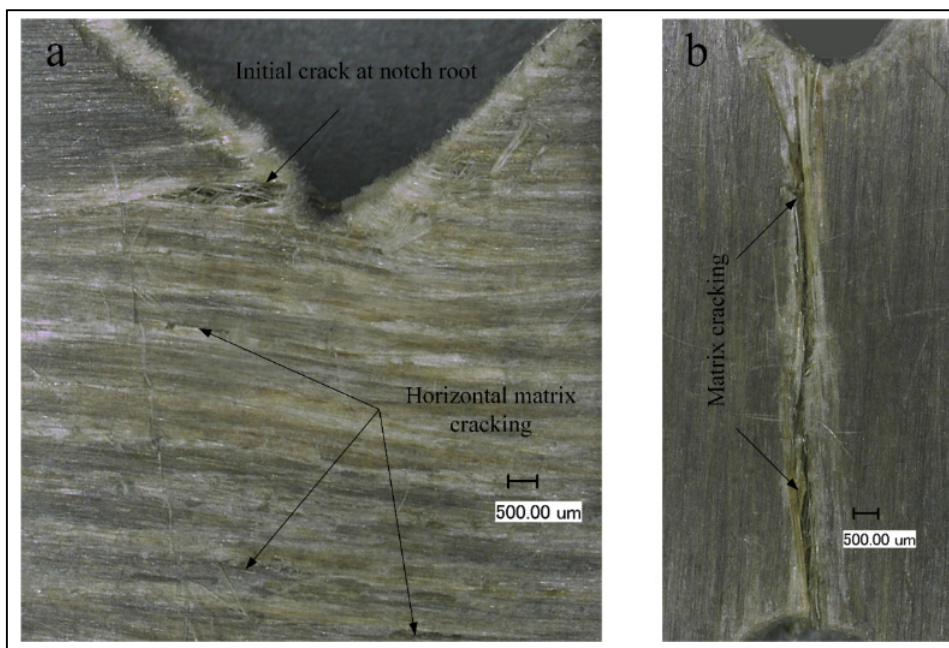
Figure 3.13 Shear failure modes in; longitudinal (a) and transverse directions (b)

The shear stress-strain curves of two typical specimens tested in the fiber direction are plotted in Figure 3.14a for the strain range that was recorded by the SGs installed on the beams. The material presents a ductile failure; at low strain levels, based on which the shear modulus (G_{12}) is determined, the material exhibits a linear behavior, nearly after 2% strain, a nonlinear response is recorded until the failure of SGs which happens above 5% strain (Figure 3.14a), and before the failure of the material. In this case, the failure strain (ε_{12}^{ult}) of the material is too large, and out of the functional range of conventional SGs, to be recorded; however, it is not required. According to ASTM, for this case, the ε_{12}^{ult} is considered at 5%, and the shear strength (τ_{12}^{ult}) is determined at ε_{12}^{ult}, as the lower of shear stress at 5% strain or ultimate load. The response of the composite to shear loading in the transverse direction is shown in Figure 3.11b and Figure 3.14b by load-displacement and shear stress-strain curves, respectively. The load-displacement curve follows the general trend presented in ASTM for 90° specimens with brittle failure, Figure 3.11c.

The photograph of a failed specimen is shown in Figure 3.12b. The observed failure modes correspond to the load-displacement curve shown in Figure 3.11b, which is an acceptable failure mode and coded as VGN (Vertical cracking-Gage section-between Notches) by ASTM (Figure 3.12c). Previous researchers observed similar failure modes for UD FRCs (J. He *et al.*, 2002; Pierron & Vautrin, 1998; Selmy, Elsesi, Azab, & Abd El-baky, 2012). As shown in this case, the material displays a brittle failure with a complex response, especially at higher deformations, but in the region where the transverse shear modulus (G_{21}) is calculated, the behavior is linear. This behavior was expected, as the epoxy matrix is directly solicited in shear in the transverse direction (El Sawi *et al.*, 2014) such that a more confined fracture is obtained. For this case, the shear strength and the maximum shear strain were determined at the ultimate load.
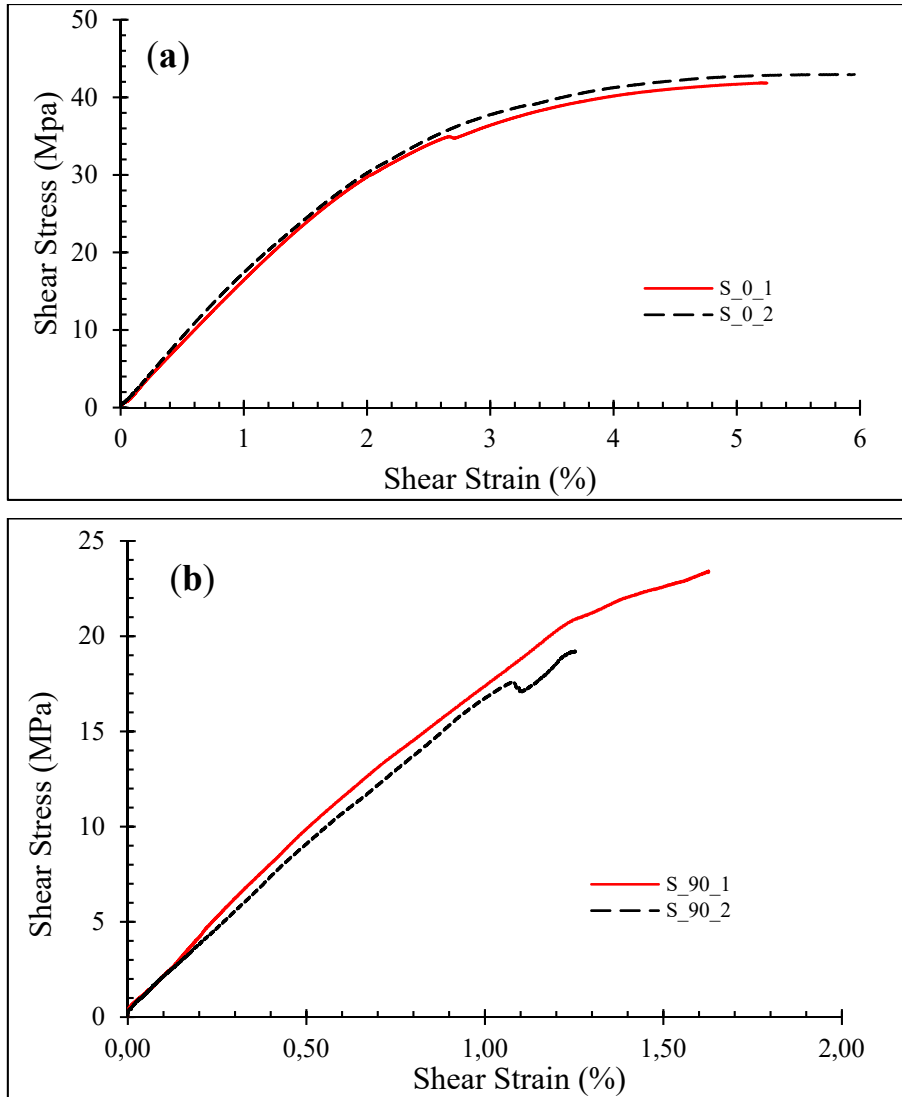
Figure 3.14 Shear behavior in longitudinal (a) and transverse
directions (b)

The material properties of the composite in shear loading are shown in Table 3.6. The variation
ranges are acceptable for this composite, considering it is reinforced with natural fibers
exhibiting high variability in the material properties. The measurements lead to higher shear
strength and higher failure shear strain in the fiber direction in comparison to those in the
transverse direction. However, the shear moduli (G_{12} and G_{21}) are very close, and considering
their STD; they can be regarded as equal. This similarity originates from the fact that shear
properties of composites are controlled mainly by the matrix and fiber-matrix interface (El
Sawi *et al.*, 2014). Since the interface bonding of the flax fiber-epoxy is weak, in both loading

directions, the dominant element determining the shear moduli is epoxy. This is shown by the micrographs of the failed specimens in Figure 3.13. It can be clearly observed that the primary failure modes are matrix fracture and fiber-matrix separation with a pre-failure debonding, spreading from the root of notch toward the tabs for the fiber-direction case, Figure 3.13a. Figure 3.13b shows the matrix fracture and fiber-matrix debonding as significant failure modes for transverse direction, spreading across the specimen width at the notch roots.

In the literature, mainly G_{12}, τ_{12}^{ult} and ε_{12}^{ult} of the flax composites are evaluated (El Sawi *et al.*, 2014; Gning, Liang, Guillaumat, & Pui, 2011; Liang *et al.*, 2015). A good correlation can be found between their results and the results of the current study; however, El Sawi et al. (El Sawi *et al.*, 2014) found higher τ_{12}^{ult} for treated flax fiber/epoxy composites processed with the compression molding and Autoclave method. The higher shear strength can be related to fiber treatment that improves the fiber-matrix bonding, which is dominant in the shear properties.

Table 3.6 Mechanical properties of FFREC in shear (1: fiber and 2: transverse direction)

	G_{12} (GPa)	τ_0^{max} (MPa)	ε_{12}^{max} (%)	G_{21} (GPa)	τ_{90}^{max} (MPa)	ε_{21}^{max} (%)
Mean	1.92	44.67	5.00	1.95	25.08	1.58
STD	0.16	2.10	0.00	0.14	2.93	0.17
COV (%)	8.49	4.70	0.00	7.39	11.69	10.88

Flexural properties

For flexural loading, the behavior in the longitudinal direction of fibers is shown in Figure 3.15, with the stress and strain calculated based on the ASTM standard for a three-point bending coupon. An initial linear behavior is observed up to 0.4%−0.5% strain, followed by a pronounced nonlinear curve with a gradually dropping slope at higher strains up to the brittle failure. Since the test specimens and configuration were prepared according to the ASTM standard, which is developed for synthetic fiber composites with higher stiffness and brittle behavior in comparison to NFRCs, the specimens exhibited large deflection to failure. The

effect of this large geometric deformation can be superimposed with composite progressive internal failures to form the nonlinear curve with the decreasing slope. The specimens exhibit a surface rupture on the lower layer with a serrated path (Figure 3.16a). The micrographs of the fracture area on the lower surface reveal fiber and matrix fracture, delamination, and some fiber pullouts (Figure 3.16b). No significant failure signs were observed on the upper surface; however, on specimen sides (cutting edges) many delamination and translaminar failures were observed (Figure 3.16c and d). The fracture mechanism corresponds to the final brittle failure shown in Figure 3.15. As observed for the two specimens shown, similar behaviors were obtained with almost the same failure strain. Sodoke et al. reported similar behavior for a plain weave flax/epoxy composite with $V_f = 0.45$; however, they observed higher failure strain and lower flexural modulus and strength values of about 3%, 8 GPa and 140 MPa, respectively (Sodoke, Laperrière, Toubal, & Khakestar, 2016). They measured an equivalent value of 8 GPa for tensile elastic modulus, which is also lower than the result of our study. The origin of this difference lies in the type of reinforcement structure, but their production process and testing procedure were also different.
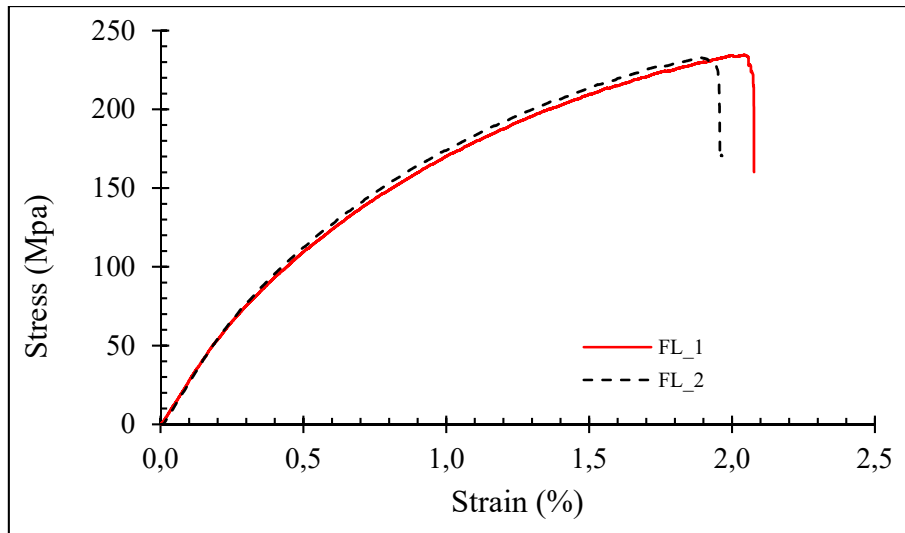
Figure 3.15 Flexural response of FFREC in the fiber direction
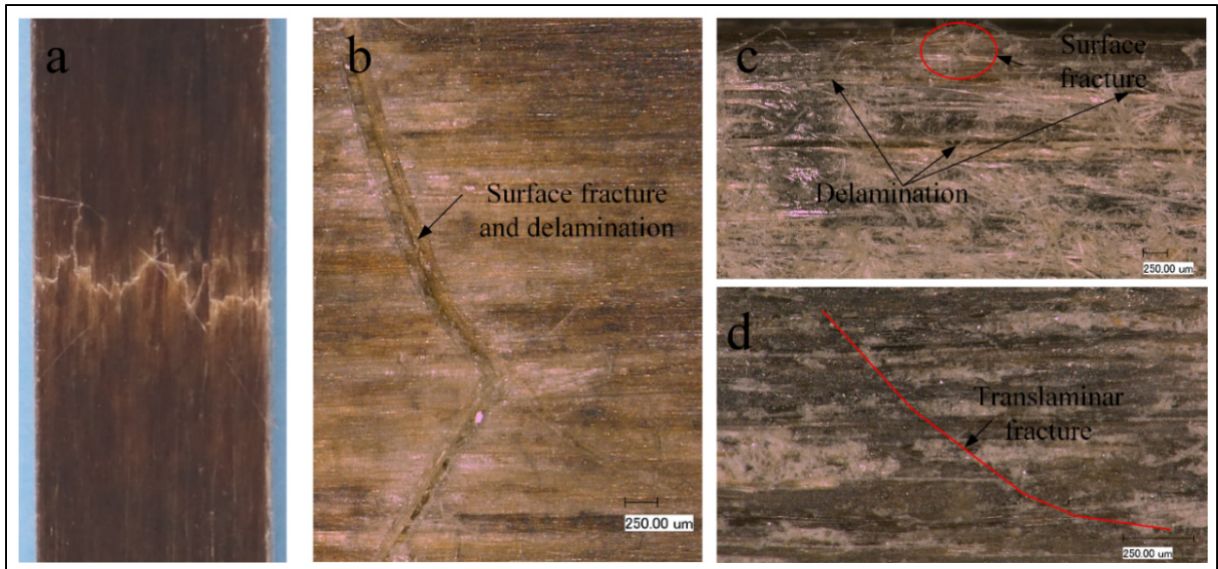
Figure 3.16 Failure modes in flexural loading; surface rupture/failure path (lower view) (a), failure modes at surface rupture (b), delamination and fracture in the lower layer (side view) (c) and connection of layer failures to form translaminar fracture (d)

The flexural properties are calculated based on ASTM D7264; the flexural modulus is calculated using the initial linear part of the testing curve (the flexural chord modulus in the standard), while the flexural strength and ultimate strain are determined based on peak load and corresponding deflection. Although the stress-strain curve is not linear up to the point of rupture, according to the standard, the results are valid, as the failures happen at 2% strain. The flexural properties are presented in Table 3.7. Small STD in the results demonstrates the repeatability and reproducibility of the results. The flexural modulus is in good correlation with elastic modulus in tension and compression, but the flexural strength value lies between that of the tensile and compression tests. This might be due to the procedure applied in the standard for the calculation of flexural strength, which is based on homogeneous beam theory for isotropic materials, whereas different behavior in tension and compression should be considered for the UD-NFRC laminates in the present case. The nonlinear behavior in the flexural loading curve can be expected considering the curves of Figure 3.5a and Figure 3.8a with the fact that flexion is a combination of tension and compression. The results for the flexural stiffness and strength are in close relationship with the results of El Sawi et al. (El Sawi *et al.*, 2014) for UD flax/epoxy composites and Moudood et al. (Moudood *et al.*, 2019b)

for flax/bio-epoxy composites. Poilane et al. (Poilâne *et al.*, 2009) found very close results for flexural modulus of flax-epoxy prepregs, whereas they reported higher ultimate stress and ultimate strain values. This is related to the much higher fiber content ($V_f = 54\%-66\%$) in their material. Therefore, the actual results are in line with those obtained by these researchers.

Table 3.7 Mechanical properties of FFREC in flexion (fiber direction)

	Flexural Modulus (GPa)	Flexural Strength (MPa)	Ultimate Strain (%)
Mean Value	24.77	236.19	2.08
STD	0.71	4.11	0.07
COV (%)	2.88	1.74	3.35

3.6.3   Conclusion

In summary, the present study aimed at evaluating the material properties of the UD flax/epoxy laminates fabricated with precisely controlled fiber content and quality. Test coupons were cut from $[0]_7$ and $[0]_{12}$ laminates, molded by RTM method, and tested according to the test methods developed for extracting material properties, reusable for design, numerical simulation, and comparison purposes.

Physical properties, such as density, specific heat capacity, and thermal diffusivity, were investigated, and the obtained average values for them are respectively 1.28 (g/cm^3), 0.6649 (J/g/K), and 1.35E-07 (m^2/S). Also, the mechanical properties of the FFREC in tension, compression, shear, and flexion were determined and measured. For instance, the average values of the elastic modulus [strength] in tension and compression, shear modulus [strength], and flexural modulus [strength] of the composite (in fiber/transverse directions) are respectively 21.26/4.24 GPa [298.39/14.73 MPa], 24.12/4.44 GPa [126.05/72.02 MPa], 1.92/1.95 GPa [44.67/25.08 MPa], and 24.77 GPa [236.19 MPa]. The resulting stress-strain curves unveiled the nonlinear or bilinear behavior of the composite, especially when loaded in

the fiber direction. However, for each type of test, the response of the specimens was very similar, and the corresponding curves were very close to each other. This behavior is well correlated with the structure of the composite and can be interpreted as the behavior of the material. Overall, our results are in the range of those reported in the literature, when available, and the reasonable variations in the measurements demonstrate that the results are reproducible. The COV is generally below 12%, except for failure strain in the fiber direction for compression loading, which is initiated from the fact that in this loading case, there is no clear failure point for the specimen.

Collectively, the results are consistent with the definitions of material property, and the data generated can confidently be considered as the material property of the unidirectional flax composite. These results provide a basis for the engineering design field and numerical simulation of this material by FEM. In order to cover the required material properties for FEM analysis of these composites with orthotropic configuration, other experimental studies are currently underway, along with numerical analysis of FFREC machining, as part of the next steps of our ongoing work.

CHAPTER 4

A STUDY OF THE INTERLAMINAR FRACTURE TOUGHNESS OF UNIDIRECTIONAL FLAX/EPOXY COMPOSITES

Yousef Saadati [1], Jean-François Chatelain [1], Gilbert Lebrun [2], Yves Beauchamp [3], Philippe Bocher [1] and Nicolas Vanderesse [1]

[1] Mechanical Engineering Department, École de technologie supérieure, 1100 Notre-Dame West, Montreal, QC H3C 1K3, Canada
[2] Mechanical Engineering Department, Université du Québec à Trois-Rivières (UQTR), 3351 Boul. des Forges, Trois-Rivières, QC G9A 5H7, Canada
[3] McGill University, 845 Sherbrooke Street West, Montreal, QC H3A 0G4, Canada

4.1 Abstract

Having environmental and economic advantages, flax fibers have been recognized as a potential replacement for glass fibers as reinforcement in epoxy composites for various applications. Its widening applications require employing failure criteria and analysis methods for engineering design, analysis, and optimization of this material. Among different failure modes, delamination is known as one of the earliest ones in laminated composites and needs to be studied in detail. However, the delamination characteristics of unidirectional (UD) flax/epoxy composites in pure Mode I has rarely been addressed, while Mode II and Mixed-mode I/II have never been addressed before. This work studies and evaluates the interlaminar fracture toughness and delamination behavior of UD flax/epoxy composite under Mode I, Mode II, and Mixed-mode I/II loading. The composites were tested following corresponding ASTM standards and fulfilled all the requirements. The interlaminar fracture toughness of the composite were determined and validated based on the specific characteristics of natural fibers. Considering the variation in the composite structure configuration and its effects, the results of interlaminar fracture toughness fit in the range of those reported for similar composites in the literature and provide a basis for the material properties of this composite.

Keywords: flax-epoxy composite; interlaminar fracture energy; fracture toughness; delamination; Mode I; Mode II and Mixed-mode I–II interlaminar fracture; critical energy release rate

4.2   Introduction

In the recent past decades, since the 1990s, the increasing public environmental awareness and commencement of new legislation are demanding more sustainable and ecologically efficient products (Gurunathan *et al.*, 2015; Lotfi *et al.*, 2019; Mohanty *et al.*, 2000; Netravali & Chabba, 2003; Pil *et al.*, 2016; Ramesh *et al.*, 2017; Sanjay *et al.*, 2019). Synthetic glass and carbon fiber-reinforced polymer composites (FRCs) have high performance and are extensively applied in different industrial sectors, but they are not environment-friendly (Netravali & Chabba, 2003; Rajak, Pagar, Menezes, & Linul, 2019; Shekar & Ramachandra, 2018); thus, environmentally sustainable replacements are required. Numerous research efforts have been dedicated to finding a sustainable substitute for synthetic FRCs, and have confirmed that plant-based natural fiber-reinforced polymer composites (NFRCs) are the most promising alternatives (to petroleum-based FRCs) for many applications (Bodros *et al.*, 2007; Chandrasekar, Ishak, Sapuan, Leman, & Jawaid, 2017; Chandrasekar *et al.*, 2019; Cristaldi *et al.*, 2010; Dicker *et al.*, 2014; Gurunathan *et al.*, 2015; Joshi, Drzal, Mohanty, & Arora, 2004; Pickering *et al.*, 2016; Pil *et al.*, 2016; Ramesh *et al.*, 2017; Yan *et al.*, 2017). Having many advantages over man-made FRCs such as improved sustainability and competitive properties at a lower cost, NFRCs have attracted much attention worldwide and have penetrated the composites world with a rapidly extending industrial applications from packaging to structural construction components (Cristaldi *et al.*, 2010; Dicker *et al.*, 2014; Fuqua *et al.*, 2012; Habibi *et al.*, 2017a; Lotfi *et al.*, 2019; Sanjay *et al.*, 2019; Darshil U Shah, 2013; Yashas Gowda *et al.*, 2018). Replacing the engineered FRCs with fully biodegradable composites is not yet an economically and mechanically desirable solution in many applications; nevertheless, the synthetic polymers reinforced with natural fibers to produce economic and partially biodegradable composites can cover the requirements of a wide variety of applications and have been a viable alternative for petroleum-based FRCs (John & Thomas, 2008; Netravali &

Chabba, 2003; Ramesh *et al.*, 2017). For example, flax, hemp, and ramie fibers, placed within the category of plant-based bast fibers, are the most widely used reinforcement in NFRCs, offering comparable mechanical properties to glass fiber-reinforced polymer composites GFRPs) (Ahmad *et al.*, 2015; Fuqua *et al.*, 2012; Pickering *et al.*, 2016; Ramamoorthy *et al.*, 2015; Ramesh, 2019). Among them, flax fibers have excellent performance, and many manufacturers are interested in using them in NFRCs for various applications (Chandrasekar *et al.*, 2019; Goudenhooft *et al.*, 2019; Habibi, Laperrière, Lebrun, & Chabot, 2016; Habibi, Lebrun, & Laperrière, 2017b; Khanlou *et al.*, 2018; Khanlou *et al.*, 2017; Mohammad Khanlou *et al.*, 2018; Moudood *et al.*, 2019a; Moudood *et al.*, 2019b; Moudood *et al.*, 2018; Rajak *et al.*, 2019; Darshil U. Shah *et al.*, 2013; Yan *et al.*, 2014; Yan *et al.*, 2017). Also, epoxy resin, a thermoset polymer matrix, offers high mechanical performance and durability and is the most commonly used matrix to produce flax fiber-reinforced polymer composites (FFRCs) (Yan *et al.*, 2014). Furthermore, the application of a unidirectional (UD) or optimally woven reinforcement structure is a primary factor in maximizing the structural performance of FFRCs (S. Goutianos & Peijs, 2003; S Goutianos, Peijs, Nystrom, & Skrifvars, 2006); therefore, UD flax fiber-reinforced epoxy composites (FFRECs) are of outstanding importance and are used ubiquitously in the industry.

There are, however, some downsides to extending their application field, for instance, workpiece defects in the machining process, required for complex components, and in-service degradation when exposed to a humid (harsh) environment (Lotfi *et al.*, 2019; Moudood *et al.*, 2019b). Accordingly, FFRECs have been the subject of several pieces of research, trying to explore their properties and enhance their performance and durability to resolve these drawbacks, aiming at facilitating their applications (El Sawi *et al.*, 2014; Khanlou *et al.*, 2017; Lefeuvre *et al.*, 2015; Pil *et al.*, 2016; Yan *et al.*, 2014; Yan, Chouw, & Yuan, 2012; Jinchun Zhu *et al.*, 2013).

One of the commonly observed and major damage phenomena in laminated composites is the separation of two adjacent laminae (plies), which is known as interlaminar failure or delamination damage. This failure mode is the primary challenge for the laminated FRCs that

generally affects the in-service functionality of the component by reducing its overall stiffness and load-bearing capacity and subsequently leading to the failure of the entire component (Chen *et al.*, 2014; Nasuha *et al.*, 2017; Tay, 2003). It might form through the production process and exist as a defect in the composite, occur under different loadings and environmental conditions, or incur during machining operations, particularly drilling (Almansour *et al.*, 2017a, 2018; Nassar *et al.*, 2017). In fracture mechanics, the interlaminar failure, according to the relative displacement of crack surfaces, has been classified into three fracture modes: opening or tensile mode (Mode I), in-plane shear or sliding mode (Mode II), and out-of-plane shear or tearing mode (Mode III) (Anderson, 2017; Tay, 2003). Figure 4.1 (Anderson, 2017) illustrates the crack propagation caused by different modes of failure and the corresponding loadings acting on the cracks. Delamination can initiate and propagate due to any of these fracture modes or any combinations of them (mixed modes).
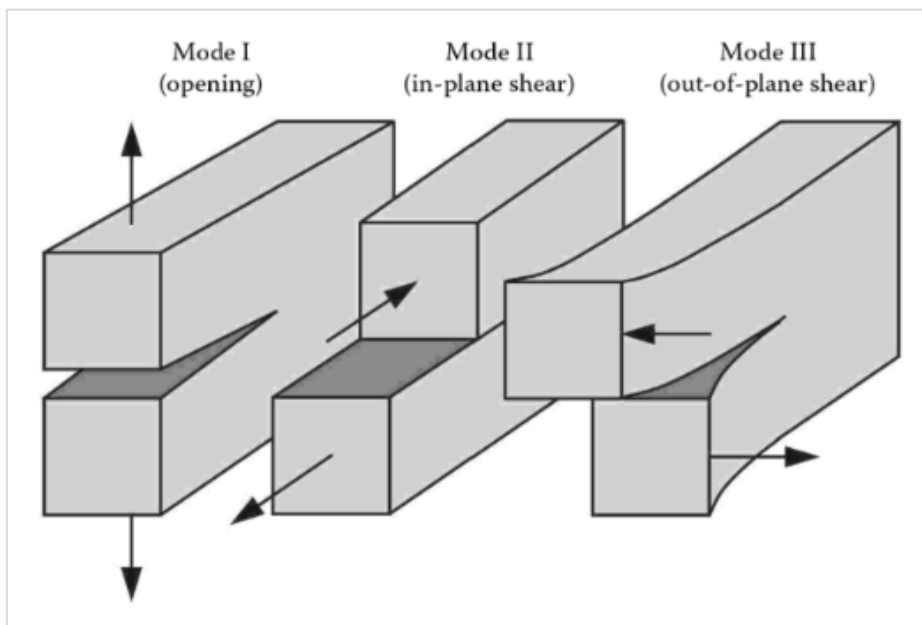
Figure 4.1 Fracture modes and applied loadings (Anderson, 2017)

The resistance of the material to crack propagation, or to delamination damages in composite laminates, is known as interlaminar fracture toughness (IFT) (Anderson, 2017). The Linear Elastic Fracture Mechanics (LEFM) approach, initially developed for isotropic materials, has

been successfully adopted and applied as a practice to characterize the IFT of the laminated FRCs (Walker & Jamasri, 1995; Y. Zhu, 2009). For fracture analysis, LEFM assumes an elastic material behavior for the whole body, except for a contained damage zone around the crack tip (which is a provision for the validity of the results). The IFT is a fundamental material property and can be determined based on either the Stress Intensity Factor (K_C) or the Critical Strain Energy Release Rate (G_C) of the material; the latter is commonly named Interlaminar Fracture Energy (IFE). They are, respectively, a measure of the stress intensity level and energy required for an increment of the crack growth (Anderson, 2017). For the isotropic, homogeneous, and relatively brittle metallic materials, IFT depends on the energy dissipation at the crack tip and can be characterized by K_C. However, for FRCs, the stress field in the vicinity of the crack tip is more complicated, and IFT is affected by the result of energy losses of different failure mechanisms such as matrix cracking, fiber fracture, fiber pullout, and fiber-matrix debonding (M. S. Prasad *et al.*, 2011; Y. Zhu, 2009). Therefore, G_C is commonly used for the determination of IFT and the study of delamination in FRC laminates for different failure modes (ASTM, 2013a, 2019a, 2019b; Nasuha *et al.*, 2017; M. S. Prasad *et al.*, 2011). By comparing the energy release rate (G) for a loading case to the G_C of the material, the capability of the body to resist crack extension can be assessed.

Ever-growing applications of laminated NFRCs and their penetration into structural applications, as well as the vital role of delamination in these composites, necessitate the investigation of the interlaminar fracture behavior and determination of IFE of these materials. IFT, as a primary property of a material, is required for engineering design purposes as well as numerical analysis methods such as the Finite Element Method (FEM). The interlaminar fracture of the synthetic FRCs under different modes of failure has been extensively investigated, and its state of the art has been comprehensively reviewed by many authors (Nasuha *et al.*, 2017; Ooi *et al.*, 2019; M. S. Prasad *et al.*, 2011; Tay, 2003; Y. Zhu, 2009). However, in the literature, limited work has been documented addressing the interlaminar fracture behavior of the laminated NFRCs, particularly FFRECs that show better toughness (Bensadoun *et al.*, 2017). Wong et al. (Wong, Shanks, & Hodzic, 2004) studied the influence of polymer modification on IFT of a randomly oriented-flax/poly(L-lactic acid) composite and

noted that by adding hyperbranched polymers (HBPs) to the matrix, G_{IC} of the composite significantly increased: from 38.9 J/m^2 for the original composite to 115 J/m^2 for the composite with the highest volume of HBP. Investigating the properties of a hybrid flax/glass UD-fabric (twisted flax yarns) reinforced phenolic resin composite, Zhang et al. (Zhang *et al.*, 2013) measured G_{IC} = 550 J/m^2 for flax composite that increased by hybridization to 560 J/m^2 for [(flax/ glass)$_n$]$_s$ composite. Their study shows that adding off-center plies of different fibers to the laminate will change the IFT, although the delamination is happening between the same type of composite plies. Li et al. (Y. Li *et al.*, 2005) investigated the effect of fiber surface treatment on the fracture properties of sisal-fabric/vinyl-ester composites with a fiber volume fraction (V_f) of around 32% ($V_f \approx 0.32$) and observed significant improvements in fracture energies of Mode I (G_{IC}) and small increases in that of Mode II (G_{IIC}) in comparison to the untreated system. While G_{IC} of the permanganate-treated fiber experienced the most significant improvement. The authors followed ASTM D5528 and measured the G_{IC} values of 320.5/1158.7 [888.0/1682.2] J/m^2, and G_{IIC} values of 2141.0 [2384.7] J/m^2 for the crack initiation/propagation of untreated and [permanganate-treated] sisal composites. In an experimental study, Chen et al. (Chen *et al.*, 2014) investigated the potential of carbon nanotube buckypaper interleaf for improving the IFT of flax-fabric/phenolic resin composites with $V_f \approx 0.73$. They followed ASTM D5528 and tested some partially and fully interleaved laminates at the mid-plane as well as laminates without interleaf for IFT. They observed a 26% [22%] and 29% [51%] increase in initiation $G_{IC,}$ and [propagation G_{IC}], respectively, for partially and fully interleaved composite in comparison to those of the original one ($\approx$4.4 and [$\approx$5.6] kJ/m^2) and related them to the extensive favorable fibrillations observed in the interleaved laminates. Trying to enhance the IFT of flax-fabric/epoxy composite of V_f = 0.60, Li et al. (Y. Li *et al.*, 2015) interleaved them at the mid-plane with chopped flax yarns of different lengths and content and followed ASTM D5528 to evaluate their G_{IC}. The authors observed a 4% to 31% improvement in the propagation G_{IC}, with the maximum increase for the moderate length and content of the chopped yarns, compared to that of the original composite, G_{IC} =1.40 kJ/m^2. It should be noted that they have used Modified Compliance Calibration method but have stated that used Modified Beam Theory (MBT). Ravandi et al. (Ravandi *et al.*, 2016a, 2016b; Ravandi *et al.*, 2018) conducted experimental investigations,

according to ASTM D5528, and numerical analysis, using FEM, to study and predict the effects of through-the-thickness stitching and reinforcement architecture on the G_{IC} of the UD ($V_f \approx 0.31$) and woven fabric ($V_f \approx 0.40$) FFRECs. The authors tested double cantilever beams (DCBs), according to ASTM D5528, to determine the G_{IC} of the FFRECs as well as UD-glass/epoxy ($V_f = 0.60$) composites, and observed that average G_{IC} of the UD-glass/epoxy was less than half of that of unstitched UD-FFRECs ($G_{IC} \approx 1.3$ kJ/m^2). Also, their findings showed that the average G_{IC} value of the UD-FFREC was three times lower than that of woven-FFRECs ($G_{IC} \approx 3.2$ kJ/m^2), and generally, stitching with flax yarns induced continuous improvement in IFT of the laminates, increasing with stitch areal fraction to a maximum of 21% for the highest investigated level (of aerial fraction). Besides, they reported that their FEM results agreed with the experimental ones giving the G_{IC} values of 0.771 and 1.25 kJ/m^2, respectively, for the crack initiation and propagation of UD-FFRECs as well as 0.671 kJ/m^2 for the G_{IC} value of glass/epoxy composite. Bensadoun et al. (Bensadoun *et al.*, 2017) tested some FFRECs reinforced with seven different fiber configurations; i.e., one plain weave, two twill weaves (low/high twist), a twisted-yarn-fabric cross-ply and an untwisted-fiber cross-ply architecture (cross-ply laminates were tested in both 0°/90° directions), to investigate the effect of the reinforcement architectures on the G_{IC} and G_{IIC} of the composites with $V_f = 0.40$. In terms of delamination fracture, their composites with untwisted-fiber cross-ply reinforcement denoted as UD [90,0], has a 0°/0° ply interface at the mid-plane of the laminate and is the closest one to the UD-FFRECs assessed in the current study. They reported initiation G_{IC} values between 457 J/m^2 for plain woven and 777 J/m^2 for twisted-yarn-fabric cross-ply composite when tested in [90,0] direction, as well as $G_{IC} = 496$ J/m^2 for UD [90,0] tests. At the same time, the propagation values of G_{IC} vary from 663 J/m^2 for UD [90,0] to 1597 J/m^2 for the low-twist twill-woven composites. Besides, they obtained G_{IIC} values between 728 J/m^2 for UD [90,0] and 1872 J/m^2 for plain weave laminates. The authors named the cross-plied twisted-yarn-fabric (with 90% of yarns in the longitudinal direction and 10% along the transverse direction) and the UD-untwisted-fiber architecture respectively "quasi-UD" and "UD" architecture, whereas, their interlaminar fracture behavior could be different with those of UD laminates, where all plies lay in one direction. Therefore, the results may not coincide exactly with the results of UD laminates. In two different works, Almansour et al. reported

their findings of the effect of water absorption on the G_{IC} (Almansour *et al.*, 2017a) and G_{IIC} (Almansour *et al.*, 2018) of the woven flax ($V_f = 0.31$) and woven flax/basalt (basalt plies in the skin of the laminates and overall $V_f = 0.33$) reinforced vinyl-ester composites in [±45°] arrangement. Their DCB test results showed that upon immersion in water, the initiation and propagation G_{IC} of the flax/vinyl-ester, as well as the initiation G_{IC} of flax/basalt hybrid composites, decreased by 27%, 10%, and 23%, respectively. In contrast, the propagation G_{IC} of flax/basalt hybrid composites increased by 15%. They have documented the average initiation/propagation G_{IC} values of 3870/12093 J/m^2, and 4431/9738 J/m^2, respectively, for flax and flax-basalt hybrid composites in dry condition. The concerning issue in this study is that the crack did not propagate in the mid-plane of the laminate and deviated from that by crossing the layers; it thus cannot be considered a pure interlaminar failure. Along with the high G_{IC} value of vinyl-ester (410 J/m^2 compared with 69–150 J/m^2 for epoxy (Bensadoun *et al.*, 2017)), this might be another reason for higher measured values of IFT. An increase in initiation G_{IC} was observed for the hybrid composites; however, their propagation G_{IC} values were lower. The latter can be associated with the ever-increasing R-curves of hybrid composites, where the final crack was shorter compared to those of flax composites. In hybrid composites, the crack deviated from the midplane and ended in a shorter length, thus resulted in lower development of R-curves and smaller growth in the propagation G_{IC}. Though, the propagation G_{IC} of hybrid composites at their final crack length was higher than that of flax composite at the crack length equal to the final crack length of hybrid composites. In terms of G_{IIC} values, testing end-notched-flexure (ENF) specimens, the authors observed that hybridization by basalt fibers (adding basalt composite plies to the skin of the flax laminates) improved the initiation G_{IIC} value of flax composite by 58%; also, moisture absorption improved the initiation G_{IIC} of flax composite by 29% and that of hybrid composite by 20%, due to improved matrix ductility. Their published average initiation G_{IIC} values for the dry flax and flax/basalt hybrid composites are 253 J/m^2, and 400 J/m^2, respectively.

Nevertheless, considering that the basalt plies are located at the surface of the laminate, while the IFT is being evaluated between flax plies at the mid-plane, the basalt layers have the same function that the stiffeners (bonded as tabs to the skin of DCB and ENF test specimens to avoid

large deformations and specimens arm failure) used by some researchers measuring the IFT of flax composites (Bensadoun *et al.*, 2017; Ravandi *et al.*, 2016a, 2016b; Ravandi *et al.*, 2018; Vo Hong *et al.*, 2018). Accordingly, the findings of these studies show that the stiffeners affect the values of both Mode I and Mode II IFT, which contradicts the assumption of these researchers. As a result, stiffening the arms of the DCB and ENF specimens will affect the IFT values and is not a proper solution, instead, increasing the thickness or changing the initial crack length to improve the specimen stiffness seems desirable, as recommended by the corresponding ASTM standards (ASTM, 2013a, 2019a).

Trying to improve the IFT of UD-flax/gliadin composites, Vo Hong et al. (Vo Hong *et al.*, 2018) investigated the influences of some processing conditions, fiber surface treatment, and matrix plasticization on IFT by fabricating and testing flax/gliadin composite laminates with $V_f = 0.40$. Testing the original composite DCB specimens according to ISO 15024 standard, the authors reported $G_{IC} = 50$ to 100 J/m^2 and $G_{IC} = 450$ to 550 J/m^2, respectively, for crack initiation and propagation measurements. Their findings show that the optimum value of IFT, $G_{IC} \approx 1000$ J/m^2, was obtained with a combination of the investigated processing and materials parameters, i.e., fiber treatment, adding glycerol to the matrix, and medium cooling rate. Rajendran et al. (Rajendran *et al.*, 2018) investigated the behavior of twill-weave flax/epoxy composites in Mode I and Mode II delamination (no V_f reported). The authors tested DCB and ENF specimens and, following the experimental calibration method, calculated a $G_{IC} = 485$ J/m^2 and $G_{IIC} = 962$ J/m^2 for the composite. In another report (Rajendran *et al.*, 2019), they published their findings of the Mode I, Mode II, and Mixed-mode I/II interlaminar fracture toughness of the same composite with $V_f \approx 0.44$. In this work, they followed ASTM D5528 and D7905 standards and tested standardized DCB and ENF specimens to determine the IFT in Mode I and Mode II, respectively, while, they tested single-leg-bending (SLB) specimens, which is not standardized, to measure the Mixed-mode I/II fracture toughness ($G_{(I/II)C}$). Their obtained values in this recent report are $G_{IC} = 363$ J/m^2, $G_{IIC} = 962$ J/m^2 and $G_{(I/II)C} = 649$ J/m^2 (for a $G_{II}/(G_I + G_{II}) = 0.43$), which shows a discrepancy in G_{IC} value for the same material from two different reports. In a recent study, Saidane et al. (Saidane *et al.*, 2019) used the acoustic emission (AE) method to investigate the Mode I fracture toughness of flax, glass, and

hybrid flax/glass woven-fiber/epoxy composites, flax laminates had a $V_f = 0.40$. They conducted DCB tests according to ASTM D5528 standard but used AE to detect the onset of delamination and the corresponding critical load to calculate G_{IC}. The initiation G_{IC} values of 1079 J/m^2, 945 J/m^{2,} and 923 J/m^2 were determined respectively for flax, hybrid flax/glass, and glass composites. Nevertheless, the method used in this work to detect the delamination initiation and the corresponding critical load used in the calculation of G_{IC} influences the obtained values, thus, this fact should be considered when using the results for comparison purposes. The interesting point in this study is that the propagation G_{IC} value of flax composites (R-curve) continuously increased with delamination length which contradicts the findings of previously cited studies, including those of Zhang et al. (Zhang *et al.*, 2013) for the similar materials which show a stabilized plateau value after a certain crack length. Also, their findings for hybrid flax/glass composites regarding the behavior of R-curves and the decrease in G_{IC} is in contrast with those of Zhang et al. (Zhang *et al.*, 2013) for the similar materials.

As summarized above, the literature review shows that the previous works addressing the IFT of flax composites have mostly studied flax-fabric reinforced composites, while few researchers investigated UD-FFRECs and only in Mode I (Ravandi *et al.*, 2016a). Also, to the knowledge of the authors, no study has, in particular, investigated their delamination behavior in Mode II and Mixed-mode I/II. Therefore, the damage tolerance and behavior knowledge of UD-FFRECs, as the basic building block of the FFRECs, particularly in Mode II and Mixed-mode I/II are missing. This is of paramount importance in using flax/epoxy composites in recently demanded structural applications as well as employing widely-used and reliability-proven FEM numerical analysis method to study this environmentally and economically-advantageous and ubiquitously used material. Consequently, an in-depth understanding of their delamination behavior in different modes is essential both for improving their material properties and for generating demanded knowledge and mechanical properties in the engineering design field and for future studies employing analytic and numerical resolutions. Because of the variations in the fabrication processes, origins and properties of raw materials, and the mechanical properties evaluation methods of these composites, the use of well-defined

and precisely controlled uniform composites as well as standard test methods is a pre-requisite to achieve reliable results.

The aim here is to investigate the interlaminar fracture behavior of the UD-FFRECs in three different modes of failure, namely, Mode I, Mode II, and Mixed-mode I/II and determine the corresponding interlaminar fracture toughness. For this purpose, UD-FFRECs are fabricated using identical raw materials and processing techniques with a precisely controlled fiber volume fraction. The commonly used ASTM standard test procedures are followed to evaluate the composites under different modes of loading to determine their IFT and produce valid and reliable data by respecting the defined validity criteria.

4.3   Materials and Methods

4.3.1   Material System and Test Specimen Preparation

Unidirectional tapes of flax fibers, FLAXTAPE™ 200 (from LINEO, Valliquerville, France, https://eco-technilin.com), with an areal density of 200 g/m^2, were cut in 300 mm × 300 mm dimensions and stacked up to form the UD reinforcement preform, Figure 4.2a. The thermosetting Marine 820 Epoxy System, mixed with 18 Wt.% Marine 824 hardener (from ADTECH® Plastic Systems, Madison Heights, MI, USA, www.axson-technologies.com), was used to impregnate the fibers employing the resin transfer molding (RTM) process. The number of layers in $[0]_n$ layup and the thickness of laminates were accurately computed according to the ASTM D3171 procedure and controlled to result in a unique V_f of ≈41% for all composite plates and meet the requirements of the employed ASTM test procedures regarding the thickness of test specimens. In order to induce a pre-crack as the initiation site for delamination, a 13 µm-thick polytetrafluoroethylene (PTFE) film, was accommodated on the mid-plane of the laminate during layup of the preform; the schematic view of the plate including the insert film is shown in Figure 4.2b.
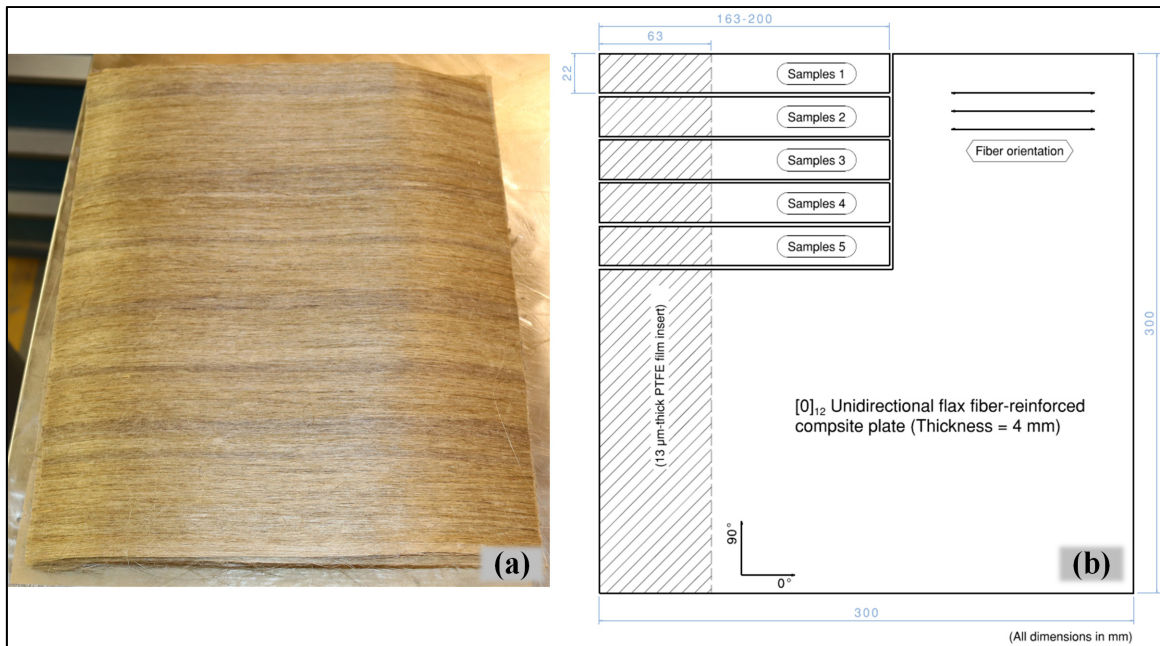
Figure 4.2 Unidirectional flax fiber preform (a) and configuration of flax/epoxy pre-cracked laminate (b)

After fabrication and post-curing of the composite laminate, the PTFE film was located via X-ray imaging, and the laminate was trimmed to reach the dimension of the insert that is recommended by the ASTM standards, as shown in Figure 4.2b. Next, the rectangular UD-laminated composite specimens with uniform thickness and containing a PTFE non-adhesive insert at one end on the mid-plane were cut to their desired dimensions by a 10-inch/90-tooth, DIABLO's cutting saw blade with high-density carbide tooltips, as illustrated in Figure 4.2b.

4.3.2   Mechanical Testing

Three different types of fracture tests were conducted to evaluate the interlaminar fracture toughness of the composite in pure Mode I and Mode II as well as in Mixed-mode I/II loading conditions. Numerous test methods and specimen configurations have been developed over the years to evaluate the IFT of the laminated FRCs; however, only some of them have been standardized (Davies, Blackman, & Brunner, 1998; Tay, 2003). In this study, the most commonly used standardized test methods by ASTM will be employed. All the tests were carried out at ambient conditions, and the specimens were exposed to the test conditions at

least 48 hours before the experiments. The details of the corresponding specimens, test procedures, and data reduction methods are described as follows.

4.3.2.1 Mode I Interlaminar Fracture Toughness

Following the ASTM D5528 standard test method, DCB specimens were prepared and tested to determine the Mode I interlaminar fracture toughness of the composite. The thickness, h, and initial delamination length, a_0, of the composite laminate were designed to fulfill the requirements of the standard. After cutting the test coupons to their desired dimensions, two piano hinges were bonded to the delaminated arms of the DCB specimen to introduce the tensile opening load and induce a Mode I delamination fracture; the configuration and nominal dimensions of the DCB specimen are illustrated in Figure 4.3a. To facilitate the detection of the onset and propagation of the crack, the side edge of the specimens was coated with white correction fluid, and the approximate location of the pre-crack tip and required final crack length were marked, as shown in Figure 4.3b. The DCB tests were conducted on an MTS Landmark 370 hydraulic machine equipped with a 1 kN-capacity load cell, and MTS 647/10 hydraulic grips. The specimens were loaded and unloaded, respectively, at a constant crosshead speed of 3 and 25 mm/min in two loading/unloading cycles. The initial loading was stopped after a crack growth of 3 to 5 mm, and the specimens were unloaded; this was a procedure to create a natural Mode I pre-crack in the DCB specimens. They were then reloaded until the delamination crack (a) propagated past 50 mm from the tip of pre-crack, and then they were unloaded.

A Digital Image Correlation (DIC) system was employed to observe and track the delamination front; the test setup is shown in Figure 4.4. DIC is an optical non-contact deformation measurement technique (Fathi, Keller, & Altstaedt, 2015; Huaiwen Wang, 2013) with adequate performance, low cost, and handy experimental setup that has been used in many research fields for strain analysis studies, including crack initiation (Tekieli, De Santis, de Felice, Kwiecień, & Roscini, 2017; D. Xu, Cerbu, Wang, & Rosca, 2019). The principle of DIC and theoretical basis for the calculation of strain fields using consecutive images has been reported

by many researchers and is available in the literature (Anzelotti, Nicoletto, & Riva, 2008; Takano, Zako, Fujitsu, & Nishiyabu, 2004; H. Wang & Hou, 2010).
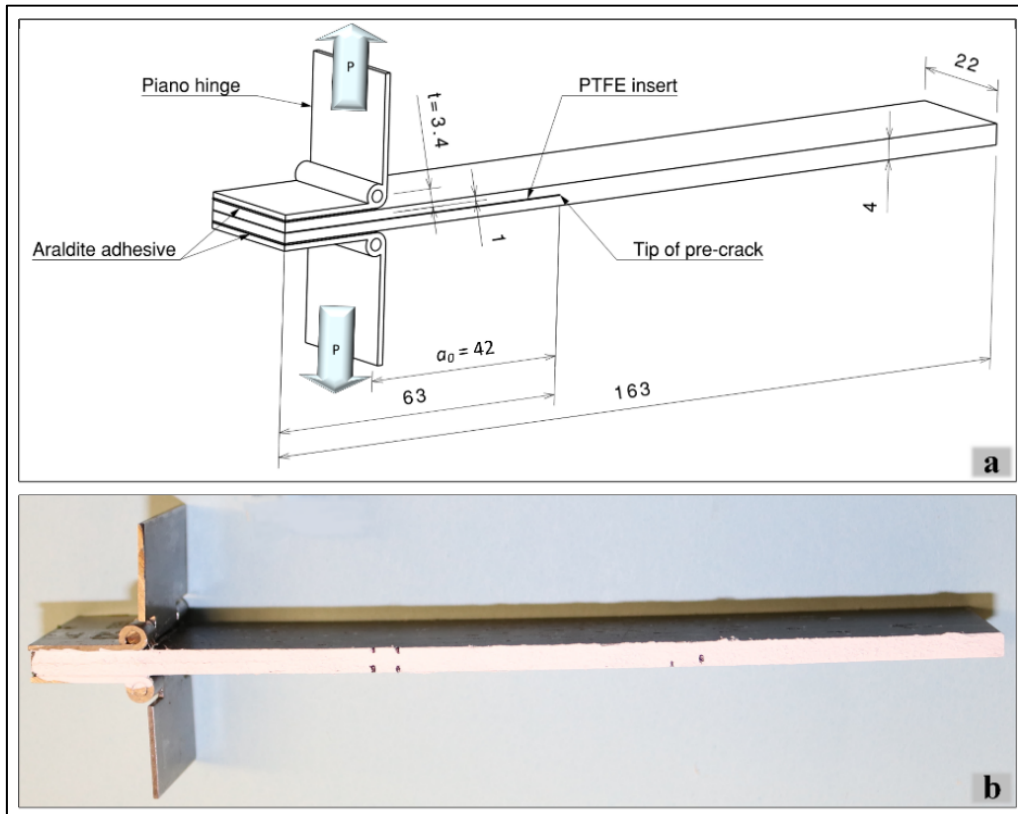
Figure 4.3 Double Cantilever Beam (DCB) specimen: (a) configuration and dimensions, (b) final test specimen

The recorded images were synchronized with the load and displacement signals of the MTS machine, the crack opening displacement (COD) was estimated as the crosshead displacement, and the data was recorded for the entire loading/unloading cycles. Then, the registered information was processed to associate the load and displacement values at the intervals of delamination growth defined by the standard. These values were used to calculate G_{IC} for different delamination lengths and to form the delamination resistance curves (R-curves). Eight DCB specimens were tested to obtain at least five valid tests to determine the G_{IC} of the composite. The piano hinges were extended with a bracket to avoid the interference that occurred between the arms of the specimen with regular piano hinges and the jaws of the grip. In order to more precisely locate the end of the insert film, the first failed sample was

completely opened, and the end of the film was marked to measure a_0 and used for marking the other samples.
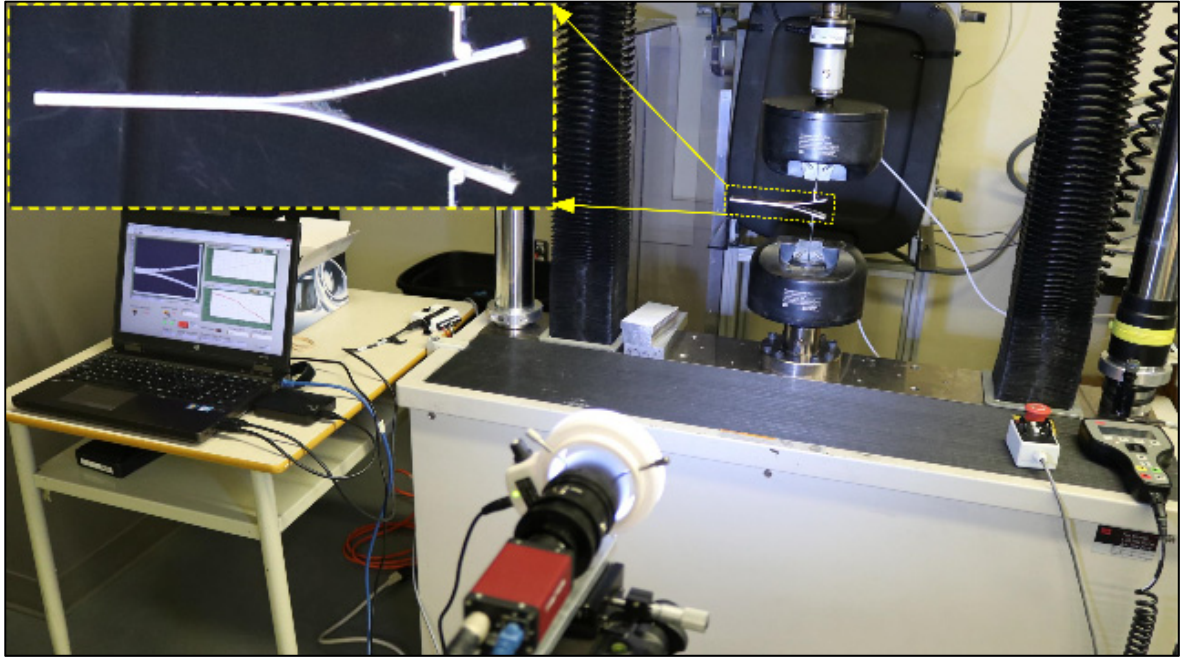
Figure 4.4 Mode I delamination test setup with a DIC system to follow crack propagation

There are various data reduction methods for calculating G_{IC} values, three of which are presented in the ASTM D5528 standard; however, the MBT method, yielding to the most conservative values, has been recommended. In this study, MBT was implemented to calculate G_{IC} values based on the processed data and using Equation (4.1);

$$G_I = \frac{3P\delta}{2b(a+|\Delta|)} \qquad (4.1)$$

where P is the applied load, δ is the COD on the load line, b is the width of the specimen, a represents the delamination crack length, and Δ is the crack length correction factor. Δ can be determined experimentally as the x-intercept of linear least squares plot of $C^{1/3}$ versus delamination length, where C is the compliance of the specimen ($C = \delta/P$). G_{IC} is the IFT of the composite, associated with critical load (P_C) determined as follows.

The crack initiation value of G_{IC} (G_{IC}^{ini}) was determined using three definitions presented in the standard, namely, at the deviation from linearity point in the load-displacement curve, when delamination is visually observed (respectively named NL and VIS by ASTM) and at 5%-increased-compliance point or the maximum load, as illustrated in Section 4.4.1. The NL G_{IC}^{ini} is the lowest and recommended for damage tolerance analysis, and the first propagation value of G_{IC} is known as Mode I pre-crack G_{IC} (ASTM, 2013a). Concerning deflections of the specimen arms due to relatively low flexural modulus of the FFREC, the values of h and a_0 were calculated according to the recommendations outlined in the ASTM standard and based on the elastic properties of the composite, leading to a shorter $a_0 = 42$ mm compared to $a_0 = 50$ mm, recommended for synthetic FRCs. Nevertheless, for some delamination lengths, the ratio of the load-line displacement to delamination length was higher than 0.4 ($\delta/a_0 > 0.4$). Consequently, according to the standard, a large-displacement correction factor (F) was calculated using Equation (4.2) and incorporated in the data reduction method by multiplying F by G_{IC} values calculated using Equation (4.1);

$$F = 1 - \frac{3}{10}(\frac{\delta}{a})^2 - \frac{3}{2}(\frac{\delta t}{a^2}) \tag{4.2}$$

where t was measured as defined in the standard and is shown in Figure 4.3.

4.3.2.2 Mode II Interlaminar Fracture Toughness

End-notched flexure (ENF) tests were conducted following the procedure outlined in ASTM D7905 to determine the Mode II interlaminar fracture toughness, G_{IIC}, of the UD-FFRECs using the compliance calibration (CC) method, which is presented as the only acceptable data reduction method for this test (ASTM, 2019a). The specimens were cut from the same laminates used for DCB specimens mentioned above (Figure 4.2b) and with the same tool to the dimensions that fall within the range of allowable lengths and widths specified in the standard. Both sides of the specimens were painted with a correction liquid to help the detection of crack initiation, and the end of pre-crack, as well as the required loading points, was marked.

Figure 4.5a illustrates the configuration and dimensions, and Figure 4.5b shows a picture of the ENF specimen with markings. The ENF specimens were mounted in a three-point-bending (TPB) fixture with a 100-mm-span and loaded on the same machine fitted with the 1kN-loadcell that was used for DCB specimens, as shown in Figure 4.6. The coupons were loaded and unloaded at 0.5 mm/min crosshead speed, and the data acquisition was performed for the entire fracture tests and the loading phase of the CC tests.
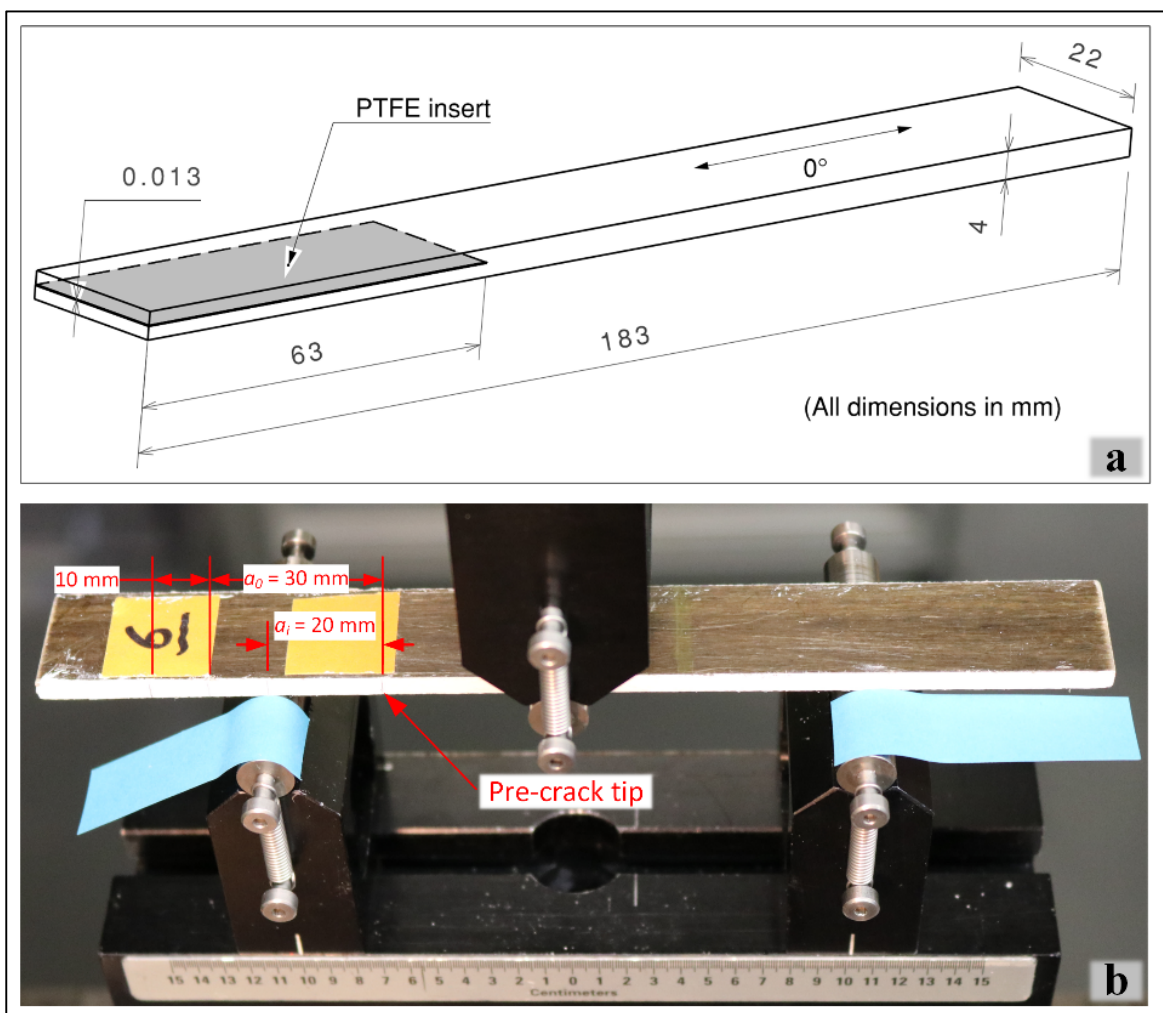
Figure 4.5 ENF specimen for Mode II delamination: (a) configuration and dimensions, (b) specimen and loading fixture
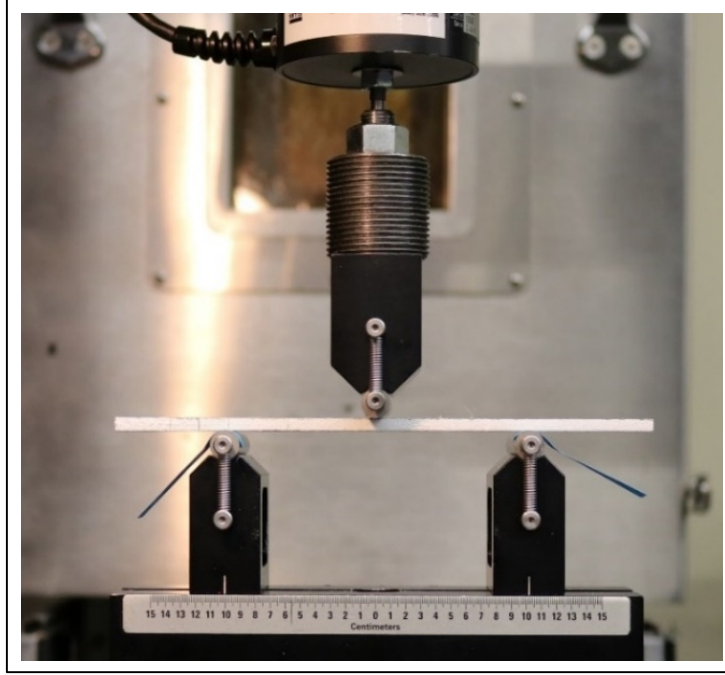
Figure 4.6 Mode II delamination test setup

According to the standard, the non-pre-cracked (NPC) and pre-cracked (PC) CC tests, at $a_i =$ 20 and 40 mm, and fracture tests, at $a_0 = 30$ mm, were carried out on the same specimen to obtain the compliance plots as well as the maximum loads (P_{Max}), to be used for determination of G_{IIC}. The initial CC forces (P_i) were approximated using the flexural modulus (E_f) of the same material (Saadati *et al.*, 2020c) and G_{IIC} of a similar material (Rajendran *et al.*, 2018), then, the result of ENF tests with accepted G_{IIC} was used to update the P_C and P_i. The calculated crack length after NPC tests (a_{calc}) was calculated using unloading data of the NPC fracture test, as mentioned in the test procedure.

At each crack length, for NPC and PC tests, the compliance (C) was specified as the slope of the load-point displacement versus load curve by linear least-squares regression analysis (LLSRA). Then, C values were plotted versus cubed crack length (a^3), and the CC coefficients, A and m in Equation (4.3), were determined using LLSRA;

$$C = A + ma^3$$

(4.3)

G_{IIC} values were calculated using Equation (4.4) and validated based on the criteria of the ASTM standard;

$$G_{IIC} = \frac{3mP_{Max}^2 a_0^2}{2B}$$

(4.4)

where m is the CC coefficient, a_0 and P_{Max} are respectively the crack length used and the maximum force measured in the fracture test, and B is the specimen width. Six ENF specimens were tested to obtain adequate results for the calculation of G_{IIC}. The value of G_{IIC} is considered as IFT, only if it satisfies the criteria defined in the standard.

4.3.2.3 Mixed-Mode I/II Interlaminar Fracture Toughness

The Mixed-Mode Bending (MMB) tests were carried out according to ASTM D6671 standard test method (ASTM, 2019b) to obtain the Mixed-mode I/II fracture toughness ($G_{(I/II)C}$) of the composite. Following the guidelines of the standard, piano hinges, with drilled holes matching to the hinge clamp of the MMB test fixture, were adhesively bonded to the pre-cracked specimens cut from the same plate as for DCB and ENF specimens, to form an initial crack length of $a_0 = 28$ mm. The length of the initial crack was calculated based on the criteria defined in the standard and using the thickness, mechanical properties, and an estimated value of fracture energy, $G_{(I/II)C}^{est}$, to result in an ultimate allowable deflection. Also, the side edges of the specimens were painted white and marked. Figure 4.7a presents the configuration, dimensions, and load application points of the MMB specimen. Figure 4.7b shows the MMB apparatus with a mounted specimen and the finalized MMB specimen. Mixed-mode delamination under a mode mixture ratio of $G_{II}/(G_I + G_{II}) = 0.55$ was applied by setting the length of the lever as $c = 47.4$ mm (Figure 4.7b). The tests were performed at a constant crosshead speed of 0.5 mm/min on an MTS-322.31 machine equipped with a 5 kN loadcell, and the force versus displacement data was recorded. A moveable microscope was synchronized with the load-displacement data and used to observe the crack tip to detect the onset and follow the propagation of the delamination; the test setup is shown in Figure 4.8.

The loading of the specimen was continued until the delamination extended past 25 mm. The required elastic and shear properties were used from our previous work (Saadati *et al.*, 2020c), and the out-of-plane shear modulus G_{13} was assumed to be equal to G_{12}. Also, for the calculations of the estimated force and deflection, the estimated Mixed-mode IFT, $G_{(I/II)C}^{est}$, was considered as the average values of the G_{IC} and G_{IIC} of the composite measured in this study.
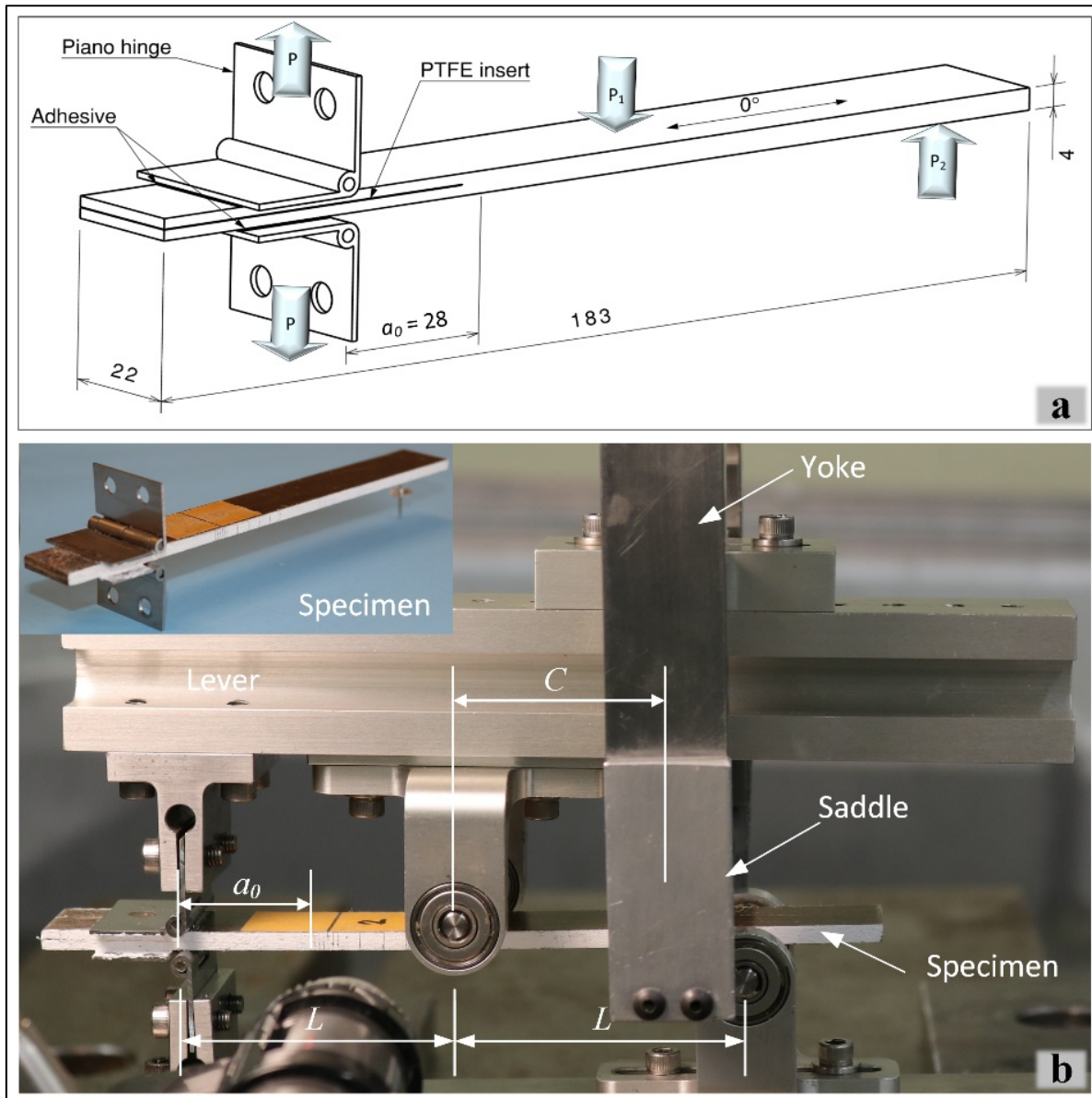
Figure 4.7 Mixed-Mode Bending (MMB) test specimen for Mixed-mode I/II delamination: (a) configuration and dimensions, (b) test fixture and final test specimen

Six MMB tests were carried out to achieve a minimum of five valid tests by controlling the failure mode and maximum allowable deflection of the specimens according to the criteria of the standard.
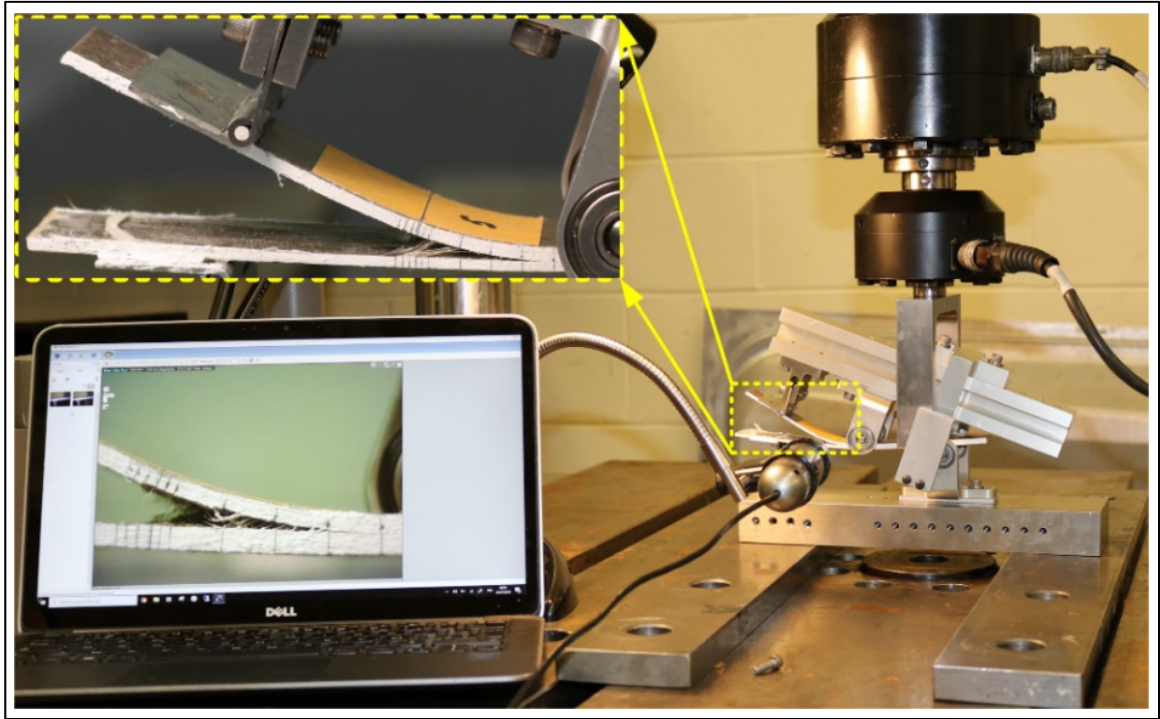
Figure 4.8 Mixed-mode I/II delamination test setup

$G_{(I/II)C}$ values were calculated using the Equations (4.5)–(4.7), as mentioned in the ASTM D6671;

$$G_{IC} = \frac{12P_C^2(3c-L)^2}{16b^2h^3L^2E_{1f}}(a_0 + \chi h)^2 \qquad (4.5)$$

$$G_{IIC} = \frac{9P_C^2(c+L)^2}{16b^2h^3L^2E_{1f}}(a_0 + 0.42\chi h)^2 \qquad (4.6)$$

$$G_{(I/II)C} = G_{IC} + G_{IIC} \qquad (4.7)$$

where G_{IC} and G_{IIC} are the Mode I and Mode II components of the Mixed-mode IFT, respectively, P_C is the critical load, in this study, it is the load associated with the VIS point, c is the lever length, b and h are respectively the specimen width and half-thickness, a_0 is the delamination length, L is the half-span length, and χ is the crack correction parameter defined in the standard.

4.4 Results and Discussion

4.4.1 Mode I Interlaminar Fracture Toughness

The load-COD curve presented in Figure 4.9a shows the response of a typical DCB specimen to the crack opening load during the second loading cycle (after inducing the natural pre-crack in the first cycle). This curve shows that the UD-FFREC DCB specimen has a perfect linear behavior up to 95% of the P_{max}, followed by a short nonlinear curve up to the P_{max} point. Upon reaching the peak point, which differs from the point at which the delamination initiates, the load drops slowly and continuously with crack propagation, indicating that stable crack propagation is happening. Figure 4.9b confirms unique behavior for all of the DCB specimens and shows good repeatability of the tests for an NFRC. This behavior of the DCBs perfectly agrees with the observations of Ravanid et al. (Ravandi *et al.*, 2016a, 2016b; Ravandi *et al.*, 2018) for woven and UD-FFREC DCBs, which were stiffened by GFRP/CFRP tabs on both sides, as well as with those of Bensadoun et al. (Bensadoun *et al.*, 2017) for cross-ply (UD [0 90]$_{4s}$) FFRECs laminate stiffened likewise and those of Saidaine et al. (Saidane *et al.*, 2019) for woven flax/epoxy composite. Investigating woven/vinyl-ester DCB specimens, Almansour et al. (Almansour *et al.*, 2017a) also observed an initial linear response followed by a nonlinear curve up to the peak load. However, this is in marked contrast to the observations of Rajendran et al. (Rajendran *et al.*, 2018; Rajendran *et al.*, 2019) for the flax fabric/epoxy DCBs., who reported a high nonlinear response up to the maximum load. Ravandi et al. (Ravandi *et al.*, 2016a) and Rajendran et al. (Rajendran *et al.*, 2019) tested epoxy composite DCBs made of relatively similar flax fabrics supplied by the same supplier with the specifications as described in the Introduction part. However, they reported an entirely different load-displacement

response and IFT values; the average G_{IC} value reported by the former ($\approx$2000 J/m^2) is much higher than that of the latter (363 J/m^2).
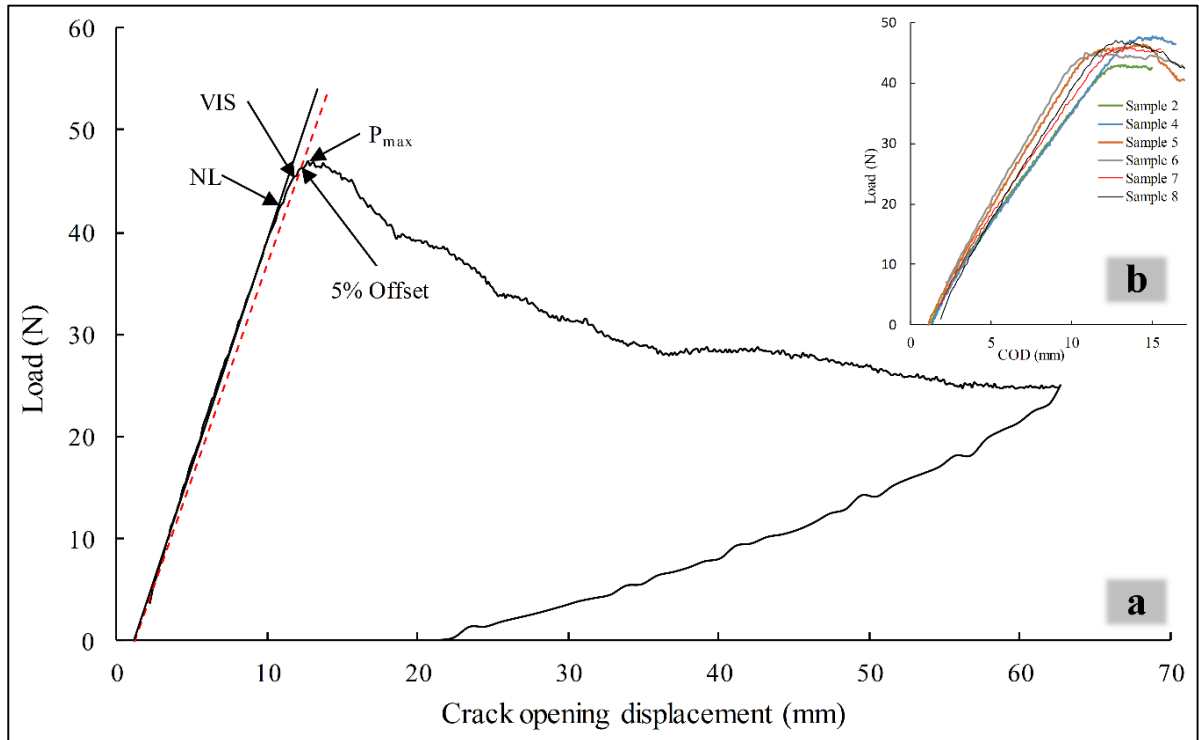
Figure 4.9 Load-crack opening displacement (COD) of the DCB specimen: (a) Typical loading/unloading cycle and initial G_{IC} measurement points, and (b) overall initial behavior

The calculated G_{IC} values for a typical DCB specimen are drawn as a function of delamination length (Figure 4.10) to generate the delamination resistance curve, known as R-curve, and to determine the initiation and propagation values of G_{IC}. As can be seen in Figure 4.10, the G_{IC} value determined at NL is the minimum followed by those at VIS and 5% Offset points, which happened before the P_{max} point for all DCB tests on the load-COD curve (Figure 4.9a). Figure 4.10 shows that G_{IC} increases by delamination growth to a maximum value and then drops to stabilize at a plateau value. Several authors observed similar R-curves, and this is a commonly occurred phenomenon for UD-FRC DCB specimens when the delamination grows parallel to the fibers between two UD plies that is attributed to the development of fiber bridging across the crack (Airoldi & Dávila, 2012; ASTM, 2013a; Bensadoun *et al.*, 2017; Chen *et al.*, 2014; Ravandi *et al.*, 2016a; Ravandi *et al.*, 2018). This resistance-type fracture behavior of UD DCB

composites is an incidence of properly implantation of the delamination insert and validates the tests. Some authors reported a much more extensive fiber bridging scale for UD-NFRCs compared to their synthetic fiber counterparts (Ravandi *et al.*, 2016a, 2016b; Ravandi *et al.*, 2018; Saidane *et al.*, 2019; Zhang *et al.*, 2013). They related this phenomenon to the high strength of the longer synthetic fibers, which tend to remain unbroken and less mobile, whereas UD natural fibers are composed of shorter technical fibers with irregular geometry and alignment that helps them bridge two opening plies. They also believe that the higher G_{IC} value determined for UD-FFECs compared to those for UD glass/epoxy composites is associated with the larger scale of fiber bridging.
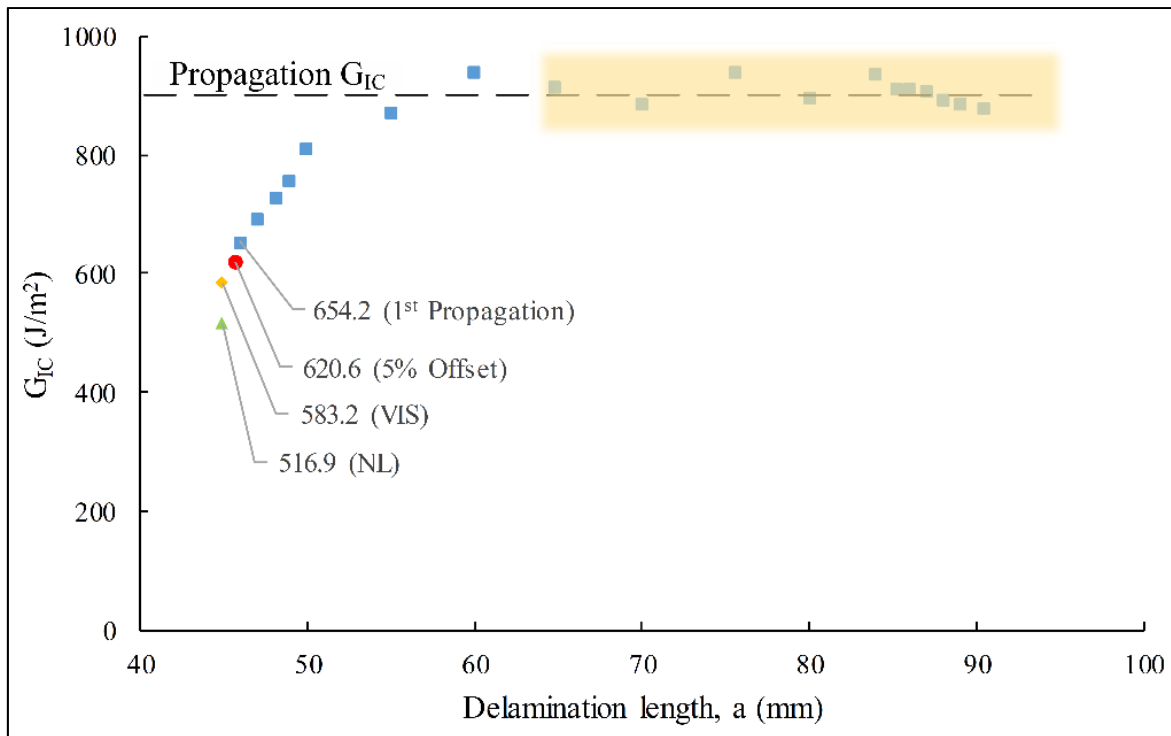
Figure 4.10 Crack Resistance Curve (R-Curve) of a typical UD-FFREC DCB, the plateau region is highlighted

The G_{IC} values, determined based on different definitions of onset of delamination, are presented in Table 4.1. However, combining some damage detection techniques, such as Radiography, strain gauge, and AE, with DCB tests, reveal that the delamination starts in the interior of the specimen width very close to NL point on the load-COD curve (ASTM, 2013a;

De Kalbermatten, Jäggi, Flüeler, Kausch, & Davies, 1992; Saidane *et al.*, 2019), and as can be seen in Figure 4.10, this point is far from propagation values, thus is considered as initiation G_{IC} value, as recommended by ASTM D5528. The plateau value of G_{IC} in the R-curve, the average value within the highlighted zone in Figure 4.10, is considered as the propagation G_{IC} value and summarized in Table 4.1.

Table 4.1 Mode I fracture toughness values for UD FFREC

Mode I G_{IC}	G_{IC} (NL Point)	G_{IC} (VIS Point)	G_{IC} (5%/Max)	G_{IC} (Propagation)
Average (J/m^2)	574	641	644	903
STD	38	31	26	55
COV (%)	6.6	4.8	4.0	6.1

STD: Standard deviation; COV: Coefficient of variation

The relevant DCB tests conducted for FFRCs and their corresponding G_{IC} values available in the literature are summarized in Table 4.2. As can be seen in Table 4.2, the most similar tests have been performed by Ravandi et al. (Ravandi *et al.*, 2018) for an analogous UD-FFECs ([0]$_{16}$) laminate containing a similar UD reinforcement with a lower surface density (110 g/m^2) compared to 200 g/m^2 used in the under-study [0]$_{12}$ laminate. However, the obtained initiation G_{IC} value at VIS point (641 J/m^2), as well as the propagation G_{IC} value (903 J/m^2) in the present study, are about 20% lower than those reported by these authors. Considering that they stiffened their DCB specimens with GFRP, this difference may be explained by referring to the work of Almansour et al. (Almansour *et al.*, 2017a), where replacing the out-most layers of flax fabric composites by the 4-fold stiffer basalt fiber plies, equivalent to stiffening flax composite DCBs, augmented the G_{IC} values by around 19%. Therefore, the obtained results in the current study are in excellent agreement with their results. The experiments of Bensadoun et al. (Bensadoun *et al.*, 2017) for the cross-ply DCB ([90,0] specimens), where the delamination occurs at 0°//0° interface, also have similar failure conditions to the present DCB tests; however, it has been shown that G_{IC} value measured for delamination at 0°//0° interface within a UD laminate is different with that within a multidirectional laminate and replacing

some off-center 0° plies with 90° layers reduce the G_{IC} value (Robinson, 1996; Shokrieh & Heidari-Rarani, 2011). Therefore, in view of this fact, the lower G_{IC} values reported by these authors, presented in Table 4.2, are also in good agreement with those of the present work. In general, from the studies summarized in Table 4.2, it can be deduced that the composites reinforced with women fibers have higher G_{IC} values compared to those with UD reinforcements. As explained before, the huge difference observed for the results of Almansour et al. (Almansour *et al.*, 2017a) can be due to the very high toughness of matrix (that is the dominant factor in this failure mode) used in their study in comparison to that used in the current study (410 J/m^2 of vinyl-ester against 69–150 J/m^2 of epoxy (Bensadoun *et al.*, 2017)). Also, the woven reinforcement structure used in their composite that exhibits higher G_{IC} compared to UD laminate, as shown in Table 4.2 and (Bensadoun *et al.*, 2017; Pinto, Chalivendra, Kim, & Lewis, 2016), can be another reason. However, for propagation values, clearly, the deviation of crack from the mid-plane of the laminates is a significant reason. Despite the similarity of their material, the value reported by Rajendran et al. (Rajendran *et al.*, 2019) seems relatively low compared to (Almansour *et al.*, 2017a). In addition to other differences listed in Table 4.2, and as discussed earlier, their load-COD curve is entirely in contrast with the findings of this study and all other authors. Moreover, they reported a 34% higher value for G_{IC} of the same material in another work (Rajendran *et al.*, 2018).

Overall, considering the differences in reinforcements architecture/source, matrix type, processing, testing, and data reduction method, the obtained results in the present study are generally consistent with the literature data given in Table 4.2. Therefore, the determined and validated values for the initiation and propagation GIC for UD-FFRECs can be considered as the material properties of these composites and be confidently applied in future research and engineering fields.

Table 4.2 Mode I interlaminar fracture toughness tests and values for FFRCs

	Current Study	(Ravandi et al., 2016a)	(Ravandi et al., 2018)	(Bensadoun et al., 2017)	(Bensadoun et al., 2017)	(Almansour et al., 2017a)	(Rajendran et al., 2019) /(Rajendran et al., 2018)	(Y. Li et al., 2015)	(Chen et al., 2014)	(Saidane et al., 2019)	(Zhang et al., 2013)	(Vo Hong et al., 2018)
Reinforcement	UD-flax (200 g/m^2) [0]$_{12}$	4 × 4 W-flax fabric (500 g/m^2)	UD-flax (110 g/m^2) [0]$_{16}$	0°//0° flax-plies [90,0]$_{2s}$	W-flax fabrics	(±45°) W-flax fabric	2 × 2 W-flax fabric (200 g/m^2)	UD-T-flax fabric (200 g/m^2)	UD-T-flax fabric	2 × 2 W-flax fabric	UD-T-flax fabric	UD-flax
Matrix	Epoxy	Epoxy	Epoxy	Epoxy	Epoxy	Vinyl ester	Epoxy	Epoxy	Phenolic resin	Epoxy	Phenolic resin	Gliadin powder
Stiffener	-	CFRP	GFRP	GFRP	GFRP	-	-	-	-	-	-	GFRP
Composite fabrication	RTM ‡	VARI †	VARI †	RTM ‡	RTM ‡	VI ±	Hand layup	CM +	VARI †	CM +	CM +	Hand layup
V_f (%)	41	31	40	40	40	31	44	60	73	40	67	40
Test /Data reduction method	ASTM D5528 /MBT	ASTM D5528 /MBT	ASTM D5528 /MBT	ASTM D5528 /MBT	ASTM D5528 /MBT	ASTM D5528 /MBT	CC	ASTM D5528 /CC *	ASTM D5528 /CC	ASTM D5528 /MBT	ASTM D5528/-	ISO 15024 /MBT
Damage initiation point	NL	-	VIS	NL	NL	VIS	SG detected /P$_{max}$	-	VIS	AE detected	-	NL
G_{IC} (J/m^2) Initiation	574	≈2000	771	496	457–754	3579	363/485	-	≈440	1079	280	50–60
G_{IC} (J/m^2) Propagation	903	≈3200	1250	663	1151–1597	11789	-	1400	≈580	≈2400	550	450–550

† Vacuum-assisted resin infusion; ‡ Resin transfer molding; ± Vacuum infusion; + Compression molding; * In the paper mentioned MTB (by mistake); AE: Acoustic Emission; W: Woven, UD: Unidirectional; T: Twisted; SG: Strain gauge; CC: Compliance Calibration; MBT: Modified Beam Theory

4.4.2 Mode II Interlaminar Fracture Toughness

Figure 4.11 presents the load-displacement curve of a typical ENF fracture test. As can be seen, the composite shows an overall linear response with a clear load drop, from which, respectively, the compliance of the specimen and the peak load can be determined. This is a normal and known behavior exhibited by ENF where, under an in-plane shear loading, the surfaces of the mid-plane plies slide over each other and lead to unstable crack growth ~~and sudden load drop~~ (ASTM, 2019a). This failure allows only the measurement of crack initiation IFT. Almansour et al. observed an analogous behavior for woven flax/vinyl-ester (Almansour *et al.*, 2018) and non-woven flax mat/vinyl-ester (Almansour *et al.*, 2017b), whereas Rajendran et al. (Rajendran *et al.*, 2018; Rajendran *et al.*, 2019) reported a complete nonlinear load-displacement curve for woven flax/epoxy composites. The experience of the latter, likewise to their DCB tests, is in stark contrast with the observations of previously cited authors (Almansour et al.) and many other authors (Al-Khudairi, Hadavinia, Waggott, Lewis, & Little, 2015; Johar, Israr, Low, & Wong, 2017; W.-X. Wang, Nakata, Takao, & Matsubara, 2009).

The Mode II interlaminar fracture energy, G_{IIC}, was calculated using the data reduction method explained in the previous section, and the averaged results of five valid Non Precracked (NPC) and Precracked (PC) tests are presented in Table 4.3. As can be noticed, considering the variations, the averaged results are in the same range and overlapping, however, NPC results have a larger variation.

Table 4.3 Mode II fracture toughness values for UD FFREC

	G_{IIC} (NPC)	G_{IIC} (PC)	G_{IIC} (Average)
Mean (J/m^2)	401	378	390
STD	18	7	18
COV (%)	4.5	1.9	4.6

STD: Standard deviation; COV: Coefficient of variation

There are very limited similar ENF test data available in the literature for comparison and validation purposes. In fact, there is no available ENF test being conducted and treated exactly in the same way for UD FFRECs; nevertheless, the closest ones are summarized in Table 4.4.
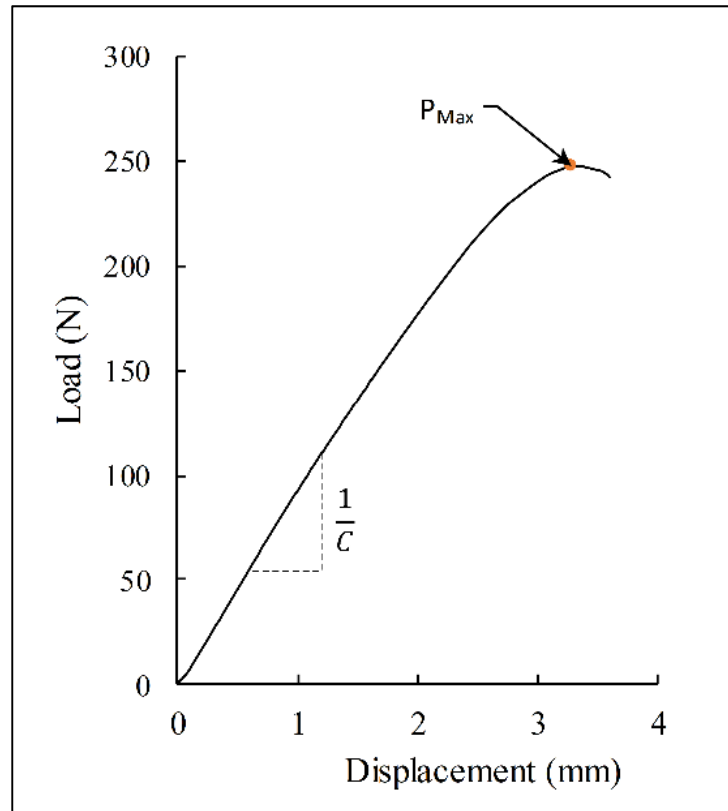
Figure 4.11 Load-displacement curve of ENF test and illustration of compliance (C) and P_{Max} determination

In Table 4.4, the obtained G_{IIC} value for the under-study UD-FFREC laminate is placed within the range of those reported for similar tests. However, it is clearly lower than that of the closest material, i.e., $[90,0]_{2s}$ laminate with $0°//0°$ UD-flax/epoxy plies in the midplane (Bensadoun *et al.*, 2017). This difference not only can be associated with the variating properties of natural fibers, but it can also be due to the difference in the reinforcement configuration of the laminates, i.e., the GFRP tabs used for stiffening $[90,0]_{2s}$ laminate. The different data reduction methods employed for the calculation of G_{IIC} can be another source of discrepancy. The results of Almansour et al. (Almansour *et al.*, 2018; Almansour *et al.*, 2017b) show that replacing the out-most plies of the flax composite with high-stiffness basalt plies, which is equivalent to

tabbing ENF specimens, augmented the G_{IIC} value of the flax composites up to 62%. Therefore, tabbing can be one of the reasons for obtaining higher value for the compared composite. In addition, for DCB tests, it is proven that alterations in the off-center plies (orientation and material) of the UD laminates with the same delamination interface layers affect G_{IIC} values (Robinson, 1996; Saidane *et al.*, 2019; Shokrieh & Heidari-Rarani, 2011). There is no research result for ENF tests; however, this might be true for them, as well.

Table 4.4 Mode II interlaminar fracture toughness tests and values for FFRCs

	Current Study	(Bensadoun *et al.*, 2017)		(Almansour *et al.*, 2018)	(Almansour et al., 2017)	(Rajendran *et al.*, 2019)
Reinforcement	UD-flax (200 g/m²)	0°//0° UD-flax plies in [90,0]$_{2s}$	W-flax fabrics	(±45°) W-flax fabric	Non-woven flax mat	W-flax fabric (200 g/m²)
Matrix	Epoxy	Epoxy	Epoxy	vinyl ester	vinyl ester	Epoxy
Stiffener	-	GFRP	GFRP	−/basalt	−/basalt	-
Composite fabrication	RTM	RTM	RTM	VARTM	Hand layup + CM	Hand layup
Fiber content	V_f= 0.41	V_f= 0.40	V_f= 0.40	100 Wt.%	V_f= 0.23	V_f= 0.44
Test /Data reduction method	ASTM D7905/ CC [SBT]	SBT	SBT	SBT	SBT	CC
G_{IIC} (J/m²)	378 [612]	728	1315-1872	266/430	1940/2173	962

UD: Unidirectional, W: Woven, RTM: Resin transfer molding, VARTM: Vacuum-assisted resin transfer molding, CM: Compression molding, SBT: Classical Simple Beam Theory, CC: Compliance Calibration.

Furthermore, the ASTM D7905 standard is followed in the current study; however, Bensadoun et al. used the classical simple beam theory method (SBT). While using different data reduction methods yields variations in the obtained G_{IIC} values, for instance, applying the classical SBT used in their study to the test data of the current study, a higher value (612 J/m^2) is obtained, Table 4.4. The findings of some authors (Bensadoun *et al.*, 2017; Compston & Jar, 1998) revealed that woven reinforcements result in higher G_{IIC} values compared to UD ones; thus, the difference between the G_{IIC} values of UD laminates and those of woven-fabric reinforced composites given in Table 4.4 is reasonable.

Some authors believe that normally G_{IIC} values are higher than G_{IC} (Bensadoun *et al.*, 2017; Lens, Bittencourt, & d'Avila, 2009), whereas some observed the opposite (Almansour *et al.*, 2017a, 2018; Rajendran *et al.*, 2019), and some believe that both can be true for laminated composites (Dillard, Singh, Pohlit, & Starbuck, 2009). As listed in Table 4.3 and Table 4.4, depending on the applied data reduction method, both cases can happen for the UD-FFREC. For the most similar instance ([90,0]$_{2s}$ laminate) discussed above, using ASTM D7905 standard for G_{IC} and SBT for G_{IIC} results in the same trend.

4.4.3 Mixed-Mode I/II Interlaminar Fracture Toughness

The mixed-mode loading behavior of the composite is plotted in Figure 4.12. For clarity, a single curve specimen is presented in Figure 4.12a and shows that in general, MMB specimens of FFREC exhibit an initial linear behavior followed by a nonlinear curve up to the peak load, after which, a plateau type curve with gradual load drop can be seen till the end of the test. Having plotted the curves of all 5 MMB specimens in Figure 4.12b, it can be seen that they exhibit a similar and consistent response with acceptable repeatability for the natural fiber composites.
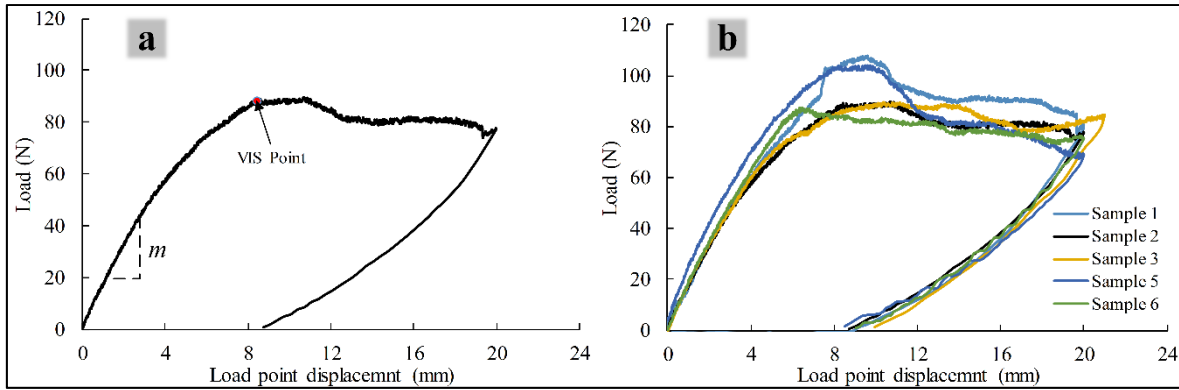
Figure 4.12 Load-displacement curves of MMB tests: (a) determination of m and P_C, and (b) all curves of the tests

The slope of the load-displacement curve (m) and the critical load (P_C) need to be determined for the calculation of mixed-mode I/II fracture energy of the composite. m was directly calculated from the linear part on the curve, as shown in Figure 4.12a. However, there are some definitions for the P_C in the standard; NL, VIS, and 5%/max points, as define for the calculations of G_{IC}, and the most suitable one should be used. Due to the large nonlinearity part in the load-displacement curves, NL and the calculated 5% offset points reach too early for most of the tests on this curve, so that do they not seem to be the failure point and using the corresponding load would result in an underestimated fracture energy. On the other hand, comparing the VIS and the maximum force points, it was observed that the former happened earlier and right before peak load. This was also observed by Rajendran et al. (Rajendran *et al.*, 2019), who used strain gauge to detect the onset of failure in similar tests. Accordingly, the VIS point was considered as the onset of delamination, and $G_{(I/II)C}$ was calculated based on the associated load at this point. For all the tests, the maximum deflection was smaller than the allowable deflection that was determined based on the criterion of the standard, and they were validated.

The obtained average mixed-mode I/II fracture energy value was $G_{(I/II)C} = 414$ J/m^2 with a 15% coefficient of variation. The variation of results seems relatively high; however, considering the nature of the natural fiber composites, the complexity of this test, and the subjective visual solution used for detecting the initiation of failure, it is reasonable. To the knowledge of the authors, MMB tests reported by Rajendran et al. (Rajendran *et al.*, 2019) are the only literature

data available for flax/epoxy composites. These authors tested three single-leg-bending specimens ($G_{II}/G_{(I/II)C}$ = 0.43) of woven-flax/epoxy composite with V_f = 0.44, and using compliance calibration method, obtained $G_{(I/II)C}$ = 649.1 J/m^2. Comparison is limited to the result of this work that is obviously higher than the value obtained in this study; nevertheless, it should be noted that the reinforcement, manufacturing method, mode mixture (mixed-mode ratio), $G_{II}/G_{(I/II)C}$, and test method in their study was different with the current one. Furthermore, in the previous section, it was seen that woven reinforcement configurations produced higher IFT, and for the same material, in another work, the authors reported a much higher G_{IIC}; therefore, this difference is reasonable. Considering that there is no other pertinent data for comparison, and compared to the obtained Mode I and Mode II fracture toughness, which were determined and validated earlier, this value of the mixed-mode fracture energy is the only value obtained for UD-FFRECs and reasonably acceptable. Therefore, it can be considered as the representative of the material property of this composite and used in engineering design and numerical simulation studies.

The B-K delamination criterion was used and fitted to the obtained data to determine the B-K fitting parameter, η, and to predict the interlaminar toughness for various mixed-mode ratios (Benzeggagh & Kenane, 1996);

$$G_{(I/II)C} = G_{IC} + (G_{IIC} - G_{IC})\left(\frac{G_{II}}{G_{(I/II)C}}\right)^{\eta} \tag{4.8}$$

Where $G_{II}/G_{(I/II)C}$ is the mixed-mode ratio, and η is the B-K fitting parameter. Using Equation (4.8), η = 0.35 is computed for the prediction of the $G_{(I/II)C}$ with other mixed-mode ratios.

4.5   Conclusions

The present study investigated the interlaminar fracture energy of unidirectional flax epoxy composites in Mode I, Mode II, and Mixed-mode I/II delamination failure. The composite laminates were manufactured via RTM method and were tailored to have a constant V_f = 0.44,

and a 13 μm-thick PTFE was placed in the midplane to induce pre-crack, it was then located by X-ray in the laminate. All the DCB, ENF, and MMB tests were conducted and validated according to corresponding ASTM standards to evaluate the fracture energies in Mode I, Mode I, and Mixed-mode I/II, respectively. For Mode I, G_{IC} = 574 and G_{IC} = 903 J/m^2 were obtained respectively for crack initiation and propagation values. The obtained value based on the standard method for Mode II delamination is G_{IIC} =378 J/m^2, which in contrast to the results of previous authors, calculated via the SBT data reduction method, is lower than G_{IC}. However, when following the SBT method, G_{IIC} =612 J/m^2 is obtained, which is consistent with their results. MMB tests resulted in $G_{(I/II)C}$ = 414.4 J/m^2 for Mixed-mode I/II fracture energy. Despite the limited, and in some cases lack of data available in the literature for comparison, the results are compared to the existing similar data and confirmed. In view of the fact that there is limited or no interlaminar fracture energy for these composites, the obtained values are valuable material properties to be further used in the design engineering field and numerical simulation methods.

CHAPTER 5

STUDY OF TRANSLAMINAR FRACTURE TOUGHNESS OF UNIDIRECTIONAL FLAX/EPOXY COMPOSITE

Yousef Saadati[1], Gilbert Lebrun[2], Christophe Bouvet[3], Jean-François Chatelain[1] and Yves Beauchamp[4]

[1] Mechanical Engineering Department, École de Technologie Supérieure, 1100 Notre-Dame West, Montreal, QC H3C 1K3, Canada
[2] Mechanical Engineering Department, Université du Québec à Trois-Rivières (UQTR), 3351 boul. des Forges, Trois-Rivières, QC G9A 5H7, Canada
[3] University of Toulouse; INSA, UPS, Mines Albi, ISAE-SUPAERO; ICA (Institut Clément Ader), 3, rue Caroline Aigle, 31400 Toulouse, France
[4] McGill University, 845 Sherbrooke Street West, Montreal, Québec, Canada

5.1   Abstract

Ever growing applications of flax fiber-reinforced polymer composites (FFRCs) and their suitability for structural uses involve implementing the design and failure criteria for these composites. Translaminar fracture is one of the primary failure modes of unidirectional (UD) fiber-reinforced composites, and measuring it is essential for design purposes and in many material failure studies. However, the translaminar fracture parameters have not been evaluated for UD-FFRCs; thus, there is no data available in the literature. Moreover, conventional test methods for this failure mode are complex, and there is no standard method for measuring this value in compression. In this study, the translaminar fracture behavior of a UD flax/epoxy composite has been examined, and its fracture toughness in tension and compression in the fiber direction are determined following existing standard methods as well as using a methodology developed using infrared thermography. Compact tension specimens were adapted and used for this purpose. A fractographic study is conducted to examine the fracture surfaces and better understand the failure mechanisms. For tensile tests, the results of infrared thermography are in good agreement with those of ASTM E1922 and lie in the range of values obtained for similar composites in the literature.

138

Keywords: Flax fiber; Translaminar fracture energy; Fracture toughness; Flax-epoxy composites; Tensile and compressive translaminar fracture; Infrared thermography

5.2   Introduction

Over the last two decades, the need for materials with enhanced properties, lower cost, and improved sustainability has rendered natural (cellulosic) fiber-reinforced polymer composites (NFRCs) an attractive alternative to their synthetic glass fiber (GFRP) counterpart in structural and non-structural applications (Fuqua *et al.*, 2012; Ramesh *et al.*, 2017; Darshil U. Shah *et al.*, 2013; Yashas Gowda *et al.*, 2018). Among natural plant fibers (NFs), flax is considered one of the most promising for polymer composites due to its unique properties (Moudood *et al.*, 2018; Darshil U. Shah *et al.*, 2013; Yan *et al.*, 2014). Using continuous unidirectional (UD) and optimally configured reinforcements in NFRCs is crucial to maximizing their load-carrying performance (S. Goutianos & Peijs, 2003; S Goutianos *et al.*, 2006; Khanlou *et al.*, 2018). Therefore, UD flax fiber-reinforced composites (FFRCs) are of prominent importance for the industry. In addition to strength and stiffness, fracture toughness is an essential property of fiber-reinforced polymer composites (FRCs) for most engineering applications (Haldar *et al.*, 2019; Hughes *et al.*, 2002; Q. Liu & Hughes, 2008). Nowadays, the engineering desire for an optimized, efficient, sustainable, cost-effective, and damage tolerant product design in conjunction with the ever-growing applications of FFRCs necessitate characterizing the fracture toughness of these composites. The fracture toughness associated with translaminar failure mode (denoted by G_{IC}, when expressed in terms of energy and by K_{IC} when expressed in terms of stress intensity factor) is one of the primary mechanical properties of the fiber-reinforced composites (FRCs). This is particularly true when using the finite element method (FEM) to simulate specific material damages occurring in composite laminates, like fiber failure, matrix breaking, and delamination (El-Hajjar & Haj-Ali, 2005; Faggiani & Falzon, 2010; Falzon & Apruzzese, 2011; Israr *et al.*, 2014; Jose *et al.*, 2001). The FEM approach requires different fracture energies as input variables, and the fracture toughness in different directions and their corresponding evaluation methods are prerequisites for the FEM simulation of FFRCs. While the significance of translaminar fracture toughness (TFT)

measurement was recognized since the late '70s, it has attracted little interest (M. J. Laffan *et al.*, 2012). This is because FRCs were not used in primary structures, where this property is mostly required. At the same time, the advanced numerical simulation methods referring to this property were not yet developed (M. J. Laffan *et al.*, 2012). The situation is now different as FRCs are used in structures, and FEM is a commonly used numerical method. With the growing application of NFRCs, their TFT is expected to play an essential role in the future. Currently, it is required in many research fields, such as the machining of composite materials, where numerical models based on FEM are involved.

In the literature, measuring the translaminar fracture toughness of NFRCs is limited to a few studies that are all conducted only in tension. Hughes et al. (Hughes *et al.*, 2002) studied the TFT of some chopped NFRCs and compared them to that of a glass fiber mat composite. The G_{IC} value of GFRP was three-fold higher than those of NFRCs. They concluded that different micro-structural toughening mechanisms were activated in the NFRCs compared to GFRP. Silva et al. (Silva *et al.*, 2006) reported an in tension G_{IC} = 11.8 kJ/m^2 for woven sisal/polyurethane (PU) composite. They observed that G_{IC} increased with fiber volume fraction (V_f) and was impaired with the alkaline treatment of the fibers. Liu and Hughes (Q. Liu & Hughes, 2008) investigated the effects of textile yarn linear density, weave configuration, and stacking sequence on G_{IC} of woven FFRECs. They measured the K_{IC} of anisotropic woven-flax/epoxy composites following BS 7448 standard. According to their findings, the fracture behavior and K_{IC} are strongly dependent on the linear density of yarns and the direction of the test but is independent of the weave type. The authors reported K_{IC} values in the range of 3–8.5 MPa m$^{1/2}$ for the composites and concluded that the fracture toughness is more dominated by the fiber properties and V_f rather than the reinforcement configuration. Following ASTM D5045, Li et al. (Y. Li *et al.*, 2005) studied the fiber surface treatment effect on fracture properties of textile-sisal/vinyl-ester composite. They obtained K_{IC} = 4.2 MPa m$^{1/2}$ for the untreated fiber composite, which increased to 5.5 and 6.0 MPa m$^{1/2}$, respectively, with Silane and KMnO$_4$ fiber treatments. Ismail et al. (A. E. Ismail *et al.*, 2016) reported values of $K_{IC} \approx 8.5$ and $K_{IC} \approx 4.5$ MPa m$^{1/2}$ respectively for UD-twisted yarn and cross-ply woven kenaf/polyester composites tested based on ASTM D5045. Chizyuka and Kanyanga

(Chizyuka & Kanyanga, 2013) investigated the effects of hydrothermal aging and moisture absorption on the K_{IC} of sisal/polyester composites. They followed the ASTM E1922 procedure to evaluate the K_{IC} of the composites and obtained $K_{IC} \approx 6.25$ MPa m$^{1/2}$. The fractographic study revealed that the reduction of K_{IC} after moisture absorption was mainly due to fiber/matrix debonding, which was the dominant fracture mechanism in the composite. Manjunath et al. (G B *et al.*, 2015) followed ASTM E1922 and investigated the K_{IC} of jute fabric reinforced epoxy composites. However, the criteria of the standard were not carefully respected, and there is a mismatch between their reported test data and the reported K_{IC} values. Their result is also one order of magnitude higher than that of Ashik et al. (Ashik *et al.*, 2017), $K_{IC} = 7.71$ MPa m$^{1/2}$, for an analogous material.

5.2.1   Translaminar fracture toughness in tension

The ASTM E1922 standard (ASTM, 2015b) suggests the extended compact tension (ECT) specimen for measuring the tensile TFT of FRCs. ECT, Figure 5.1, is an extended configuration of the compact tension (CT) specimen, Figure 5.2, which was developed to overcome undesirable failure modes such as crack growth perpendicular to the pre-notch (Piascik *et al.*, 1997; Underwood *et al.*, 1995). ASTM E1922 was developed and adapted to measure the fracture toughness of FRCs in tension, while a number of studies have used CT specimens, along with ASTM E399, D5045, or other methods (Catalanotti *et al.*, 2010; M. J. Laffan *et al.*, 2010a, 2010b; Leonard *et al.*, 2009; H. Liu *et al.*, 2018; S. T. Pinho *et al.*, 2006). Without mentioning any particular reason, several researchers tested cross-ply laminates and utilized a rule-of-mixtures type approach to measure the fracture toughness of UD-FRCs (M. J. Laffan *et al.*, 2012). Jose et al. (Jose *et al.*, 2001) evaluated the tensile TFT of a carbon/epoxy cross-ply laminate [0/90]$_{15}$ as well as its constituent UD laminates, [0]$_{30}$ and [90]$_{30}$. They presented an analytical relationship between the K_{IC} of the laminate and those of its constituent UD sub-laminates. However, some of their specimens failed improperly, and their derived equation seems to have inconsistent dimensions. Pinho et al. (S. T. Pinho *et al.*, 2006) used a similar approach to determine the G_{IC} associated with the tensile and compressive failure of UD carbon/epoxy laminates using a cross-ply [0/90]$_{8S}$ laminate. They used CT and CC

specimens with the dimensions and fiber direction shown respectively in Figures 5.2a and 5.2b and followed the ASTM E399 procedure. However, they regenerated a finite-width correction factor based on FEM to replace the one defined in ASTM derived for isotropic materials. The authors assumed: (i) that the mode-I critical energy release rate of the cross-ply laminate is the sum of energies associated with the fiber fracture in the 0° layers and matrix cracking in the 90° layers (they thus neglected other damage modes and interaction between neighboring layers) and (ii) that the matrix cracking in the 90° layers occurred as a single crack parallel to the notch (similar to delamination mode-I). With this last assumption, the critical energy release rate in tension is quantitatively equivalent to that of mode-I delamination. This assumption seems reasonable, as the 0° layers are much tougher than the 90° layers, and is found to be a good approximation based on their findings in a previous work (S. Pinho *et al.*, 2009). For the particular cross-ply lay-up studied, they derived an equation used to calculate the G_{IC} for the UD laminate. Later on, Laffan et al. (M. J. Laffan *et al.*, 2010b) used the following generalized form of the derived equation (with the same assumptions) to study the lay-up effects on the fracture toughness of carbon/epoxy composites in tensile fiber failure mode;

$$G_{IC}^0 = \frac{t_{lam}}{t_0} G_{IC}^{lam} - \frac{t_{90}}{t_0} G_{IC}^{90} \tag{5.1}$$

where t_{lam}, t_0 and t_{90} are the thicknesses of the laminate, 0° and 90° layers within the laminate, respectively. G_{IC}^0 is the fracture energy associated with the fiber tensile failure mode, and G_{IC}^{90} represents the intralaminar mode-I matrix cracking fracture energy. In another study, Laffan et al. (M. J. Laffan *et al.*, 2011) observed that there was no interaction between the failure modes occurring in the 0° and 90° plies. This result confirms their approach. Nevertheless, it has been shown that the lay-up in the cross-ply laminates can affect the G_{IC} measured for the 0° plies (M. Laffan *et al.*, 2009; M. J. Laffan *et al.*, 2012; M. J. Laffan *et al.*, 2010b; Teixeira *et al.*, 2016). Donadon et al. (Donadon *et al.*, 2007) followed the same approach to calculate the fracture energy in woven cross-ply laminates along with a numerical method. The agreement of the experimental and numerical results confirmed the validity of this approach.

5.2.2 Translaminar fracture toughness in compression

By contrast to TFT in tension, there is no standard test method available to evaluate the fracture toughness of FRCs in compression. In a few works (Catalanotti *et al.*, 2010; S. T. Pinho *et al.*, 2006), modified CT specimens are used in compression with the test coupon renamed compact compression (CC). Pinho et al. (S. T. Pinho *et al.*, 2006) used the same approach explained in the previous section for determining TFT in compression of UD laminates. They used CC specimens with the configuration shown in Figure 5.2c and Figure 5.2d and followed the ASTM E399 procedure. They made the same assumptions considering that in compression loading, the matrix cracking in the 90° layers is close to what happens in delamination mode-II. Thus, the critical energy release rate in compression is quantitatively equivalent to that of mode-II delamination. They used Equation (5.2) to calculate the G_{IC} for the UD laminate in the fiber direction;

$$G_{IC} \mid_{fiber\ kinking} = 2G_{IC} \mid_{lam\ comp} - G_{IIC} \mid_{matrix\ intra} \tag{5.2}$$

where $G_{IC}|_{lam\ comp}$ is the critical energy release rate of the laminate, as measured by a CC test, $G_{IIC}|_{matrix\ intra}$ is the mode-II matrix failure intralaminar fracture energy, and $G_{IC}|_{fiber\ kinking}$ is the fracture energy associated with fiber-kinking failure mode. Overall, there is a significant difference between the fracture toughness values reported by the authors using different approaches to measure compressive TFT (M. J. Laffan *et al.*, 2012; H. Liu *et al.*, 2018). Perhaps this indicates that conventional mechanical tests are not suitable for this purpose. The compressive fiber failure mode in laminated composites is known as a very complex phenomenon, which is the result of fibers micro-buckling and formation of kink-bands or crushing (Gutkin *et al.*, 2010; S. T. Pinho *et al.*, 2006; Soutis & Curtis, 2000). So, and unlike tension, the authors observed large damage zones. Therefore, to measure the pure TFT in compression, the damage mechanisms should be separated.

5.2.3   Infrared thermography/Translaminar fracture toughness measurement

In the past two decades, infrared thermography (IRT) has been broadly used to investigate the energy-dissipative processes in materials, for example, plastic deformation in metals (Dumoulin *et al.*, 2010) or damage in polymeric materials (Wattrisse *et al.*, 2002). For composite materials, Naderi et al. (Naderi *et al.*, 2012) used IRT to characterize the damage evolution in fatigue loading. They found that the results were consistent with those obtained by acoustic emission, while Lisle et al. (T. Lisle *et al.*, 2013; T. Lisle *et al.*, 2015) used it to study damage development in fabric-glass/epoxy composites. The relation between fracture toughness and dissipative work has already been proved (Freund & Hutchinson, 1985), and depending on the material, the ratio of the dissipative work converted into thermal energy can vary between 10 and 100% (Kapoor & Nemat-Nasser, 1998; Z. Li & Lambros, 2001). Lisle et al. (Teddy Lisle *et al.*, 2015) showed that for a carbon/epoxy composite, the ratio of dissipative work converted to heat should be close to 100%, but for metallic materials, this ratio is usually lower. The authors used the IRT to measure the fracture toughness of the GFRP in tension (T. Lisle *et al.*, 2013) and that of the UD-carbon fiber-reinforced polymer (CFRP) composite in compression (Teddy Lisle *et al.*, 2015; Teddy Lisle *et al.*, 2014). IRT made it possible to separately assess the dissipated energy due to fiber failure in compression and eliminate those associated with material crushing at loading points or secondary cracks. They obtained a value of G_{IC} = 42.5 N/mm in compression and found their results consistent with those of Hongkarnjanakul et al. (Hongkarnjanakul *et al.*, 2013) (40 N/mm) and other researchers (S. T. Pinho *et al.*, 2006; Soutis & Curtis, 2000). There is no previous research using this approach to address NFRCs.

In summary, no standard test methods have been developed for measuring G_{IC} of NFRCs and of FRCs in compression, and a very limited number of studies have addressed these topics, while all NFRCs have been tested in tension. These are essential properties for engineering design purposes and the modeling of these materials with numerical methods, such as FEM. Moreover and to our knowledge, no fractographic and micrographic analysis of this subject have been performed for UD-flax fiber-reinforced epoxy composites (FFRECs). The work

presented in this study aims at evaluating the fracture energy associated with the translaminar failure of the UD-FFRECs, using two methodologies, along with an investigation of the fracture behavior and viability of the standard test procedures for FFRECs considering that these procedures are used for synthetic (glass or carbon) FRCs. In the first method, the composite was tested according to the existing ASTM E1922 standard. The translaminar fracture was studied, and the G_{IC} value in tension for crack propagating perpendicular to fibers was determined and validated. In the second method, employing the IRT-based methodology developed and implemented for this purpose by Lisle et al. (Teddy Lisle *et al.*, 2015; T. Lisle *et al.*, 2013; Teddy Lisle *et al.*, 2014) as well as ASTM D5045 standard, G_{IC} of UD-FFRECs in tension and compression was determined, and the material behavior was assessed.

5.3   Material system and test specimens

Unidirectional flax fibers, FLAXTAPE™ 200 (from LINEO – France), with a width of 400 mm and surface density of 200 g/m^2, were used to reinforce Marine 820 Epoxy System, mixed with 18 Wt% Marine 824 hardener (from ADTECH® Plastic Systems), to prepare the UD-FFREC laminates. The composite laminates were molded using the RTM process. The layers of flax fibers were stacked up according to the required number of layers and orientation of fibers. 300 mm × 300 mm composite plates were molded, starting with $[0]_{12}$ and $[(0/90)_4/0]_s$ laminates, respectively for ECT and CT/CC specimens; then, a third configuration, $[(90/0)_4/90]_s$, has been used to improve the translaminar crack propagation for ECT specimens, as detailed in Table 5.1.

Table 5.1 Configuration and applications of flax/epoxy laminates

Plate	Application Test	Specimen type	Layup	Reinforcement surface density (g/m^2)	Volume fraction (%)	Thickness (mm)
1	E1922	ECT	$[0]_{12}$	200	41	4.04
2	IRT	CT & CC	$[(0/90)_4/0]_s$	200	41	6.06
3	E1922	ECT	$[(90/0)_4/90]_s$	200	41	6.06

The number of layers and thickness of laminates were precisely calculated, according to the ASTM D3171 procedure, and controlled with spacers during molding to result in a unique V_f = 0.41 for all composite plates while attaining the required thickness for the test specimens.

ECT specimens were prepared according to ASTM E1922 for evaluating the TFT in tension. Figure 5.1 shows the configuration and photograph of a typical specimen. The CT and CC specimens used for TFT measurement in combination with IRT were prepared according to in-plane dimensions specified in Pinho et al. study (S. T. Pinho *et al.*, 2006). The configurations and photographs of typical specimens are shown in Figure 5.2. The same type of CT specimen was also used in (M. J. Laffan *et al.*, 2010a, 2010b; M. J. Laffan *et al.*, 2011). Pujols Gonzalez et al. (Pujols Gonzalez, Bouvet, & Vieille, 2020) used CT and CC specimens to evaluate in tension and compression TFT of CFRP composites using IRT-based methodology, respectively. A similar methodology is adapted and employed in this study. Rectangular specimens were cut by a 10-inch/90-tooth, DIABLO's cutting saw blade, with high-density carbide tooltips. Then, the loading-pin holes were drilled with the help of sacrificed plates to avoid damages to the specimens. A Protostar® mini corner radius solid carbide shoulder/slot milling cutter (Protostar®-Walter tools) was used to cut the notch in ECT specimens. As can be seen in Figure 5.1d, despite the low machinability of NFRCs in terms of surface quality, a very neat notch is cut without damaging the composite. The 4 mm-notch on the CT and CC specimens were cut using a milling cutter; the notch mouth on the CC was widened, and the final notch (pre-crack) on CT was cut using a wire saw. Two clevises were designed and manufactured to eccentrically introduce the load to the specimens (Figure 5.1c).
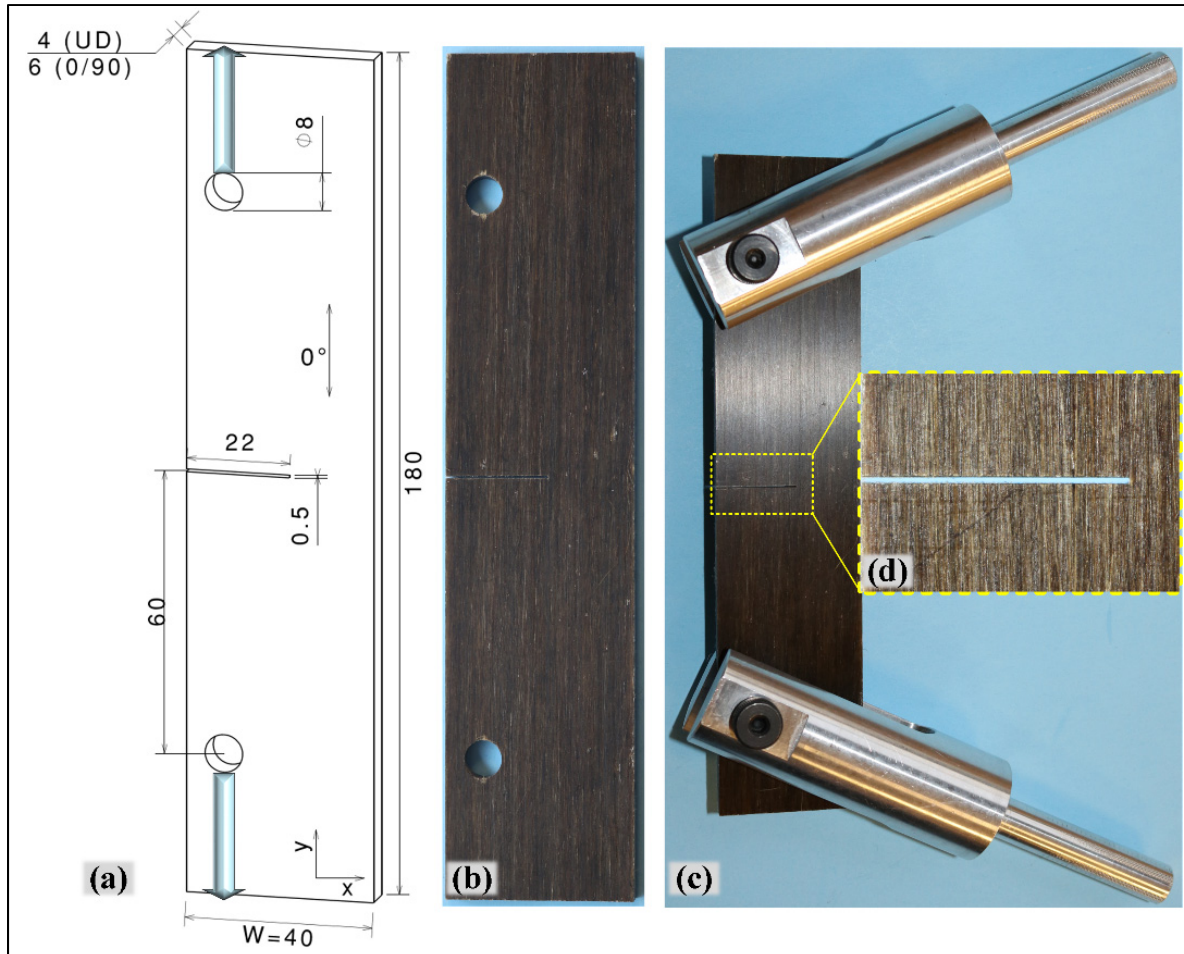
Figure 5.1 The ECT configuration (a), test specimen (b), load application configuration (c), and notch (d) (Dimensions in mm)

5.4 Translaminar fracture tests and data reduction methods

5.4.1 Standard tension testing of ECT specimens

ASTM E1922 standard (ASTM, 2015b) involves tension testing of single-edge-notch specimens to determine the tensile TFT of various carbon and glass/polymer composites. However, it can be applied to other FRCs, provided that the specimen dimensions and the test results satisfy the requirements of the standard. Following the guidelines of this standard and aiming at measuring the TFT of the UD-FFRECs, ECT specimens (Figure 5.1b) were cut from the UD-FFREC laminate with a nominal thickness of 4 mm (plate 1 in Table 5.1). Here,
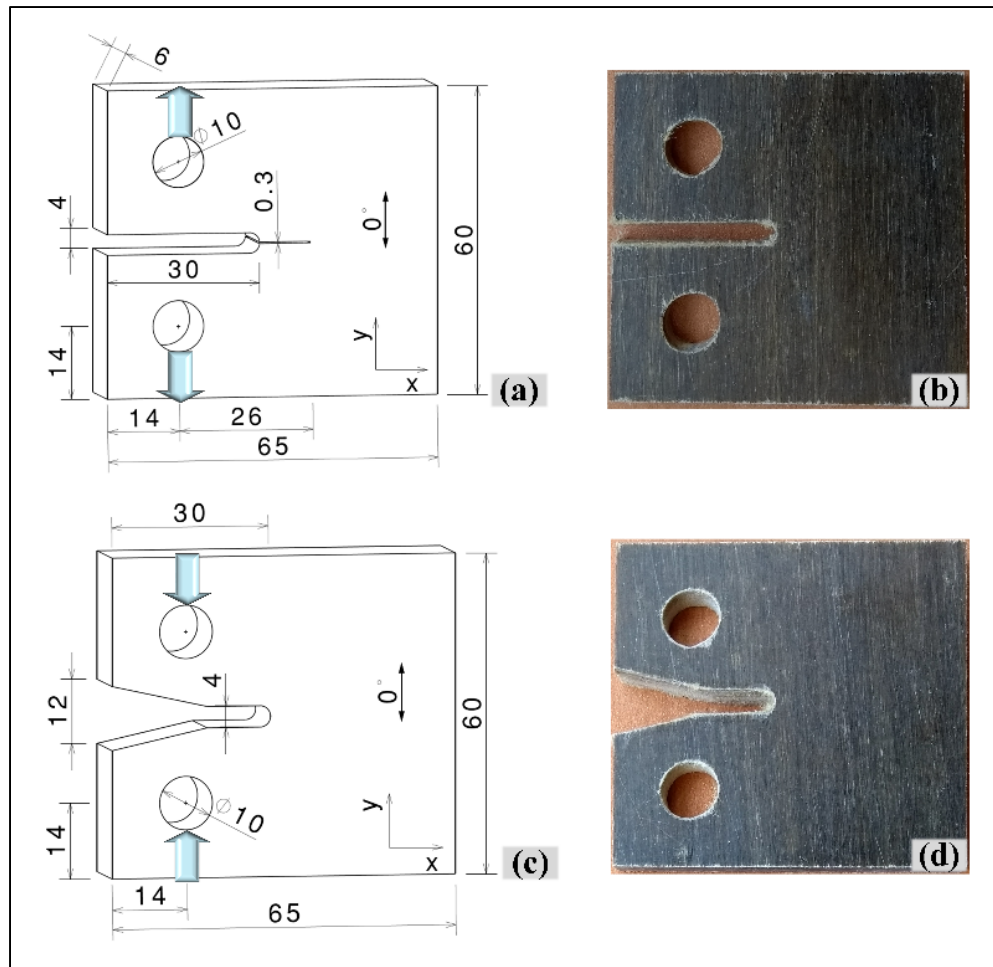
Figure 5.2 The CT (a) and CC (c) configurations and CT (b) and CC (d) test
specimens (Dimensions in mm)

the low stiffness of the ECT specimens made it impossible to install the conventional extensometers, using knife edges, at the notch-mouth to measure the notch mouth opening displacement (NMOD). Alternatively, a digital image correlation (DIC) setup, synchronized with load application, was used for this purpose, as shown in Figure 5.3a. However, none of the five ECT specimens tested with such setup experienced a self-similar (parallel to the pre-notch) crack growth and did not result in effective translaminar crack growth of concern in this test method. Indeed, the crack propagated perpendicular to the notch and in the fiber direction, which invalidated the tests, as shown in Figure 5.3b. To the authors' knowledge, no ECT specimens of synthetic or natural UD-FRCs have been tested in the literature. Also, the reported ECT tests are mostly for natural/synthetic fabric or cross-ply reinforcement

architectures (Chizyuka & Kanyanga, 2013; G B *et al.*, 2015; Hou & Hong, 2014; M. J. Laffan *et al.*, 2012), and a few were from pultruded composites (El-Hajjar & Haj-Ali, 2005). Therefore, no benchmark study was possible, and these experiments were unavoidable.
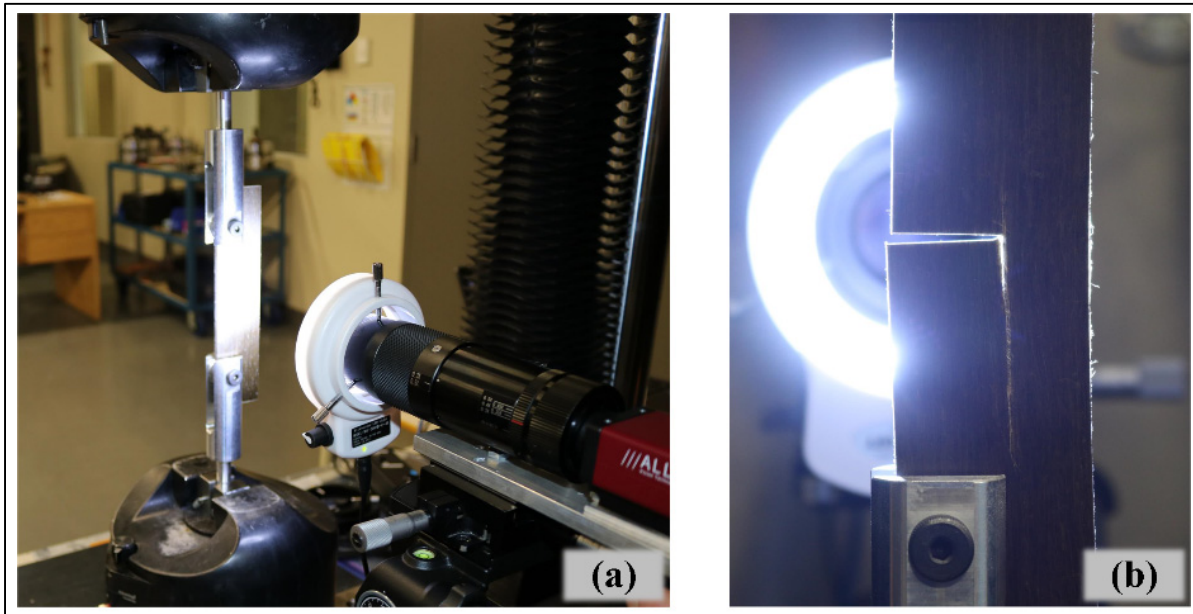
Figure 5.3 Test setup with DIC used to measure NMOD (a) and failed ECT UD specimen (b)

To overcome this difficulty, cross-ply laminates were used to avoid the large difference in strength between the longitudinal and transverse direction of the test specimen, such that each 0° layer is backed by a 90° layer to inhibit crack propagation perpendicular to the notch, similar to the approach in (M. J. Laffan *et al.*, 2010b; S. T. Pinho *et al.*, 2006). Equation (5.1) is used to calculate the translaminar fracture energy of UD plies using that of a cross-ply laminate and the Mode I and Mode II interlaminar fracture energies of the UD laminate. For this purpose, a second laminate was fabricated (plate 3 with the lamination sequence of $[(90/0)_4/90]_s$ and nominal thickness of 6 mm), and ECT specimens (Figure 5.1a) were cut and prepared. These thick and stiff enough specimens made possible the installation of an extensometer to measure the mouth opening. Therefore, precisely machined knife edges were bonded to the specimens' edge on both sides of the notch mouth, Figure 5.4, and the extensometer MTS (632.02F-20) was installed to measure the notch-mouth-opening displacement (NMOD). The tests were conducted with a 0.7 mm/min crosshead displacement rate on an MTS (858 Mini Bionix-II)

machine, with a mounted 15 kN load-cell. The test setup and specimen are shown in Figure 5.4a and Figure 5.4b. The tests continued until the applied force dropped to a magnitude of less than 50% of the peak load. The specimen exhibited a translaminar self-similar crack growth, as expected, Figure 5.4c.
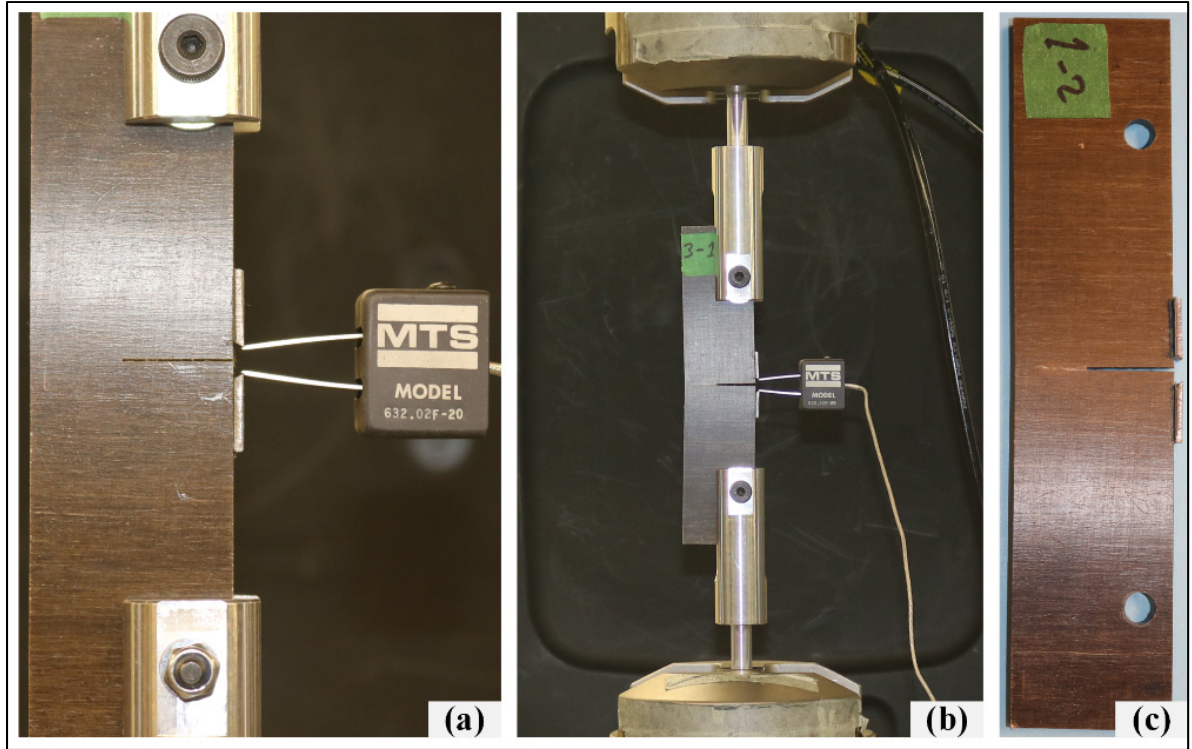
Figure 5.4 ECT specimen; knife edges and installed extensometer (a) test setup (b), and failed sample (c)

Data reduction was performed according to ASTM E1922, and the TFT was calculated through the stress intensity factor approach, as;

$$K_{Ic} = \left[\frac{P_{max}}{BW^{1/2}}\right] \frac{\alpha^{1/2}[1.4 + \alpha][3.97 - 10.88\alpha + 26.25\alpha^2 - 38.9\alpha^3 + 30.15\alpha^4 - 9.27\alpha^5]}{[1 - \alpha]^{3/2}} \quad (5.3)$$

where K_{Ic} is the critical stress intensity factor (MPa-m$^{1/2}$), P_{max} is the maximum applied or fracture load (MN), $\alpha = a/W$ is a dimensionless parameter, while a is the notch length, B is

specimen thickness, and W is specimen width (a, B and W are in meter). According to the standard, K_{Ic} provides a valid measure of TFT, when the damage zone is relatively small. This criterion is defined based on NMOD values at maximum load as $\Delta V_n / V_{n-0} \leq 0.3$, for ΔV_n and V_{n-0} shown in Figure 5.6. For orthotropic plates under plane stress (with a pre-crack subjected to in-plane loading), the fracture energy G_{IC} can be calculated from K_{Ic} as follow (Jose *et al.*, 2001; Lin, Feng, & Rowlands, 1997; Paris & Sih, 1965; S. T. Pinho *et al.*, 2006; Soutis & Curtis, 2000);

$$G_{Ic}^{lam} = \frac{K_{Ic}^2}{\sqrt{2E_{xx}E_{yy}}}\left[\left(\frac{E_{xx}}{E_{yy}}\right)^{1/2} + \frac{E_{xx}}{2G_{xy}} - v_{xy}\right]^{1/2} \tag{5.4}$$

where E_{xx}, E_{yy} are the laminate elastic moduli respectively in the x and y directions (shown in Figure 5.1a, Figure 5.2a, and Figure 5.2c), G_{xy} is the laminate shear modulus, and v_{xy} is the Poisson's ratio. For the [(90/0)4/90]s laminate, these properties, presented in Table 5.3, are calculated from those of the UD laminate given in Table 5.2, published in a previous work (Saadati et al., 2020c), by using the classical laminate theory (Hyer & White, 2009).

Table 5.2 Mechanical and thermal properties of UD-FFREC ply (Saadati *et al.*, 2020c)

Longitudinal elastic modulus, E_{11}	22.69[*] GPa
Transverse elastic modulus,E_{22}	4.34[*] GPa
Shear modulus, G_{12}	1.92 GPa
Poisson's ratio, v_{12}	0.4[*]
Density, ρ	1280 kg/m^3
Specific heat, C	665J/kg/K
Thermal conductivity in normal (z) direction, k_{33}	0.115W/m/K

*Average of the values in tension and compression

Table 5.3 Elastic properties of [(90/0)4/90]s

E_{xx} (GPa)	E_{yy} (GPa)	G_{xy} (GPa)	v_{xy}
14.74	12.68	1.92	0.14

5.4.2   Infrared thermography method

In order to overcome the problems experienced with experimental methods used to study the translaminar fracture of composite materials, it was proposed to develop an approach allowing estimating the rate of energy release via the temperature measurement in (Teddy Lisle *et al.*, 2015; T. Lisle *et al.*, 2013; Teddy Lisle *et al.*, 2014; Naderi *et al.*, 2012). Characterizing the fracture energy utilizing IRT is an idea conceptualized based on the principles of irreversible thermodynamics and thermo-mechanical laws. The complete details of the methodology, including all assumptions made and their validity, are well described in (Teddy Lisle *et al.*, 2015; T. Lisle *et al.*, 2013; Teddy Lisle *et al.*, 2014) for evaluating the tensile and compressive fracture energy of FRCs, and the reader should refer to these documents for more details.

Having the dissipated energy evaluated with IRT, the fracture energy, G_{IC}, can be determined using Equation (5.5) (Teddy Lisle *et al.*, 2015; T. Lisle *et al.*, 2013);

$$G_{IC} = \frac{dW_{irrev}}{dA} = \frac{dW_{diss}}{\beta.dA} \tag{5.5}$$

where dW_{irrev} denotes the total irreversible energy, dW_{diss} is the energy dissipated as heat, dA is the crack surface growth and $\beta = \frac{dW_{diss}}{dW_{irrev}}$ is the Taylor–Quinney coefficient ($0 \leq \beta \leq 1$).

Some studies of metallic materials reported $\beta \approx 1$ for Tantalum (Kapoor & Nemat-Nasser, 1998; Teddy Lisle *et al.*, 2015) and $0.5 \leq \beta \leq 1$ for stainless steel, depending on the applied strain rate (Teddy Lisle *et al.*, 2015). However, allocating value for this ratio remains a delicate issue in this study, because, no values are available for the flax/epoxy composite under study.

Furthermore, the magnitude of the coefficient is strain and strain-rate dependent (Z. Li & Lambros, 2001; Teddy Lisle *et al.*, 2015; T. Lisle *et al.*, 2013). Li and Lambros (Z. Li & Lambros, 2001) investigated PMMA and PC polymers in terms of the value of β and its sensitivity to strain and strain-rate. The authors found it impossible to measure β for PMMA; however, they reported values between 50% for high strain and 100% for low strain, independent of the strain-rate in the ranges of the investigation. Considering the available β values for polymers in the literature, values of $\beta = 0.5$ and $\beta = 0.9$ were chosen for this study. The results are then compared to those obtained from the ASTM E1922 standard test method to evaluate the validity of the assumptions.

In this study, the 3D thermal analysis methodology developed in (Teddy Lisle *et al.*, 2015; T. Lisle *et al.*, 2013) is utilized to evaluate the heat sources in the composite using the thermal properties in Table 5.2. From the generated heat, the dissipated energy, and then, using Equation (5.5), the critical energy release rate or fracture energy G_{IC} is calculated. For this purpose, the adapted CT and CC specimens from (S. T. Pinho *et al.*, 2006), shown in Figure 5.2, were cut from $[(0/90)_4/0]_s$ laminate (Plate 2 in Table 5.1) and mechanically loaded in tension and compression respectively. CT tests were conducted following ASTM D5045 standard, and CC tests were performed with the same procedure with a compression loading. The temperature change at the surface of the specimen (outermost 0°-ply of the $[(0/90)_4/0]_s$ laminate) was simultaneously recorded and synchronized with the load and displacement data. The test setup is shown in Figure 5.5a. It can be noticed that for the CC tests, the grip of the machine was only put on the axis of load introduction in order to have a larger filmed area (Figure 5.5c). The translaminar fracture tests were carried out on an electromechanical traction machine (INSTRON 100kN) at ambient temperature ($\approx 25\,°C$) and a constant displacement rate of 2 mm/min. The thermal data of the specimen surface was recorded at a frequency of 50 Hz using an infrared camera (FLIR SC7000) with a resolution of 320×256 pixels, and a thermal resolution of 0.025 K for temperature variation measurement. The spatial resolution (pixel size) determined by the focal distance is set at 0.264 mm. The target surface of the specimen was painted black in order to maximize the emissivity coefficient, and then the value is supposed to equal 1 for data treatment. As expected, for CT specimens, the through-the-

thickness crack propagated parallel to the 90° fibers by breaking the fibers in the 0° layers and created almost a planar fracture path, Figure 5.5a. The fracture path at the edge of the specimen opposite to the notched side shows that the crack path is almost planar.
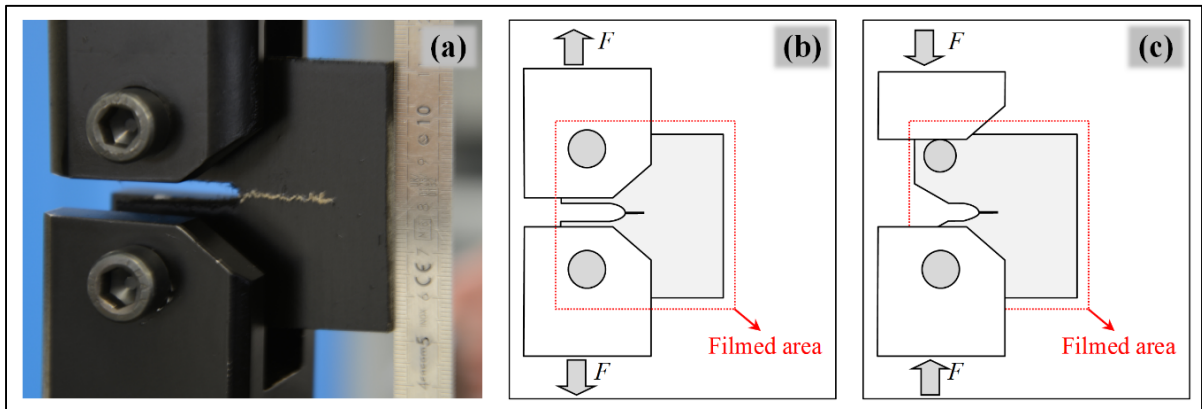
Figure 5.5 Experimental setup for IRT methodology (a), test specimen and thermal investigation area for CT (b) and CC (c)

5.5   Results and discussion

5.5.1   Standard tension testing of ECT specimens

A typical load vs. NMOD curve of a cross-ply ($[(90/0)_4/90]_s$) ECT specimen is shown in Figure 5.6. From this curve, it can be observed that the composite exhibits a linear behavior (R^2 =0.997) up to around 80% of the maximum load. Subsequently, upon initiating the damage zone ahead of the notch tip, a gradual deviation from linearity appears and continues up to the peak load. After reaching the peak value, the load decreases slowly with no sudden drops, meaning that a stable translaminar fracture occurs and propagates, consistent with the observations during the test. Similar behavior was observed for woven-flax/epoxy composites tested using CC specimens (Q. Liu & Hughes, 2008), woven-sisal/polyester composites tested using ECT (Chizyuka & Kanyanga, 2013), and woven-sisal/PU composites tested by CT specimens (Silva *et al.*, 2006). On a macroscopic scale, the wake of self-similar crack can be seen on a failed specimen in Figure 5.4c, satisfying the requirement of the ASTM E1922 concerning effective translaminar crack growth. As shown for the typical specimen in Figure

5.6, the additional NMOD during fracture, ΔV_n, fulfills the criterion of ASTM E1922, in this case with $\Delta V_n/V_{n-0} = 0.18 \leq 0.3$, and validates the translaminar fracture toughness (K_{IC}) obtained using Equation (5.3) for all the tests.
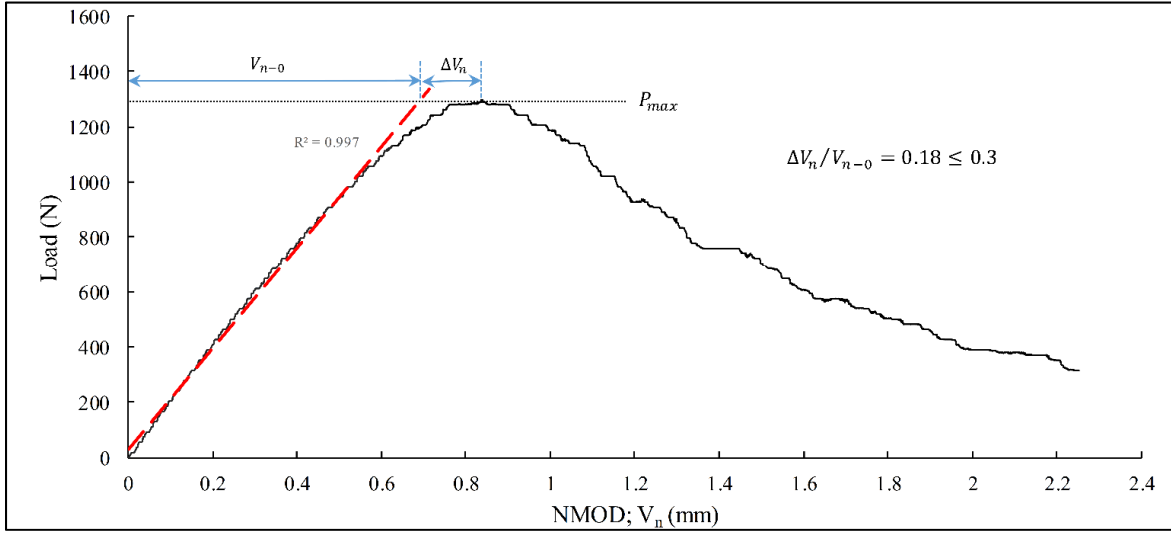
Figure 5.6 Load vs. Notch-mouth-opening displacement (NMOD) curve

Substituting the α parameter value in Equation (5.3) and using the maximum load, the K_{IC} of the cross-ply specimens ($[(90/0)_4/90]$s) was computed, and the results are summarized in Table 5.4. The fracture energy (G_{IC}^{lam}) was subsequently obtained from the data in Table 5.3 and Equation (5.4) and is also presented in Table 5.4. As discussed earlier, Equation (5.1) is used to calculate the fracture energy of the $0°$ sub-laminates (G_{IC}^0) where G_{IC}^{90} is assumed to be equivalent in magnitude to the mode-I interlaminar fracture energy of the UD-FFREC, G_{IC}^{delam}, which was evaluated in a separate study as $G_{IC}^{delam} = 0.691$ kJ/m^2 (Saadati et $al.$, 2020a). Accordingly, t_0 and t_{90} were obtained by considering they are proportional to the number of the corresponding plies in the laminate, i.e., 8 and 10 plies. For comparison purposes with the literature data, K_{IC}^0 of the UD-FFREC laminate was calculated back from G_{IC}^0 and its elastic properties (given in Table 5.2) using Equation (5.4). The results are presented in Table 5.4.

Table 5.4 Fracture toughness and fracture energy of UD-FFREC

	K_{IC}^{lam} (MPa m$^{1/2}$)	G_{IC}^{lam} (kJ/m^2)	K_{IC}^{0} (MPa m$^{1/2}$)	G_{IC}^{0} (kJ/m^2)
Mean	8.07	7.37	14.27	15.71
STD	0.30	0.55	0.57	1.23
COV (%)	3.78	7.41	3.99	7.82

It is difficult to compare these results with the literature considering the very limited works published on the measurement of TFT in NFRCs, particularly FFRECs. Nevertheless, the value obtained for K_{IC}^{lam} is in excellent agreement with the results published by Liu et al. (Q. Liu & Hughes, 2008) for woven-flax/epoxy CT tests, shown in Table 5.5. They published K_{IC}^{lam} values in the range of 3 to 8.5 MPa m$^{1/2}$, albeit at lower V_f (from 31% to 35%), that covers the obtained value in this study. The K_{IC}^{lam} = 7.2 MPa m$^{1/2}$ mentioned in Table 5.5, with the reinforcement configuration most consistent with the cross-ply laminate tested in this present study but for a fabric instead of UD reinforcement in the present study, should be compared to the value of K_{IC}^{lam} in Table 5.4. Overall, considering the difference in V_f and ply architecture, their results are consistent with the findings of the present study, and these two studies confirm each other. K_{IC} = 7.71 MPa m$^{1/2}$ reported by Ashik et al. (Ashik *et al.*, 2017) for 50 wt% woven jute/epoxy composite (Table 5.5) is also in the range of the obtained results. The higher fiber content, but lower strength of jute fibers could have balanced the toughness to be consistent with the result of the present work (Hughes *et al.*, 2002; Rajak *et al.*, 2019; Ramesh *et al.*, 2017). Chizyuka and Kanyanga (Chizyuka & Kanyanga, 2013) obtained K_{IC} = 6.5 MPa m$^{1/2}$ for fabric-sisal/polyester composites with V_f between 50% to 55% (Table 5.5). The lower K_{IC} of this composite can be attributed to the lower tensile strength of sisal fibers compared to flax fibers (Hughes *et al.*, 2002; Rajak *et al.*, 2019; Ramesh *et al.*, 2017). On the other hand, Silva et al. (Silva *et al.*, 2006) reported G_{IC} ≈ 11.5 and G_{IC} ≈ 7 kJ/m^2 respectively for a fabric and short fiber sisal/PU composite with V_f ≈ 0.30 (Table 5.5). The G_{IC} of short fiber sisal/PU composite is in the range of our results, but that of sisal-fabric is much higher. Due to reporting the toughness of sisal-fabric/PU in the form of G_{IC}, it cannot be compared with those of similar materials; fabric-sisal/polyester composite reported in (Chizyuka & Kanyanga, 2013) and

textile sisal/vinyl-ester reported in (Y. Li *et al.*, 2005), both indicated by K_{IC}, see Table 5.5. The authors attributed the high performance of fabric-reinforced PU to the better compatibility between NFs and natural resins and to the structure of the reinforcement. Li et al. (Y. Li *et al.*, 2005) reported a $K_{IC} = 4.2$ MPa m$^{1/2}$ for a textile sisal/vinyl ester composite at $V_f \approx 0.32$, which increased to 6 MPa m$^{1/2}$ after applying a fiber surface treatment. Hughes et al. (Hughes *et al.*, 2002) measured $K_{IC} = 5.04$ and $K_{IC} = 5.62$ MPa m$^{1/2}$ respectively for jute and hemp non-woven felt reinforced polyester, Table 5.5. The reported $K_{IC} \approx 8.5$ MPa m$^{1/2}$ by Ismail et al. (A. E. Ismail *et al.*, 2016) for UD twisted-kenaf-yarn/polyester composites is also consistent with the values determined in this research, Table 5.5. Considering the reasonable variability of the results and after comparing them to the available literature data, it can be concluded that the measured values are a realistic representation of the fracture toughness and fracture energy of the FFREC.

Table 5.5 Literature data for fracture toughness of NFRCs

	K_{IC}^{lam} (MPa m$^{1/2}$)	K_{IC}^{lam} (MPa m$^{1/2}$)	K_{IC}^{lam} (MPa m$^{1/2}$)	G_{IC}^{lam} (kJ/m^2)	K_{IC}^{lam} (MPa m$^{1/2}$)	K_{IC}^{lam} (MPa m$^{1/2}$)	K_{IC}^{lam} (MPa m$^{1/2}$)
Ref.	(Q. Liu & Hughes, 2008)	(Ashik *et al.*, 2017)	(Chizyuka & Kanyanga, 2013)	(Silva *et al.*, 2006)	(Y. Li *et al.*, 2005)	(Hughes *et al.*, 2002)	(A. E. Ismail *et al.*, 2016)
Material system	Woven flax/epoxy	Woven jute/epoxy	Fabric sisal/polyester	Fabric & short fiber sisal/PU	Fabric sisal/VE	Jute&hemp mat/polyester	Woven kenaf/polyester
Fiber content	V_f = 0.31 - 0.35	50 Wt.%	V_f = 0.50 - 0.55	$V_f \approx 0.30$	$V_f \approx 0.32$	$V_f \approx 0.41$	No available
Toughness	(3 - 8.5) 7.2 ($V_f \approx 0.33$)	7.71	6.5	11.5 & 7	4.2 - 6	5.04 & 5.62	8.5

5.5.2   Fractography of the ECT specimens

The fracture paths of ECT specimens when the load dropped to about $0.2P_{max}$, are shown in Figure 5.4c and Figure 5.7a. The failed specimen is not separated into two parts to expose the fracture surface, so it is difficult to examine the fracture in terms of failure mechanisms. On the other hand, separating the two parts of the specimen would alter the rupture faces. Nevertheless, to perform a microstructural study and explore the fracture mechanisms, one of the specimens was loaded up to full separation to expose the fracture surface near the notch tip.

The micrographs are shown in Figure 5.7a and Figure 5.7b. At the surface ply, which is a 90° ply oriented parallel to the notch, matrix cracking and splitting of the ply has occurred, and then, with crack growth, fiber-matrix debonding and fiber bridging have developed. In addition, the crack emanated from the corner of the notch and propagated in a self-similar manner. For further analysis of the failure mechanisms, the fracture surface is investigated from three viewing directions, as indicated in Figure 5.8a. The normal view of the fracture surface, Figure 5.8b, clearly shows the 0° and 90° layers. Fiber-matrix debonding and matrix cracking can be observed in the 90° plies, while fiber fracture occurred in the 0° plies. The side view in Figure 5.8c shows a huge fiber pull-out, fiber bundle fracture, and fiber bundle splintering. These phenomena are accepted as the dominant failure modes contributing to fracture toughness in composites (M. J. Laffan *et al.*, 2010b; M. J. Laffan *et al.*, 2011; S. T. Pinho *et al.*, 2006; Silva *et al.*, 2006). The high volume of fiber pull-out is an indication of the poor fiber-matrix adhesion (due to poor compatibility of hydrophilic NFs towards the hydrophobic polymer matrix), resulting in weak interfaces that have been observed in several works (Habibi *et al.*, 2017b; Hughes *et al.*, 2002; Y. Li *et al.*, 2005; Saadati *et al.*, 2020c). Although fiber pull-out is a mechanism that accounts for significant energy absorption in FRCs (Hughes *et al.*, 2002), poor fiber-matrix adhesion along with the elementary flax fiber slippage inside the flax bundle after fiber fracture could ease the fiber pull-out without a corresponding large energy absorption. This effect will cause fiber pull-out to share a smaller contribution to fracture toughness. There is no information in the literature about the fracture toughness of flax

fibers; however, these might be some reasons why FFREC is offering lower TFT compared to engineered FRCs. The top view, Figure 5.8d, reveals the depth of the pulled-out fibers and the severity of this phenomenon.
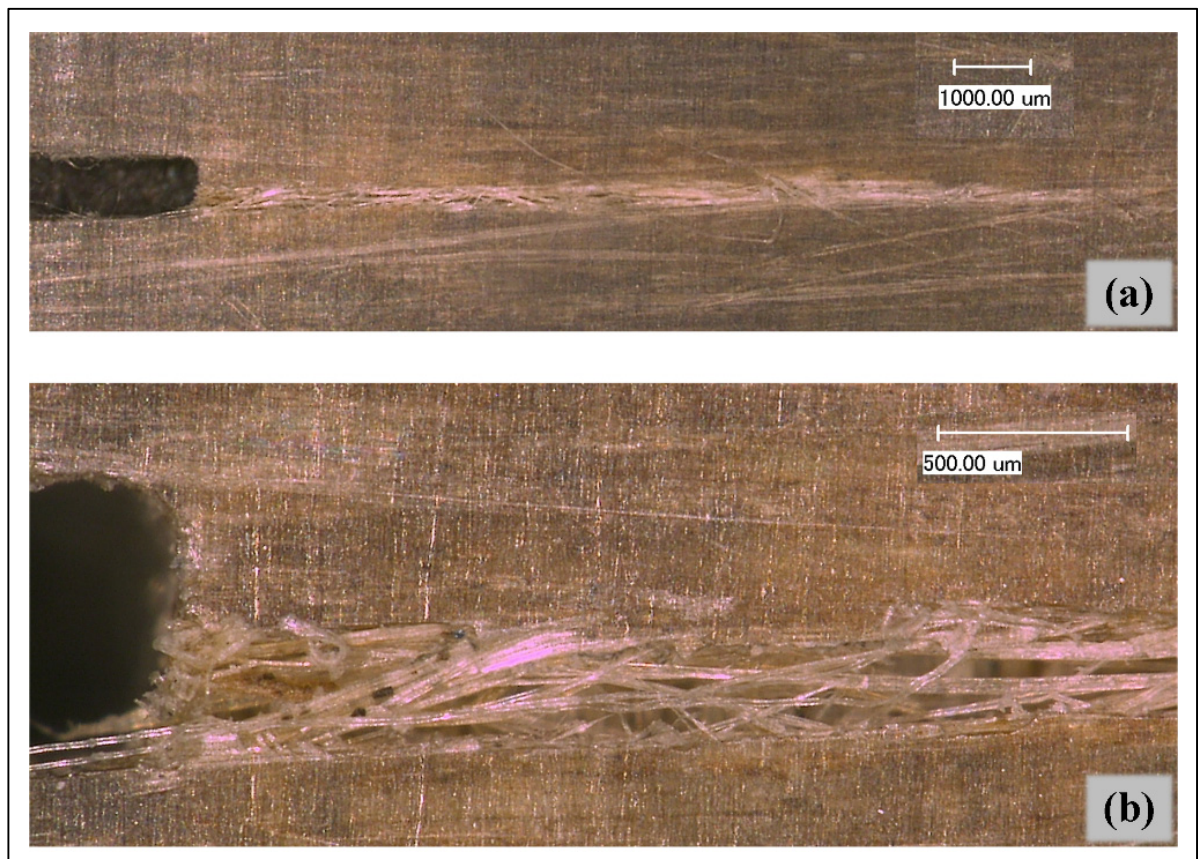
Figure 5.7 Fracture path of cross-ply ECT specimen; (a) whole crack growth after failure, and (b) fiber bridging
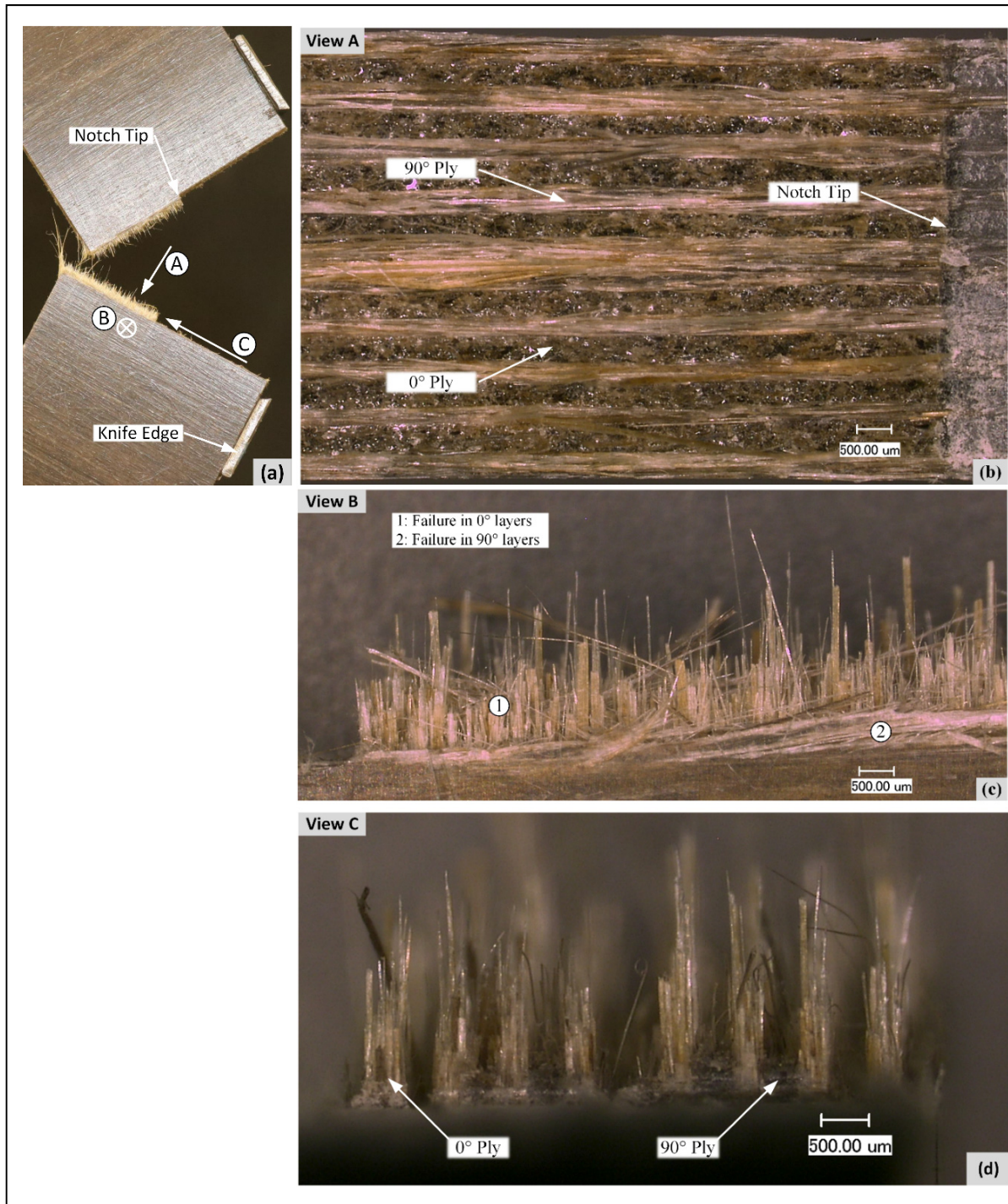
Figure 5.8 Fracture surface of cross-ply ECT specimen; (a) definition of the viewing directions, (b) normal view to fracture surface, (c) normal view to specimen surface, and (d) view parallel to the notch

5.5.3 Infrared thermography method

Subjecting six CT to tensile load and seven CC specimens to compression load, the translaminar fracture tests were conducted according to the method described above. Typical temperature variation fields measured using IRT associated with the crack propagation are presented in Figure 5.9. The temperature increase observed during crack propagation is clearly higher for the CT specimens than for the CC ones: increasing of about 5 °C for CT and less than 2 °C for CC. This result confirms the usual conclusion that the fracture toughness of translaminar failure is higher in tension than in compression (Catalanotti *et al.*, 2010; M. J. Laffan *et al.*, 2011; H. Liu *et al.*, 2018; S. T. Pinho *et al.*, 2006). Moreover, the extent of warming over the coupon is larger for compression; this means the phenomenon of compressive failure creates a larger area of damage.

The corresponding load-displacement curves of CT and CC tests are plotted in Figure 5.10a and Figure 5.10b, respectively. For all the CT and CC tests, the crack propagation started about at maximum load. The CT specimens experienced a progressive propagation of crack during the load drop. The two first CC tests, CC1 and CC2, had to be stopped at 6.5 mm of displacement due to a contact between the edges of the notch. Then the other CC tests were continued until 5.5 mm of displacement and the sample unloaded until diminishing of the load.

Finally, the intrinsic dissipation was evaluated using the IRT measure for CT (Figure 5.10c) and CC specimens (Figure 5.10d). For the CT specimens, the intrinsic dissipation is significant (value higher than 4×10^6 J/m^3) and concentrated at the crack edges. In Figure 5.10c, the edges of the sample are also seen due to the movement of the sample during the test. Evidently, the value of the intrinsic dissipation evaluated at the sample edges should not be considered. For the CC specimens, the intrinsic dissipation is relatively low (a value lower than 0.5×10^6 J/m^3), and the crack path is barely detectable. Moreover, due to the scale used in Figure 5.10d, some measured noises are visible. As will be explained in the two subsequent sections, according to the literature data for synthetic FRCs, G_{IC} in compression is lower than in tension. Therefore, knowing that the generated heat is proportional to G_{IC}, it is logical to obtain lower intrinsic

dissipation for CC specimens than for CT specimens. However, for the authors, the obtained result for CC tests seems too low. Since IRT measures the temperature only at the surface, this might be due to the delamination (observed in compression testing of FFREC (Saadati *et al.*, 2020c)) and possible buckling of the outer plies, which would hide a significant part of the created heat. Hence, it will not be possible to evaluate the real temperature inside the laminate.
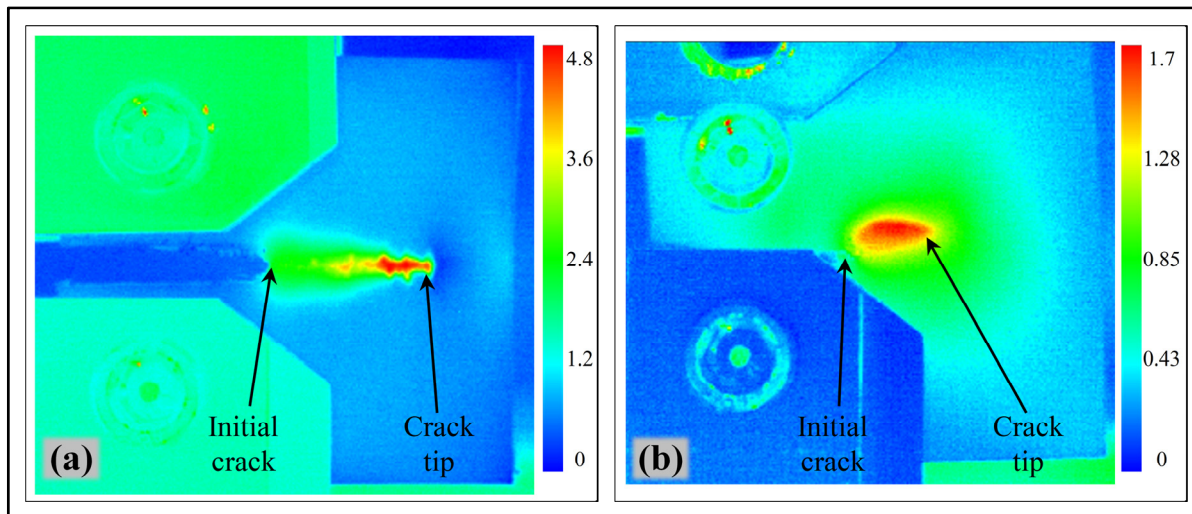
Figure 5.9 Temperature variation field observed during the crack propagation of CT, (a) and CC, (b) specimens
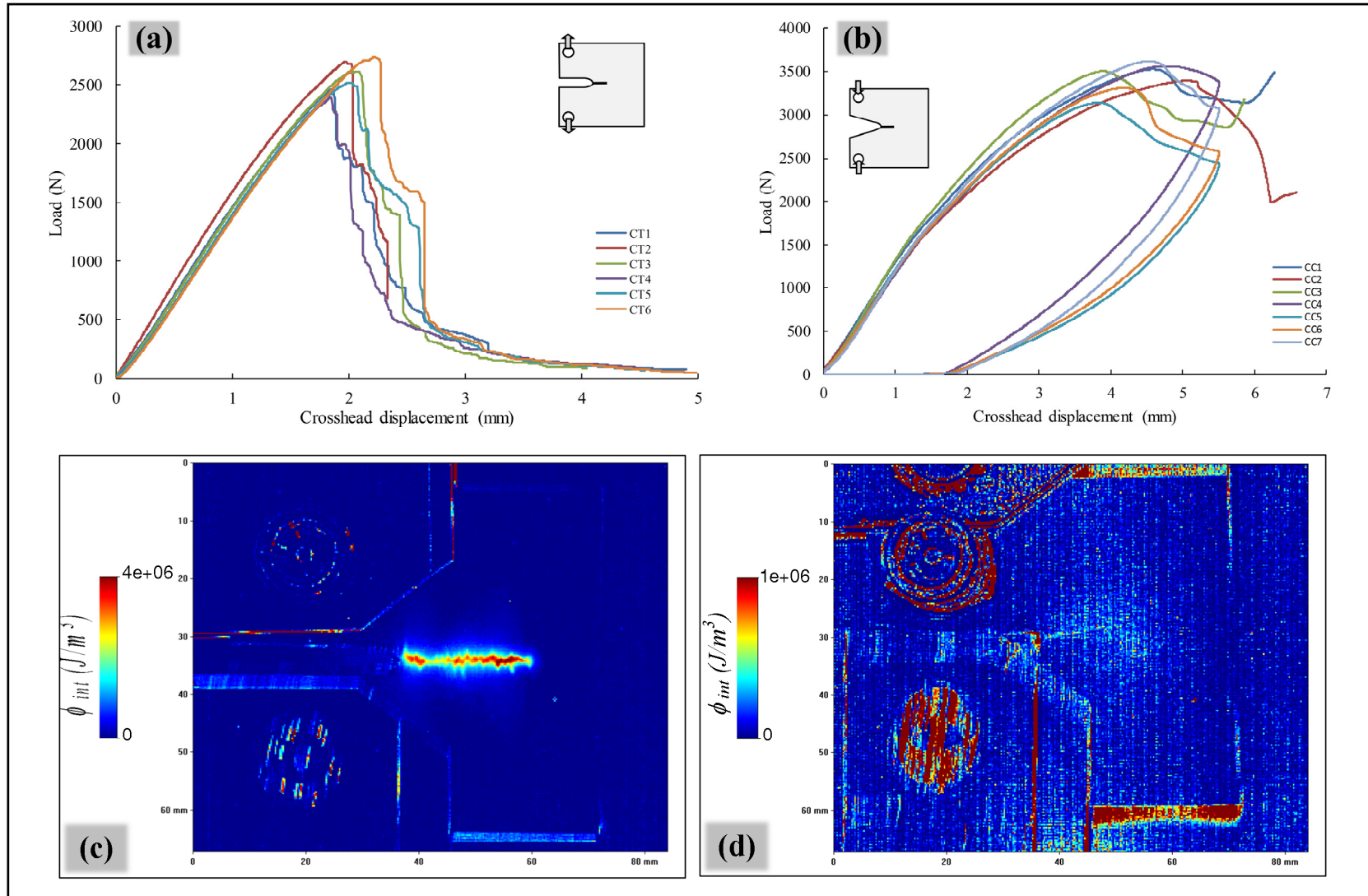
Figure 5.10 Load-displacement curves for the CT (a) and CC (b) specimens, and intrinsic heat measured by IRT for the CT (c) and CC (d) specimens

5.5.3.1 Tension testing of CT specimens

Globally, CT specimens exhibit a brittle behavior with a relatively linear response up to almost the maximum load, which is followed by a sudden and then continuous force drop, indicating consistent crack growth and stiffness reduction, as shown in Figure 5.10a. These curves are very similar and are in good agreement with those reported in the literature for CT specimens of carbon/epoxy composites (M. J. Laffan *et al.*, 2010a, 2010b; M. J. Laffan *et al.*, 2011; S. T. Pinho *et al.*, 2006), which is as such an indication of the validity of the current tests. Therefore, they seem to have small enough damage zone to use the ASTM D5045 standard, which is developed for isotropic plastic materials, to evaluate the fracture toughness for comparison purposes. The fracture energy of the UD laminate (G_{IC}^{Ten}) was calculated using the same approach applied to ECT specimens, and the results are summarized in Table 5.6.

As shown in Figure 5.9, for CT specimens, the damage zone is minimal; this was also observed by Pinho et al. (S. T. Pinho *et al.*, 2006) using C-Scan. The propagation of the crack is perceivable from the thermal image exposed in Figure 5.9. As discussed above, considering the available values for β of polymers in the literature, two cases were investigated; first assuming $\beta = 0.5$ and second, $\beta = 0.9$. Data treatment in the selected zones was performed according to the developed and validated methodology in (Teddy Lisle *et al.*, 2015; T. Lisle *et al.*, 2013). The obtained fracture energy value is presented in Table 5.6.

Table 5.6 Fracture energy of UD-FFREC evaluated by IRT and standard methods

	IRT				ASTM standards			
	G_{IC}^{Ten} (kJ/m^2)		G_{IC}^{Comp} (kJ/m^2)		G_{IC}^{Ten} (kJ/m^2)	G_{IC}^{Ten} (kJ/m^2)	G_{IC}^{Comp} (kJ/m^2)	$G_{IC}^{Comp(Linear)}$ (kJ/m^2)
	$\beta = 0.50$	$\beta = 0.90$	$\beta = 0.50$	$\beta = 0.90$	E1922	D5045		
						Max Load		Max Linear
Mean	19.88	11.10	1.30	0.77	15.71	23.37	41.29	9.84
STD	2.68	1.49	0.119	0.066	1.23	2.28	3.56	0.39
COV (%)	13.48	13.42	9.15	8.57	7.82	9.76	8.62	4.00

It can be seen that the value of G_{IC}^{Ten} obtained by ASTM D5045, which was developed for isotropic plastic materials, is much ($\approx$49%) higher than that determined by ASTM E1922, specially developed for FRCs. The latter was particularly developed and validated based on synthetic FRCs, though, according to the standard, it is applicable to other types of FRCs provided that the criteria are met. However, in this study, it was applied to NFRCs, which have a more complicated microstructure and may behave differently. This is because NFs are composite by themselves that normally come in bundles containing technical fibers that are composed of helically arranged microfibrils as the main force carrying elements. Therefore, they exhibit more complex failure behavior with high variability in the material properties. The complex microstructure of the NFs will impose a complex fiber fracture leading to different mechanisms of energy absorption. Consequently, as a dominant failure mechanism, the complex fracture of NFs will influence the fracture toughness of the composite and may require a different determination method.

Nevertheless, there is no standard test method developed for testing NFRCs and no literature data available to validate the results. Consequently, for the time being, G_{IC}^{Ten} determined by ASTM E1922 can be considered as the most reliable tensile TFT value for the understudy FFRECs. This value is placed between the values obtained by IFT analysis for $\beta = 0.90$ and $\beta = 0.90$ by $\pm 29\%$ difference. Considering the high variability of material properties for NFs, these values could be considered consistent with that of the standard method. In general, even the data available for synthetic FRCs are scattered, for instance, CT tests of a unique CFRP composite show more than 15% variation (Catalanotti *et al.*, 2010; M. J. Laffan *et al.*, 2011). However, assuming the result of the standard method as the real value, it may be concluded that the realistic value of β for the understudy flax/epoxy is between the margins (0.50 and 0.90) used for analysis, or, technically speaking, the ratio of dissipative work converted into heat in this composite is between 50% and 90%. Considering that G_{IC} is an inverse linear function of β, this ratio for the composite can be calculated back from the result of the standard test ($\beta = 0.69$) and be used in the future calculation of the fracture energy, for instance in compressive failure mode, presented in the following section. Consequently, having a precise

enough value for β, the employed method based on IRT can be confidently used to determine the fracture energy of the composites.

Naturally, the failure modes in CT specimens are the same occurring in ECT, as discussed in the previous section.

5.5.3.2 Compression testing of CC specimens

The load-displacement response of the CC tests (Figure 10b) is more difficult to interpret. As can be observed, CC specimens exhibited complex, but similar behavior in compression loading. The similarity of the curves indicates a good reproducibility and the certainty of the data recorded for the composites under study. The composite displays a linear behavior up to a displacement of about 1.2 mm (1500 N of loading), where a clear slope reduction happens. After this point, a relatively linear response continues until a displacement of 3 mm followed by a nonlinear curve up to the maximum load. For all of the specimens, the visual signs of failure occurred at the maximum load, and upon reaching this point, the load slowly dropped until the test was stopped. The load-displacement response of these CC specimens is more or less analogous to that of carbon/epoxy CC specimens (Catalanotti *et al.*, 2010; S. T. Pinho *et al.*, 2006); however, flax/epoxy composite demonstrates much higher nonlinearity. The ASTM D5045 standard was first employed to evaluate the fracture toughness in compression of the cross-ply laminate using the maximum load. Then, the fracture energy of the UD laminate in compression (G_{IC}^{Comp}) was calculated following the aforementioned approach used by Pinho et al. (S. T. Pinho *et al.*, 2006) for CC specimens. Assuming that G_{IC}^{90} is equivalent in magnitude to the mode-II interlaminar fracture energy of the UD-FFREC, $G_{IIC}^{delam} = 0.378$ kJ/m², which was evaluated in a separate study (Saadati *et al.*, 2020a), the results are calculated and summarized in Table 5.6. However, the result is unreasonably higher compared to G_{IC}^{Ten}, whereas it is expected to be lower for compression testing (Catalanotti *et al.*, 2010; M. J. Laffan *et al.*, 2011; H. Liu *et al.*, 2018; S. T. Pinho *et al.*, 2006). This should be due to the nonlinearity that corresponds to some damages or plasticity in the sample and means that an important part

of the dissipated energy is not due to the crack propagation but to other secondary damage phenomena. Therefore, the onset of damage must have happened much before reaching the maximum load point. Considering the low stiffness of flax fibers in compression and the poor fiber-matrix adhesion, this failure mode is a matrix-driven failure. Thus, it is expected that the isotropic epoxy matrix exhibits a linear behavior up to failure. Therefore, theoretically, the composite translaminar failure in compression should start in the endpoint of the first linear part, after which, by the development of other secondary material damages, the stiffness of the sample and the slope of the curve reduce. As a result, the load at this point is considered as the compressive translaminar failure load and is used to evaluate the G_{IC}^{Comp} of the composite, the result is presented in Table 5.6. The literature data for G_{IC}^{Comp} is very scattered, for instance, conducting 4-point bending tests, Laffan et al. (M. Laffan et $al.$, 2012) measured value of $G_{IC}^{Comp} = 25.9$ kJ/m² for IM7/8552 CFRP, while Catalanotti et al. (Catalanotti et $al.$, 2010) reported $G_{IC}^{Comp} = 47.5$ kJ/m² for the same material system and Pinho et al. (S. T. Pinho et $al.$, 2006) published $G_{IC}^{Comp} = 79.9$ kJ/m² for another CFRP, both using CC specimens. Therefore, the value in this range can be a good representative of the fracture energy of the composite. Nevertheless, the complex microstructure of the NF composite and, consequently, its complex behavior increases the difficulty of recognizing the precise failure point and needs deeper analysis.

Figure 5.9 shows that CC specimens experience much broader damage zone compared to CT specimens, also observed by Pinho et al. (S. T. Pinho et $al.$, 2006). However, the onset of failure and propagation of the crack couldn't be recognized in the thermal images and the experimental heat source fields.

In a similar approach to CT tests, assuming $\beta = 0.50$ and $\beta = 0.90$ the data were processed to determine the translaminar fracture energy in compression (G_{IC}^{Comp}), results are given in Table 5.6. As expected, the values are lower than those for CT tests. However, they are obviously too low, indicating that IRT is underestimating the fracture energy in compression for UD-FFRECs. There is no available literature data for G_{IC}^{Comp} to be compared with the obtained

values; however, the proportion of G_{IC}^{Ten} to G_{IC}^{Comp} for other composites evidently shows that the measured values by IRT do not represent the G_{IC}^{Comp} of the composite. Considering the presence of complex failure modes in CC specimens, which is more complicated for NF composites, it is not trivial to perform a root-cause-analysis for this issue; however, some hypotheses can be made. A previous study shows that the UD-FFREC experiences delamination damage in compression failure (Saadati *et al.*, 2020c); this may be the case for the cross-ply CC specimen. Therefore, the surface layer might have been delaminated before a translaminar failure occurs and then buckled in the out-of-plane direction so that the generated heat in the surface ply is not associated with a translaminar failure and could be the result of other failure modes, like buckling, producing much less heat. It could also be related to the microstructure of the flax fibers so that, under compression loading, their internal structure collapses, with the fibers being compressed in themselves to generate reversible energy, rather than failing to produce thermal energy. Finally, the poor fiber-matrix adhesion could make the fibers ineffective in carrying the compression load; thus, the fracture energy could be mostly related to matrix failure in compression. This hypothesis is supported by Mode-II interlaminar fracture energy of UD-FFREC, $G_{IIC}^{delam} = 0.378$ kJ/m^2, measured in another study (Saadati *et al.*, 2020a), as their failure modes are similar, and the fracture energy values are close.

In summary, using IRT and cross-ply laminates, valid values cannot be determined for G_{IC}^{Comp} of the UD-FFRECs. However, assuming that the failure starts at the end of the first linear part of the load-displacement curve and using the ASTM D5045 standard, a reasonable value can be achieved for G_{IC}^{Comp} of the UD-FFRECs.

5.6 Conclusions

This study has investigated the fracture behavior and evaluated the fracture toughness parameters of the UD-FFRECs under quasi-static tensile and compressive loads. The existing ASTM E1922 standard test method was employed to examine the fracture toughness of ECT specimens in tension, and an already developed methodology based on IRT, as well as ASTM

D5045, were applied to study the fracture energy in tension and compression respectively using CT and CC specimens. Afterward, combining the micrographs and the load-NMOD curves, the fracture behavior and the fracture mechanisms of the composite were studied.

Applying the ASTM E1922 standard test method to determine the tensile fracture toughness using UD laminates was impossible, and the self-similar translaminar crack growth of concern was not exhibited. A cross-ply laminate was instead used to evaluate the fracture toughness of the laminate and extract that of UD composite following an approach that was already used and proved valid in some earlier studies. Although there are no published fracture property data for these composites for comparison, the obtained values (G_{IC} = 15.71 kJ/m^2 and K_{IC} = 14.27 MPa-m$^{1/2}$) fit very well in the range of those of the similar NFPCs available in the literature.

Experimental tests using IRT were conducted, and employing the developed program, the data were treated to determine the fracture toughness of the composite in tensile and compressive loadings using CT and CC cross-ply composite specimens, respectively. An assumption of β = 0.5 and β = 0.9 was made for the Taylor–Quinney coefficient based on the existing values for similar materials. Compared to the standard test results, CT specimens demonstrated proper adequacy for this purpose; however, the results of CC tests were too low and thus unsatisfactory. Employing this methodology to CT tests, the values of G_{IC}^{Ten} = 19.88 and 11.1 kJ/m^2, respectively for β = 0.5 and β = 0.9, were obtained. The results of IRT are consistent with and are covering those of the ASTM standard, showing that the real value of β is between the two assumed values. Therefore, the application of the IRT method for evaluating tensile translaminar fracture energy of UD-flax/epoxy composites using CT tests is validated; however, the accuracy of IRT for determining the compressive translaminar fracture energy using CC specimens is not proved. Instead, for CC tests it was concluded that using the maximum load of the initial linear load-displacement curve as the failure load and ASTM D5045 standard leads to a reasonable compressive fracture energy G_{IC}^{Comp} = 9.84 kJ/m^2. The fractography study reveals that the primary mechanisms activated in translaminar failure are fiber pull-out, fiber breakage, and fiber-matrix debonding. To conclude, a view of the

translaminar fracture behavior of the UD-FFRECs has been drawn, and the translaminar fracture toughness parameters in the fiber direction and under tensile and compressive loadings are determined. These values are the most reliable data ever obtained to be used in engineering design and numerical simulation studies.

CONCLUSION

In this research work, first, the complications of the trimming process of the unidirectional flax fiber-reinforced epoxy composites (UD-FFRECs) were analyzed. Then, the literature works investigating the machining processes of fiber-reinforced polymer composites (FRCs) were reviewed. It was deduced that the experimental methods are not sufficient for deep analysis of the cutting process of these composites. Also, the capability and application of the finite element method (FEM) to model the cutting process was investigated. Overall, it was concluded that involving FEM in studying the cutting process of FFRECs is crucial for better understanding their cutting mechanisms, thus, for predicting machining damages, and improving their machining quality. However, the extensive literature review revealed that the required properties for finite element modeling of their cutting process are not available in the literature.

Then, UD-FFRECs with unique specifications were molded by the resin transfer molding (RTM) method. In the absence of standardized test methods for natural fiber composites (NFRCs), the best matching test methods for FFRECs were selected. Following these test procedures, proper test specimens were prepared and tested for desired properties. The obtained results are consistent with the definitions of the material properties in each ASTM standard followed in this work, thus, the data generated can confidently be considered as the material property of this composite. These results are the most reliable data ever obtained for this material and provide a basis for the engineering design field and numerical simulation of this material by FEM.

In light of the results obtained, the major findings are summarized as follows:

- According to the results of this study, Archimedes' density measurement method using water as the immersion fluid is not recommended for measuring the density of FFRP composites due to water absorption that leads to inaccurate results. In contrast, Archimedes' method using ethanol or gas pycnometry method are recommended. A

density value of $\rho = 1.281$ g/cm^3 was obtained for FFECs with $V_f = 0.41$ studied in this work.

- Specific heat capacity measurements resulted in $C_p = 0.665$ J/g.K, while a thermal diffusivity $\alpha = 1.35 \times 10^{-7}$ m^2/s was obtained for the composite. Having ρ, C_p and α, the thermal conductivity, $\lambda = 0.115$ W/m.K, was calculated.

- The tensile tests in the fiber direction revealed that the composite exhibited two stiffness. The modulus of elasticity of the material at the beginning of the elongation, before 0.1% strain, is 30.04 GPa, then changes to 21.26 GPa and remains constant up to the ultimate strain at 1.35%. The average values of the ultimate tensile strength and Poisson's ratio in the fiber direction are respectively 298.39 MPa and 0.373.

- The fractured samples of the tensile tests exhibited a serrated fracture surface, mainly generated by transverse fracture of fiber and matrix, accompanied by longitudinal splitting after longitudinal matrix shear. Post-failure examinations of the split surfaces, revealed a significant amount of fiber pullout, demonstrating a weak fiber-matrix interfacial bonding. The matrix was broken, and the flax fiber bundles were ruptured and splintered into smaller bundles and single fibers.

- Tensile tests in the transverse direction presented a bilinear load-displacement curve with a mild slope change of around 0.25-0.3% strain. The tensile stiffness, failure strength, Poisson's ratio, and ultimate strain in the transverse direction are respectively 4.24 GPa, 14.73 MPa, 0.054, and 0.38%.

- The fractography study showed that the failure path in the transverse direction under tensile loading was a straight line. Matrix fracture, fiber-matrix debonding, and flax bundle fuzzing are the main failure mechanisms in this loading case. Fiber bridging is happening due to crack crossing the flax bundles because of the slight misalignment of fibers with the normal direction to the loading axis.

- Under fiber direction-compression loading, the laminate displayed a linear behavior, turning to highly nonlinear at around 0.3%–0.4% strain. The obtained compressive stiffness, failure strength, Poisson's ratio, and ultimate strain in the longitudinal direction are respectively 24.12 GPa, 126.05 MPa, 0.431, and 2.02%. However, in this case, the composite failure behavior is very complex, and any initial slight fiber deviations may trigger a premature failure. Thus, the values can be considered as a lower limit.

- Post-failure examinations of the specimens showed that the compressive failure modes in the fiber direction are one or two 45°-kink band, fiber failure, fiber-matrix debonding, and propagated delamination from the kink band. This combination of failure modes can explain the behavior of the composite in compression. In this case, the linear response, before micro-buckling of the reinforcement, transits to be nonlinear by starting the fibers micro-buckling and the internal failure modes. These occur along with a continuously dropping of the rigidity.

- In the transverse direction compression loading, the composite presents a linear behavior up to 1.3% strain, which is almost 80% of the deformation. After initiation of failure, the rigidity decreases, ending to a brittle shear-failure. The values of 4.44 GPa, 72.02 MPa, 0.0.054, and 2.1% were determined respectively for compressive stiffness, failure strength, Poisson's ratio, and ultimate strain in the transverse direction.

- The fractographic analysis showed that the transverse shear fracture in the transverse compressive loading occurs on a $30\pm5°$ fracture plane. As expected, in this case, where the matrix property is dominant, the main failure mode is matrix fracture.

- One of the interesting findings of this study is the difference between the Poisson's ratios obtained in compression and tension loadings. Theoretically, these values shouldn't be different, and this difference is not seen for other materials. It could be

originated from the complex microstructure of the flax fibers; however, a specific study is required to investigate it.

- The in-plane shear properties of the FFREC were evaluated in the principal material directions by testing V-notched shear beams according to the corresponding ASTM standard. The tests perfectly fulfilled the requirements of the norm, and the shear property values were measured as follows. The shear modulus, shear strength, and maximum shear strain in the fiber direction were respectively, 1.92 GPa, 44.67 MPa, and 5.0%. In the transverse direction, they were respectively 1.95 GPa, 25.08 MPa, and 1.58%. The shear moduli in both directions are very close. This can be explained by the fact that shear properties of composites are controlled mainly by the matrix and fiber-matrix interface.

- In the fiber direction shear loading, the composite presents a ductile failure; whereas, in the transverse direction, a brittle failure is observed. The micrographs showed that the primary failure modes are matrix fracture and fiber-matrix separation.

- The flexural tests were carried out only in the longitudinal direction, and an initial linear behavior turning to nonlinear ending to a brittle fracture was observed. The failure modes, in this case, included lower surface ply rupture, delamination, and finally, translaminar fracture. The flexural modulus, strength, and maximum strain of the composite were determined respectively as 24.77 GPa, 236.19 MPa, and 2.08%.

- DCB tests, with the help of the DIC method, were conducted and validated according to the related ASTM standard to measure the Mode I interlaminar fracture energy of the composite. The load vs crack opening displacement curves of the tests fulfilled the criteria of the standard. Huge fiber-bridging was observed for these specimens, leading to an increase in R-curves and confirming the appropriateness of the pre-crack induced by the 13μm-thick insert film. For Mode I, $G_{IC} = 574$ and $G_{IC} = 903$ J/m^2 were obtained respectively for crack initiation and propagation values. (In this study, the recorded

images by DIC had to be processed subjectively to be able to recognize the delamination front more accurately.)

- To measure the Mode II interlaminar fracture energy, first, exploratory ENF tests were conducted to find the proper test parameters. Then, the real tests were carried out and validated based on the criteria of the associated ASTM standard. The obtained value for Mode II delamination is G_{IIC} =378 J/m^2. In contrast to the results of previous authors who used the SBT data reduction method, this value is lower than G_{IC}. However, when applying the SBT method for the current study, G_{IIC} =612 J/m^2 is obtained, which is consistent with their results.

- MMB tests were conducted and validated according to the corresponding ASTM standard to evaluate the interlaminar fracture energy in Mixed-mode I/II. Similar to DCB tests, significant fiber-bridging was observed in these tests, which is related to the nature of the natural fibers. MMB tests resulted in $G_{(I/II)C}$ = 414.4 J/m^2 for Mixed-mode I/II fracture energy. Also, using the B-K (Benzeggagh & Kenane) delamination criterion, the B-K fitting parameter, $\eta = 0.35$, was calculated. Since there is no Mixed-mode interlaminar fracture energy for these composites, the obtained values are valuable material properties to be further used in the design engineering field and numerical simulation methods.

- Trying to evaluate the translaminar fracture toughness (TFT) of UD-FFREC in tension, UD ECT specimens were prepared and tested according to ASTM E1922. However, the samples didn't fail properly, and it was concluded that it was impossible to test UD ECT samples for TFT. Instead, the fracture toughness of a cross-ply laminate was evaluated, from which that of UD composite was extracted: G_{IC}^{Ten}= 15.71 kJ/m^2 and K_{IC}= 14.27 MPa-m$^{1/2}$.

- Due to lack of standardized test methods for evaluating the fracture toughness in compression of FRCs, an Infrared Thermography (IRT)-based methodology was

employed to study the fracture energy in tension and compression respectively using CT and CC specimens. Compared to the standard test results, CT specimens demonstrated proper adequacy; however, the results of CC tests were too low and thus unsatisfactory. Therefore, the application of the IRT method for evaluating tensile TFT of UD-FFRECs is validated. However, the accuracy of IRT for determining the compressive TFT using CC specimens was not proved and thus it is not recommended. Instead, for CC tests it was concluded that using the maximum load of the initial linear load-displacement curve as the failure load and ASTM D5045 standard led to a reasonable compressive fracture energy $G_{IC}^{Comp} = 9.84$ kJ/m^2.

- An assumption of $\beta = 0.5$ and $\beta = 0.9$ was made for the Taylor–Quinney coefficient. Employing this methodology to CT tests, the values of $G_{IC}^{Ten} = 19.88$ and 11.1 kJ/m^2, respectively for $\beta = 0.5$ and $\beta = 0.9$, were obtained. Indicating that the real value of β for this material was between the two assumed values.

- The fractography study reveals that the primary mechanisms activated in translaminar failure are fiber pull-out, fiber breakage, and fiber-matrix debonding.

RECOMMENDATIONS

The primary purpose of the present study was a comprehensive investigation of unidirectional flax/epoxy composites in terms of their physical, mechanical, and fracture properties. This was conducted to develop essential knowledge and adequate data for finite element (FE) modeling of the cutting process of these composites.

Evidently, the next step would be the implementation of the FEM to study their cutting process, conduct efficient analysis and, eventually, propose practical suggestions to improve their machining quality. In line with this general target that was already defined, some stepwise directions for future research work related to this study are proposed as follows:

- As an efficient alternative for experimental methods, first, a 2D FE model of the orthogonal cutting process would be developed using the generated data in this study to simulate the cutting forces and predict the machining damages. Then, the effects of cutting conditions would be evaluated. Thanks to the capability of the FEM, this can include any combinations of the cutting conditions i.e., feed rate, depth of cut, cutting speed, as well as, cutting tool geometry such as rake angle, clearance angle, and cutting edge radius in edge trimming of UD-FFRECs.

- In this study, an attempt was made to fabricate the flax/epoxy laminate with the specifications of those used in a previous study, (Karabibene, 2017), in order to benefit from its experimental results. Therefore, the second step will be validating the FE model using the experimental data reported in that work.

- The FE model will be extended to 3D geometry.

- Having the 3D FE model validated, optimization of the machining parameters for improving machining quality will be carried out. Then, conducting experiments with

the optimized parameters, the accuracy of the model will be checked. Then efficient cutting strategies can be developed to improve the machining quality of the composite.

- Having the cutting forces from the FE model and using the material properties of the composite obtained in this study, the FE model can also be used for investigating the workpiece deflections and machining errors.

- Regarding the discrepancy between the Poisson's ratio in tension and compression loading, a study can be organized to examine the composite for this effect.

- Considering that in the Infrared Thermography method, it was not possible to measure the translaminar fracture energy in compression, and thus it was calculated from the maximum force of the linear part of the load-displacement curve. Research work can be defined to evaluate the accuracy of this assumption.

- Finding improvements on the composite such as fiber-matrix bonding improvements, to improve its machinability can be another research topic.

- Considering that there is an empty hole inside the flax fibers, their fracture and deformation behavior may be different, especially under compression loading. Therefore, it is recommended to consider this fact in future studies.

LIST OF REFERENCES

Ahmad, F., Choi, H. S., & Park, M. K. (2015). A Review: Natural Fiber Composites Selection in View of Mechanical, Light Weight, and Economic Properties. *Macromolecular Materials and Engineering, 300*(1), 10-24. doi:10.1002/mame.201400089

Aiman Akmal, A., Azmi, A., & Khalil, A. (2014). *Investigating the Effect of Machining Parameters on Mechanical Performance of Flax Natural Fibre Composites with Circular Holes*. Paper presented at the Advances in Material Processing Technologies (AMPT 2014), Dubai, UAE.

Airoldi, A., & Dávila, C. G. (2012). Identification of material parameters for modelling delamination in the presence of fibre bridging. *Composite Structures, 94*(11), 3240-3249. doi:https://doi.org/10.1016/j.compstruct.2012.05.014

Al-Khudairi, O., Hadavinia, H., Waggott, A., Lewis, E., & Little, C. (2015). Characterising mode I/mode II fatigue delamination growth in unidirectional fibre reinforced polymer laminates. *Materials & Design, 66*, 93-102. doi:10.1016/j.matdes.2014.10.038

Almansour, F., Dhakal, H., & Zhang, Z. Y. (2017a). Effect of water absorption on Mode I interlaminar fracture toughness of flax/basalt reinforced vinyl ester hybrid composites. *Composite Structures, 168*, 813-825. doi:http://dx.doi.org/10.1016/j.compstruct.2017.02.081

Almansour, F., Dhakal, H., & Zhang, Z. Y. (2018). Investigation into Mode II interlaminar fracture toughness characteristics of flax/basalt reinforced vinyl ester hybrid composites. *Composites Science and Technology, 154*, 117-127. doi:https://doi.org/10.1016/j.compscitech.2017.11.016

Almansour, F., Dhakal, H. N., Zhang, Z. Y., & Ghasemnejad, H. (2017b). Effect of hybridization on the mode II fracture toughness properties of flax/vinyl ester composites. *Polymer Composites, 38*(8), 1732-1740. doi:10.1002/pc.23743

Amiri, A., Triplett, Z., Moreira, A., Brezinka, N., Alcock, M., & Ulven, C. A. (2017). Standard density measurement method development for flax fiber. *Industrial Crops and Products, 96*, 196-202. doi:https://doi.org/10.1016/j.indcrop.2016.11.060

Anderson, T. L. (2017). *Fracture Mechanics: Fundamentals and Applications* (4 ed.). Boca Raton, FL, USA: CRC Press.

Anderson, T. L., & Anderson, T. L. (2005). *Fracture Mechanics: Fundamentals and Applications, Third Edition*: Taylor & Francis.

Anzelotti, G., Nicoletto, G., & Riva, E. (2008). Mesomechanic strain analysis of twill-weave composite lamina under unidirectional in-plane tension. *Composites Part A: Applied*

Science and Manufacturing, 39(8), 1294-1301. doi:https://doi.org/10.1016/j.compositesa.2008.01.006

Arbelaiz, A., Cantero, G., Fernandez, B., Mondragon, I., Ganan, P., & Kenny, J. (2005a). Flax fiber surface modifications: effects on fiber physico mechanical and flax/polypropylene interface properties. *Polymer Composites, 26*(3), 324-332. Retrieved from https://onlinelibrary.wiley.com/doi/pdf/10.1002/pc.20097

Arbelaiz, A., Fernandez, B., Ramos, J., Retegi, A., Llano-Ponte, R., & Mondragon, I. (2005b). Mechanical properties of short flax fibre bundle/polypropylene composites: Influence of matrix/fibre modification, fibre content, water uptake and recycling. *Composites Science and Technology, 65*(10), 1582-1592.

Arola, D., & Ramulu, M. (1997). Orthogonal cutting of fiber-reinforced composites: a finite element analysis. *International journal of mechanical sciences, 39*(5), 597-613.

Arola, D., Sultan, M., & Ramulu, M. (2002). Finite element modeling of edge trimming fiber reinforced plastics. *Journal of Manufacturing Science and Engineering, 124*(1), 32-41.

Ashik, K. P., Sharma, R. S., & Raghavendra, N. (2017). Evaluation of Tensile, Modal and Fracture Properties of Jute/Epoxy Natural Composites with addition of Silicon Di Oxide as Filler Material. *Materials Today: Proceedings, 4*(9), 9586-9591. doi:https://doi.org/10.1016/j.matpr.2017.06.229

ASTM. (2012). Standard Test Method for Shear Properties of Composite Materials by the V-Notched Beam Method. ASTM Standard D5379/D5379M-12. West Conshohocken, PA: ASTM International. doi:https://doi.org/10.1520/D5379_D5379M-12

ASTM. (2013a). Standard Test Method for Mode I Interlaminar Fracture Toughness of Unidirectional Fiber-Reinforced Polymer Matrix Composites. ASTM Standard D5528-13. West Conshohocken, PA: ASTM International. doi:https://doi.org/10.1520/D5528-13

ASTM. (2013b). Standard Test Method for Thermal Diffusivity by the Flash Method. ASTM Standard E1461-13. West Conshohocken, PA: ASTM International. doi:https://doi.org/10.1520/E1461-13

ASTM. (2013c). Standard Test Methods for Density and Specific Gravity (Relative Density) of Plastics by Displacement. ASTM Standard D792-13. West Conshohocken, PA: ASTM International. doi:https://doi.org/10.1520/D0792-13

ASTM. (2014). Standard Test Method for Density of Solid Pitch (Helium Pycnometer Method). ASTM Standard D4892-14. West Conshohocken, PA: ASTM International. doi:https://doi.org/10.1520/D4892-14R19E01

ASTM. (2015a). Standard Test Method for Flexural Properties of Polymer Matrix Composite Materials. ASTM Standard D7264/D7264M-15. West Conshohocken, PA: ASTM International. doi:https://doi.org/10.1520/D7264_D7264M-15

ASTM. (2015b). Standard Test Method for Translaminar Fracture Toughness of Laminated and Pultruded Polymer Matrix Composite Materials. ASTM Standard E1922-04. West Conshohocken, PA: ASTM International. doi:https://doi.org/10.1520/E1922-04R15

ASTM. (2015c). Standard Test Methods for Constituent Content of Composite Materials. ASTM Standard D3171-15. West Conshohocken, PA: ASTM International. doi:https://doi.org/10.1520/D3171-15

ASTM. (2016). Standard Test Method for Compressive Properties of Polymer Matrix Composite Materials Using a Combined Loading Compression (CLC) Test Fixture. ASTM Standard D6641/D6641M-16. West Conshohocken, PA: ASTM International. doi:https://doi.org/10.1520/D6641_D6641M-16E01

ASTM. (2017). Standard Test Method for Tensile Properties of Polymer Matrix Composite Materials. ASTM Standard D3039/D3039M-17. West Conshohocken, PA: ASTM International. doi:https://doi.org/10.1520/D3039_D3039M-17

ASTM. (2018). Standard test method for determining specific heat capacity by differential scanning calorimetry. ASTM Standard E1269-11. West Conshohocken, PA: ASTM International. doi:https://doi.org/10.1520/E1269-11R18

ASTM. (2019a). Standard Test Method for Determination of the Mode II Interlaminar Fracture Toughness of Unidirectional Fiber-Reinforced Polymer Matrix Composites. ASTM Standard D7905/D7905M-19. West Conshohocken, PA: ASTM International. doi:https://doi.org/10.1520/D7905_D7905M-19E01

ASTM. (2019b). Standard Test Method for Mixed Mode I-Mode II Interlaminar Fracture Toughness of Unidirectional Fiber Reinforced Polymer Matrix Composites. ASTM Standard D6671/D6671M-19. West Conshohocken, PA: ASTM International. doi:https://doi.org/10.1520/D6671_D6671M-19

Avril, C., Bailly, P., Njuguna, J., Nassiopoulos, E., & De Larminat, A. (2012, 24-28 June 2012). *Development of flax-reinforced bio-composites for high-load bearing automotive parts.* Paper presented at the 15th European Conference on Composite Materials (ECCM15) Venice, Italy.

Azmi, A., Lin, R., & Bhattacharyya, D. (2013). Machinability study of glass fibre-reinforced polymer composites during end milling. *The International Journal of Advanced Manufacturing Technology, 64*(1-4), 247-261.

Azmi, H., Haron, C., Ghani, J., Suhaily, M., Sanuddin, A., & Song, J. (2016). Study on machinability effect of surface roughness in milling kenaf fiber reinforced plastic

composite (unidirectional) using response surface methodology. *ARPN Journal of Engineering and Applied Sciences, 11*(7), 4761-4766.

Azmi, H., Haron, C. H. C., Ghani, J. A., Suhaily, M., & Yuzairi, A. R. (2018). Machinability Study on Milling Kenaf Fiber Reinforced Plastic Composite Materials using Design of Experiments. *IOP Conference Series: Materials Science and Engineering, 344*(1), 012027. doi:10.1088/1757-899X/344/1/012027

Babu, G. D., Babu, K. S., & Gowd, B. U. M. (2013). Effect of machining parameters on milled natural fiber-reinforced plastic composites. *Journal of Advanced Mechanical Engineering, 1*, 1-12.

Baiardo, M., Zini, E., & Scandola, M. (2004). Flax fibre–polyester composites. *Composites Part A: Applied Science and Manufacturing, 35*(6), 703-710. doi:https://doi.org/10.1016/j.compositesa.2004.02.004

Baley, C. (2002). Analysis of the flax fibres tensile behaviour and analysis of the tensile stiffness increase. *Composites Part A: Applied Science and Manufacturing, 33*(7), 939-948. doi:https://doi.org/10.1016/S1359-835X(02)00040-4

Baley, C., Gomina, M., Breard, J., Bourmaud, A., & Davies, P. (2019). Variability of mechanical properties of flax fibres for composite reinforcement. A review. *Industrial Crops and Products*, 111984. doi:https://doi.org/10.1016/j.indcrop.2019.111984

Baley, C., Perrot, Y., Busnel, F., Guezenoc, H., & Davies, P. (2006). Transverse tensile behaviour of unidirectional plies reinforced with flax fibres. *Materials Letters, 60*(24), 2984-2987. doi:https://doi.org/10.1016/j.matlet.2006.02.028

Bavan, D. S., & Kumar, G. C. M. (2013). Finite Element Analysis of a Natural Fiber (Maize) Composite Beam. *Journal of Engineering, 2013*. doi:10.1155/2013/450381

Behzad, T., & Sain, M. (2007). Measurement and prediction of thermal conductivity for hemp fiber reinforced composites. *Polymer Engineering & Science, 47*(7), 977-983. doi: https://doi.org/10.1002/pen.20632

Bensadoun, F. (2016). *Bensadoun, Farida. In-service Behaviour of Flax Fibre Reinforced Composites for High Performance Applications.* (PhD Paper-based). Retrieved from https://limo.libis.be/primo-explore/fulldisplay?docid=LIRIAS1674573&context=L&vid=Lirias&search_scope=Lirias&tab=default_tab&lang=en_US&fromSitemap=1

Bensadoun, F., Verpoest, I., & Van Vuure, A. W. (2017). Interlaminar fracture toughness of flax-epoxy composites. *Journal of Reinforced Plastics and Composites, 36*(2), 121-136. doi:https://doi.org/10.1177/0731684416672925

Benzeggagh, M. L., & Kenane, M. (1996). Measurement of mixed-mode delamination fracture toughness of unidirectional glass/epoxy composites with mixed-mode bending

apparatus. *Composites Science and Technology, 56*(4), 439-449. doi:https://doi.org/10.1016/0266-3538(96)00005-X

Bodros, E., Pillin, I., Montrelay, N., & Baley, C. (2007). Could biopolymers reinforced by randomly scattered flax fibre be used in structural applications? *Composites Science and Technology, 67*(3), 462-470. doi:https://doi.org/10.1016/j.compscitech.2006.08.024

Bos, H. L. (2004). *The potential of flax fibres as reinforcement for composite materials*: Technische Universiteit Eindhoven Eindhoven.

Bos, H. L., Molenveld, K., Teunissen, W., van Wingerde, A. M., & van Delft, D. R. V. (2004). Compressive behaviour of unidirectional flax fibre reinforced composites. *Journal of Materials Science, 39*(6), 2159-2168. doi:10.1023/b:jmsc.0000017779.08041.49

Calzada, K. A. (2010). *Modeling and interpretation of fiber orientation-based failure mechanisms in machining of carbon fiber-reinforced composites.* (Master). University of Illinois at Urbana-Champaign, Urbana, Illinois.

Calzada, K. A., Kapoor, S. G., DeVor, R. E., Samuel, J., & Srivastava, A. K. (2012). Modeling and interpretation of fiber orientation-based failure mechanisms in machining of carbon fiber-reinforced polymer composites. *Journal of Manufacturing Processes, 14*(2), 141-149. doi:10.1016/j.jmapro.2011.09.005

Catalanotti, G., Camanho, P. P., Xavier, J., Dávila, C. G., & Marques, A. T. (2010). Measurement of resistance curves in the longitudinal failure of composites using digital image correlation. *Composites Science and Technology, 70*(13), 1986-1993. doi:https://doi.org/10.1016/j.compscitech.2010.07.022

Chabbert, B., Padovani, J., Djemiel, C., Ossemond, J., Lemaître, A., Yoshinaga, A., . . . Kurek, B. (2020). Multimodal assessment of flax dew retting and its functional impact on fibers and natural fiber composites. *Industrial Crops and Products, 148*, 112255. doi:https://doi.org/10.1016/j.indcrop.2020.112255

Chakrapani, P., & Sekar, V. (2018). 3D finite element analysis of slot milling of unidirectional glass fiber reinforced polymer composites. *Journal of the Brazilian Society of Mechanical Sciences and Engineering, 40*, 279. doi:10.1007/s40430-018-1195-4

Chandramohan, D., & Rajesh, S. (2014). Study of machining parameters on natural fiber particle reinforced polymer composite material. *Academic Journal of Manufacturing Engineering, 12*(3), 72-77.

Chandrasekar, M., Ishak, M., Sapuan, S., Leman, Z., & Jawaid, M. (2017). A review on the characterisation of natural fibres and their composites after alkali treatment and water absorption. *Plastics, Rubber and Composites, 46*(3), 119-136. doi:https://doi.org/10.1080/14658011.2017.1298550

Chandrasekar, M., Shahroze, R. M., Ishak, M. R., Saba, N., Jawaid, M., Senthilkumar, K., . . . Siengchin, S. (2019). Flax and sugar palm reinforced epoxy composites: effect of hybridization on physical, mechanical, morphological and dynamic mechanical properties. *Materials Research Express, 6*(10), 105331. doi:https://doi.org/10.1088/2053-1591/ab382c

Charlet, K., Baley, C., Morvan, C., Jernot, J. P., Gomina, M., & Bréard, J. (2007). Characteristics of Hermès flax fibres as a function of their location in the stem and properties of the derived unidirectional composites. *Composites Part A: Applied Science and Manufacturing, 38*(8), 1912-1921. doi:https://doi.org/10.1016/j.compositesa.2007.03.006

Charlet, K., Jernot, J.-P., Gomina, M., Bizet, L., & Bréard, J. (2010). Mechanical properties of flax fibers and of the derived unidirectional composites. *Journal of Composite Materials, 44*(24), 2887-2896.

Charlet, K., Jernot, J. P., Eve, S., Gomina, M., & Bréard, J. (2010). Multi-scale morphological characterisation of flax: From the stem to the fibrils. *Carbohydrate polymers, 82*(1), 54-61. doi:https://doi.org/10.1016/j.carbpol.2010.04.022

Chatelain, J. F., Zaghbani, I., & Monier, J. (2012). Effect of ply orientation on roughness for the trimming process of CFRP laminates. *International Journal of Industrial and Manufacturing Engineering, 6*(8), 1516-1522.

Che, D., Saxena, I., Han, P., Guo, P., & Ehmann, K. F. (2014). Machining of carbon fiber reinforced plastics/polymers: A literature review. *Journal of Manufacturing Science and Engineering, 136*(3), 034001.

Chegdani, F., & El Mansori, M. (2018). New multiscale approach for machining analysis of natural fiber reinforced bio-composites. *Journal of Manufacturing Science and Engineering.* doi:10.1115/1.4041326

Chegdani, F., & Mansori, M. E. (2018). Mechanics of material removal when cutting natural fiber reinforced thermoplastic composites. *Polymer Testing, 67*, 275-283. doi:https://doi.org/10.1016/j.polymertesting.2018.03.016

Chegdani, F., Mezghani, S., & El Mansori, M. (2015a). Experimental study of coated tools effects in dry cutting of natural fiber reinforced plastics. *Surface and Coatings Technology, 284*, 264-272. doi:https://doi.org/10.1016/j.surfcoat.2015.06.083

Chegdani, F., Mezghani, S., & El Mansori, M. (2016). On the multiscale tribological signatures of the tool helix angle in profile milling of woven flax fiber composites. *Tribology International, 100*, 132-140. doi:10.1016/j.triboint.2015.12.014

Chegdani, F., Mezghani, S., El Mansori, M., & Mkaddem, A. (2015b). Fiber type effect on tribological behavior when cutting natural fiber reinforced plastics. *Wear, 332-333*, 772-779. doi:10.1016/j.wear.2014.12.039

Chegdani, F., Takabi, B., Tai, B. L., Mansori, M. E., & Bukkapatnam, S. T. S. (2018). Thermal Effects on Tribological Behavior in Machining Natural Fiber Composites. *Procedia Manufacturing, 26*, 305-316. doi:https://doi.org/10.1016/j.promfg.2018.07.039

Chen, C., Li, Y., & Yu, T. (2014). Interlaminar toughening in flax fiber-reinforced composites interleaved with carbon nanotube buckypaper. *Journal of Reinforced Plastics and Composites, 33*(20), 1859-1868. doi:10.1177/0731684414548084

Chizyuka, C. G., & Kanyanga, S. B. (2013). Effects of Hydrothermal Ageing on the Fracture Damage of Sisal Fibre Reinforced Polyester Composites. *The Zambian Engineer, 46*(1), 11-19. Retrieved from https://www.researchgate.net/publication/262321283

Compston, P., & Jar, P. Y. B. (1998). Comparison of Interlaminar Fracture Toughness in Unidirectional and Woven Roving Marine Composites. *Applied Composite Materials, 5*(3), 189-206. doi:10.1023/A:1008899628807

Coroller, G., Lefeuvre, A., Le Duigou, A., Bourmaud, A., Ausias, G., Gaudry, T., & Baley, C. (2013). Effect of flax fibres individualisation on tensile failure of flax/epoxy unidirectional composite. *Composites Part A: Applied Science and Manufacturing, 51*, 62-70.

Couture, A., Lebrun, G., & Laperrière, L. (2016). Mechanical properties of polylactic acid (PLA) composites reinforced with unidirectional flax and flax-paper layers. *Composite Structures, 154*, 286-295. doi:https://doi.org/10.1016/j.compstruct.2016.07.069

Cristaldi, G., Latteri, A., Recca, G., & Cicala, G. (2010). Composites based on natural fibre fabrics. In P. D. Dubrovski (Ed.), *Woven fabric engineering* (pp. 317-342). doi:10.5772/10465

Dandekar, C. R., & Shin, Y. C. (2008). Multiphase Finite Element Modeling of Machining Unidirectional Composites: Prediction of Debonding and Fiber Damage. *Journal of Manufacturing Science and Engineering, 130*(5), 051016. doi:10.1115/1.2976146

Dandekar, C. R., & Shin, Y. C. (2012). Modeling of machining of composite materials: a review. *International Journal of Machine Tools and Manufacture, 57*, 102-121.

Daniel, I. M., Ishai, O., Daniel, I. M., & Daniel, I. (2006). *Engineering mechanics of composite materials* (Vol. 3). New York: Oxford university press.

Davies, P., Blackman, B. R. K., & Brunner, A. J. (1998). Standard Test Methods for Delamination Resistance of Composite Materials: Current Status. *Applied Composite Materials, 5*(6), 345-364. doi:10.1023/a:1008869811626

Davila, C. G., Camanho, P. P., & Rose, C. A. (2005). Failure Criteria for FRP Laminates. *Journal of Composite Materials, 39*(4), 323-345. doi:10.1177/0021998305046452

Davim, J. P., & Reis, P. (2005). Damage and dimensional precision on milling carbon fiber-reinforced plastics using design experiments. *Journal of Materials Processing Technology, 160*(2), 160-167.

De Kalbermatten, T., Jäggi, R., Flüeler, P., Kausch, H. H., & Davies, P. (1992). Microfocus radiography studies during mode I interlaminar fracture tests on composites. *Journal of Materials Science Letters, 11*(9), 543-546. doi:10.1007/BF00728603

Delahaigue, J. (2015). *Influence de la temperature de coupe sur les propriétés mécaniques en traction uni-axiale d'un composite carbone/époxy et étude de l'usinabilité d'un composite lin/époxy.* (Master). École de technologie supérieure, Montreal, Canada. Retrieved from https://espace.etsmtl.ca/id/eprint/1471

Delahaigue, J., Chatelain, J. F., & Lebrun, G. (2017). Machining analysis of unidirectional and bi-directional flax-epoxy composite laminates. *Proceedings of the Institution of Mechanical Engineers, Part L: Journal of Materials: Design and Applications, 231*(1-2), 196-209. doi:10.1177/1464420716671970

Dicker, M. P. M., Duckworth, P. F., Baker, A. B., Francois, G., Hazzard, M. K., & Weaver, P. M. (2014). Green composites: A review of material attributes and complementary applications. *Composites Part A: Applied Science and Manufacturing, 56*, 280-289. doi:https://doi.org/10.1016/j.compositesa.2013.10.014

Dillard, D. A., Singh, H. K., Pohlit, D. J., & Starbuck, J. M. (2009). Observations of Decreased Fracture Toughness for Mixed Mode Fracture Testing of Adhesively Bonded Joints. *Journal of Adhesion Science and Technology, 23*(10-11), 1515-1530. doi:10.1163/156856109X452701

Donadon, M. V., Falzon, B. G., Iannucci, L., & Hodgkinson, J. M. (2007). Intralaminar toughness characterisation of unbalanced hybrid plain weave laminates. *Composites Part A: Applied Science and Manufacturing, 38*(6), 1597-1611. doi:https://doi.org/10.1016/j.compositesa.2006.12.003

Dumoulin, S., Louche, H., Hopperstad, O. S., & Børvik, T. (2010). Heat sources, energy storage and dissipation in high-strength steels: Experiments and modelling. *European Journal of Mechanics - A/Solids, 29*(3), 461-474. doi:https://doi.org/10.1016/j.euromechsol.2009.11.005

El-Hajjar, R., & Haj-Ali, R. (2005). Mode-I fracture toughness testing of thick section FRP composites using the ESE(T) specimen. *Engineering Fracture Mechanics, 72*(4), 631-643. doi:https://doi.org/10.1016/j.engfracmech.2004.03.013

El Sawi, I., Bougherara, H., Zitoune, R., & Fawaz, Z. (2014). Influence of the Manufacturing Process on the Mechanical Properties of Flax/Epoxy Composites. *Journal of Biobased Materials and Bioenergy, 8*, 69-76. doi:10.1166/jbmb.2014.1410

Faggiani, A., & Falzon, B. (2010). Predicting low-velocity impact damage on a stiffened composite panel. *Composites Part A: Applied Science and Manufacturing, 41*(6), 737-749.

Falzon, B. G., & Apruzzese, P. (2011). Numerical analysis of intralaminar failure mechanisms in composite structures. Part I: FE implementation. *Composite Structures, 93*(2), 1039-1046. doi:https://doi.org/10.1016/j.compstruct.2010.06.028

Fathi, A., Keller, J.-H., & Altstaedt, V. (2015). Full-field shear analyses of sandwich core materials using Digital Image Correlation (DIC). *Composites Part B: Engineering, 70*, 156-166. doi:https://doi.org/10.1016/j.compositesb.2014.10.045

Freund, L. B., & Hutchinson, J. W. (1985). High strain-rate crack growth in rate-dependent plastic solids. *Journal of the Mechanics and Physics of Solids, 33*(2), 169-191. doi:https://doi.org/10.1016/0022-5096(85)90029-8

Fuqua, M., Huo, S., & Ulven, C. (2012). Natural Fiber Reinforced Composites. *Polymer Reviews, 52*(3), 259-320. doi:10.1080/15583724.2012.705409

G B, M., Vijaykumar, T. N., K N, D. B., & Jmsse. (2015). Optimization of Notch Parameter on Fracture Toughness of Natural Fiber Reinforced Composites Using Taguchi Method. *Journal of Materials Science & Surface Engineering, 3*, 244-248.

Garkhail, S., Heijenrath, R., & Peijs, T. (2000). Mechanical properties of natural-fibre-mat-reinforced thermoplastics based on flax fibres and polypropylene. *Applied Composite Materials, 7*(5-6), 351-372.

Ghafarizadeh, S. (2015). *Experimental investigation and modeling of surface machining of high performance CFRP for the aerospace industry.* (Ph.D.). École de technologie supérieure, Montreal, Canada. Retrieved from https://espace.etsmtl.ca/id/eprint/1593

Ghafarizadeh, S., Chatelain, J.-F., & Lebrun, G. (2014). Effect of cutting tool lead angle on machining forces and surface finish of CFRP laminates. *Science and Engineering of Composite Materials*.

Ghafarizadeh, S., Chatelain, J.-F., & Lebrun, G. (2016). Finite element analysis of surface milling of carbon fiber-reinforced composites. *The International Journal of Advanced Manufacturing Technology*, 1-11.

Gning, P. B., Liang, S., Guillaumat, L., & Pui, W. J. (2011). Influence of process and test parameters on the mechanical properties of flax/epoxy composites using response surface methodology. *Journal of Materials Science, 46*(21), 6801-6811. doi:https://doi.org/10.1007/s10853-011-5639-9

Goudenhooft, C., Bourmaud, A., & Baley, C. (2019). Flax (Linum usitatissimum L.) Fibers for Composite Reinforcement: Exploring the Link Between Plant Growth, Cell Walls Development, and Fiber Properties. *Frontiers in Plant Science, 10.* doi:10.3389/fpls.2019.00411

Goutianos, S., & Peijs, T. (2003). The Optimisation of Flax Fibre Yarns for the Development of High-Performance Natural Fibre Composites. *Advanced Composites Letters, 12*(6), 237-241. doi:https://doi.org/10.1177/096369350301200602

Goutianos, S., Peijs, T., Nystrom, B., & Skrifvars, M. (2006). Development of flax fibre based textile reinforcements for composite applications. *Applied Composite Materials, 13*(4), 199-215. doi:10.1007/s10443-006-9010-2

Grandidier, J. C., Casari, P., & Jochum, C. (2012). A fibre direction compressive failure criterion for long fibre laminates at ply scale, including stacking sequence and laminate thickness effects. *Composite Structures, 94*(12), 3799-3806. doi:https://doi.org/10.1016/j.compstruct.2012.06.013

Gurunathan, T., Mohanty, S., & Nayak, S. K. (2015). A review of the recent developments in biocomposites based on natural fibres and their application perspectives. *Composites Part A: Applied Science and Manufacturing, 77,* 1-25. doi:https://doi.org/10.1016/j.compositesa.2015.06.007

Gutkin, R., Pinho, S. T., Robinson, P., & Curtis, P. T. (2010). On the transition from shear-driven fibre compressive failure to fibre kinking in notched CFRP laminates under longitudinal compression. *Composites Science and Technology, 70*(8), 1223-1231. doi:https://doi.org/10.1016/j.compscitech.2010.03.010

Habibi, M., Laperrière, L., Lebrun, G., & Chabot, B. (2016). Experimental Investigation of the Effect of Short Flax Fibers on the Permeability Behavior of a New Unidirectional Flax/Paper Composite. *Fibers, 4*(3), 22. doi:doi:10.3390/fib4030022

Habibi, M., Laperrière, L., Lebrun, G., & Toubal, L. (2017a). Combining short flax fiber mats and unidirectional flax yarns for composite applications: Effect of short flax fibers on biaxial mechanical properties and damage behaviour. *Composites Part B: Engineering, 123,* 165-178. doi:https://doi.org/10.1016/j.compositesb.2017.05.023

Habibi, M., Lebrun, G., & Laperrière, L. (2017b). Experimental characterization of short flax fiber mat composites: tensile and flexural properties and damage analysis using acoustic emission. *Journal of Materials Science, 52*(11), 6567-6580. doi:https://doi.org/10.1007/s10853-017-0892-1

Haldar, S., Herráez, M., Naya, F., González, C., & Lopes, C. S. (2019). Relations between intralaminar micromechanisms and translaminar fracture behavior of unidirectional FRP supported by experimental micromechanics. *Composites Part B: Engineering, 174,* 107000. doi:https://doi.org/10.1016/j.compositesb.2019.107000

Hashin, Z. (1980). Failure criteria for unidirectional fiber composites. *Journal of applied mechanics, 47*(2), 329-334.

He, J., Chiang, M. Y. M., Hunston, D. L., & Han, C. C. (2002). Application of the V-Notch Shear Test for Unidirectional Hybrid Composites. *Journal of Composite Materials, 36*(23), 2653-2666. doi:10.1177/002199802761675566

He, Y.-L., Davim, J.-P., & Xue, H.-Q. (2018). 3D Progressive Damage Based Macro-Mechanical FE Simulation of Machining Unidirectional FRP Composite. *Chinese Journal of Mechanical Engineering, 31*(1), 51. doi:https://doi.org/10.1186/s10033-018-0250-5

Hongkarnjanakul, N., Bouvet, C., & Rivallant, S. (2013). Validation of low velocity impact modelling on different stacking sequences of CFRP laminates and influence of fibre failure. *Composite Structures, 106*(Supplement C), 549-559. doi:https://doi.org/10.1016/j.compstruct.2013.07.008

Hou, F., & Hong, S. (2014). Characterization of R-curve behavior of translaminar crack growth in cross-ply composite laminates using digital image correlation. *Engineering Fracture Mechanics, 117*, 51-70. doi:https://doi.org/10.1016/j.engfracmech.2014.01.010

Hughes, M., Hill, C., & Hague, J. (2002). The fracture toughness of bast fibre reinforced polyester composites Part 1 Evaluation and analysis. *Journal of Materials Science, 37*(21), 4669-4676. doi:https://doi.org/10.1023/A:1020621020862

Hyer, M. W., & White, S. R. (2009). *Stress analysis of fiber-reinforced composite materials*: DEStech Publications, Inc.

Ismail, A. E., Masran, S. H., Jamian, S., Kamarudin, K. A., Mohd Nor, M. K., Nor, N. H. M., . . . Awang, M. K. (2016). Fracture toughness of woven kenaf fibre reinforced composites. *IOP Conference Series: Materials Science and Engineering, 160*, 012020. doi:http://dx.doi.org/10.1088/1757-899X/160/1/012020

Ismail, S. O., Dhakal, H. N., Popov, I., & Beaugrand, J. (2016). Comprehensive study on machinability of sustainable and conventional fibre reinforced polymer composites. *Engineering Science and Technology, an International Journal, 19*(4), 2043-2052. doi:https://doi.org/10.1016/j.jestch.2016.07.010

Israr, H. A., Rivallant, S., Bouvet, C., & Barrau, J. J. (2014). Finite element simulation of 0°/90° CFRP laminated plates subjected to crushing using a free-face-crushing concept. *Composites Part A: Applied Science and Manufacturing, 62*, 16-25. doi:https://doi.org/10.1016/j.compositesa.2014.03.014

Johar, M., Israr, H. A., Low, K. O., & Wong, K. J. (2017). Numerical simulation methodology for mode II delamination of quasi-isotropic quasi-homogeneous composite laminates. *Journal of Composite Materials, 51*(28), 3955-3968. doi:10.1177/0021998317695414

John, M. J., & Thomas, S. (2008). Biofibres and biocomposites. *Carbohydrate polymers, 71*(3), 343-364. doi:10.1016/j.carbpol.2007.05.040

Jose, S., Kumar, R. R., Jana, M., & Rao, G. V. (2001). Intralaminar fracture toughness of a cross-ply laminate and its constituent sub-laminates. *Composites Science and Technology, 61*(8), 1115-1122.

Joshi, S. V., Drzal, L., Mohanty, A., & Arora, S. (2004). Are natural fiber composites environmentally superior to glass fiber reinforced composites? *Composites Part A: Applied Science and Manufacturing, 35*(3), 371-376. doi:10.1016/j.compositesa.2003.09.016

Kapoor, R., & Nemat-Nasser, S. (1998). Determination of temperature rise during high strain rate deformation. *Mechanics of materials, 27*(1), 1-12. doi:https://doi.org/10.1016/S0167-6636(97)00036-7

Karabibene, N. (2017). *Optimisation des paramètres de détourage des composites à fibres de lin et comparaison avec le détourage des composites à fibres de verre.* (Master). École de technologie supérieure, Montreal, Canada. Retrieved from https://espace.etsmtl.ca/id/eprint/2066

Karabibene, N., Chatelain, J.-F., Beauchamp, Y., & Lebrun, G. (2018). Effect of machining parameters on the uncut fibers of a unidirectional flax fiber reinforced composite. *Journal of Management & Engineering Integration, 11*(1), 54-63.

Khan, Z., Yousif, B. F., & Islam, M. (2017). Fracture behaviour of bamboo fiber reinforced epoxy composites. *Composites Part B: Engineering, 116*, 186-199. doi:https://doi.org/10.1016/j.compositesb.2017.02.015

Khanlou, H. M., Woodfield, P., Summerscales, J., Francucci, G., King, B., Talebian, S., . . . Hall, W. (2018). Estimation of mechanical property degradation of poly(lactic acid) and flax fibre reinforced poly(lactic acid) bio-composites during thermal processing. *Measurement, 116*, 367-372. doi:https://doi.org/10.1016/j.measurement.2017.11.031

Khanlou, H. M., Woodfield, P., Summerscales, J., & Hall, W. (2017). Consolidation process boundaries of the degradation of mechanical properties in compression moulding of natural-fibre bio-polymer composites. *Polymer Degradation and Stability, 138*, 115-125. doi:http://dx.doi.org/10.1016/j.polymdegradstab.2017.03.004

La Mantia, F. P., & Morreale, M. (2011). Green composites: A brief review. *Composites Part A: Applied Science and Manufacturing, 42*(6), 579-588. doi:https://doi.org/10.1016/j.compositesa.2011.01.017

Laffan, M., Pinho, S., Robinson, P., & Iannucci, L. (2009). *Fracture Toughness Measurement for Mode I Fibre Tensile Failure in FRP.* Paper presented at the International Conference on Composite Materials.

Laffan, M., Pinho, S., Robinson, P., Iannucci, L., & McMillan, A. (2012). Measurement of the fracture toughness associated with the longitudinal fibre compressive failure mode of laminated composites. *Composites Part A: Applied Science and Manufacturing, 43*(11), 1930-1938.

Laffan, M. J., Pinho, S., Robinson, P., & McMillan, A. (2012). Translaminar fracture toughness testing of composites: A review. *Polymer Testing, 31*, 481–489. doi:10.1016/j.polymertesting.2012.01.002

Laffan, M. J., Pinho, S. T., Robinson, P., & Iannucci, L. (2010a). Measurement of the in situ ply fracture toughness associated with mode I fibre tensile failure in FRP. Part I: Data reduction. *Composites Science and Technology, 70*(4), 606-613. doi:https://doi.org/10.1016/j.compscitech.2009.12.016

Laffan, M. J., Pinho, S. T., Robinson, P., & Iannucci, L. (2010b). Measurement of the in situ ply fracture toughness associated with mode I fibre tensile failure in FRP. Part II: Size and lay-up effects. *Composites Science and Technology, 70*(4), 614-621. doi:https://doi.org/10.1016/j.compscitech.2009.12.011

Laffan, M. J., Pinho, S. T., Robinson, P., & McMillan, A. J. (2011). Translaminar fracture toughness: The critical notch tip radius of 0° plies in CFRP. *Composites Science and Technology, 72*(1), 97-102. doi:https://doi.org/10.1016/j.compscitech.2011.10.006

Lasri, L., Nouari, M., & El Mansori, M. (2009). Modelling of chip separation in machining unidirectional FRP composites by stiffness degradation concept. *Composites Science and Technology, 69*(5), 684-692. doi:https://doi.org/10.1016/j.compscitech.2009.01.004

Le Gall, M., Davies, P., Martin, N., & Baley, C. (2018). Recommended flax fibre density values for composite property predictions. *Industrial Crops and Products, 114*, 52-58. doi:https://doi.org/10.1016/j.indcrop.2018.01.065

Lefeuvre, A., Bourmaud, A., & Baley, C. (2015). Optimization of the mechanical performance of UD flax/epoxy composites by selection of fibres along the stem. *Composites Part A: Applied Science and Manufacturing, 77*, 204-208. doi:http://dx.doi.org/10.1016/j.compositesa.2015.07.009

Lefeuvre, A., Bourmaud, A., Lebrun, L., Morvan, C., & Baley, C. (2013). A study of the yearly reproducibility of flax fiber tensile properties. *Industrial Crops and Products, 50*, 400-407.

Lens, L. N., Bittencourt, E., & d'Avila, V. M. R. (2009). Constitutive models for cohesive zones in mixed-mode fracture of plain concrete. *Engineering Fracture Mechanics, 76*(14), 2281-2297. doi:https://doi.org/10.1016/j.engfracmech.2009.07.020

Leonard, L. W. H., Wong, K. J., Low, K. O., & Yousif, B. F. (2009). Fracture behaviour of glass fibre-reinforced polyester composite. *Proceedings of the Institution of Mechanical Engineers, Part L: Journal of Materials: Design and Applications, 223*(2), 83-89. doi:https://doi.org/10.1243/14644207JMDA224

Li, X., Tabil, L. G., Oguocha, I. N., & Panigrahi, S. (2008). Thermal diffusivity, thermal conductivity, and specific heat of flax fiber–HDPE biocomposites at processing temperatures. *Composites Science and Technology, 68*(7), 1753-1758. doi:https://doi.org/10.1016/j.compscitech.2008.02.016

Li, Y., Mai, Y.-W., & Ye, L. (2005). Effects of fibre surface treatment on fracture-mechanical properties of sisal-fibre composites. *Composite Interfaces, 12*(1-2), 141-163. doi:https://doi.org/10.1163/1568554053542151

Li, Y., Wang, D., & Ma, H. (2015). Improving interlaminar fracture toughness of flax fiber/epoxy composites with chopped flax yarn interleaving. *Science China Technological Sciences, 58*(10), 1745-1752. doi:https://doi.org/10.1007/s11431-015-5911-3

Li, Z., & Lambros, J. (2001). Strain rate effects on the thermomechanical behavior of polymers. *International Journal of Solids and Structures, 38*(20), 3549-3562. doi:https://doi.org/10.1016/S0020-7683(00)00223-7

Liang, S., Gning, P.-B., & Guillaumat, L. (2014). Properties evolution of flax/epoxy composites under fatigue loading. *International Journal of Fatigue, 63*, 36-45. doi:https://doi.org/10.1016/j.ijfatigue.2014.01.003

Liang, S., Gning, P.-B., & Guillaumat, L. (2015). Quasi-static behaviour and damage assessment of flax/epoxy composites. *Materials & Design, 67*, 344-353.

Lin, S. T., Feng, Z., & Rowlands, R. E. (1997). Thermoelastic determination of stress intensity factors in orthotropic composites using the J-integral. *Engineering Fracture Mechanics, 56*(4), 579-592. doi:https://doi.org/10.1016/S0013-7944(96)00062-8

Lisle, T., Bouvet, C., Hongkarnjanakul, N., Pastor, M.-L., Rivallant, S., & Margueres, P. (2015). Measure of fracture toughness of compressive fiber failure in composite structures using infrared thermography. *Composites Science and Technology, 112*, 22-33. doi:https://doi.org/10.1016/j.compscitech.2015.03.005

Lisle, T., Bouvet, C., Pastor, M. L., Margueres, P., & Prieto Corral, R. (2013). Damage analysis and fracture toughness evaluation in a thin woven composite laminate under static tension using infrared thermography. *Composites Part A: Applied Science and Manufacturing, 53*(Supplement C), 75-87. doi:https://doi.org/10.1016/j.compositesa.2013.06.004

Lisle, T., Bouvet, C., Pastor, M. L., Rouault, T., & Marguerès, P. (2015). Damage of woven composite under tensile and shear stress using infrared thermography and micrographic cuts. *Journal of Materials Science, 50*(18), 6154-6170. doi:10.1007/s10853-015-9173-z

Lisle, T., HONGKARNJANAKUL, N., BOUVET, C., PASTOR, M.-L., MARGUERES, P., & RIVALLANT, S. (2014). *MEASURE OF FRACTURE TOUGHNESS IN COMPOSITE STRUCTURES USING INFRARED THERMOGRAPHY*. Paper presented at the ECCM16 - 16TH EUROPEAN CONFERENCE ON COMPOSITE MATERIALS, Seville, Spain.

Liu, H., Falzon, B., Catalanotti, G., & Tan, W. (2018). An experimental method to determine the intralaminar fracture toughness of high-strength carbon-fibre reinforced composite aerostructures. *The Aeronautical Journal, 122*(1255), 1352-1370.

Liu, Q., & Hughes, M. (2008). The fracture behaviour and toughness of woven flax fibre reinforced epoxy composites. *Composites Part A: Applied Science and Manufacturing, 39*(10), 1644-1652. doi:https://doi.org/10.1016/j.compositesa.2008.07.008

Lotfi, A., Li, H., Dao, D. V., & Prusty, G. (2019). Natural fiber–reinforced composites: A review on material, manufacturing, and machinability. *Journal of Thermoplastic Composite Materials*, 1-47. doi:10.1177/0892705719844546

Madsen, B. (2004). *Properties of plant fibre yarn polymer composites*. Lyngby: Technical University of Denmark.

Madsen, B., & Lilholt, H. (2003). Physical and mechanical properties of unidirectional plant fibre composites—an evaluation of the influence of porosity. *Composites Science and Technology, 63*(9), 1265-1272. doi:https://doi.org/10.1016/S0266-3538(03)00097-6

Mahboob, Z., Chemisky, Y., Meraghni, F., & Bougherara, H. (2017). Mesoscale modelling of tensile response and damage evolution in natural fibre reinforced laminates. *Composites Part B: Engineering, 119*, 168-183. doi:https://doi.org/10.1016/j.compositesb.2017.03.018

Mahdi, M., & Zhang, L. (2001). A finite element model for the orthogonal cutting of fiber-reinforced composite materials. *Journal of Materials Processing Technology, 113*(1), 373-377.

Mahmoudi, S., Kervoelen, A., Robin, G., Duigou, L., Daya, E. M., & Cadou, J. M. (2019). Experimental and numerical investigation of the damping of flax-epoxy composite plates. *Composite Structures, 208*, 426–433. doi:https://doi.org/10.1016/j.compstruct.2018.10.030

Martin, N., Mouret, N., Davies, P., & Baley, C. (2013). Influence of the degree of retting of flax fibers on the tensile properties of single fibers and short fiber/polypropylene

194

composites. *Industrial Crops and Products, 49*, 755-767. doi:https://doi.org/10.1016/j.indcrop.2013.06.012

Mbakop, R. S., Lebrun, G., & Brouillette, F. (2019). Effect of compaction parameters on preform permeability and mechanical properties of unidirectional flax fiber composites. *Composites Part B: Engineering, 176*, 107083. doi:https://doi.org/10.1016/j.compositesb.2019.107083

Mkaddem, A., Demirci, I., & El Mansori, M. (2008). A micro–macro combined approach using FEM for modelling of machining of FRP composites: Cutting forces analysis. *Composites Science and Technology, 68*(15), 3123-3127. doi:https://doi.org/10.1016/j.compscitech.2008.07.009

Mkaddem, A., & El Mansori, M. (2009). Finite element analysis when machining UGF-reinforced PMCs plates: Chip formation, crack propagation and induced-damage. *Materials & Design, 30*(8), 3295-3302. doi:https://doi.org/10.1016/j.matdes.2008.12.009

Mohamed, S. B., Rashid, R. A., Muhamad, M., & Ismail, J. (2019). Composite Materials and Types of Machining. In *Down Milling Trimming Process Optimization for Carbon Fiber-Reinforced Plastic* (pp. 1-14). Singapore: Springer Singapore.

Mohammad Khanlou, H., Hall, W., Woodfield, P., Summerscales, J., & Francucci, G. (2018). The mechanical properties of flax fibre reinforced poly(lactic acid) bio-composites exposed to wet, freezing and humid environments. *Journal of Composite Materials, 52*(6), 835-850. doi:10.1177/0021998317714857

Mohanty, A., Misra, M., & Hinrichsen, G. (2000). Biofibres, biodegradable polymers and biocomposites: an overview. *Macromolecular Materials and Engineering, 276*(1), 1-24.

Moudood, A., Hall, W., Öchsner, A., Li, H., Rahman, A., & Francucci, G. (2019a). Effect of Moisture in Flax Fibres on the Quality of their Composites. *Journal of Natural Fibers, 16*(2), 209-224. doi:https://doi.org/10.1080/15440478.2017.1414651

Moudood, A., Rahman, A., Khanlou, H. M., Hall, W., Öchsner, A., & Francucci, G. (2019b). Environmental effects on the durability and the mechanical performance of flax fiber/bio-epoxy composites. *Composites Part B: Engineering, 171*, 284-293. doi:https://doi.org/10.1016/j.compositesb.2019.05.032

Moudood, A., Rahman, A., Öchsner, A., Islam, M., & Francucci, G. (2018). Flax fiber and its composites: An overview of water and moisture absorption impact on their performance. *Journal of Reinforced Plastics and Composites, 38*(7), 323-339. doi:https://doi.org/10.1177/0731684418818893

Muralidhar, B. A. (2013a). Tensile and compressive behaviour of multilayer flax-rib knitted preform reinforced epoxy composites. *Materials & Design, 49*, 400-405. doi:https://doi.org/10.1016/j.matdes.2012.12.040

Muralidhar, B. A. (2013b). Tensile and compressive properties of flax-plain weave preform reinforced epoxy composites. *Journal of Reinforced Plastics and Composites, 32*(3), 207-213. doi:https://doi.org/10.1177/0731684412469136

Mustafa, A. R., Azmi, A. I., Zakaria, M. S., & Lih, T. C. (2019). Evaluation of delamination damage and surface roughness in end milling flax fibre composites. *IOP Conference Series: Materials Science and Engineering, 670*, 012009. doi:http://dx.doi.org/10.1088/1757-899X/670/1/012009

Naderi, M., Kahirdeh, A., & Khonsari, M. M. (2012). Dissipated thermal energy and damage evolution of Glass/Epoxy using infrared thermography and acoustic emission. *Composites Part B: Engineering, 43*(3), 1613-1620. doi:https://doi.org/10.1016/j.compositesb.2011.08.002

Naik, P. K., Londe, N. V., Yogesha, B., Laxmana Naik, L., & Pradeep, K. V. (2018). Mode I Fracture Characterization of Banana Fibre Reinforced Polymer Composite. *IOP Conference Series: Materials Science and Engineering, 376*, 012041. doi:http://dx.doi.org/10.1088/1757-899X/376/1/012041

Nasir, A. A., Azmi, A., & Khalil, A. (2015). Parametric Study on the Residual Tensile Strength of Flax Natural Fibre Composites after Drilling Operation. *Procedia Manufacturing, 2*, 97-101.

Nassar, M., Nassar, M. M. A., Arunachalam, R., & Alzebdeh, K. (2017). Machinability of natural fiber reinforced composites: a review. *The International Journal of Advanced Manufacturing Technology, 88*(9-12), 2985-3004. doi:10.1007/s00170-016-9010-9

Nasuha, N., Azmi, A., & Lih, T. (2017). A review on mode-I interlaminar fracture toughness of fibre reinforced composites. *IOP Conf. Series: Journal of Physics: Conf. Series, 908*, 012024. doi:10.1088/1742-6596/908/1/012024

Nayak, D., Bhatnagar, N., & Mahajan, P. (2005). Machining studies of UD-FRP composites part 2: finite element analysis. *Machining Science and Technology, 9*(4), 503-528.

Netravali, A. N., & Chabba, S. (2003). Composites get greener. *Materials Today, 6*(4), 22-29. doi:https://doi.org/10.1016/S1369-7021(03)00427-9

Oksman, K. (2001). High Quality Flax Fibre Composites Manufactured by the Resin Transfer Moulding Process. *Journal of Reinforced Plastics and Composites, 20*, 621-627. doi:10.1106/CA5A-6FAX-VJRB-80P0

Ooi, C., Tan, C., & Azmi, A. (2019). Experimental study towards inter-laminar fracture toughness of different fibre reinforced polymer composites. *Journal of Physics: Conference Series, 1150*(1), 012029. doi:10.1088/1742-6596/1150/1/012029

Paris, P., & Sih, G. (1965, June 21-26). *Stress analysis of cracks.* Paper presented at the Fracture toughness testing and its applications Chicago.

Petersen, E., Cuntze, R. G., & Hühne, C. (2016). Experimental determination of material parameters in Cuntze's Failure-Mode-Concept-based UD strength failure conditions. *Composites Science and Technology, 134*, 12-25. doi:https://doi.org/10.1016/j.compscitech.2016.08.006

Piascik, R., Newman, J., & Underwood, J. (1997). The extended compact tension specimen. *Fatigue & Fracture of Engineering Materials & Structures, 20*(4), 559-563. doi:https://doi.org/10.1111/j.1460-2695.1997.tb00287.x

Pickering, K. L., Efendy, M. G. A., & Le, T. M. (2016). A review of recent developments in natural fibre composites and their mechanical performance. *Composites Part A: Applied Science and Manufacturing, 83*, 98-112. doi:https://doi.org/10.1016/j.compositesa.2015.08.038

Pierron, F., & Vautrin, A. (1998). Measurement of the in-plane shear strengths of unidirectional composites with the Iosipescu test. *Composites Science and Technology, 57*(12), 1653-1660. doi:https://doi.org/10.1016/S0266-3538(97)00099-7

Pil, L., Bensadoun, F., Pariset, J., & Verpoest, I. (2016). Why are designers fascinated by flax and hemp fibre composites? *Composites Part A: Applied Science and Manufacturing, 83*, 193-205. doi:http://dx.doi.org/10.1016/j.compositesa.2015.11.004

Pinho, S., Robinson, P., & Iannucci, L. (2009). Developing a four point bend specimen to measure the mode I intralaminar fracture toughness of unidirectional laminated composites. *Composites Science and Technology, 69*(7), 1303-1309. doi:https://doi.org/10.1016/j.compscitech.2009.03.007

Pinho, S. T., Robinson, P., & Iannucci, L. (2006). Fracture toughness of the tensile and compressive fibre failure modes in laminated composites. *Composites Science and Technology, 66*(13), 2069-2079. doi:10.1016/j.compscitech.2005.12.023

Pinto, M., Chalivendra, V. B., Kim, Y. K., & Lewis, A. F. (2016). Improving the strength and service life of jute/epoxy laminar composites for structural applications. *Composite Structures, 156*, 333-337. doi:https://doi.org/10.1016/j.compstruct.2015.10.005

Poilâne, C., Vivet, A., Momayez, L., Doudou, A. B., Ayachi, M. h., & Chen, J. (2009). *Propriétés mécaniques de préimprégnés lin/époxyde - Mechanical properties of flax/epoxy industrial prepregs* Paper presented at the Compte rendu des JNC16, Toulouse, France.

Prasad, M. S., Venkatesha, C., & Jayaraju, T. (2011). Experimental methods of determining fracture toughness of fiber reinforced polymer composites under various loading conditions. *Journal of Minerals and Materials Characterization and Engineering, 10*(13), 1263.

Prasad, V., Venkatachalam, G., Rathi, A., & Rajakumar, S. (2014). *Finite element analysis of jute fibre made hybrid polymer matrix composite.* Paper presented at the 2014 International Mechanical Engineering Congress, IMEC 2014, June 13, 2014 - June 15, 2014, Tiruchirappalli, TN, India.

Pujols Gonzalez, J. D., Bouvet, C., & Vieille, B. (2020). *Translaminar cracking modelling in woven ply composite laminates at high temperature*. Paper presented at the ECCM19-19TH EUROPEAN CONFERENCE ON COMPOSITE MATERIALS, Nantes, France.

Rajak, D. K., Pagar, D. D., Menezes, P. L., & Linul, E. (2019). Fiber-Reinforced Polymer Composites: Manufacturing, Properties, and Applications. *Polymers, 11*(10), 1667. doi:https://doi.org/10.3390/polym11101667

Rajendran, T., Johar, M., Hassan, S., & Wong, K. J. (2018, June 28). *Mode I and Mode II Delamination of Flax/Epoxy Composite Laminate.* Paper presented at the MATEC Web of Conferences (AAME 2018), Les Ulis Cedex A, France.

Rajendran, T., Johar, M., Low, K. O., Abu Hassan, S., & Wong, K. J. (2019). Interlaminar fracture toughness of a plain weave flax/epoxy composite. *Plastics, Rubber and Composites, 48*(2), 74-81. doi:10.1080/14658011.2018.1550235

Rajmohan, T., Vinayagamoorthy, R., & Mohan, K. (2018). Review on effect machining parameters on performance of natural fibre–reinforced composites (NFRCs). *Journal of Thermoplastic Composite Materials, 32*(9), 1282-1302. doi:https://doi.org/10.1177/0892705718796541

Ramamoorthy, S. K., Skrifvars, M., & Persson, A. (2015). A Review of Natural Fibers Used in Biocomposites: Plant, Animal and Regenerated Cellulose Fibers. *Polymer Reviews, 55*(1), 107-162. doi:https://doi.org/10.1080/15583724.2014.971124

Ramesh, M. (2019). Flax (Linum usitatissimum L.) fibre reinforced polymer composite materials: A review on preparation, properties and prospects. *Progress in Materials Science, 102*, 109-166. doi:https://doi.org/10.1016/j.pmatsci.2018.12.004

Ramesh, M., Palanikumar, K., & Reddy, K. (2017). Plant fibre based bio-composites: Sustainable and renewable green materials. *Renewable and Sustainable Energy Reviews, 79*, 558-584. doi:10.1016/j.rser.2017.05.094

Ramulu, M. (1997). Machining and surface integrity of fibre-reinforced plastic composites. *Sadhana, 22*(3), 449-472. Retrieved from https://link.springer.com/content/pdf/10.1007/BF02744483.pdf

Rao, G. V. G., Mahajan, P., & Bhatnagar, N. (2008). Three-dimensional macro-mechanical finite element model for machining of unidirectional-fiber reinforced polymer composites. *Materials Science & Engineering A, 498*(1), 142-149. doi:10.1016/j.msea.2007.11.157

Ravandi, M., Teo, W., Tran, L., Yong, M., & Tay, T. (2016a). The effects of through-the-thickness stitching on the Mode I interlaminar fracture toughness of flax/epoxy composite laminates. *Materials & Design, 109*, 659-669. doi:http://dx.doi.org/10.1016/j.matdes.2016.07.093

Ravandi, M., Teo, W., Tran, L., YONG, M., & TAY, T. (2016b). *Mode I Interlaminar Fracture Toughness of Natural Fiber Stitched Flax/Epoxy Composite Laminates–Experimental and Numerical Analysis.* Paper presented at the Proceedings of the American Society for Composites: Thirty-First Technical Conference.

Ravandi, M., Teo, W. S., Yong, M. S., & Tay, T. E. (2018). Prediction of Mode I interlaminar fracture toughness of stitched flax fiber composites. *Journal of Materials Science, 53*(6), 4173-4188. doi:https://doi.org/10.1007/s10853-017-1859-y

Robinson, P. (1996). The effects of starter film thickness, residual stresses and layup on GIc of a 0°/0° interface. *Advanced Composites Letters, 5*(6), 159-163. doi:https://doi.org/10.1177/096369359600500601

Romhány, G., Karger-Kocsis, J., & Czigány, T. (2003). Tensile Fracture and Failure Behavior of Thermoplastic Starch with Unidirectional and Cross-Ply Flax Fiber Reinforcements. *Macromolecular Materials and Engineering, 288*(9), 699-707. doi:10.1002/mame.200300040

Saadati, Y., Chatelain, J.-F., Lebrun, G., & Beauchamp, Y. (2019). *Comparison of density measurement methods for unidirectional flax-epoxy polymer composites*. Paper presented at the EMuS 2019, Barcelona, Spain.

Saadati, Y., Chatelain, J.-F., Lebrun, G., Beauchamp, Y., Bocher, P., & Vanderesse, N. (2020a). A Study of the Interlaminar Fracture Toughness of Unidirectional Flax/Epoxy Composites. *Journal of Composites Science, 4*(2), 66. doi:https://doi.org/10.3390/jcs4020066

Saadati, Y., Lebrun, G., Bouvet, C., Chatelain, J.-F., & Beauchamp, Y. (2020b). Study of translaminar fracture toughness of unidirectional flax/epoxy composite. *Composites Part C: Open Access*, 100008. doi:https://doi.org/10.1016/j.jcomc.2020.100008

Saadati, Y., Lebrun, G., Chatelain, J.-F., & Beauchamp, Y. (2020c). Experimental investigation of failure mechanisms and evaluation of physical/mechanical properties of unidirectional flax–epoxy composites. *Journal of Composite Materials, 54*(20), 2781–2801. doi:https://doi.org/10.1177/0021998320902243

Saidane, E. H., Scida, D., Pac, M.-J., & Ayad, R. (2019). Mode-I interlaminar fracture toughness of flax, glass and hybrid flax-glass fibre woven composites: Failure mechanism evaluation using acoustic emission analysis. *Polymer Testing, 75*, 246-253. doi:https://doi.org/10.1016/j.polymertesting.2019.02.022

Sanjay, M. R., Madhu, P., Jawaid, M., Senthamaraikannan, P., Senthil, S., & Pradeep, S. (2018). Characterization and properties of natural fiber polymer composites: A comprehensive review. *Journal of Cleaner Production, 172*, 566-581. doi:https://doi.org/10.1016/j.jclepro.2017.10.101

Sanjay, M. R., Siengchin, S., Parameswaranpillai, J., Jawaid, M., Pruncu, C. I., & Khan, A. (2019). A comprehensive review of techniques for natural fibers as reinforcement in composites: Preparation, processing and characterization. *Carbohydrate polymers, 207*, 108-121. doi:https://doi.org/10.1016/j.carbpol.2018.11.083

Santiuste, C., Soldani, X., & Miguélez, M. H. (2010). Machining FEM model of long fiber composites for aeronautical components. *Composite Structures, 92*(3), 691-698. doi:10.1016/j.compstruct.2009.09.021

Schellekens, J. C. J., & de Borst, R. (1990). The use of the Hoffman yield criterion in finite element analysis of anisotropic composites. *Computers & Structures, 37*(6), 1087-1096. doi:https://doi.org/10.1016/0045-7949(90)90020-3

Selmy, A. I., Elsesi, A. R., Azab, N. A., & Abd El-baky, M. A. (2012). In-plane shear properties of unidirectional glass fiber (U)/random glass fiber (R)/epoxy hybrid and non-hybrid composites. *Composites Part B: Engineering, 43*(2), 431-438. doi:https://doi.org/10.1016/j.compositesb.2011.06.001

Shah, D. U. (2013). Developing plant fibre composites for structural applications by optimising composite parameters: a critical review. *Journal of Materials Science, 48*(18), 6083-6107. doi:10.1007/s10853-013-7458-7

Shah, D. U., Schubel, P. J., & Clifford, M. J. (2013). Can flax replace E-glass in structural composites? A small wind turbine blade case study. *Composites Part B: Engineering, 52*, 172-181. doi:https://doi.org/10.1016/j.compositesb.2013.04.027

Shakir Radif, Z., & Ali, A. (2011). Fracture toughness of kenaf mat reinforced polyester composite. *Pertanika Journal of Science and Technology, 19*, 177.

Sheikh-Ahmad, J. Y. (2009). *Machining of polymer composites*. New York, NY: Springer.

200

Shekar, H. S. S., & Ramachandra, M. (2018). Green Composites: A Review. *Materials Today: Proceedings, 5*(1, Part 3), 2518-2526. doi:https://doi.org/10.1016/j.matpr.2017.11.034

Shetty, N., Shahabaz, S. M., Sharma, S. S., & Divakara Shetty, S. (2017). A review on finite element method for machining of composite materials. *Composite Structures, 176*, 790-802. doi:https://doi.org/10.1016/j.compstruct.2017.06.012

Shokrieh, M. M., & Heidari-Rarani, M. (2011). Effect of stacking sequence on R-curve behavior of glass/epoxy DCB laminates with 0°//0° crack interface. *Materials Science and Engineering: A, 529*, 265-269. doi:https://doi.org/10.1016/j.msea.2011.09.027

Siddharth, M., Anand, K., Vijay Sekar, K., & Suresh Kumar, S. (2015). An investigation of the effects of fiber orientation in GFRP machining using FEM. *International Journal of Applied Engineering Research, 10*(51), 2015.

Silva, R. V., Spinelli, D., Bose Filho, W. W., Claro Neto, S., Chierice, G. O., & Tarpani, J. R. (2006). Fracture toughness of natural fibers/castor oil polyurethane composites. *Composites Science and Technology, 66*(10), 1328-1335. doi:https://doi.org/10.1016/j.compscitech.2005.10.012

Singh, T. J., & Samanta, S. (2016). *Multi-response parametric optimization in drilling of bamboo/Kevlar fiber reinforced sandwich composite.* Paper presented at the IOP Conference Series: Materials Science and Engineering.

Singleton, A. C. N., Baillie, C. A., Beaumont, P. W. R., & Peijs, T. (2003). On the mechanical properties, deformation and fracture of a natural fibre/recycled polymer composite. *Composites Part B: Engineering, 34*(6), 519-526. doi:https://doi.org/10.1016/S1359-8368(03)00042-8

Sodoke, K. F., Laperrière, L., Toubal, L., & Khakestar, R. S. (2016). Fuzzy logic response to Young's modulus characterization of a flax–epoxy natural fiber composite. *Materials & Design, 89*, 273-285.

Soutis, C., & Curtis, P. (2000). A method for predicting the fracture toughness of CFRP laminates failing by fibre microbuckling. *Composites Part A: Applied Science and Manufacturing, 31*(7), 733-740.

Sridharan, V., & Muthukrishnan, N. (2013). Optimization of machinability of polyester/modified jute fabric composite using grey relational analysis (GRA). *Procedia engineering, 64*, 1003-1012.

Takano, N., Zako, M., Fujitsu, R., & Nishiyabu, K. (2004). Study on large deformation characteristics of knitted fabric reinforced thermoplastic composites at forming temperature by digital image-based strain measurement technique. *Composites Science and Technology, 64*(13), 2153-2163. doi:https://doi.org/10.1016/j.compscitech.2004.03.016

Tay, T. (2003). Characterization and analysis of delamination fracture in composites: an overview of developments from 1990 to 2001. *Applied Mechanics Reviews-ASME, 56*(1), 1-32. doi:10.1115/1.1504848

Taylor, G. I., & Quinney, H. (1934). The latent energy remaining in a metal after cold working. *Proceedings of the Royal Society of London. Series A, Containing Papers of a Mathematical and Physical Character, 143*(849), 307-326.

Teixeira, R. F., Pinho, S. T., & Robinson, P. (2016). Thickness-dependence of the translaminar fracture toughness: Experimental study using thin-ply composites. *Composites Part A: Applied Science and Manufacturing, 90*, 33-44. doi:https://doi.org/10.1016/j.compositesa.2016.05.031

Tekieli, M., De Santis, S., de Felice, G., Kwiecień, A., & Roscini, F. (2017). Application of Digital Image Correlation to composite reinforcements testing. *Composite Structures, 160*, 670-688. doi:https://doi.org/10.1016/j.compstruct.2016.10.096

Teti, R. (2002). Machining of composite materials. *CIRP Annals-Manufacturing Technology, 51*(2), 611-634. doi:https://doi.org/10.1016/S0007-8506(07)61703-X

Truong, M., Zhong, W., Boyko, S., & Alcock, M. (2009). A comparative study on natural fibre density measurement. *The Journal of The Textile Institute, 100*(6), 525-529. doi:https://doi.org/10.1080/00405000801997595

Underwood, J., Kortschot, M., Lloyd, W., Eidinoff, H., Wilson, D., & Ashbaugh, N. (1995). Translaminar Fracture Toughness Test Methods and Results from Interlaboratory Tests of Carbon/epoxy Laminates. *Fracture Mechanics: 26th Volume, ASTM STP 1256*, 486-508.

Vaidya, R. S., & Sun, C. (1997). Fracture criterion for notched thin composite laminates. *AIAA journal, 35*(2), 311-316.

Väisänen, T., Das, O., & Tomppo, L. (2017). A review on new bio-based constituents for natural fiber-polymer composites. *Journal of Cleaner Production, 149*, 582-596. doi:https://doi.org/10.1016/j.jclepro.2017.02.132

Van de Weyenberg, I., Ivens, J., De Coster, A., Kino, B., Baetens, E., & Verpoest, I. (2003). Influence of processing and chemical treatment of flax fibres on their composites. *Composites Science and Technology, 63*(9), 1241-1246.

Vinayagamoorthy, R., & Rajeswari, N. (2012). Analysis of cutting forces during milling of natural fibered composites using fuzzy logic. *International Journal of Composites Materials and Manufacturing, 2*(3), 15-21.

Vinayagamoorthy, R., Rajeswari, N., Sivanarasimha, S., & Balasubramanian, K. (2015). Fuzzy based optimization of thrust force and torque during drilling of natural hybrid

composites. *Applied Mechanics and Materials, 787*, 265-269. doi:http://dx.doi.org/10.4028/www.scientific.net/AMM.787.265

Vinayagamoorthy, R., & Thiagarajan, R. (2018). Machining and its challenges on bio-fibre reinforced plastics: A critical review. *Journal of Reinforced Plastics and Composites*, 073168441877835. doi:10.1177/0731684418778356

Vo Hong, N., Beckers, K., Goderis, B., Van Puyvelde, P., Verpoest, I., & Willem Van Vuure, A. (2018). Fracture toughness of unidirectional flax fiber composites with rigid gliadin matrix. *Journal of Reinforced Plastics and Composites, 37*(18), 1163-1174. doi:10.1177/0731684418789780

Walker, C. A., & Jamasri. (1995). Mixed-mode stress intensity factors in finite, edge-cracked orthotropic plates. *The Journal of Strain Analysis for Engineering Design, 30*(2), 83-90. doi:https://doi.org/10.1243/03093247V302083

Wambua, P., Ivens, J., & Verpoest, I. (2003). Natural fibres: can they replace glass in fibre reinforced plastics? *Composites Science and Technology, 63*(9), 1259-1264. doi:https://doi.org/10.1016/S0266-3538(03)00096-4

Wan, M., Li, S.-E., Yuan, H., & Zhang, W.-H. (2019). Cutting force modelling in machining of fiber-reinforced polymer matrix composites (PMCs): A review. *Composites Part A: Applied Science and Manufacturing, 117*, 34-55. doi:https://doi.org/10.1016/j.compositesa.2018.11.003

Wang, H. (2013). Marker Identification Technique for Deformation Measurement. *Advances in Mechanical Engineering, 5*, 246318. doi:https://doi.org/10.1155/2013/246318

Wang, H., & Hou, Z. (2010, 10-12 Aug. 2010). *Application of Genetic Algorithms in a surface deformation measurement technique.* Paper presented at the 2010 Sixth International Conference on Natural Computation.

Wang, W.-X., Nakata, M., Takao, Y., & Matsubara, T. (2009). Experimental investigation on test methods for mode II interlaminar fracture testing of carbon fiber reinforced composites. *Composites Part A: Applied Science and Manufacturing, 40*(9), 1447-1455. doi:https://doi.org/10.1016/j.compositesa.2009.04.029

Wang, X., & Zhang, L. (2003). An experimental investigation into the orthogonal cutting of unidirectional fibre reinforced plastics. *International Journal of Machine Tools and Manufacture, 43*(10), 1015-1022. doi:https://doi.org/10.1016/S0890-6955(03)00090-7

Wattrisse, B., Muracciole, J.-M., & Chrysochoos, A. (2002). Thermomechanical effects accompanying the localized necking of semi-crystalline polymers. *International Journal of Thermal Sciences, 41*(5), 422-427. doi:https://doi.org/10.1016/S1290-0729(02)01334-0

Wong, S., Shanks, R. A., & Hodzic, A. (2004). Mechanical Behavior and Fracture Toughness of Poly(L-lactic acid)-Natural Fiber Composites Modified with Hyperbranched Polymers. *Macromolecular Materials and Engineering, 289*(5), 447-456. doi:10.1002/mame.200300366

Xiong, X., Shen, S. Z., Hua, L., Liu, J. Z., Li, X., Wan, X., & Miao, M. (2018). Finite element models of natural fibers and their composites: A review. *Journal of Reinforced Plastics and Composites, 37*(9), 617-635.

Xu, D., Cerbu, C., Wang, H., & Rosca, I. C. (2019). Analysis of the hybrid composite materials reinforced with natural fibers considering digital image correlation (DIC) measurements. *Mechanics of materials, 135*, 46-56. doi:https://doi.org/10.1016/j.mechmat.2019.05.001

Xu, W., & Zhang, L. (2017). A new approach to characterising the surface integrity of fibre-reinforced polymer composites during cutting. *Composites Part A: Applied Science and Manufacturing, 103*, 272-282. doi:https://doi.org/10.1016/j.compositesa.2017.10.015

Yan, L., & Chouw, N. (2013). Crashworthiness characteristics of flax fibre reinforced epoxy tubes for energy absorption application. *Materials & Design, 51*, 629-640. doi:https://doi.org/10.1016/j.matdes.2013.04.014

Yan, L., Chouw, N., & Jayaraman, K. (2014). Flax fibre and its composites–A review. *Composites Part B: Engineering, 56*, 296-317. doi:http://dx.doi.org/10.1016/j.compositesb.2013.08.014

Yan, L., Chouw, N., & Yuan, X. (2012). Improving the mechanical properties of natural fibre fabric reinforced epoxy composites by alkali treatment. *Journal of Reinforced Plastics and Composites, 31*(6), 425-437. doi:10.1177/0731684412439494

Yan, L., Wang, B., & Kasal, B. (2017). Can Plant-Based Natural Flax Replace Basalt and E-Glass for Fiber-Reinforced Polymer Tubular Energy Absorbers? A Comparative Study on Quasi-Static Axial Crushing. *Frontiers in Materials, 4*. doi:10.3389/fmats.2017.00042

Yashas Gowda, T. G., Sanjay, M. R., Subrahmanya Bhat, K., Madhu, P., Senthamaraikannan, P., & Yogesha, B. (2018). Polymer matrix-natural fiber composites: An overview. *Cogent Engineering, 5*(1), 1446667. doi:10.1080/23311916.2018.1446667

Zaghbani, I., Chatelain, J.-F., Berube, S., Songmene, V., & Lance, J. (2012a). Analysis and modelling of cutting forces during the trimming of unidirectional CFRP composite laminates. *International Journal of Machining and Machinability of Materials, 12*(4), 337-357. doi:10.1504/ijmmm.2012.050433

Zaghbani, I., Chatelain, J.-F., Songmene, V., Bérubé, S., & Atarsia, A. (2012b). A comprehensive analysis of cutting forces during routing of multilayer carbon fiber-reinforced polymer laminates. *Journal of Composite Materials, 46*(16), 1955-1971. doi:https://doi.org/10.1177/0021998311428362

Zenia, S., Ayed, L. B., Nouari, M., & Delamézière, A. (2015). An elastoplastic constitutive damage model to simulate the chip formation process and workpiece subsurface defects when machining CFRP composites. *Procedia CIRP, 31*, 100-105.

Zhang, Y., Li, Y., Ma, H., & Yu, T. (2013). Tensile and interfacial properties of unidirectional flax/glass fiber reinforced hybrid composites. *Composites Science and Technology, 88*, 172-177. doi:https://doi.org/10.1016/j.compscitech.2013.08.037

Zhu, J., Abhyankar, H., Nassiopoulos, E., & Njuguna, J. (2012). *Tannin-based flax fibre reinforced composites for structural applications in vehicles.* Paper presented at the IOP Conference Series: Materials Science and Engineering.

Zhu, J., Sauget, A., Nassiopoulos, E., Pizzi, A., Avril, C., Njuguna, J., & Abyhankar, H. (2014). *Structural performances of flax reinforced composites from tannin resin and bio-epoxy.* Paper presented at the Transport Research Arena (TRA) 5th Conference: Transport Solutions from Research to Deployment Paris, France.

Zhu, J., Zhu, H., Njuguna, J., & Abhyankar, H. (2013). Recent development of flax fibres and their reinforced composites based on different polymeric matrices. *Materials, 6*(11), 5171-5198. doi:10.3390/ma6115171

Zhu, Y. (2009). *Characterization of Interlaminar Fracture Toughness of a Carbon/epoxy Composite Material.* (Master). Pennsylvania State University, University Park, PA 16802, USA. Retrieved from https://books.google.ca/books?id=KEehAQAACAAJ